

University of Alberta
Department of Civil and
Environmental Engineering



Structural Engineering Report No. 215

SEISMIC BEHAVIOUR OF STEEL PLATE SHEAR WALLS

by

Robert G. Driver

Geoffrey L. Kulak

D.J. Laurie Kennedy

and

Alaa E. Elwi

February 1997

Recent Structural Engineering Reports

Department of Civil Engineering

University of Alberta

187. *Shear Lag in Bolted Single and Double Angle Tension Members* by Yue Wu and Geoffrey L. Kulak, June 1993.
188. *A Shear-Friction Truss Model for Reinforced Concrete Beams Subjected to Shear* by Simon A. Chen and James G. MacGregor, June 1993.
189. *An Investigation of Hoist-Induced Dynamic Loads* by Douglas A. Barrett and Terry M. Hrudey, July 1993.
190. *Analysis and Design of Fabricated Steel Structures for Fatigue: A Primer for Civil Engineers* by Geoffrey L. Kulak and Ian F.C. Smith, July 1993.
191. *Cyclic Behavior of Steel Gusset Plate Connections* by Jeffrey S. Rabinovitch and J.J. Roger Cheng, August 1993.
192. *Bending Strength of Longitudinally Stiffened Steel Cylinders* by Qishi Chen, Alaa E. Elwi and Geoffrey L. Kulak, August 1993.
193. *Web Behaviour in Wood Composite Box Beams* by E. Thomas Lewicke, J.J. Roger Cheng and Lars Bach, August 1993.
194. *Experimental Investigation of the Compressive Behavior of Gusset Plate Connections* by Michael C.H. Yam and J.J. Roger Cheng, September 1993.
195. *Some Behavioural Aspects of Composite Trusses* by Berhanu Woldegiorgis and D.J. Laurie Kennedy, January 1994.
196. *Flexural Behavior of High Strength Concrete Columns* by Hisham H.H. Ibrahim and James G. MacGregor, March 1994.
197. *Prediction of Wrinkling Behavior of Girth-Welded Line Pipe* by Luis T. Souza, Alaa E. Elwi, and David W. Murray, April 1994.
198. *Assessment of Concrete Strength in Existing Structures* by F. Michael Bartlett and James G. MacGregor, May 1994.
199. *The Flexural Creep Behavior of OSB Panels Under Various Climatic Conditions* by Naiwen Zhao, J.J. Roger Cheng, and Lars Bach, June 1994.
200. *High Performance Concrete Under High Sustained Compressive Stresses* by Said Irvani and James G. MacGregor, June 1994.

SEISMIC BEHAVIOUR OF STEEL PLATE SHEAR WALLS

by

Robert G. Driver

Geoffrey L. Kulak

D.J. Laurie Kennedy

and

Alaa E. Elwi

Structural Engineering Report 215

**Department of Civil and Environmental Engineering
University of Alberta
Edmonton, Alberta, Canada**

February, 1997

ABSTRACT

Steel plate shear walls are an innovative lateral load-resisting system capable of effectively bracing a building against both wind and earthquake forces. The system consists of vertical steel infill plates one storey high and one bay wide connected to the surrounding beams and columns. The plates are installed in one or more bays for the full height of a building to form a stiff cantilever wall. Steel plate shear walls are well-suited for new construction and they also offer a relatively simple means for the seismic upgrading of existing steel or concrete structures.

A large-scale four storey, single bay specimen with unstiffened panels was tested under controlled cyclic loading to determine its behaviour under an idealized severe earthquake event. The shear wall had moment-resisting beam-to-column connections, resulting in a lateral load-resisting system that possessed an inherent redundancy. During the test, the specimen endured 30 cycles of loading, including 20 cycles in the inelastic range. Prior to failure of the specimen, the deflection reached in the lowest storey was nine times the yield deflection. The test specimen proved to be initially very stiff, showed excellent ductility and energy dissipation characteristics, and exhibited stable behaviour at very large deformations and after many cycles of loading.

Results of another large-scale test to evaluate the performance of the corner detail to be used in the main test specimen are reported. Other ancillary tests included an evaluation of residual stresses in the shear wall frame members and a series of material tests on both the members and infill plates.

A non-linear finite element model for steel plate shear walls was developed using the as-built dimensions and measured material properties of the test specimen. A non-planar initial plate geometry and residual stresses obtained experimentally

were included. Cyclic and monotonic load vs. deflection responses and the internal member forces are compared with experimental results.

A simplified method for predicting the monotonic response and two models for predicting the hysteresis behaviour of steel plate shear walls are described. The models account for inelastic behaviour in both the infill panels and the frame members. The predicted behaviour of the four storey shear wall specimen is compared with the test results.

RÉSUMÉ

Les murs de refend en acier représentent un système innovateur résistant aux charges latérales susceptible de contreventer efficacement un bâtiment contre les forces de vent et de séisme. Ce système est constitué de plaques verticales en acier placées à l'intérieur de la hauteur d'un étage et d'une largeur d'une baie, reliées aux poutres et aux colonnes adjacentes. Les plaques sont installées dans une ou plusieurs baies sur toute la hauteur du bâtiment pour former un porte-à-faux vertical. Les murs de refend en acier sont bien appropriés pour les nouvelles constructions et ils offrent aussi un moyen relativement simple pour rendre les structures existantes en acier ou en béton conformes aux nouvelles normes para-sismiques.

Un échantillon d'une seule baie et de quatre étages, à grande échelle, avec des panneaux non rigides a été testé sous un chargement cyclique contrôlé afin de déterminer son comportement face à un séisme sévère idéalisé. Le mur de refend a été conçu avec des assemblages rigides poutres-poteaux, donnant au système une résistance supplémentaire. Durant l'essai, l'échantillon a subi 30 cycles de chargement, incluant 20 cycles dans le domaine inélastique. Avant la rupture de l'échantillon, le déplacement atteint au plus bas étage représentait neuf fois le déplacement élastique. Le modèle expérimental s'est démontré initialement très rigide, mais a ensuite démontré une excellente ductilité et des caractéristiques de dissipation d'énergie. L'échantillon a aussi présenté un comportement stable après de très grandes déformations et plusieurs cycles de chargement.

Des résultats d'autres essais à grande échelle pour évaluer la performance du détail de coin utilisé dans l'échantillon principal sont rapportés. D'autres essais complémentaires ont inclus une évaluation des contraintes résiduelles dans les membrures du mur de refend et des séries d'essais de matériaux sur les membrures et les plaques.

Un modèle non-linéaire par éléments finis pour le mur de refend en acier a été développé en utilisant les dimensions exactes de l'échantillon et les propriétés des matériaux mesurées par des essais sur éprouvettes. La géométrie initiale non plane des plaques et les contraintes résiduelles obtenues expérimentalement sont inclus. Les réponses charges cycliques et monotones en fonction du déplacement et des forces internes des membrures sont comparées avec les résultats expérimentaux.

Une méthode simplifiée pour prédire la réponse monotone et deux modèles de comportement hystérétique des murs de refend en acier sont présentés. Les modèles tiennent compte du comportement inélastique des panneaux insérés et des membrures du cadre. Le comportement théorique du mur de cisaillement à quatre étages est comparé avec les résultats des essais.

ZUSAMMENFASSUNG

Stahlschubwände sind ein innovatives Seitenlastwiderstandssystem, mit dem ein Gebäude wirksam gegen Wind- und Erdbebenkräfte gestützt werden kann. Das System besteht aus senkrechten Stahlplatten, die ein Stockwerk hoch, ein Feld breit und mit den umgebenden Trägern und Stützen verbunden sind. Die Stahlplatten werden in ein oder mehrere Felder für die volle Höhe des Gebäudes eingebaut, sodaß sie eine steife Kragwand bilden. Stahlschubwände eignen sich ausgezeichnet für Neubauten, sind aber auch eine relativ einfache Möglichkeit zum erdbebensicheren Umbau vorhandener Stahl- und Betonbauten.

Zur Bestimmung des Verhaltens bei einem schweren Erdbeben unter idealisierten Bedingungen wurde ein großes, vier Stockwerke hohes und ein Feld breites Modell mit unversteiften Stahlplatten unter kontrollierten zyklischen Belastungen getestet. Die Stahlschubwand besaß biegungsfeste Träger-zu-Stützen-Verbindungen, die ein Seitenlastwiderstandssystem mit inhärentem Überschuß ergaben. Während des Versuchs hielt das Modell 30 Lastzyklen stand; wovon 20 im unelastischen Bereich lagen. Vor seinem Versagen erreichte es im untersten Geschoß die neunfache Fließabweigung. Das Versuchsmodell erwies sich als am Anfang sehr steif, zeigte ausgezeichnete Dehnbarkeit und Energieverzehrungsmerkmale und stabiles Verhalten bei sehr großen Umformungen und nach vielen Belastungszyklen.

Ergebnisse eines anderen Großtests zur Auswertung der Leistung des im Haupttest zu verwendenden Eckendetails werden beschrieben. In anderen Nebentests erfolgte unter anderem eine Auswertung der Restspannung in den Schubwandrahmengliedern und eine Reihe von Materialtests an den Rahmengliedern und Stahlplatten.

Es wurde ein nichtlineares, Finite-Elemente-Modell für Stahlschubwände mit den genauen Abmessungen und gemessenen Materialeigenschaften des

Versuchsmodelles entwickelt. Es umfaßte auch eine experimentell ermittelte unebene anfängliche Stahlplattengeometrie und Restspannung. Zyklische und gleichförmige Belastung im Verhältnis zu Abweichungsreaktionen und die internen Stabkräfte werden mit Versuchsergebnissen verglichen.

Es werden eine vereinfachte Methode zum Berechnen der gleichförmigen Reaktionen und zwei Modelle zur Berechnung des Hystereseverhaltens von Stahlschubwänden beschrieben. Die Modelle erklären das unelastische Verhalten in den Stahlplatten und Rahmengliedern. Das vorhergesagte Verhalten des vierstöckigen Schubwandmodelles wird mit den Versuchsergebnissen verglichen.

ACKNOWLEDGEMENTS

This project was conducted with research funding from the Natural Sciences and Engineering Research Council of Canada. The first author wishes also to acknowledge personal financial support in the form of scholarships from the University of Alberta, the Province of Alberta, the Steel Structures Education Foundation, the Alberta Research Council, the Canadian Society for Civil Engineering, and the Izaak Walton Killam Trust.

Many people contributed to the success of the physical testing programme. Those who made particularly significant contributions are Prof. S. Alexander (interactive data acquisition interface), A. Boucher, J. DiBattista, and R. Savage (construction), R. Helfrich (instrumentation), and M. Medhekar (testing and photography). Several of the AutoCADTM drawings of the tests in the thesis were created by T. Manuel.

Cooperation of the staff at the Centre for Engineering Research (C-FER), and in particular T. Zimmerman, G. Beaulac, and A. Betts, is gratefully acknowledged. Allowing the test to be conducted in their facility, and making an effort to ensure that the logistics of moving many tonnes of equipment in and out proceeded smoothly, contributed greatly to the success of the project.

The helpful comments of Profs. L.-W. Lu of Lehigh University, H.G.L. Prion of the University of British Columbia, and M.G. Faulkner and A.E. Peterson of the University of Alberta are also very much appreciated.

TABLE OF CONTENTS

1. INTRODUCTION	1
1.1 Foreword	1
1.2 Objectives and Scope	3
1.3 Organization of the Thesis	4
2. PREVIOUS STEEL PLATE SHEAR WALL RESEARCH	7
2.1 Introduction	7
2.2 Takahashi <i>et al.</i> (1973)	8
2.3 Mimura and Akiyama (1977)	10
2.4 Agelidis and Mansell (1980)	12
2.5 Thorburn <i>et al.</i> (1983)	13
2.6 Timler and Kulak (1983)	14
2.7 Tromposch and Kulak (1987)	15
2.8 Elgaaly and Caccese (1990)	17
2.9 Sabouri-Ghomi and Roberts (1991)	19
2.10 Xue and Lu (1994)	21
2.11 Other Related Research	23
3. PRELIMINARY FINITE ELEMENT MODEL	32
3.1 Introduction	32
3.2 Description of Model	32
3.2.1 Elements	32
3.2.2 Material Properties	34
3.2.3 Initial Conditions	35
3.2.4 Solution Strategy	35
3.3 Numerical Analysis of Timler and Kulak Specimen	36
3.3.1 Finite Element Model	36
3.3.2 Results of Analysis	39
3.4 Summary	39

4. EXPERIMENTAL PROGRAMME – GENERAL	49
4.1 Objectives	49
4.2 Specimen Details and Fabrication Procedures	50
4.3 Test Design Considerations and Constraints	52
4.4 Preliminary Numerical Analysis of Specimen	54
4.5 As-built Measurements	56
4.6 Summary	58
5. ANCILLARY TESTS.....	64
5.1 Introduction	64
5.2 Corner Detail Test	64
5.2.1 Introduction.....	64
5.2.2 Test Set-up and Procedures.....	65
5.2.3 Test Results	67
5.2.4 Conclusion	69
5.3 Residual Stress Measurements	69
5.3.1 Introduction.....	69
5.3.2 Standards and Procedures	69
5.3.3 Results.....	73
5.3.4 Summary	75
5.4 Tension Coupon Tests	75
5.4.1 Introduction.....	75
5.4.2 Standards and Procedures	75
5.4.3 Test Results.....	76
5.4.3.1 Infill Plates	76
5.4.3.2 Boundary Members.....	76
5.4.4 Summary	78

6. MULTI-STOREY STEEL PLATE SHEAR WALL TEST.....	89
6.1 Introduction	89
6.2 Test Set-up.....	89
6.3 Instrumentation and Data Acquisition	91
6.4 Load and Deflection History	92
6.5 Specimen Behaviour During Test.....	96
6.5.1 Gravity Load Application	96
6.5.2 Cycles Prior to Significant Yielding.....	96
6.5.3 Cycles Subsequent to Significant Yielding.....	97
6.5.4 Specimen Failure.....	99
7. DISCUSSION OF SHEAR WALL TEST RESULTS	108
7.1 Introduction	108
7.2 Hysteretic Behaviour	108
7.3 General Observations	113
7.4 Failure Mode	117
7.5 Force Modification Factor, R (NBCC 1995a).....	119
8. FINITE ELEMENT ANALYSIS OF TEST SPECIMEN	132
8.1 Introduction	132
8.2 Description of Model	132
8.2.1 Elements.....	132
8.2.2 Geometry.....	133
8.2.3 Connectivity and Bracing.....	134
8.2.4 Residual Stresses.....	134
8.2.5 Material Properties.....	136
8.2.6 Geometric Non-linearity	136
8.3 Results of Analyses.....	137
8.3.1 Monotonic Loading.....	137
8.3.2 Cyclic Loading.....	139
8.4 Summary.....	140

9. SIMPLIFIED ANALYSIS.....	152
9.1 Introduction	152
9.2 Strip Model.....	153
9.2.1 Analysis Method	153
9.2.2 Angle of Inclination of Tension Field.....	156
9.3 Comparison with Test Results.....	158
9.3.1 Introduction.....	158
9.3.2 Analyses and Results	158
9.4 Hysteresis Models.....	163
9.4.1 Hysteresis Model of Tromposch and Kulak (1987).....	163
9.4.2 Proposed Hysteresis Model.....	166
9.4.3 Comparison of Hysteresis Models.....	172
9.5 General Discussion	174
9.6 Summary.....	177
10. EVALUATION OF STRAIN DATA	194
10.1 Introduction	194
10.2 Beam and Column Strains	195
10.3 Panel 2 Strains.....	199
10.4 General Discussion	201
10.5 Summary.....	203
11. SUMMARY, CONCLUSIONS, and RECOMMENDATIONS	214
11.1 Summary.....	214
11.2 Conclusions and Recommendations.....	216
11.3 Recommendations for Future Research	219
REFERENCES	222

LIST OF TABLES

Table	Page
5.1 Infill Panel Tension Coupon Test Results.....	79
5.2 W310x118 Tension Coupon Test Results.....	80
5.3 W310x60 Tension Coupon Test Results.....	81
5.4 W530x82 Tension Coupon Test Results.....	82
10.1 Panel 2 Stress Data at Rosette Locations	205
10.2 Force Effects at Base of Panel 1	206

LIST OF FIGURES

Figure	Page
2.1 Idealized Deformed Panel (Mimura and Akiyama 1977)	27
2.2 Hysteresis Model (Mimura and Akiyama 1977)	27
2.3 Strip Model Representation of a Typical Storey (Thorburn <i>et al.</i> 1983)	28
2.4 Schematic Diagram of Test Specimen (Timler and Kulak 1983)	29
2.5 Schematic Diagram of Test Specimen (Tromposch and Kulak 1987)	30
2.6 Load vs. Deflection Curve (Tromposch and Kulak 1987)	31
3.1 Cross-section of the ABAQUS B32 Beam Element	41
3.2 Modified Riks Solution Strategy	42
3.3 Schematic Diagram of Test Specimen (Timler and Kulak 1983)	43
3.4 Timler and Kulak Specimen – Finite Element Model	43
3.5 Timler and Kulak Specimen – Infill Plate Material Model	44
3.6 Timler and Kulak Specimen – Initial Imperfections	45
3.7 Load vs. Elongation Response of Test Strips	46
3.8 Load vs. Panel Deflection of Timler and Kulak Specimen	47
3.9 Load vs. Panel Deflection – Sensitivity to Material Properties	48
4.1 Steel Plate Shear Wall Test Specimen (North Face)	59
4.2 Fish Plate Detail Used in Test Specimen	60
4.3 Finite Element Model of Test Specimen (Deflected Shape)	61
4.4 Predicted Storey Shear vs. Storey Deflection	62
4.5 Predicted Base Shear vs. Top Deflection	63
5.1 Corner Test Set-up – South Elevation	83
5.2 Corner Test Specimen (North Face)	84
5.3 Tears in Corner Region at Conclusion of Test (North Face)	85
5.4 W310x118 Residual Stress Distribution	86
5.5 W310x60 Residual Stress Distribution	87
5.6 W530x82 Residual Stress Distribution	88
6.1 Test Set-up – North Elevation	100
6.2 Test Set-up – West Elevation	100
6.3 Overview of Test Set-up	101
6.4 Four Storey Shear Wall Specimen	102
6.5 Data Acquisition Locations	103
6.6 Tears at Top West Corner of Panel 1	104
6.7 Tear in Panel 1 Initiated by Cyclic Kinking	104
6.8 West Column Local Distortion	105

6.9	Tears in Panel 1 at Conclusion of Test (North Face)	106
6.10	Fracture at Base of West Column.....	107
7.1	Storey Shear vs. Storey Deflection – Panel 1	125
7.2	Typical Loading Cycle – Panel 1	126
7.3	Base Shear vs. Top Deflection	127
7.4	Actual Energy Dissipation During Test	128
7.5	Adjusted Energy Dissipation During Test.....	129
7.6	Elastic and Inelastic Response of a Structural System.....	130
7.7	Envelope of Cyclic Test Curves.....	131
8.1	W310X118 Flange Residual Stresses.....	142
8.2	Comparison of Monotonic Finite Element Analysis with Test Results – Panel 1	143
8.3	Comparison of Monotonic Finite Element Analysis with Test Results – Panel 2	144
8.4	Comparison of Monotonic Finite Element Analysis with Test Results – Panel 3	145
8.5	Comparison of Monotonic Finite Element Analysis with Test Results – Panel 4	146
8.6	Comparison of Monotonic Finite Element Analysis with Test Results – Overall	147
8.7	Comparison of Initial Finite Element Curves with Test Results – Panel 1	148
8.8	Comparison of Initial Finite Element Curves with Test Results – Panel 2	148
8.9	Comparison of Initial Finite Element Curves with Test Results – Panel 3	149
8.10	Comparison of Initial Finite Element Curves with Test Results – Panel 4	149
8.11	Comparison of Initial Finite Element Curves with Test Results – Overall	150
8.12	Comparison of Finite Element Hysteresis Analysis with Test Results – Panel 1	151
9.1	Plane Frame Strip Model of Test Specimen.....	179
9.2	Comparison of Strip Model Analyses with Test Results – Panel 1.....	180
9.3	Comparison of Strip Model Analyses with Test Results – Panel 2.....	181
9.4	Comparison of Strip Model Analyses with Test Results – Panel 3.....	182
9.5	Comparison of Strip Model Analyses with Test Results – Panel 4.....	183
9.6	Comparison of Strip Model Analyses with Test Results – Overall	184
9.7	Sequence of Plastic Hinging and Strip Yielding	185
9.8	Effect of Number of Tension Strips in Strip Model – Panel 1	186

9.9	Hysteresis Model (Tromposch and Kulak 1987).....	187
9.10	Comparison of Hysteresis Models with Test Results – Panel 1 / Cycle 15	188
9.11	Comparison of Hysteresis Models with Test Results – Panel 1 / Cycle 18	189
9.12	Comparison of Hysteresis Models with Test Results – Panel 1 / Cycle 21	190
9.13	Storey Shear vs. Storey Deflection Behaviour of Shear Wall Components....	191
9.14	Proposed Hysteresis Model.....	192
9.15	Panel Thickness Ratio vs. Angle of Inclination of Tension Field.....	193
10.1	Bending Moment Diagrams – Storey 1 / East Column.....	207
10.2	Bending Moment Diagrams – Storey 1 / West Column.....	207
10.3	Bending Moment Diagrams – Storey 2 / East Column.....	208
10.4	Bending Moment Diagrams – Storey 2 / West Column.....	208
10.5	Bending Moment Diagrams – Level 1 Beam.....	209
10.6	Bending Moment Diagrams – Level 2 Beam.....	209
10.7	Axial Force Diagrams – Storey 1 / East Column.....	210
10.8	Axial Force Diagrams – Storey 1 / West Column.....	210
10.9	Axial Force Diagrams – Storey 2 / East Column.....	211
10.10	Axial Force Diagrams – Storey 2 / West Column.....	211
10.11	Axial Force Diagrams – Level 1 Beam.....	212
10.12	Axial Force Diagrams – Level 2 Beam.....	212
10.13	Panel 1 Stress Distribution – Finite Element Model.....	213

LIST OF SYMBOLS

- A_b = cross-sectional area of beam
- A_c = cross-sectional area of column
- C = applied axial compressive force
- C_y = plastic axial compressive capacity
- E = error of the mean of a sample from the population mean;
modulus of elasticity
- G = elastic shear modulus
- h_s = storey height
- I_c = moment of inertia of column
- K = steel plate shear wall stiffness
- $[K]$ = structure stiffness matrix
- K_f = moment-resisting frame stiffness
- $[K_G]$ = structure geometric stiffness matrix
- K_p = infill panel stiffness
- L = width of shear wall panel
length of column
- M = applied bending moment
- M_p = plastic moment capacity
- n = sample size
- r = correlation coefficient
- R = force modification factor (NBCC 1995a)

- $\{R\}$ = load vector
- s = estimate of the standard deviation of a population
- s_x^- = estimate of the standard deviation of the mean
- t = number of standard deviations of the mean from the population mean
- t = infill plate thickness
- t_e = effective infill plate thickness
- U = design base shear calibration factor (NBCC 1995a)
- U_σ = strain energy of a panel in pure diagonal tension
- U_τ = strain energy of a panel in pure shear
- V = storey shear;
design base shear (NBCC 1995a)
- V_e = elastic base shear (NBCC 1995a)
- V_{\max} = base shear capacity of a structural system
- \bar{x} = sample mean
- $\{X\}$ = nodal displacement vector
- α = angle of inclination of the tension field from the vertical
- δ = deflection
- δ_v = elastic deflection under a base shear V
- δ_{V_e} = elastic deflection under a base shear V_e
- δ_{\max} = maximum deflection where a base shear of V_{\max} can be maintained
- δ_{NBC} = estimated maximum inelastic deflection (NBCC 1995a)
- δ_y = deflection at the point of significant yielding

Δ_{uf} = deflection recovery for moment-resisting frame to completely unload

Δ_{up} = deflection recovery for infill panel to completely unload

Δ_{yf} = deflection at yield point of moment-resisting frame

Δ_{yp} = deflection at yield point of infill panel

μ = population mean

σ = standard deviation of a population;
normal stress

σ_1 = major principal stress

σ_2 = minor principal stress

$\sigma_{\bar{x}}$ = standard deviation of the mean

σ_y = yield stress

τ_{max} = maximum shear stress

τ_{xy} = in-plane shear stress

1. INTRODUCTION

1.1 Foreword

Steel plate shear walls are an innovative lateral load-resisting system capable of effectively and economically bracing a building against both wind and earthquake forces. This type of shear wall consists of vertical steel plates—referred to as *infill plates*—one storey high and one bay wide connected to the surrounding beams and columns. The surrounding steel frame may use either simple or moment-resisting beam-to-column connections. The plates can be installed in one or more bays for the full height of a building to form a stiff cantilever wall. The panels themselves can be either stiffened or unstiffened, depending on the design philosophy. Steel plate shear walls are well-suited for new construction and they also provide a relatively simple means for the seismic upgrading of existing steel and concrete structures.

Steel plate shear walls possess properties that are fundamentally beneficial in resisting seismically-induced loads. These include superior ductility, a robust resistance to degradation under cyclic loading, high initial stiffness, and, when moment-resisting beam-to-column connections are present, inherent redundancy and a capacity for significant energy dissipation. Moreover, the low mass of a steel plate shear wall—as compared with an equivalent reinforced concrete shear wall—reduces both the gravity loads and the seismic loads transmitted to the foundation. This can lead to considerable cost savings in construction.

In a steel framed building, the use of a steel system for resisting lateral loads can lead to significant cost savings as compared to systems that use a steel frame in conjunction with a concrete shear core, as is often the practice in Canada. This is because the number of trades required on the site is reduced. Considerable construction scheduling advantages should also be realized, especially for mid- to high-rise structures. Other economical advantages of steel plate shear walls arise from

their relative simplicity and repetition during fabrication. In order to reduce the amount of relatively costly field fabrication, steel shear walls can be prefabricated in the shop in two or three storey tiers and then assembled on-site.

Most existing steel plate shear wall buildings were designed with shear panels that are stiffened in an attempt to preclude out-of-plane buckling. Although it has been shown that stiffening the panel heavily can produce a significant increase in the amount of energy dissipated under cyclic loading (Takahashi *et al.* 1973), the cost involved is likely to be prohibitive in most markets. Wagner (1931), however, demonstrated that buckling does not necessarily represent the limit of useful behaviour and that the post-buckling strength of an unstiffened shear panel can be considerable. At the point of buckling, the load-resisting mechanism changes from in-plane shear to an inclined tension field that develops along the elongated diagonal. When the panel is thin, buckling will occur at very low loads and the resistance of the panel is dominated by tension field action. The consideration of the post-buckling strength of plates has been accepted in the design of plate girder webs for many years, based largely on the work of Basler (1961).

The Canadian steel design standard, CAN/CSA-S16.1-94 (CSA 1994), includes an appendix that outlines design requirements for steel plate shear walls. These requirements are based on the unstiffened thin-panel concept that relies on post-buckling strength. The methodology is derived primarily from an analytical model developed by Thorburn *et al.* (1983), which has been substantiated by physical tests conducted on single storey shear wall panels employing either true pins (Timler and Kulak 1983) or standard bolted shear-type connections (Tromposch and Kulak 1987) at the beam-to-column joints. Because no large-scale multi-storey test had been conducted on shear walls with thin, unstiffened panels, extrapolation to multi-storey applications has had to be based on computer analysis and engineering judgement. The research described herein includes a large-scale four storey cyclic steel plate shear wall test. This test has provided important additional evidence supporting the

suitability of unstiffened thin-panel steel shear walls for seismic applications. To maximize the ability of the shear wall to dissipate energy under seismic loading, moment-resisting beam-to-column connections were used in the test specimen.

1.2 Objectives and Scope

The primary objective of this research was to study the behaviour of steel plate shear walls when subjected to extreme cyclic loading, such as would be expected in a severe earthquake. To examine this behaviour, the first-ever test was conducted of a large-scale multi-storey steel plate shear wall with thin, unstiffened panels. The test specimen was intended to simulate as closely as practicable a steel shear wall as it would be constructed in practice. No special or unusual fabrication techniques were employed. The test was conducted according to established methods for applying simulated earthquake loading and gravity loads were applied to the columns throughout the test.

There were two general objectives in conducting the test. One was to evaluate the performance of the details used in the test specimen. The other objective was to evaluate the overall performance of the shear wall, particularly in the context of the “force modification factor,” as defined in the National Building Code of Canada (NBCC 1995a). This allows a measure of comparison of inelastic seismic performance between the steel plate shear wall and other systems. Factors analogous to the force reduction factor are used in design codes of other countries, and so similar evaluations of the performance of the test specimen can be made.

Other objectives of the test were to assess how the storey shear forces were shared between the panels and the moment-resisting frame and to conduct a detailed evaluation of the strains at various locations in the frame and at different load levels. The ability of the shear wall to dissipate energy during inelastic cyclic loading, and the contribution of the moment-resisting frame thereto, was also of primary interest.

Another objective of this research was to develop in parallel with the experimental work an analytical tool for predicting the behaviour of steel plate shear walls subjected to lateral loading up to the ultimate capacity. A detailed non-linear finite element analysis, verified by the test results, was selected to achieve this objective.

A simplified method of analysis was considered to be important for use by structural designers. Therefore, a further objective was to assess the ability of the strip model (Thorburn *et al.* 1983) to predict the observed behaviour of the four storey test specimen. Furthermore, a simple method of predicting hysteretic behaviour was to be identified. Again, the test results provide the means of verifying the validity of the models.

Finally, a comprehensive review of the existing published body of research on steel plate shear wall behaviour was needed. A summary of this review is presented herein.

1.3 Organization of the Thesis

As an overview of the thesis structure, this section provides a description of the manner in which the remainder of the manuscript is organized.

Chapter 2 provides a chronological review of the previously published research on steel plate shear wall behaviour. Summaries of both analytical and experimental investigations are presented.

Chapter 3 describes the finite element model that was developed to predict the behaviour of the multi-storey shear wall specimen to be tested subsequently. As a means of verifying the model, it was first used to simulate the test of Timler and Kulak (1983) and a comparison of the test and analytical results is made.

In Chapter 4, an overview of the experimental programme is provided. The objectives of the test, a description of the specimen details, and the test design considerations are described. A summary of the preliminary numerical analysis of the test specimen is also presented.

Chapter 5 presents the ancillary tests that were conducted as a part of the experimental programme. A large-scale cyclic test on a corner of a steel plate shear wall panel is described. Investigations into the material behaviour and the initial residual stress distributions in the main test specimen are also presented.

The four storey cyclic test is described in Chapter 6. Both the test set-up and the manner in which the test was conducted are discussed. Observations made during the test about the behaviour of the specimen and its components are also described.

In Chapter 7, the results of the four storey test are discussed. The stages of the hysteretic response are described and an evaluation of the performance of the test specimen is made.

A discussion of the finite element model incorporating the as-built dimensions and measured material properties is presented in Chapter 8. Monotonic and cyclic analyses are described and the results of the numerical analyses are compared with the test results.

Chapter 9 describes a simplified method of analysing steel plate shear walls. A model for determining monotonic behaviour and two methods for predicting hysteresis behaviour are presented. The model predictions are compared with the experimental findings.

The strain data are evaluated in Chapter 10, where measured strains are compared with those predicted by the finite element and simplified models.

Chapter 11 provides a summary of the research and a discussion of the conclusions drawn therefrom. Areas of further research required are also identified.

2. PREVIOUS STEEL PLATE SHEAR WALL RESEARCH

2.1 Introduction

Research on steel plate shear walls began in the early 1970s. Although the body of research that has accumulated since that time clearly shows that steel shear walls provide an effective and economical way of resisting wind and earthquake loads, relatively few buildings have been constructed using this form of lateral load-resisting system. There are perhaps two reasons for this. First, much of the early research was conducted in Japan and published only in Japanese, limiting its accessibility to engineers in other parts of the world. Second, consensus on some aspects regarding design, analysis, and detailing concepts has not yet been achieved.

The majority of steel plate shear wall buildings constructed to date are in Japan and the United States and they take a variety of forms. Heavily stiffened thin-panel shear walls have been favoured historically in Japan, whereas unstiffened or moderately stiffened thick-panel shear walls have dominated in the United States. However, as the international interaction of researchers in this area increases, this distinction is rapidly becoming less clear cut. Thorburn *et al.* (1983) present a survey of existing steel plate shear wall buildings, with a brief discussion of the characteristics of each. Since that report was published, several other steel shear wall buildings have been reported in the literature, notably, the five storey Veterans' Administration Medical Center in Charleston, South Carolina (Baldelli 1983) and an eight storey office block in Benoni, South Africa (Anon. 1989). The former is an example of the seismic upgrading of a reinforced concrete building using steel plate shear walls. The shear walls were connected to the existing structure with drilled-in anchors and were stiffened using channel sections. The South African building is thought to be the first major implementation of unstiffened thin-panel shear walls that

rely primarily on the post-buckling behaviour of the shear panels in resisting lateral loads.

Research has been conducted on steel plate shear walls having a multiplicity of forms. However, steel shear walls can be broken down conceptually into two types: those in which the plate is prevented from buckling under the design loads and those that rely on the post-buckling strength of the panels. Research on both of these types is ongoing. A chronological review of previous steel plate shear wall research is presented here.

2.2 Takahashi *et al.* (1973)

The first extensive research programme on the behaviour of steel plate shear wall panels was conducted by Takahashi *et al.* (1973) in Japan. The objective was to study various configurations of stiffened shear panels subjected to inelastic cyclic loading in order to determine their suitability for use as a lateral load-resisting system for buildings.

The experimental programme was carried out in two parts. The first phase consisted of cyclic tests on 12 panels with varying plate thicknesses (2.3 mm to 4.5 mm) and stiffener arrangements. The stiffeners were cut in various widths from flat plate and welded to the panels on one or both sides. One of the 12 panels was a control specimen with no stiffeners installed. All of the test panels were 900 mm in height and 1200 mm in length. Each panel was bounded by a very stiff rectangular pin-jointed frame and connected thereto with high-strength bolts. From four to six complete cycles of shear loading were applied with increasing deformations in each cycle.

The researchers demonstrated that the stiffened panels dissipated significantly more energy than did the unstiffened panel, although both types generally behaved in a stable and ductile manner. The panels with stiffeners on both sides tended to show

more stable behaviour than those with single sided stiffeners. Based on the results of these tests, Takahashi *et al.* (1973) recommended that stiffened steel plate shear walls be designed so that the shear panel does not buckle elastically. Furthermore, it was recommended that should inelastic buckling occur, it be limited to local buckling between the stiffening elements, that is, overall buckling of the stiffened panel should not occur. Guidance was provided as to how to achieve this. Although the benefit of increased energy dissipation resulting from stiffening the shear panels was demonstrated, no evaluation of the additional cost involved was made. The additional fabrication costs encountered with heavily stiffened steel plate shear walls could preclude their use in North America.

The second phase of the experimental programme consisted of two full-scale tests of a section of a stiffened shear wall taken from the design of a 32 storey building. The design was carried out using the principles established from the results of the first series of tests. The two test specimens were one bay wide and two storeys high, one with stiffened door openings and one without. In order to produce similar shear stiffness and strength, the panels without openings were 4.5 mm thick and the panels with openings were 6 mm thick.

Horizontal in-plane loads were applied at the tops of the test specimens. The specimens were loaded and unloaded in one direction, with a few fully reversed loading cycles interspersed. Both specimens showed good ductility and energy dissipation characteristics.

The full-scale test specimens were modelled using the finite element method. Elasto-plastic material behaviour was assumed, together with the von Mises yield criterion. Fully planar behaviour was assumed so that plate buckling did not need to be taken into account. The finite element analyses used monotonic loading, but good agreement was achieved with the envelope of the experimental load vs. deflection curves.

Based on the results of the second series of tests, Takahashi *et al.* (1973) concluded that the principles upon which the design was based (established from the first series) were adequate and that the equations presented for the stiffener spacing and stiffness, formulated to prevent plate buckling, could be used for design. Furthermore, they concluded that the stiffness and strength of the panel could be calculated using conventional shear theory.

2.3 Mimura and Akiyama (1977)

Mimura and Akiyama (1977) developed a method for predicting the monotonic and hysteretic behaviour of unstiffened steel plate shear walls with plates that buckle prior to reaching the shear yield load. The method described for monotonic loading considers the contributions of the panel and the surrounding frame separately. The shear buckling load of the plate is calculated assuming a pinned boundary and using classical elastic plate buckling theory. At loads greater than the elastic plate buckling load, the panel shear is assumed to be resisted by a diagonal tension field, as described by Wagner (1931). Assuming pure diagonal tension, inclined at an angle in accordance with the derivation provided by Wagner, the panel yield and ultimate shear strength can be determined. The contribution of the moment-resisting frame to the shear wall behaviour is determined by an elasto-plastic frame analysis. The overall monotonic load vs. deflection behaviour is taken as the sum of the contributions from the panel and the frame.

The hysteresis model proposed by Mimura and Akiyama (1977) is based on the monotonic curve described above and a number of assumptions regarding hysteretic response. Because the model accounts for inelastic stretching of the panel along the diagonal, slack in the panel is present upon reversal of the load. In order to define the displacement required to redevelop the tension field after a load reversal, a simplified representation of the shear panel is assumed. Figure 2.1 shows a single buckled panel deformed inelastically by a load Q , to a deflection δ . The tension field

is assumed to have an angle of inclination of 45° . The elastic portion of the deformation is considered to be negligible and the deflection, δ , results in an applied diagonal tensile strain equal to ϵ_a . Furthermore, it is assumed that the inelastic Poisson's ratio is 0.5 and that no significant force develops in the compression diagonal. This results in a plastic shortening strain perpendicular to the tensile strain of $0.5\epsilon_a$. Therefore, upon reversal of the loading, the panel does not have to return to its original position for the new diagonal tension field to develop. In fact, the tension field begins to carry load when the deflection of the panel is reduced to 0.5δ .

The hysteresis model developed by Mimura and Akiyama (1977) is shown in Fig. 2.2. The line O-A-H is the idealized load vs. deflection behaviour of the steel plate shear wall panel subjected to monotonic loading. The panel is loaded initially up to the yield level at point A. Thereafter, the panel behaves inelastically up to an arbitrary deflection at point B. If the load is then removed, the panel unloads elastically to point C'. As the panel is then loaded in the opposite (negative) direction, the elastic curve is followed to point C, where the infill plate reaches its elastic shear buckling capacity. At this point, the storey shear that was carried by shear stresses in the unbuckled plate must be resisted by tension field action and the frame deflects until this tension field force is developed at point D. Because the model assumes that the boundary frame has zero stiffness after the panel buckles, the line C-D is horizontal. If the panel were then unloaded along line D-D', parallel to the elastic curve O-A, the residual deflection O-D' would be equal to 0.5 times the deflection O-C' because of the shortening of the diagonal due to the Poisson effect during the inelastic deformation A-B. If, instead, the loading in the negative direction *increases* from point D, an empirical linear path D-A' is assumed where the deflection at point A' is equal and opposite to that of point A. Further loading follows the inelastic path A-E, parallel to line A-B. At an arbitrary deflection at point E, the panel is unloaded elastically to point F'.

The elastic curve is followed as loading commences again in the positive direction to the plate buckling load at point F. The panel then deflects with zero stiffness to point G, where the tension field resists the current storey shear. The curve from point G to the point where unloading occurred in the previous cycle (point B) is assumed to be linear. Any further inelastic loading in the same direction follows the path B-H. Subsequent cycles can be derived in a similar manner. This hysteresis model forms the basis of a proposed new model presented in Section 9.4.2.

In order to provide evidence to support their theoretical model, Mimura and Akiyama (1977) tested a series of small scale, simply supported stiffened plate girder specimens subjected to a single cyclic point load at midspan. The panel aspect ratio, the web thickness, the number of panels per girder (from two to eight), and the flange and stiffener member sizes were varied. Steel angles were used for both the flanges and the stiffeners. Generally, only two cycles of loading were applied, although they demonstrated reasonable agreement with the predictive model. Because of the small number of load cycles, no conclusions about the resistance of the panels to degradation under cyclic loading can be drawn.

2.4 Agelidis and Mansell (1980)

An innovative form of steel shear wall built-up from prefabricated stiffened plate components was described by Agelidis and Mansell (1980). The system consists of relatively thin steel panels stiffened by either angle, flat plate, or trapezoidal “trough” stiffeners oriented in the vertical direction only. The prefabricated panels are assembled to form a central building service core that has no integral heavy columns to carry gravity loads. Rather, the continuous stiffened panels resist all tributary vertical loads plus the horizontal loads. In order to stiffen the system without obscuring the corridor space within the service core, individual shear walls are coupled by built-up beams.

A 20 storey building with a steel service core utilizing this concept was analysed both manually and also using a finite element computer program. For the latter, they used plane stress plate elements with orthotropic properties to achieve a linear, planar analysis with the stiffeners “smeared” throughout the panels. Combinations of dead, live, and wind loads were considered for both strength and drift. The elements of the service core were designed to an extent sufficient to perform a comprehensive cost analysis. Costs were determined for panels having ten different stiffener types and arrangements. Details of the analyses and design, and the results therefrom, are presented in Agelidis and Mansell (1982). No physical tests to substantiate the analytical methods have been reported.

2.5 Thorburn *et al.* (1983)

Thorburn *et al.* (1983) recognized that steel plate shear walls with thin panels buckle at very low in-plane shear loads but can resist considerable loads through post-buckling behaviour. A model was developed based on the theory of pure diagonal tension by Wagner (1931). The so-called strip model assumes that the resistance of the panel prior to buckling is negligible and that the dominant action in resisting storey shear is the diagonal tension field. The panel is modelled as a series of discrete pin-ended diagonal tension strips representing the tension field. The strips are oriented so as to lie parallel to the tension field in the panel. The discretization of the panel into a series of tension strips implies that the compressive stresses perpendicular to the strips are negligible. The strips are assigned an area equal to the plate thickness multiplied by the width of the strips. If a typical panel (neither the top nor the bottom panel) is isolated from the remainder of the structure, as shown in Fig. 2.3, the strip model assumes that the bounding beams are infinitely stiff. This reflects the presence of opposing tension fields above and below the modelled panel. At the top and the bottom of the shear wall, the actual stiffnesses of the bounding members are used. In all cases, the columns are assigned their actual stiffness.

Figure 2.3 shows beams with simple connections, but other end conditions can also be modelled.

In carrying out an ultimate strength analysis, strips are removed from the model as they reach the yield stress and are then replaced by their equivalent reactive forces at each end. This procedure implies elasto-plastic material behaviour. Alternatively, a non-linear analysis program can account for the yielding of the strip automatically. Plastic hinging of the surrounding frame members is also taken into account. A discussion of the strip model analysis procedure is given in Section 9.2.

Thorburn *et al.* (1983) also studied the use of a single equivalent diagonal brace for simplifying the analysis of multi-storey shear walls. The area of the brace is such that the stiffness of the panel is equivalent to that derived from the strip model. Given that column and beam sizes and infill plate thicknesses will be changed only at intervals in the height of a building, this procedure allows the designer to analyse only a few storeys of a multi-storey building using the somewhat more complex strip model. A multi-storey model using equivalent diagonal braces can then be assembled. Each storey brace is assigned an area that was derived for a panel having the same or similar properties.

The researchers conducted a parametric study to assess the effect on the panel stiffness and strength of the plate thickness, the panel height, the panel width, and the column stiffness. The parameters studied were found to be closely interrelated and their interaction complex. However, it was proposed that design aid curves could be developed.

2.6 Timler and Kulak (1983)

Timler and Kulak (1983) tested a pair of single storey steel plate shear walls in order to verify the analytical technique established by Thorburn *et al.* (1983). The test specimen, shown in Fig. 2.4, consisted of vertically oriented beams and horizontally

oriented columns, connected by pinned joints at the four extreme corners. The member sizes were chosen so as to be representative of typical building construction. By testing the two shear walls together, as illustrated in the figure, the need for an external loading frame was eliminated. The test specimen is discussed further in Section 3.3.

The specimen was loaded statically, with three complete cycles of loading to a service load deflection limit of $h_s / 400$, or 6.25 mm. During these cycles, the test specimen behaved elastically. Subsequently, the shear wall was loaded to its ultimate capacity in one direction with a maximum applied load of 5395 kN. Axial loads were not applied to the columns.

Strains were measured at five boundary member cross-sections, with six strain gauges at each cross-section. Extensive strain measurements were taken on the infill panels using strain rosettes. A displacement transducer mounted on a track continually measured the profile of the buckled panel during the test.

The test specimen was analysed using the strip model technique. In general, the analysis provided a good prediction of the panel and member strains and the deflection behaviour of the test specimen. The infill plate material used in the specimen, which showed a continuously curved stress vs. strain relation characteristic of cold-worked steel, was approximated in the analysis by a bilinear curve (linearly elastic – perfectly plastic). If material with the classical hot-rolled behaviour had been used, the model likely would have underestimated the elastic stiffness of the shear wall, as is discussed in Section 9.5.

2.7 Tromposch and Kulak (1987)

Tromposch and Kulak (1987) tested a two-panel shear wall similar to the one tested by Timler and Kulak (1983). The test specimen, illustrated in Fig. 2.5, also represented two single storey steel plate shear walls. Important modifications from the

Timler and Kulak specimen include the use of typical bolted shear connections in the frame, the use of a thinner infill panel, and the use of very stiff vertical beam members. The stiff beams were intended to provide anchorage to the infill panel similar to that which would occur in a multi-storey condition with panels above and below. The column size (horizontal members in Fig. 2.5) was selected to be representative of typical building construction.

Prior to the application of lateral loading to the specimen, the columns were preloaded using two full length prestressing bars in each column, as shown in Fig. 2.5. These loads represented the gravity loads present in a building that act concurrently with the lateral loads. Fully reversed cyclic lateral loads were then applied. They were of gradually increasing magnitude and reached a maximum of 67% of the ultimate load obtained subsequently, which corresponded to a maximum deflection of $h_s / 129$, or 17 mm. This sequence comprised 28 load cycles. Beyond this load level, the testing machine was only capable of loading in one direction and the final test phase consisted of monotonic loading to the ultimate capacity of the specimen. The column prestressing rods were removed prior to this final loading in order to eliminate the possibility of restraint to the specimen occurring at large deformations.

The response of the test specimen during the cyclic loading phase, shown in Fig. 2.6, indicates very ductile behaviour, but the hysteresis curves are severely pinched because of the very thin infill plate and the flexible boundary frame. The ductility of the specimen was demonstrated even more convincingly during the final monotonic loading excursion up to a maximum deflection of $h_s / 31$, or 71 mm. However, the cyclic behaviour at this extreme deformation was not investigated.

The envelope of cyclic response curves in the two different loading directions were compared with the results of a series of strip model analyses. Tromposch and Kulak (1987) demonstrated that good agreement between the test results and the

analysis could be achieved. This was obtained by considering the frame connections to be fixed at low loads and pinned after slip had occurred and by including an estimate of the welding residual stresses in the infill panel.

In order to represent the hysteretic behaviour analytically, Tromposch and Kulak (1987) proposed a method based on the model described by Mimura and Akiyama (1977). Two modifications to represent specifically the behaviour of the shear wall specimen they tested were suggested. First, the strength prior to buckling for a very thin infill plate is neglected. Second, the stiffness of the shear wall is taken to be equal to the elastic stiffness of the boundary frame during the deflection required to develop the tension field. Should the deflections become large enough for the frame to form a mechanism, the subsequent stiffness becomes zero. Effectively, these modifications mean that the line C'-C in Fig. 2.2 has zero length and the line C-D has a shape that reflects elasto-plastic moment-resisting frame behaviour. The revised model is described in Section 9.4.1. Although the model can be used to predict the behaviour of steel plate shear walls with moment-resisting beam-to-column connections, no such tests were performed.

2.8 Elgaaly and Caccese (1990)

An experimental programme conducted by Elgaaly and Caccese (1990) investigated the behaviour of ten one-quarter scale steel plate shear wall models subjected to cyclic loading. Six of the tests were described in the paper. These tests, and the associated analytical study, are described in further detail in the companion papers Caccese *et al.* (1993) and Elgaaly *et al.* (1993). The test specimens were three storeys high and one bay wide. Parameters that were varied were the panel thickness and the beam-to-column connection (fixed or shear-type). Panel thicknesses ranged from 0.76 mm to 2.66 mm.

The test specimens were loaded with a single in-plane horizontal load at the top of the shear wall. Each specimen was loaded cyclically with gradually increasing deflections up to a maximum of 51 mm (2% drift) measured at the top of the shear wall. The peak deflection was increased in 6 mm increments, with three cycles applied at each deflection level. The complete loading series consisted of 24 fully reversed cycles and each specimen was subjected to two of these loading series. After the second series was completed, the specimens were loaded monotonically to failure.

Two analytical models were considered in the study. The first was a finite element model with beam elements representing the frame and a 6x6 mesh of shell elements representing each infill plate. In the second, the shell elements were replaced by a perpendicular grid of truss elements oriented in the directions of the principal tensile and compressive stresses. Each model was subjected to monotonic loading.

In the truss model, elasto-plastic material behaviour in the diagonals was assumed, with a yield stress of 248 MPa. Three possible buckling stresses were considered for the compression members. In the end, the truss members in compression were considered to buckle at the onset of applied loading, making the truss model analogous to the strip model proposed by Thorburn *et al.* (1983).

The finite element model that used shell elements to represent the infill plate greatly overestimated both the stiffness and the ultimate strength of the test specimens. The mesh was considered to be too coarse to represent accurately the large number of buckle wavelengths that were observed in the panels during the tests. Because of the severe demands on computing resources that an adequately refined mesh would pose, this model was abandoned.

The truss model was able to predict the ultimate strength of the test specimens, but overestimated the stiffness by a considerable margin. The material model was then modified to include an empirically derived bilinearly elastic –

perfectly plastic stress vs. strain relation in order to fit the test data well. An empirical method was also described for predicting the hysteretic behaviour of steel plate shear walls. The parameters used for defining this behaviour were established from their test results.

Two of the most significant conclusions from this research are summarized here. First, based on their test results, the authors concluded that there is no significant difference in behaviour between shear walls with moment-resisting beam-to-column connections and those with simple connections. Second, they concluded that panels have an optimum plate thickness that, if exceeded, produces no increase in strength and that the wall fails by either column yielding or buckling.

The first conclusion was addressed by Kulak *et al.* (1994), who pointed out that differences in plate thicknesses and material properties among the specimens, plus the effect of a failed weld that was reported in one of the specimens, prevent a direct comparison with regard to the effect of the connection type. Furthermore, Tromposch and Kulak (1987) showed through an analytical study that using moment-resisting beam-to-column connections results in a significant increase in energy dissipation. The effect of the connection type on energy dissipation is discussed further in Section 7.2.

Kennedy *et al.* (1994) have asserted that the second conclusion should not be considered to be general. Rather, the columns can be designed to resist the loads imparted to them from the other components of the structure, preventing premature failure.

2.9 Sabouri-Ghomi and Roberts (1991)

A general method of dynamic analysis of thin-panel steel plate shear walls was developed by Sabouri-Ghomi and Roberts (1991). The method uses a time stepping finite difference technique to solve the governing differential equation of

motion. The structure is idealized as a vertical cantilever beam that has masses lumped at each floor level. The time-dependent loading is also assumed to act discretely at each floor. Initially, the governing equation was formulated assuming that the floor beams and associated slab remain horizontal. Therefore, the bending deformations within each panel were considered to be negligible and only shear deformations were included in the model. A more general method was presented subsequently (Sabouri-Ghomi and Roberts 1992) that includes the consideration of both shear and flexural behaviour of the shear wall.

In order to include non-linear material behaviour in the proposed analytical method, an approximate elasto-plastic hysteresis model was proposed that included the influence of shear buckling and yielding of the web plate and surrounding frame. The model was developed from a series of quasi-static cyclic loading tests on small scale models. These tests (Roberts and Sabouri-Ghomi 1991) were conducted on single panel unstiffened plates with a stiff, pin-ended boundary frame. The panels were either 300 mm x 300 mm or 300 mm x 450 mm in size and had thicknesses ranging from 0.54 mm to 1.23 mm. The thinnest panels were aluminium alloy and the remainder steel. The material properties reported were the initial modulus of elasticity and the 2% offset yield stress. However, the overall stress vs. strain relation was not described. The panel was loaded at two opposite corners in the direction of the panel diagonal. Initially, a tensile load was applied until significant inelastic behaviour was evident. This was followed by a similar compressive load. A total of at least four complete cycles of loading with gradually increasing peak displacements were applied to each specimen in this manner. All panels exhibited stable, ductile behaviour and the amount of energy dissipated increased with the increasing peak displacements in each cycle.

The researchers demonstrated the proposed non-linear analytical technique by presenting the results of three analyses. Solutions were obtained for the dynamic response of a five storey single bay steel shear wall subjected to periodic loading. In

two of the analyses, equal pulse loads were applied to each storey. In the first case, the response was elastic, whereas in the second, the pulse loads were increased to elicit an inelastic response. In the latter case, the analysis showed that the inelastic behaviour in the first storey tended to induce the higher modes of vibration. The final case presented was for a sinusoidal ground motion input that was chosen to be approximately equal to the fundamental frequency of the shear wall. This analysis demonstrated that, although the frequency of the forcing function was similar to that of the shear wall in its elastic state, the onset of plastic behaviour inhibited resonance and resulted in a reduction in the amplitude of vibration.

2.10 Xue and Lu (1994)

Xue and Lu (1994a) carried out an analytical study on four thin-panel steel plate shear wall configurations. In each case, a 12 storey three bay frame with moment-resisting beam-to-column connections in the exterior bays and with steel infill plates in the interior bay was used. Frames with either moment-resisting or simple beam-to-column connections in the interior bay were studied and infill plates were connected either on all four sides or only to the beams (with no connection to the columns), resulting in a total of four combinations. For comparison, a frame with all moment-resisting connections and with an infill plate fully connected and prevented from buckling was analysed as an upper bound case. A frame with simple beam-to-column connections in the interior bay and no infill panel was analysed as a lower bound case. The lowest storey was 4572 mm high and the remainder were 3658 mm high. The exterior bays were 9144 mm wide and the interior bay was 3658 mm wide. The infill panels varied from a thickness of 2.8 mm at the bottom of the shear wall to 2.2 mm at the top.

The six frame-wall structures described above were modelled using the finite element method. The beams and columns were modelled using elastic beam elements

and the panels were modelled using elasto-plastic shell elements. An initial out-of-flatness was specified for the panels based on several shear buckling modes.

The structures were loaded monotonically with lateral forces at each floor level. Gravity loads were not applied.

From the analyses it was concluded that the type of beam-to-column connection used in the bay with infill panels had only a small effect on the lateral stiffness of the entire frame. It was also observed that the two structures with infill plates connected to both the beams and the columns had a stiffness almost as high as the upper bound case and that the two structures with infill plates connected only to the beams had a stiffness much higher than the lower bound case. Despite the somewhat higher stiffness with the infill plates connected to both the beams and the columns, a number of factors led to the conclusion that the system with the infill panels connected only to the beams was superior. The main factor that led to this conclusion is that the analysis predicted that the columns of the stiffer system carry a proportionately larger share of the storey shears which could, in turn, lead to early failure of the columns. The analyses also showed that, in the system with the panels connected only to the beams, the panels resisted a significant proportion of the storey shears at lower load levels. This behaviour was attributed to the fact that in-plane flexural loading of the plate, causing compressive stresses that reduce the shear buckling strength, was largely avoided. Thus, the panels were considered to be more effectively utilized.

Xue and Lu (1994b) also studied the effect of the width/thickness ratio of the panel and the panel aspect ratio on the load vs. deflection behaviour of a single storey, single bay steel plate shear wall with pinned beam-to-column connections and with the infill panel connected only to the beams. The single panel represented one storey from the interior bay of the multi-storey, multi-bay concept, as described above (Xue and Lu 1994a). Moment-resisting beam-to-column connections would be present in

the adjacent bays without infill panels. In each of 20 cases, an ultimate strength analysis was conducted using the finite element model. The researchers found that when the load and the deflection are non-dimensionalized using the panel shear yield load and the panel shear yield deflection, respectively, certain observations can be made. Significantly, they observed that the influence of the width/thickness ratio on the response was small. From the results of the 20 cases studied, simplified empirical equations were presented to predict load vs. deflection response.

A brief discussion of a cyclic finite element analysis was also presented. A single panel of the 12 storey three bay structure described by Xue and Lu (1994a) was analysed. Six cycles of gradually increasing deflections were applied up to a maximum storey drift of about $h_s / 60$. The non-dimensionalized load vs. deflection response was presented and significant energy dissipation was observed.

The innovative approach to steel plate shear wall design of Xue and Lu (1994a) represents a significant departure from the more traditional single bay configuration with the panels fully connected to both the beams and the columns. Therefore, a comparative study is desirable to assess their relative merits. Issues such as the ability of the shear wall to dissipate energy, the failure mode, and relative construction costs should be addressed. Clearly, with shear panels and moment-resisting connections, both configurations have the benefit of providing an inherently redundant lateral load-resisting system.

2.11 Other Related Research

In addition to the research programmes described in the previous sections, several other investigations have taken place on closely related topics. Seven tests were performed (Aoyama and Yamamoto 1984; Yamamoto and Aoyama 1985) to study methods of strengthening reinforced concrete frames with stiffened thin-panel steel infill plates. Each test specimen was a one-third scale single storey, single bay

frame. The infill plates were connected to the surrounding frame using a combination of headed studs and drilled resin anchors. The main parameters that were varied were the concrete frame reinforcement, the anchor spacing and the location of openings in the steel infill plate.

The test specimens were loaded with axial column loads combined with cyclic horizontal loads to determine the hysteretic behaviour. Either three or four cycles of loading were applied up to a maximum deflection of about $h_s / 50$, which generally constituted failure of the specimens. Based on the results of these tests, the researchers drew several conclusions. First, it was observed that a major portion of the deflection occurred as a result of interfacial slip between the steel panel and the concrete frame. Combined with the fact that specimens that ultimately failed at the interface showed inferior ductility, this led to the conclusion that closely spaced anchors are required. Second, the researchers concluded that even when shear cracks form in the concrete columns, the infill panels assist in allowing them to continue to support axial loads. Third, when a rectangular opening occupying about 12% of the area of the panel was present, its location and orientation had little effect on the response. Fourth, although installing the steel panels into existing reinforced concrete frames tended to strengthen and stiffen them, the increase in ductility was limited due to the relatively early failure of the connectors.

Yamada (1992) investigated the behaviour of composite concrete encased steel plate and other shear walls. A total of 11 one-fifth scale single storey, single bay concrete encased steel moment-resisting frames were tested. Four incorporated concrete panel infills, two were infilled with steel flat bar cross bracing encased in concrete panels, two were infilled with a concrete encased steel panel, and two used plain steel panel infills. For purposes of comparison, one specimen was also tested with no infill panel.

The test specimens were loaded monotonically in shear to failure. Responses were examined to determine an optimum system in terms of stiffness, strength, and ductility. The systems infilled with concrete or those utilizing concrete encasement of the steel infill plates or cross bracing showed a high initial stiffness, apparently arising from a diagonal compression field that formed at very small deflections. The thicker concrete panels also exhibited very high strength. However, the ultimate strength was reached at relatively small deflections and was followed by a rapid decrease in strength as the concrete crushed. Conversely, the specimens with plain steel infill plates, although initially less stiff and in some cases with a lower ultimate strength, maintained their ultimate capacities through large deflections. This high degree of ductility was achieved primarily through the yielding of a diagonal tension band in the plate. From the distinct differences in the behaviour of the concrete and steel panels, it was concluded that structural behaviour could be optimized by selecting an appropriate combination.

Sugii and Yamada (1996) conducted an additional 23 tests on one-tenth scale specimens in order to investigate further the optimal behaviour of concrete encased steel plate shear walls. Each specimen, consisting of two adjacent identical panels, was loaded as a deep beam with a concentrated load at midspan in a manner similar to that used by Timler and Kulak (1983). The two panels were, therefore, loaded in shear in an identical manner. In all cases, the surrounding moment-resisting frame consisted of wide-flange steel sections encased by reinforced concrete. Both monotonic and cyclic loading cases were investigated. Parameters that were varied included the aspect ratio, the steel panel thickness, whether or not the steel panel was encased in concrete and, if present, the concrete panel thickness.

Theoretical equations are presented for calculating both monotonic and cyclic behaviour based on an assumed response of both the panels and the surrounding frame plus an assumed effective width of the tension and compression fields. Reasonable agreement with the test results was obtained. The method allows the steel

panel and concrete encasement thicknesses to be selected optimally for the desired structural behaviour.

Variations on the use of steel plate shear panels as the primary energy absorbing mechanism in buildings during an earthquake have also been presented. Nakashima *et al.* (1994) developed a type of steel panel hysteretic damper that utilizes a steel possessing a yield strength approximately one-third that of typical mild steels. The damper consists of a relatively small (1200 mm x 1200 mm) stiffened steel panel similar to the steel plate shear wall concept that is connected in each storey to the building frame. Another application developed by Tsai and Wang (1996) uses a steel shear panel as the ductile link that is the primary energy dissipating mechanism in an eccentrically braced frame. Although not directly equivalent, the use of this concept in a hysteretic damper and in a hysteretic ductile link is further confirmation of the superior inelastic performance of steel shear panels in effectively dissipating seismic energy.

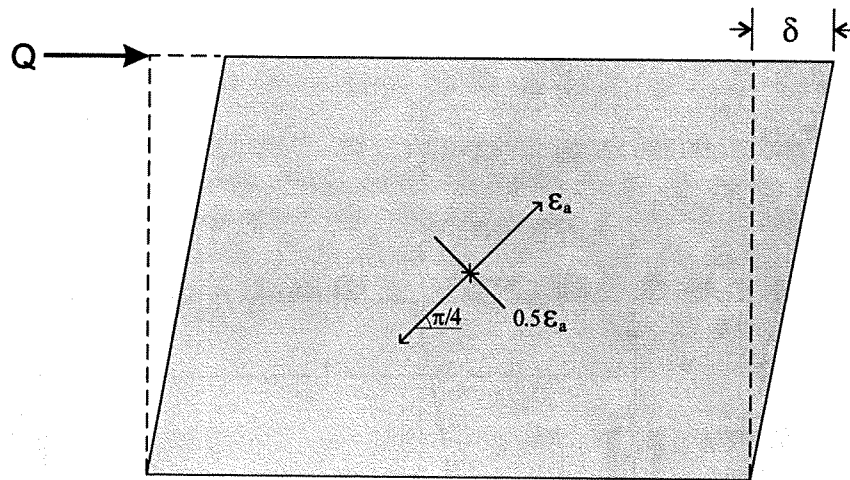


Fig. 2.1 Idealized Deformed Panel (Mimura and Akiyama 1977)

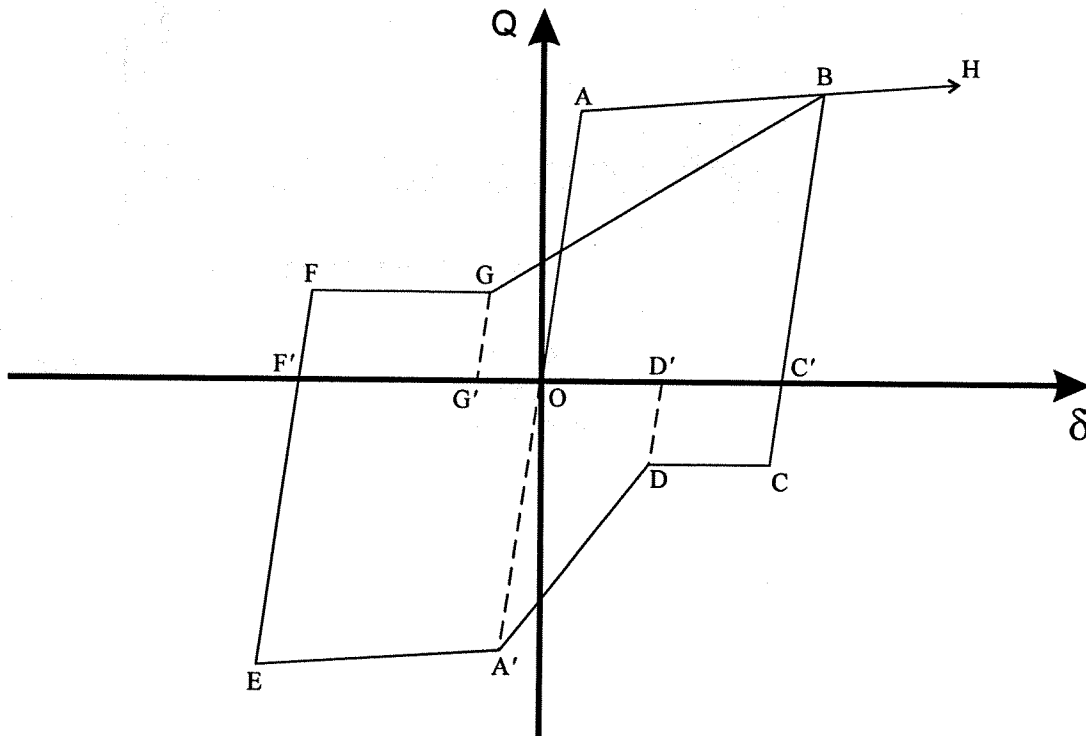


Fig. 2.2 Hysteresis Model (Mimura and Akiyama 1977)

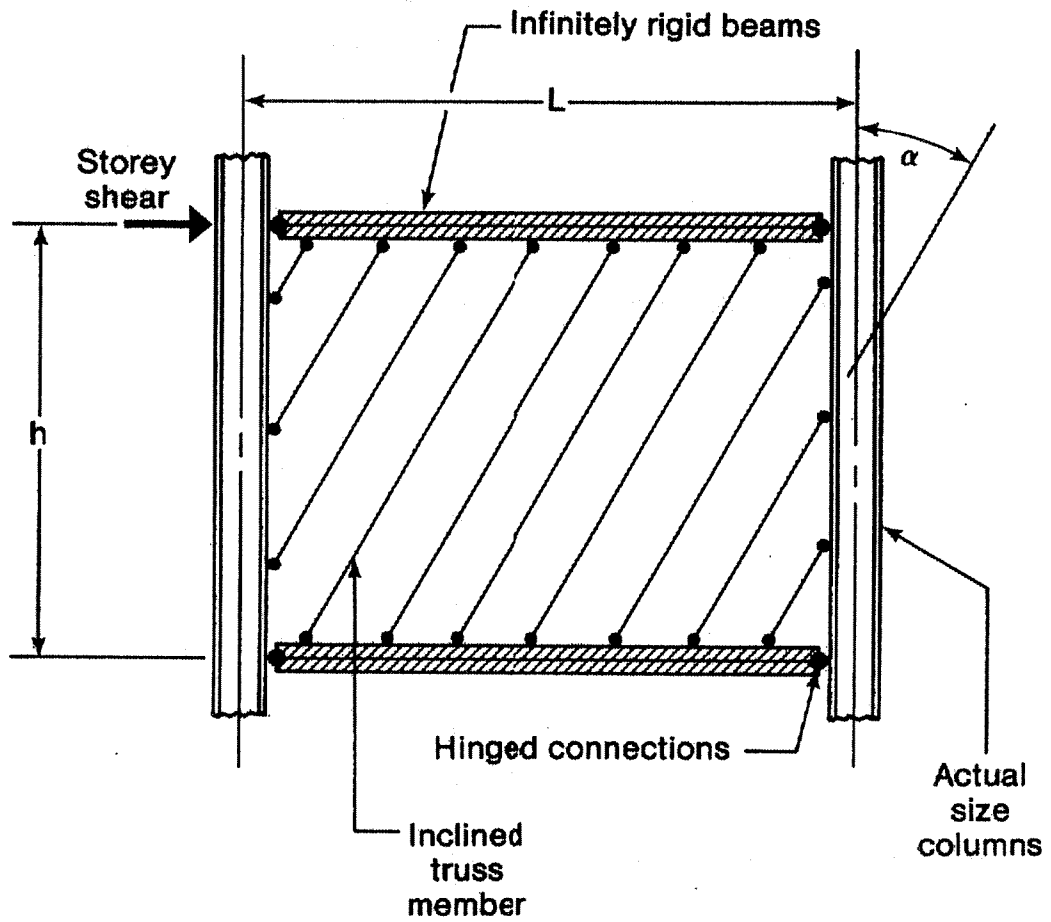


Fig. 2.3 Strip Model Representation of a Typical Storey (Thorburn *et al.* 1983)

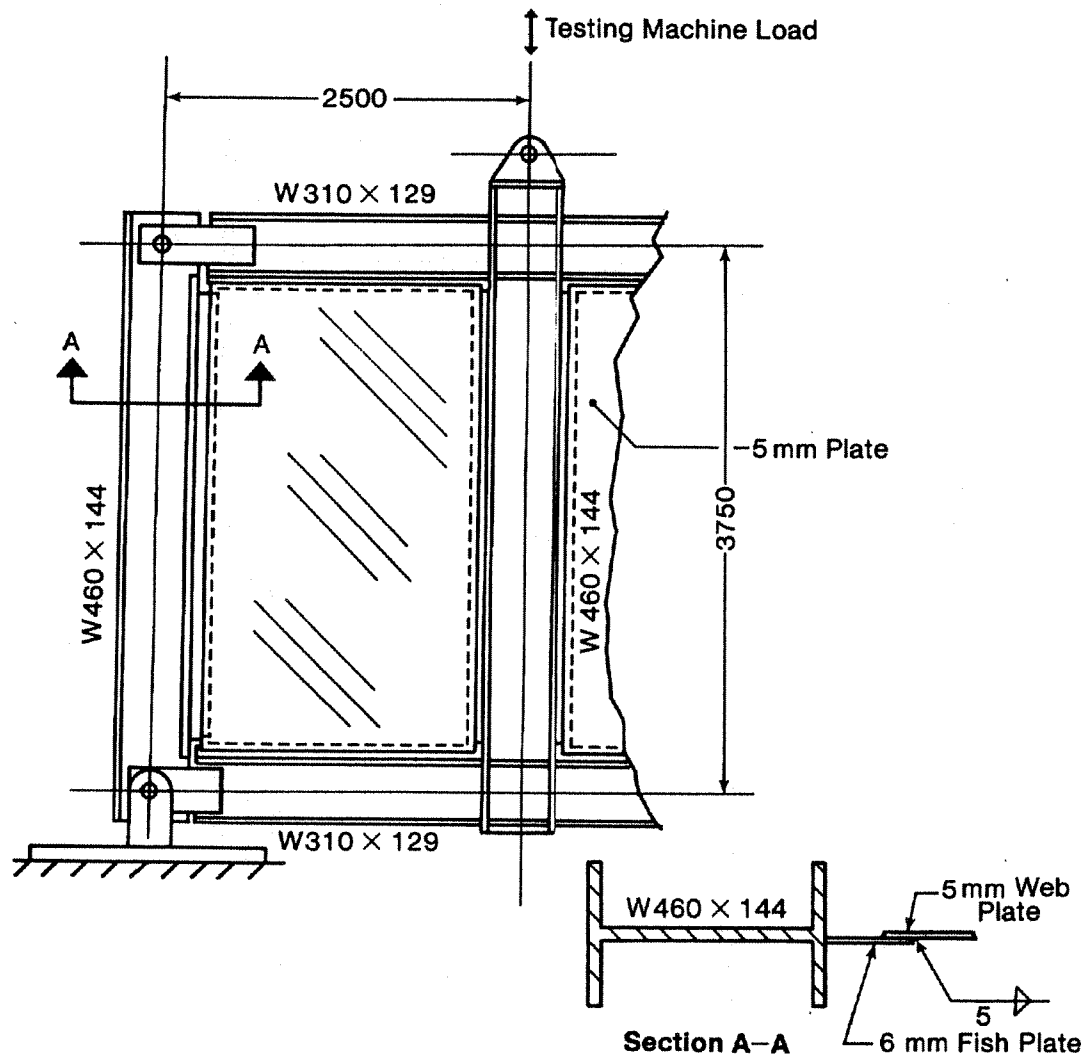


Fig. 2.4 Schematic Diagram of Test Specimen (Timler and Kulak 1983)

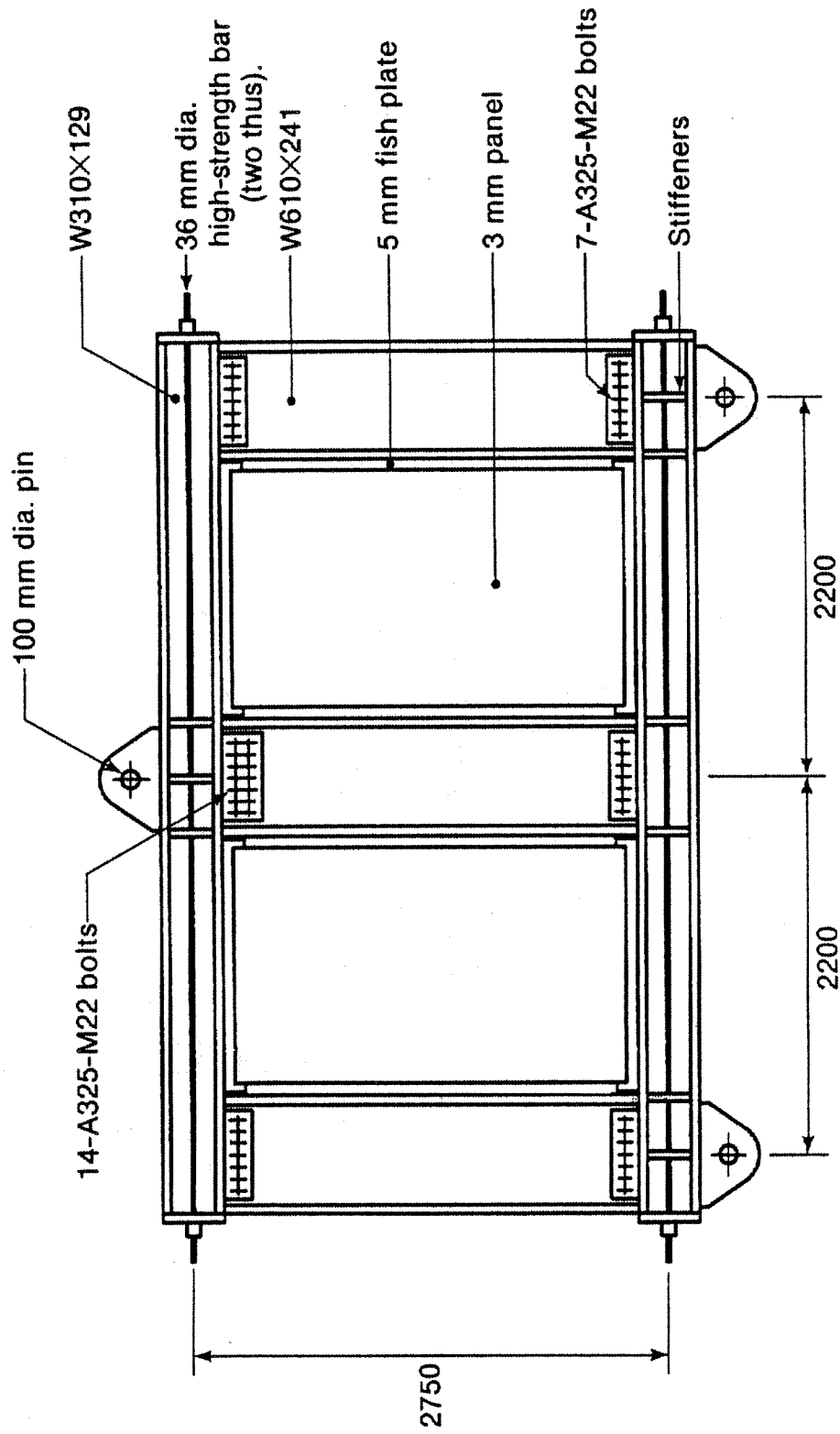


Fig. 2.5 Schematic Diagram of Test Specimen (Tromposch and Kulak 1987)

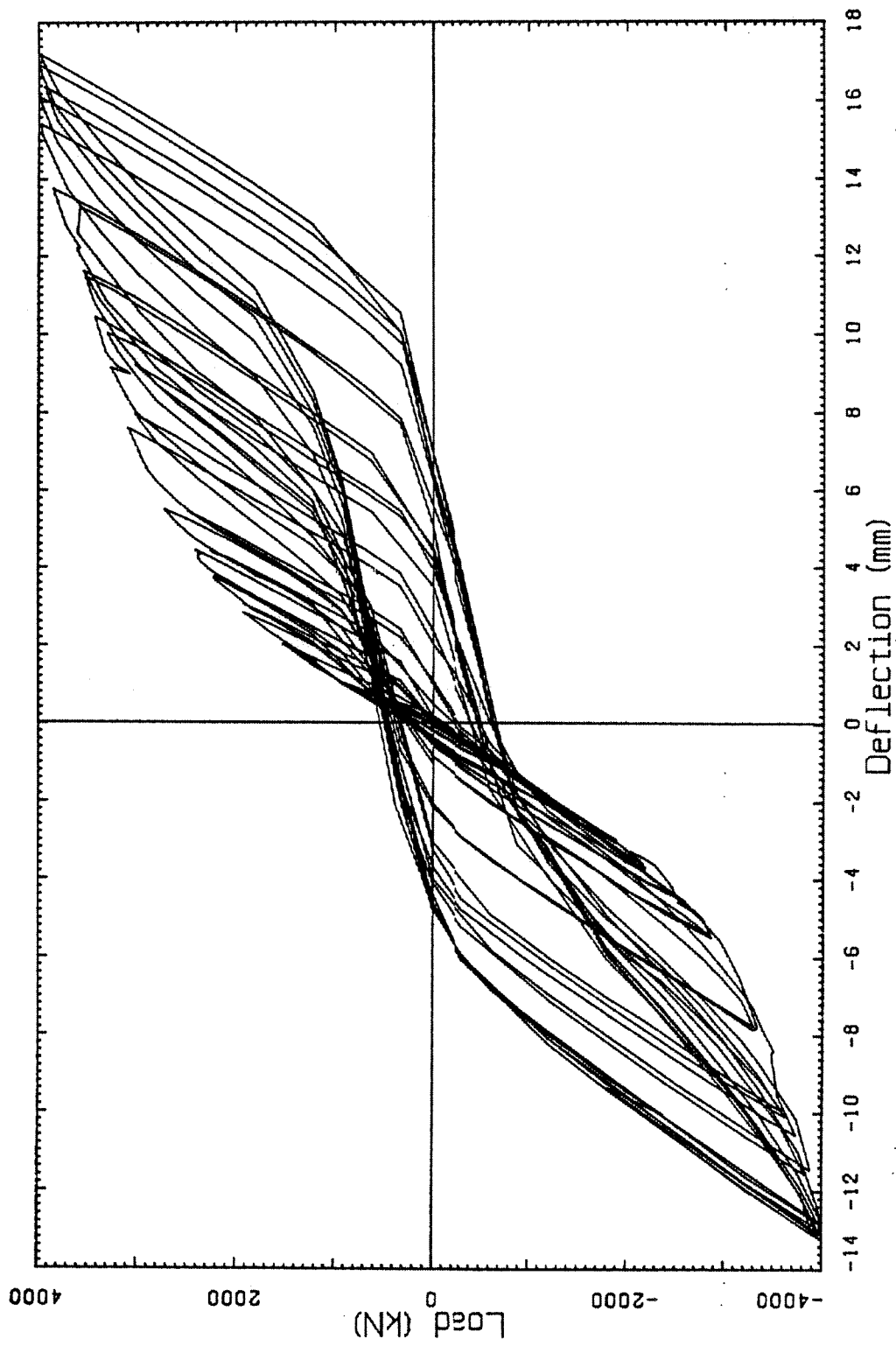


Fig. 2.6 Load vs. Deflection Curve (Tromposch and Kulak 1987)

3. PRELIMINARY FINITE ELEMENT MODEL

3.1 Introduction

A large-scale multi-storey steel plate shear wall test was designed to examine the behaviour of such lateral load-resisting systems during severe cyclic loading. Prior to conducting the experimental programme, a method of analysis was required in order to be able to predict the behaviour of the test specimen so that the test could be properly designed. Using the model, the required hydraulic jack capacities and strokes and the movements of measuring devices could be predicted. Because of the expense of conducting a test of this scale, only one specimen could be tested. Furthermore, based on the test data, the analytical model can be calibrated and refined as necessary, so that other shear wall configurations can be analysed.

A preliminary finite element model of the shear wall specimen tested by Timler and Kulak (1983) is presented. The model was developed using the commercial general purpose non-linear program ABAQUS (Hibbitt *et al.* 1994). ABAQUS runs on a 32-bit UNIX platform, and the analysis was conducted on a SUN SPARC workstation.

A brief description of the general model criteria is presented. The elements, the material properties, the initial conditions and the solution strategy are all discussed in general terms. A description of the manner in which the Timler and Kulak specimen was modelled and a brief discussion of the results are presented.

3.2 Description of Model

3.2.1 Elements

A steel shear wall system consists of beams and columns in a frame forming rectangular openings and steel plates that fill in the regions within the boundary

members. The columns and beams were modelled with beam-type finite elements and the steel infill plates with plate/shell finite elements.

The beams and columns are modelled using a three-node quadratic beam element (ABAQUS element B32). This element allows biaxial bending, axial stretching, and warping of the cross-section. It also accounts for linearly elastic transverse shear deformation according to the Timoshenko beam theory (Timoshenko and Goodier 1970). The element formulation also allows for large axial strains. This particular element was chosen from the extensive element library in ABAQUS as being the most representative of actual behaviour of the members and allows out-of-plane behaviour to be considered.

Figure 3.1 shows a typical I-shaped cross-section used for the beam-type elements. The cross-section is described with 13 integration points: five in each flange and five in the web, with two common locations. This allows an accurate description of both the residual stress distribution and the non-linear constitutive material behaviour. Describing the mid-surface of the flanges and web of the element in this manner presumes that the stresses through the thickness are negligible.

The width and thickness of each flange and the web of the cross-section may be specified individually. The only geometric constraint is that the overall cross-section must possess symmetry about the weak axis. Because the origin of the local cross-section may be placed anywhere in the plane of symmetry, the cross-section may be eccentric in the strong axis direction to the actual line of the beam element.

Despite the fact that a finite cross-section is defined, the nodes of the beam elements lie on a line. Therefore, outrigger elements of high axial and flexural stiffness are required in some cases to link the beam and plate elements to ensure compatibility of deformations between them and to allow loads to be applied at their correct locations. This is discussed in Section 3.3.1 for the Timler and Kulak (1983)

specimen and in Section 4.4 for the four storey steel plate shear wall tested during this research.

The shear wall infill plates are modelled using an eight-node quadratic plate/shell element (ABAQUS element S8R5). This element has five degrees of freedom per node, although a sixth (rotation about the out-of-plane axis) is invoked automatically under particular circumstances. Therefore, out-of-plane behaviour of the plate is included in the model. Because the rotational degrees of freedom are described independently from the translational degrees of freedom, transverse shear deformation of the cross-section is automatically taken into account. Therefore, the Kirchhoff shear constraints are relaxed. The spatial strain field distribution is sampled at four Gaussian integration points located on the mid-surface. At each Gauss point, the flexural behaviour of the shell element is numerically integrated across five integration points through the thickness, allowing accurate tracing of the non-linear constitutive material behaviour across the thickness of the infill plates.

The presence of a connection tab, or “fish plate,” to connect the infill plate to the boundary members is not represented in the finite element model. Rather, the infill plates are considered to be connected directly to the beams and columns. The effects of this approximation are studied in Section 3.3.1.

3.2.2 Material Properties

All material is modelled as isotropic with a simple rate-independent elastic – plastic constitutive behaviour, including the effects of strain hardening. The properties are identical in tension and compression, with the constitutive parameters based on measured material properties when they are available. The von Mises yield surface model is used as the yield criterion. Other aspects such as the particular stress vs. strain relation used for the various shear wall structures analysed are discussed in subsequent sections.

3.2.3 Initial Conditions

The behaviour of thin plates in real structures subjected to in-plane membrane forces can be significantly affected by initial out-of-plane deformations, and this must be taken into account in the analytical model. The stiffness of a perfectly flat plate is very high under in-plane shear stresses. However, even slight initial imperfections will substantially reduce the in-plane shear stiffness.

The geometry of steel plate shear wall infill panels is such that some out-of-flatness, accentuated by effects such as distortion due to welding, floor beam deflections, and eccentric fish plate connections, is certain to occur prior to the application of in-plane shear loading. The initial plate imperfections must be modelled prior to the strength analysis and may be obtained from measurement of the actual initial conditions in similar structures. Alternatively, the first buckling mode of the plate may be used, obtained from an eigenvalue buckling analysis of the shear wall system, with the loading applied in the same manner as for the subsequent strength analysis. The latter approach is used in all analyses conducted during this research. However, a series of trial initial plate configurations showed that the overall load vs. deflection behaviour is largely independent of the geometry selected, so long as some initial deformed configuration is imposed.

Residual stresses were not included in the modelling of the Timler and Kulak specimen because these quantities were not measured in that research programme. They were, however, included in the model of the four storey test specimen, as described in detail in Chapter 8.

3.2.4 Solution Strategy

The non-linear nature of the problem dictates that an iteration scheme be used to achieve successive solutions along the equilibrium path. In general, ABAQUS uses a load control Newton-Raphson scheme as a default solution strategy. However, this

method diverges in the neighbourhood of unstable response, including local instabilities. The local instabilities of the plate as it re-oriented itself as deformations increased made it extremely difficult to obtain a complete solution up to the ultimate capacity using a load control strategy. Therefore, the modified Riks solution algorithm (Riks 1979; Ramm 1981), treating both the loads and displacements as unknowns, was used. The basic algorithm remains the Newton-Raphson method, but the search for equilibrium is controlled based on an iterative path perpendicular to the first iterate in any step, as shown in Fig. 3.2. This perpendicular path is easily controlled to intersect and converge on the required solution path, whether the response is stable or unstable.

In general, the Newton-Raphson strategy is used at low load levels up to the point where a solution can no longer be achieved. Subsequently, the modified Riks method is used to explore higher load levels. In all cases, the step sizes used must be small in order to achieve convergence.

Geometric non-linearity was accounted for in modelling the Timler and Kulak specimen with monotonic loading. However, the more complex four-storey specimen led to solution difficulties in the presence of geometric non-linearity. Therefore, the cyclic analysis was performed without consideration of geometric non-linearity. In order to determine the effect this has on the model behaviour, a study was performed that includes geometric non-linearity in the initial portion of the load vs. deflection response using monotonic loading. This is discussed in Chapter 8.

3.3 Numerical Analysis of Timler and Kulak Specimen

3.3.1 Finite Element Model

Figure 3.3 shows a diagram of the specimen tested by Timler and Kulak (1983), and Fig. 3.4 depicts the finite element mesh used to analyse the structure. Because of symmetry in the specimen, only one-half was modelled and the edge of

the panel corresponding to the axis of symmetry was assigned full fixity. Because the beam elements lie eccentric to the cross-sectional centroid of the boundary members they represent, a rigid outrigger (as seen in the lower left corner of Fig. 3.4) was utilized to provide a concentric reaction point. The test specimen employed a cylindrical pin and clevis system between the column and beam members. Therefore, these connections were modelled as pinned about the out-of-plane axis.

The test specimen was braced out-of-plane at three locations on the exterior vertical members and these constraints were also incorporated into the model.

Geometric dimensions for the model were taken from the fabrication shop drawing and included the dimensions of the boundary members that were fabricated as three-plate built-up members. However, the as-built measured thickness of the infill plate was used.

Since no material tests had been conducted for the beam and column sections, a bilinearly elastic – perfectly plastic stress vs. strain relation was used and the values $E = 200\,000\text{ MPa}$ and $\sigma_y = 300\text{ MPa}$ were assumed.

Material properties of the infill plate used in the finite element model were based on measured values. However, due to an error in conducting the tension tests, the initial portion of the stress vs. strain curve is not well defined, although it has been shown to be of a shape more typical of cold-worked than hot-rolled steel. A multi-linear approximation of this curve with eight segments was used to model the material properties of the infill plate, as given in Fig. 3.5. The figure shows both the measured stress vs. strain multi-linear representation and also a curve modified to give an elastic stiffness more typical of structural steels.

The coordinates of the buckled shape were used to model the initial imperfections of the infill plate in the manner described in Section 3.2.3. The modal amplitude of the buckled shape was set to a peak value of 7.5 mm, which is equal to

the measured peak amplitude for the test specimen prior to the final test-to-failure excursion. (Prior to this, three cycles were performed with loading up to the service load level.) Figure 3.6 shows the initial geometry, with the out-of-plane deformations amplified 20 times.

Although the infill plates of the test specimen were connected to the boundary members by means of a fish plate connection tab, in the finite element model the infill plates were simply connected directly to the beam and column members. In order to assess the difference in tensile behaviour of a plate with and without fish plate connections, a 100 mm wide strip of plate was modelled with each type of end condition separately. These models represent a diagonal strip of the infill plate from the specimen tested by Timler and Kulak, taken parallel to the tension field developed.

The strip with the fish plate connections was modelled as three separate plates. The adjacent nodes at the overlap locations (along the lines of fillet welds) were constrained to behave as though they are joined together with a rigid link. All shell elements used were of the same type as those used in the infill plates of the shear wall model. For this study, a bilinearly elastic – plastic constitutive stress vs. strain relation was used to represent the behaviour of a typical hot-rolled structural steel up to the hardening strain. Each strip was loaded with a monotonically increasing load at one end of the strip and the other end was fixed.

Figure 3.7 shows the load vs. elongation response of the two strips. The two responses are similar, especially at low and intermediate load levels where they are virtually identical. As the loading increases, the curves tend to diverge slightly. At higher load levels, the strip with fish plates exhibits marginally stiffer behaviour because of the sharing of the tensile load where the infill and fish plates overlap. The similarity of the two curves supports the position that omitting the fish plates in the shear wall model is unlikely to cause any significant change in the overall behaviour.

3.3.2 Results of Analysis

The finite element model was loaded monotonically to a deflection approximately equal to that achieved in the test. This corresponds to a load near the ultimate capacity of the specimen. The load vs. panel deflection responses for both the test and the model are shown in Fig. 3.8. The test curve represents the final loading excursion after three cycles of loading at service load levels.

The model differs considerably from the test results. It is somewhat stiffer, but shows a trend towards the same ultimate capacity. There are several reasons that further refinements to the model of this specimen were not made. As discussed in Section 3.3.1, the actual stress vs. strain characteristics of the boundary members and the characteristics of the infill plates at low stress levels are not known. It was found, however, that the overall behaviour of the shear wall model *is* sensitive to the material properties of the infill plate, as demonstrated in Fig. 3.9. Here, the differences in response of the model representing the Timler and Kulak specimen are shown using the two material curves depicted in Fig. 3.5.

Another reason that further refinements to the model were not made was that the specimen of Timler and Kulak had pinned beam-to-column connections, whereas the proposed multi-storey test specimen had moment-resisting connections. The ability of the model to predict the multi-storey test results is not dependent upon its ability to model the pin-and-clevis joints. Finally, residual stresses measurements were not part of that study and, thus, their effect on the yielding of the boundary members could not be included.

3.4 Summary

The finite element model gave a somewhat stiffer representation of the load vs. panel deflection curve of the test conducted by Timler and Kulak. Although the

model was by no means complete, it served to highlight a number of significant effects.

The material properties of the infill plate have a significant effect on the overall behaviour, and they must be represented in the model as accurately as possible. Although initial imperfections must be modelled in some manner, the particular way in which they are represented is of considerably less importance. The omission of the fish plates in the modelling of the finite element mesh does not have a significant effect on the panel behaviour.

Within the constraints outlined above, the model provides a tool for predicting the behaviour of the multi-storey steel plate shear wall test specimen. The model can then be refined based on the test results.

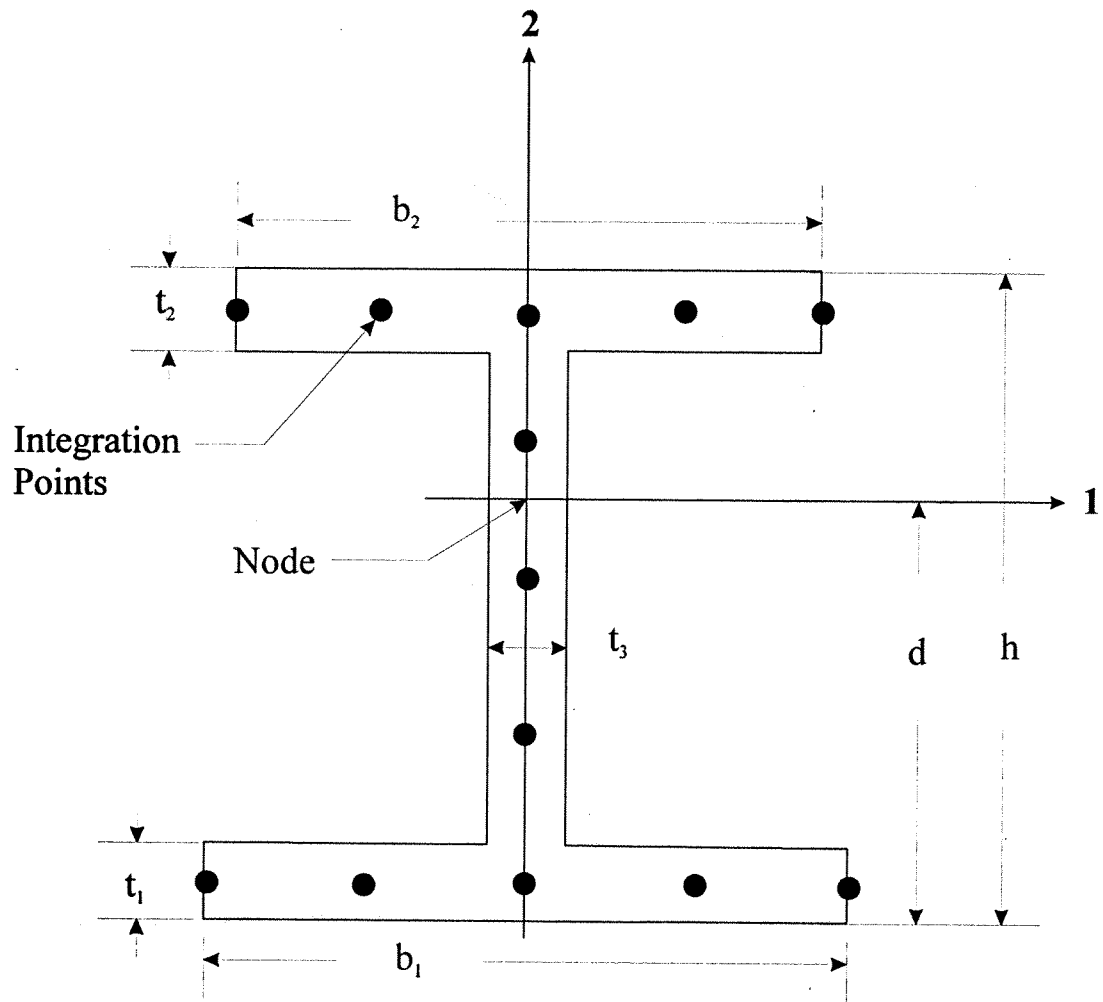
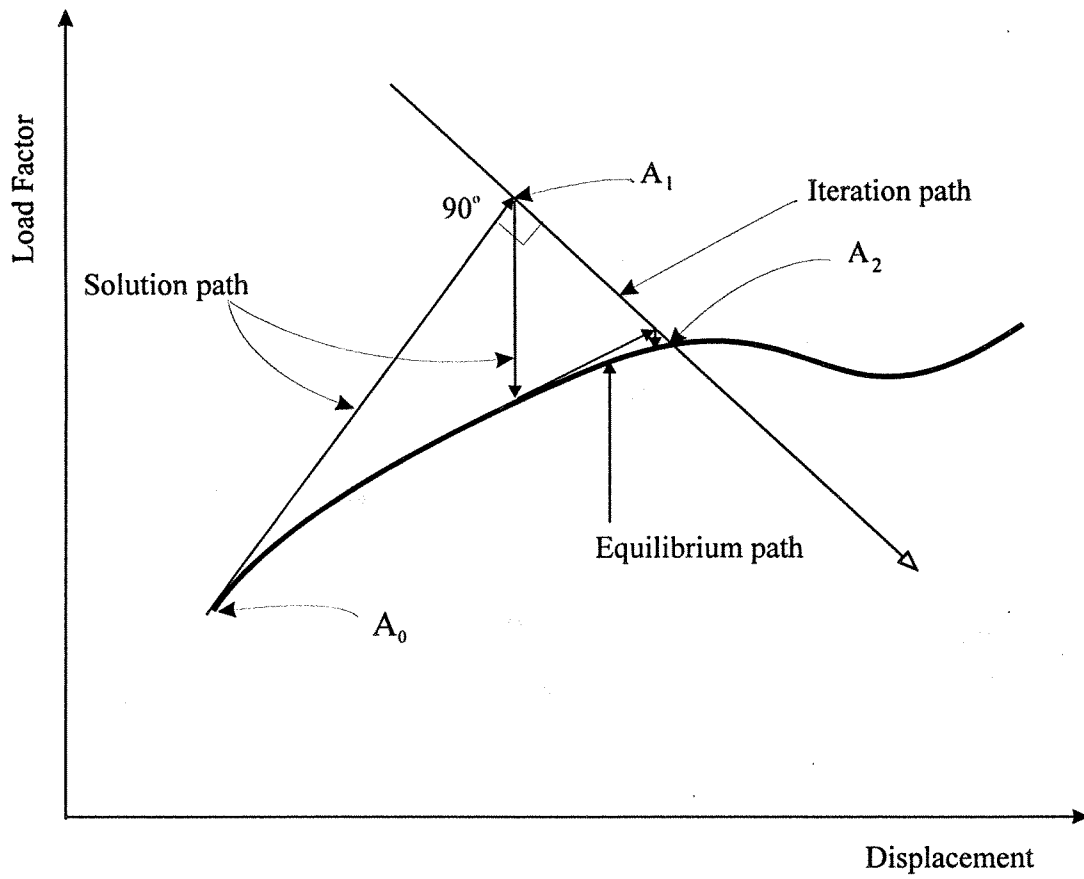


Fig. 3.1 Cross-section of the ABAQUS B32 Beam Element



A_0 --- Initial solution point

A_1 --- Solution point after moving a user-controlled distance along solution path

A_2 --- Solution point after convergence

Fig. 3.2 Modified Riks Solution Strategy

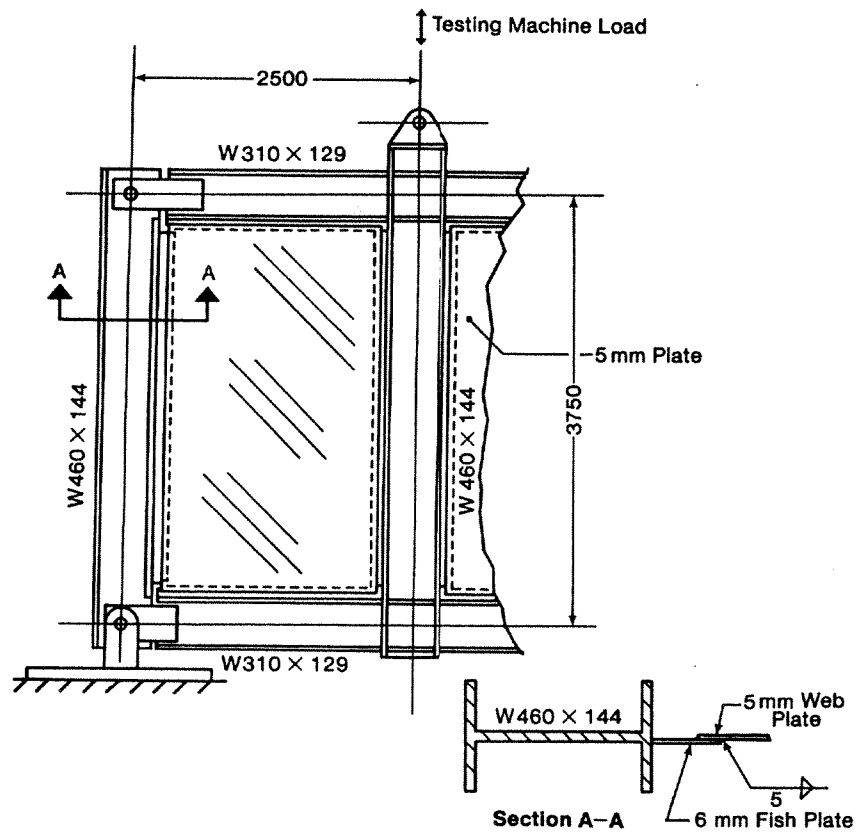


Fig. 3.3 Schematic Diagram of Test Specimen (Timler and Kulak 1983)

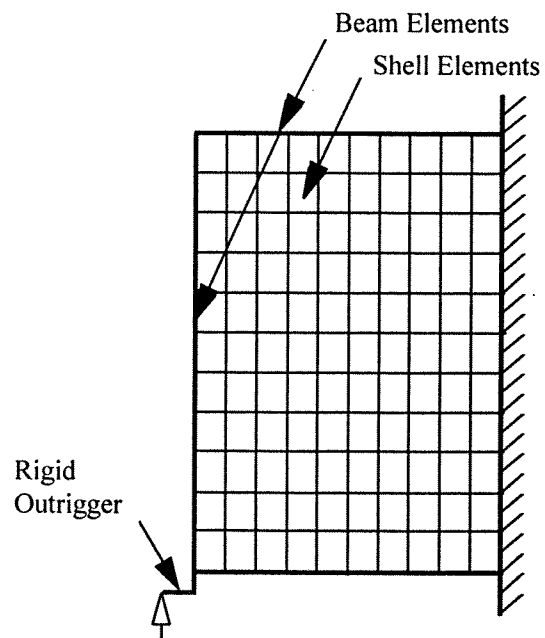


Fig. 3.4 Timler and Kulak Specimen - Finite Element Model

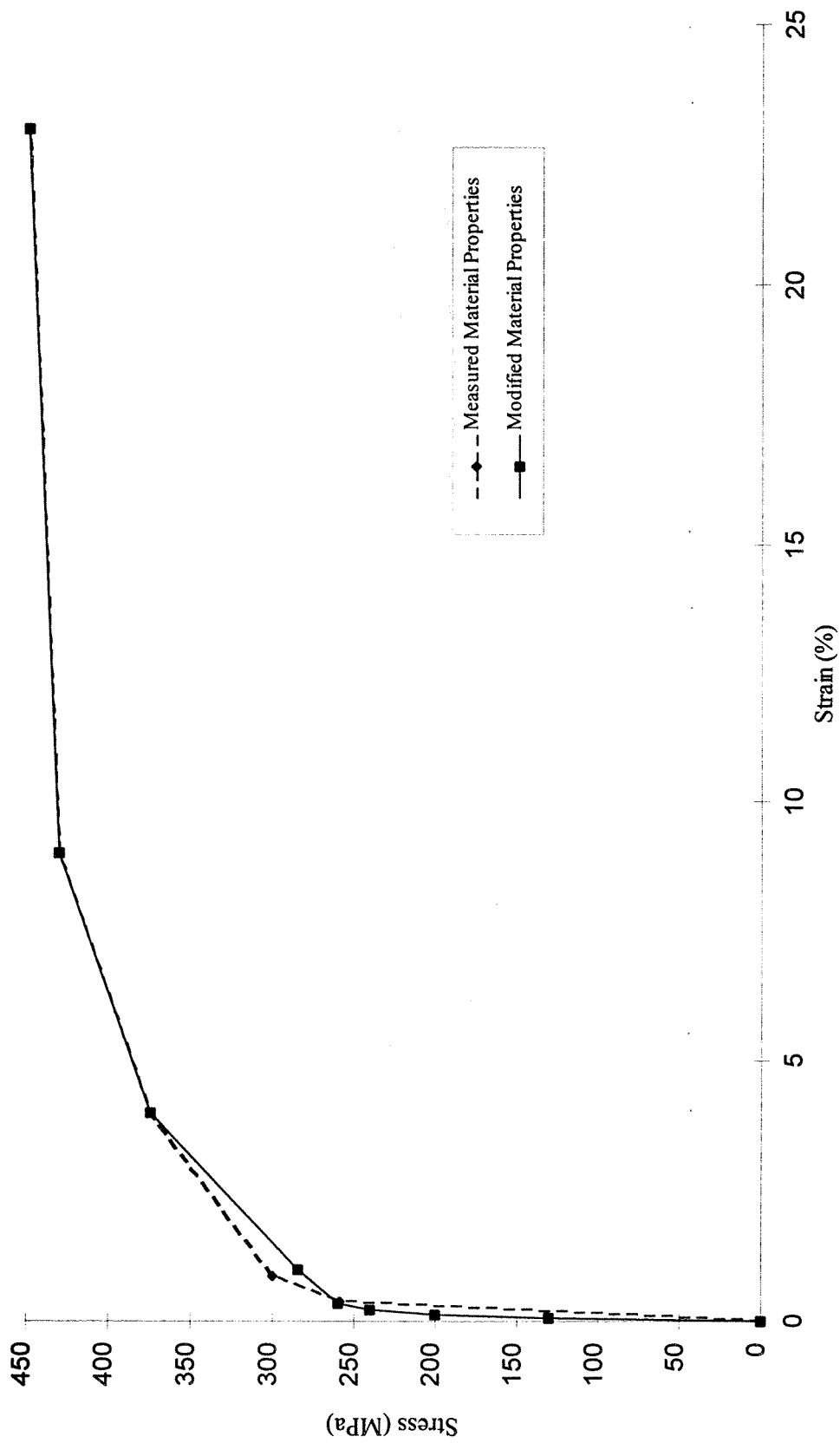


Fig. 3.5 Timler and Kulak Specimen – Infill Plate Material Model

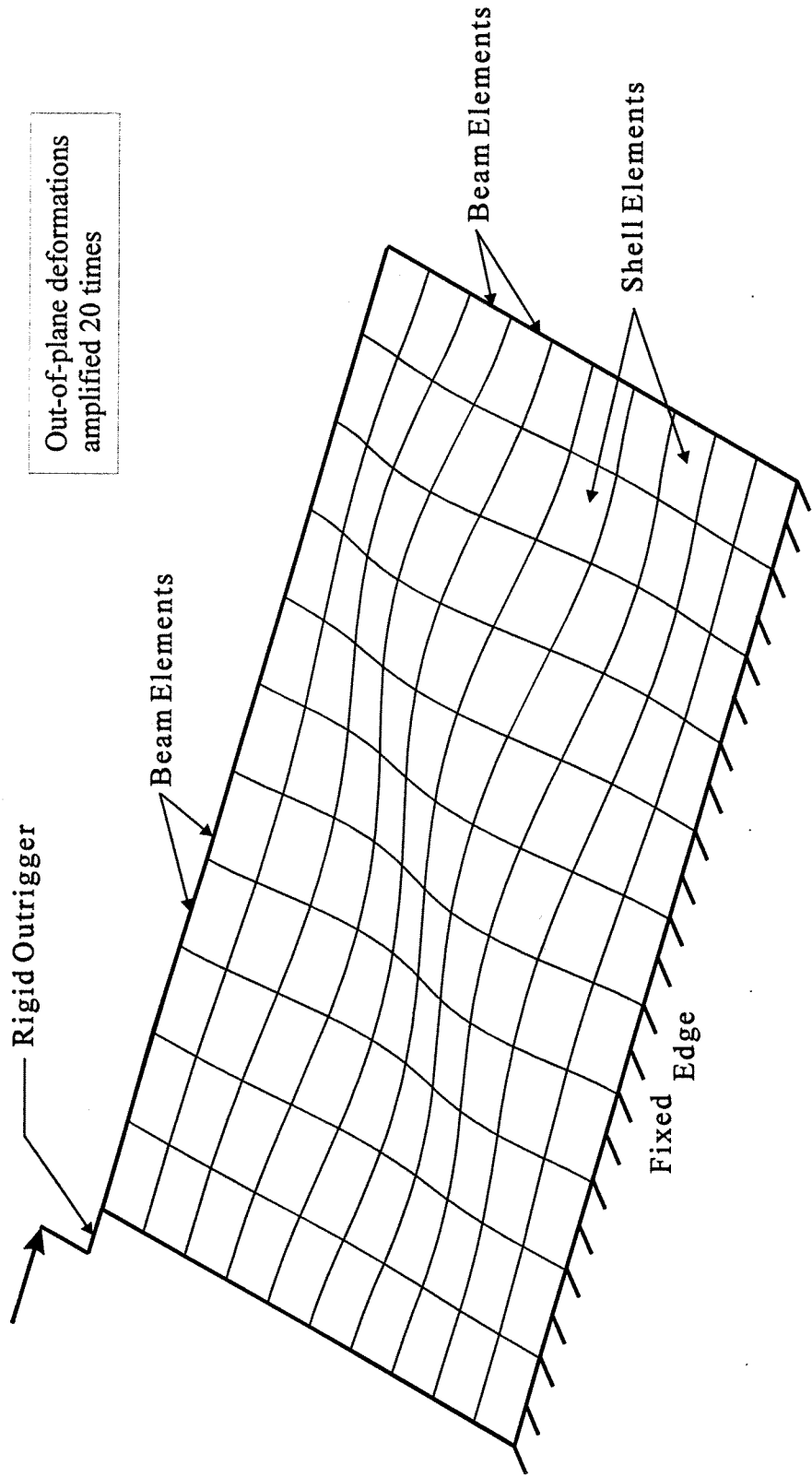


Fig. 3.6 Timler and Kulak Specimen – Initial Imperfections

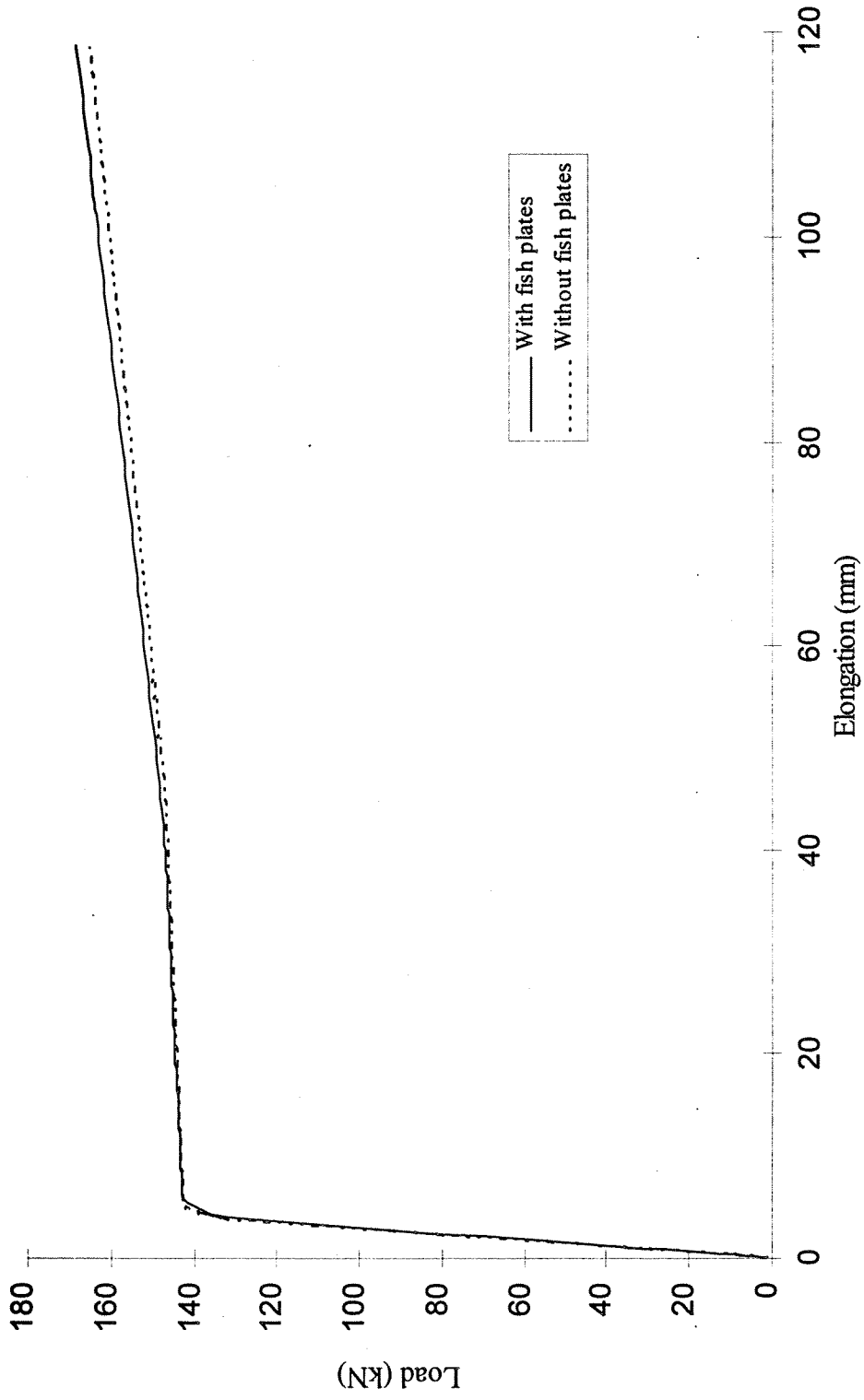


Fig. 3.7 Load vs. Elongation Response of Test Strips

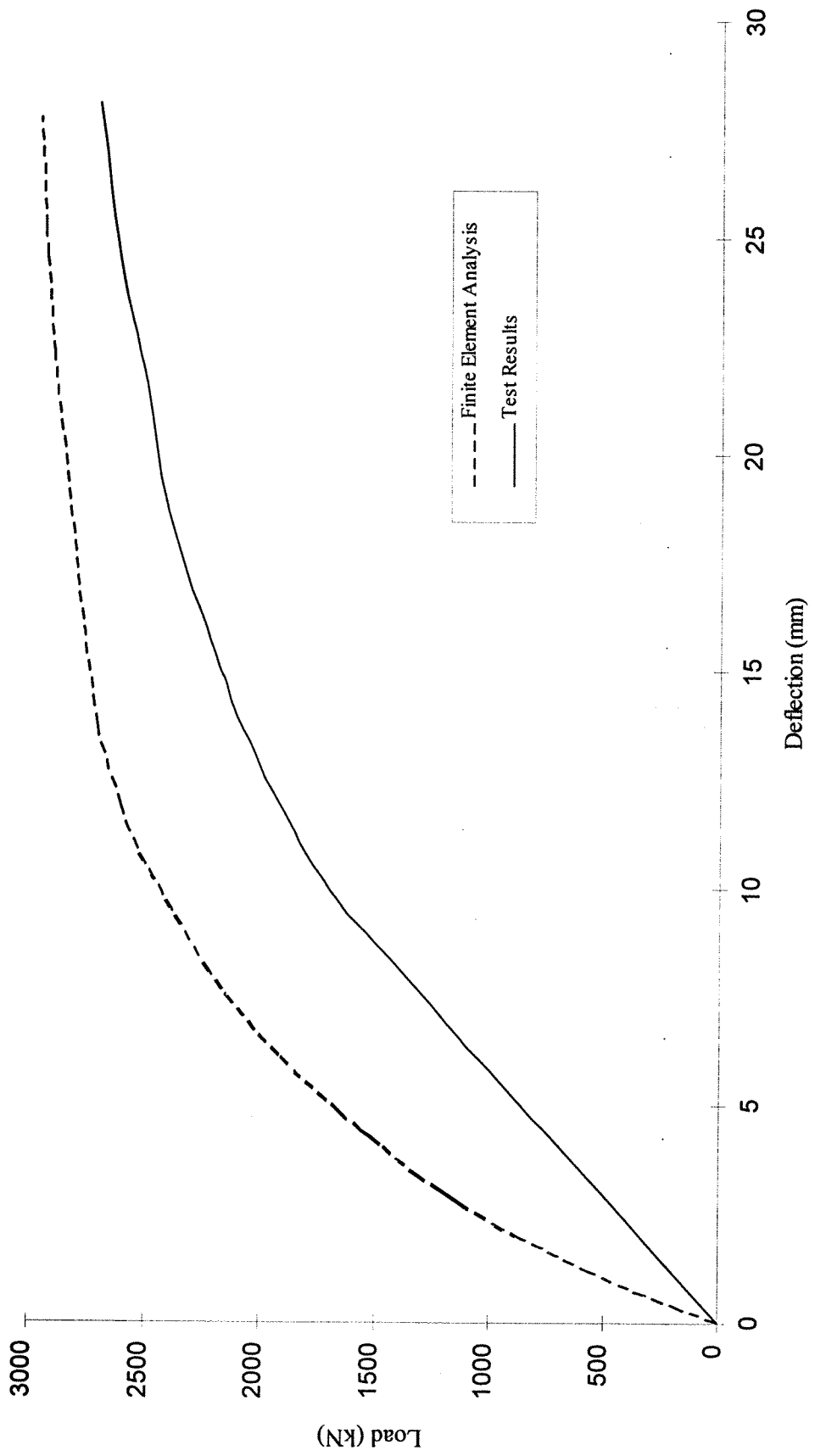


Fig. 3.8 Load vs. Panel Deflection of Timler and Kulak Specimen

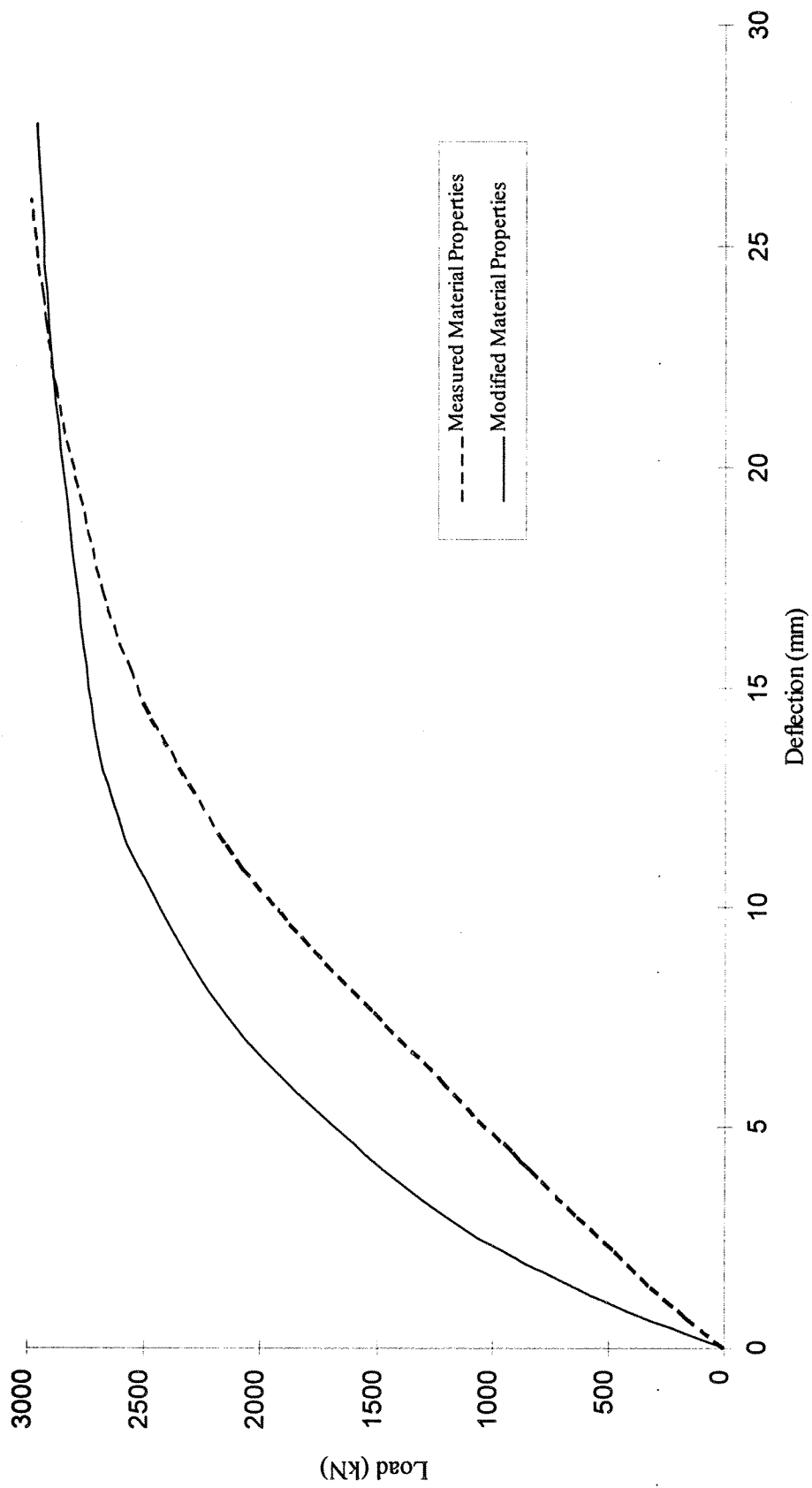


Fig. 3.9 Load vs. Panel Deflection – Sensitivity to Material Properties

4. EXPERIMENTAL PROGRAMME – GENERAL

4.1 Objectives

Previous analytical work (Thorburn *et al.* 1983, Timler and Kulak 1983) produced a simple method for predicting the behaviour of unstiffened thin-panel steel plate shear walls subject to monotonic loading up to the ultimate strength. The method was substantiated by a test of a pair of single storey shear wall panels (Timler and Kulak 1983). An additional test on a similar specimen (Tromposch and Kulak 1987) investigated the ability of the shear wall to resist cyclic loading.

Although these tests provided much useful information, experimental verification of the expected performance of steel plate shear walls undergoing very large, cyclic deformations—as would be expected in a severe earthquake—was required. Also, no large-scale tests on multi-storey shear walls had ever been conducted.

The objective of this test was to provide information about the behaviour of multi-storey steel plate shear walls under the effect of very severe cyclic loading representing an idealized earthquake. The particular arrangement used moment-resisting frame connections. Aspects of prime interest are the elastic stiffness, load level at which yielding first occurs, ductility, energy absorption, cyclic stability, and failure mode of the shear wall. Also of interest is the manner in which the steel infill panels and the moment-resisting frame share the applied load at various stages.

A further objective of the main test was to substantiate the results of the finite element model and to allow calibration of the model. In this way, other shear wall configurations can be effectively tested through computer simulation, thereby avoiding the expense of large-scale testing and the physical restrictions on the size of the specimen tested.

In order to design the test and interpret the test results, many ancillary tests were required. In addition to material tests on all components of the test specimen, a large-scale test was conducted on a corner of one panel of a shear wall. Because the frame tends to stretch and pinch the panel corner cyclically, an unsatisfactory detail could produce premature degradation of the panel. The objective of this test was to investigate the performance of the detail proposed for connecting the panels to the surrounding frame and to assess its suitability for use in the main test. The ancillary tests are described in Chapter 5.

4.2 Specimen Details and Fabrication Procedures

A diagram of the specimen tested is shown in Fig. 4.1. The overall height of the specimen, excluding the loading pedestals at the top and the base plate, is 7.4 m and the overall width, excluding the base plate, is 3.4 m. The typical storey height is 1.83 m (top three storeys) and the first storey is 1.93 m high. The columns are 3.05 m apart, measured from centreline to centreline. These dimensions are representative of a shear wall at 50% scale for an office building of 3.66 m (12 ft) typical storey height, or about 60% scale for a residential building. The test specimen was constructed entirely in a commercial steel fabrication shop using normal industry procedures. The loading clevises on the east side were added at the test site. The total mass of the test specimen was 5.6 t.

The W310x118 columns run the full height of the shear wall without splices. Beam sections at Levels 1, 2, and 3 are W310x60 and the beam section at Level 4 is a W530x82. All beam and column members in the shear wall have the cross-sectional proportions of Class 1 beam-columns. Connection of the beam flanges to the columns was made using complete penetration groove welds, using a backing bar and run-off tabs that were left in place. These welds were made using 1.6 mm flux core wire, controlled hydrogen electrodes (E4802T-9-CH) with a specified minimum tensile strength of 480 MPa. No pre- or post-heat was applied in the welding process.

Welding access holes in the beam webs of 20 mm radius were used to help ensure the continuity of the groove weld from one side of the flange to the other. The beam webs were connected to the column flange by means of fillet welds on both sides of the web. The columns were connected to the base plate using full penetration groove welds for the flanges and fillet welds for the webs.

The plates used for Panels 1 and 2 are nominally 4.8 mm thick and the plates used for Panels 3 and 4 are nominally 3.4 mm thick. (Section 4.5 gives a full description of the as-built measurements.) The panel aspect ratios (height/width) for Panels 1 to 4 are 0.59, 0.56, 0.56, and 0.48, respectively.

The grade of steel of the panels in the lower two storeys is G40.21–300W (CSA 1992b), and the plate selected is the thinnest plate readily available in this grade. In order to obtain the thinner plate in the upper two storeys, commercial quality hot-rolled steel was selected, which generally exhibits a somewhat lower yield strength than does 300W steel. Grade A569 (ASTM 1991) plate was used in Panel 3 and grade J403 GR1010 (SAE 1994) was used in Panel 4. Information obtained from the material tests on the infill plates is given in Section 5.4.

The panels were connected to the boundary members using the fish plate connection shown in Fig. 4.2. The continuous fish plates are 100 mm wide and 6 mm thick and are welded to the beams and columns by means of fillet welds on both sides. Where column fish plates and beam fish plates meet at the panel corners, they are connected using small strap plates to provide continuity. The infill panels are, in turn, fitted against one side of the fish plates, with a lap of 40 mm all around, and then welded with continuous fillets on both sides. This detail allows a simple means of compensating for normal fabrication tolerances in the plane of the plate, thereby avoiding fit-up problems in the field. The fillet welds connecting the infill plate to the fish plate and the fish plate to the boundary members are capable of developing the

ultimate strength of the infill plate. These welds were made using 3.2 mm E48024 electrodes with a specified minimum tensile strength of 480 MPa.

4.3 Test Design Considerations and Constraints

Design of the test specimen was influenced by a number of factors. The scale, complexity, and cost of the experimental programme dictated that only one specimen could be tested. The specimen was to be fabricated to as large a scale as practicable, while still satisfying the constraints imposed by the physical space limitations in the laboratory and the limitations of the testing equipment. A four storey specimen was selected in order to provide information on multi-storey steel plate shear wall behaviour. By using a four storey shear wall, two panels could be considered to have typical boundary conditions, whereas the bottom and top panels in a multi-storey shear wall have unique boundary conditions at the base and the roof beam, respectively.

The column spacing and storey heights were constrained by the location of anchor holes in the laboratory reaction wall and strong floor. The storey heights were selected to be as close to equal as this constraint permitted.

The specimen was to be constructed of elements and materials commonly available in Canada and fabricated using industry-standard details and methods. As closely as possible, it was to be representative of a shear wall that would actually be used in practice.

Column sizes were selected to maintain stability throughout the test up to the ultimate strength of the shear wall. Heavy columns such as these would be expected as part of a lateral load-resisting system in a severe earthquake zone. A Class 1 (plastic design) beam-column section was used in order that local buckling be precluded, at least up to the attainment of significant curvature at the fully plastic

moment. One column size was used throughout the height of the shear wall so as to avoid the need for a column splice.

Beams with relatively shallow depths were used at all but the top level to reflect the fact that opposing tension fields occur above and below the beam. A stiff, deep beam was used at the top level in order to anchor the tension field below. All beams were selected such that out-of-plane buckling would not occur, eliminating the need for intermediate lateral bracing.

Full moment connections were used at all beam-to-column joints. This configuration was chosen in order to produce expanded hysteresis curves as compared to a frame with simple connections (Tromposch and Kulak 1987), thereby increasing the amount of energy absorbed. The requirements of Clause 27.2 (Ductile Moment-resisting Frames) of Canadian standard CAN/CSA-S16.1-94 (CSA 1994) were met.

Plate thicknesses were selected to allow a resistance level that could be tested effectively in the laboratory. This was achieved by selecting thicknesses that represent the lower limits for plate that exhibits the classical linearly elastic – perfectly plastic plus strain hardening stress vs. strain curve of hot-rolled structural quality steel, as would be expected in a real structure. This characteristic is considered to be extremely important in order that the test results be generally applicable. Because of the potential for cold-working of thin plates during rolling, tension coupons were tested before any plate was confirmed for use. This procedure ensured that the stress vs. strain curve was characteristic of hot-rolled steel and that the steel was neither grossly over- nor under-strength. These material tests are discussed further in Section 5.4.

Because gravity loads acting on a deflected shear wall (the $P-\Delta$ effect) would have a significant effect on the overall behaviour under the action of cyclic horizontal loading, vertical loads of a magnitude representing reasonable unfactored gravity loads for a typical building at the lowest storey were applied to the columns. To avoid

a significant increase in complexity of the test set-up, these full gravity loads were applied at the tops of the columns.

Equal horizontal loads, representing the action of an idealized earthquake, were applied cyclically at each floor level. In reality, the relative values of these lateral loads depend upon the earthquake input being modelled, the assumed mass at each level, the mode shapes (which change with time for non-linear behaviour), the modal frequencies, and the damping ratios (which have different values for each mode). Additional complexity arises because these ratios of horizontal loads are also functions of time. Equal horizontal loads were considered to be no better or worse than other rational configurations and were adopted for simplicity. The loads were applied at the level of the beam top flange to simulate the location of inertia forces induced by floor masses. This loading configuration also results in varying combinations of storey shear and overturning moment at the four levels.

4.4 Preliminary Numerical Analysis of Specimen

Based on nominal dimensions (as given on the design drawings), the finite element model described in Section 3.2 was adapted to predict the behaviour of the multi-storey test specimen. The deformed configuration of the steel plate shear wall model when loaded to a base shear of approximately 2200 kN is shown in Fig. 4.3. The deformations in the figure are magnified five times for clarity.

Because the beams were modelled as line elements, rigid vertical outriggers were used above and below at each node, as shown in Fig. 4.3, to allow the infill plates to extend only to the beam top and bottom flanges. In this manner, beams of finite depth were simulated without the numerical complexity of using multiple plate elements. The outriggers ensure deformation compatibility at the interface with the infill plates.

The columns were also modelled with line elements, but they were specified as eccentric to the centroidal axis of the column cross-section. This allows the plate elements to be connected directly to the column elements. However, additional outriggers were required at the column tops, as shown in Fig. 4.3, in order that the gravity loads could be applied concentrically to the cross-section.

The columns were fully fixed at their bases, as was the lower edge of the infill plate in the lowest storey. The shear wall was braced out-of-plane at each end of each beam, as these locations were constrained from out-of-plane movement by articulated braces during the test. All other nodes were free to displace in any direction.

Estimated material properties were used in the preliminary model. The tension coupon tests subsequently conducted on the infill plate material confirmed that the parameters used for the most highly stressed panels (Panels 1 and 2) were very close to the true values. Revisions to the stress vs. strain relations used in the final analyses are discussed in Section 8.2.5. The material behaviour for both the infill plates and the boundary members is taken to be linearly elastic – perfectly plastic, with linear strain-hardening.

Initial plate imperfections were specified that model the first plate buckling mode of the shear wall. The peak amplitude was set to a value of 10 mm in order to represent a reasonable maximum out-of-flatness that might be present in an installed plate of this size. However, as described in Section 3.2.3, the value selected is unlikely to have a significant effect on the overall shear wall behaviour. Residual stresses were not included in the model at this stage.

A 6x9 element mesh was used for Panel 1, a 4x9 mesh was used for Panel 4, and a 5x9 mesh was used in the remaining two panels, resulting in a total of 5638 degrees of freedom in the model.

Because the computational demands of the problem are high, monotonic loading was used to estimate the envelope of load vs. deflection response up to the ultimate capacity of the test specimen. The model was then completely unloaded and then reloaded again well into the inelastic region. Non-linear geometric behaviour was included in the analysis. The predicted storey shear vs. storey deflection and base shear vs. top deflection curves are shown in Figs. 4.4 and 4.5, respectively. In predicting the behaviour of the steel plate shear wall specimen, the required jack and reaction wall capacities and the ranges of motion required for the jacks and instrumentation are also obtained. Figure 4.4 also shows that some plasticity was to be expected in each panel and that the great majority of the inelastic deformation would take place in the lowest storey.

4.5 As-built Measurements

Prior to the start of testing, as-built measurements of the steel plate shear wall specimen were taken in great detail. Beam elevations were measured on each side of each beam at the two ends and at the centreline, and the elevation of each loading clevis on the specimen was determined. The distances between the columns were measured at the elevation of the top and bottom flanges of each beam. Measurements of the panel diagonal were also taken in order to assess whether the frame had been fabricated squarely. In these respects, it was judged that the specimen had been fabricated to tight tolerances and the variations are considered to be negligible.

Precise locations of the column bases were determined to compare with the assumed locations on the base plate. Again, deviations from the prescribed locations are considered to be negligibly small. Column orientation measurements revealed that the west column had been welded to the base plate with approximately a one degree counter-clockwise rotation in plan. Although this does affect the stress distribution in the column cross-section, it is unlikely to have had any significant effect on the overall cyclic behaviour of the shear wall. Sweep and camber were measured for all

beams and both columns. The maximum sweep and camber for the beams were each about 2 mm (L/1368) and the maximum sweep for the columns was also about 2 mm (L/3780). There was no measurable camber in the columns. All cambers and sweeps are well within the limit prescribed by Canadian standard CAN/CSA-G40.20-92 (CSA 1992a) of L/1000.

Out-of-plumb measurements were taken for both columns in the directions of the two principal axes using a plumb-line. These measurements showed that the columns were out-of-plumb perpendicular to the plane of the wall in opposite directions. Partial correction was achieved by careful shimming of the base plate to create a very slight torsional deformation in the base plate. The final out-of-plumb of the east column was 10 mm (L/755) to the north and for the west column it was 5 mm (L/1510) to the south. The out-of-plumb of the columns in the direction parallel to the plane of the wall were within 2 mm (L/3780) of vertical. The maximum deviation from the vertical allowed by Canadian standard CAN/CSA-S16.1-94 (CSA 1994) is L/1000 for exterior columns and columns adjacent to elevator shafts and L/500 for all other columns.

Column and beam cross-sectional dimensions were determined at a total of 34 locations. Canadian standard CAN/CSA-G40.20-92 (CSA 1992a) provides production tolerance limits for various aspects of the cross-sectional dimensions of rolled shapes, as well as a permissible overall tolerance on the cross-sectional area. Although in a few individual cases, these tolerances were exceeded marginally, in all cases the mean measured values were well within the tolerances prescribed by the standard. The thickness of all stiffeners was also measured.

The thickness of each infill plate was measured at 12 locations with an ultrasound probe that had been calibrated against a micrometer. The thicknesses were found to vary in the most extreme cases by 2.2% over the area of the plate. The mean measured panel thicknesses for infill Panels 1 to 4 are 4.54 mm, 4.65 mm 3.35 mm,

and 3.40 mm, respectively. These thicknesses are within the permissible variations from the specified values that are prescribed in CAN/CSA-G40.20-92 (CSA 1992a). The thickness of the fish plates were also measured in this manner at 14 locations per panel.

When the shear wall specimen had been bolted to the floor in the testing location, the elevation of the top of the grouted base plate was determined. The thickness of grout was approximately 5 mm.

4.6 Summary

A test programme was planned to investigate the behaviour of a four storey steel plate shear wall subjected to idealized severe earthquake loading. The test specimen consisted of a moment-resisting frame with thin steel infill panels. The infill panel materials were tested prior to installation into the shear wall to confirm that they had properties typical of hot-rolled structural plate.

The test specimen was fabricated using standard industry procedures. After fabrication, detailed as-built measurements were taken for use in subsequent analyses.

The shear wall specimen was loaded with constant vertical loads at the tops of the columns and equal cyclic horizontal loads at each of the four floor levels. The finite element model described in Section 3.2 was adapted to model the test specimen and was loaded in a similar manner. However, instead of loading cyclically, the horizontal loads were applied monotonically into the inelastic range followed by a single unloading and subsequent reloading. This procedure produced predicted load vs. deflection curves that were used in designing the test.

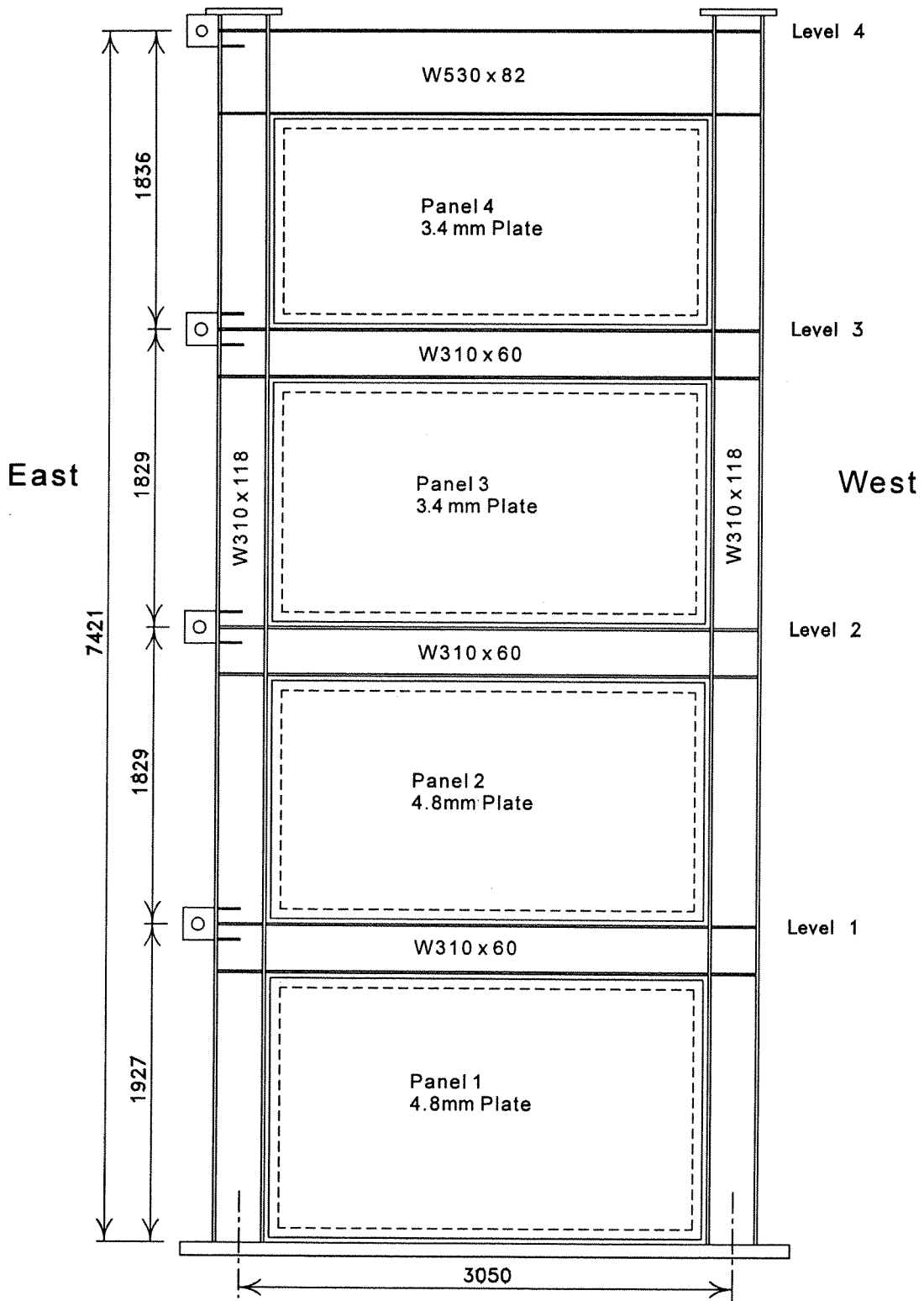


Fig. 4.1 Steel Plate Shear Wall Test Specimen (North Face)

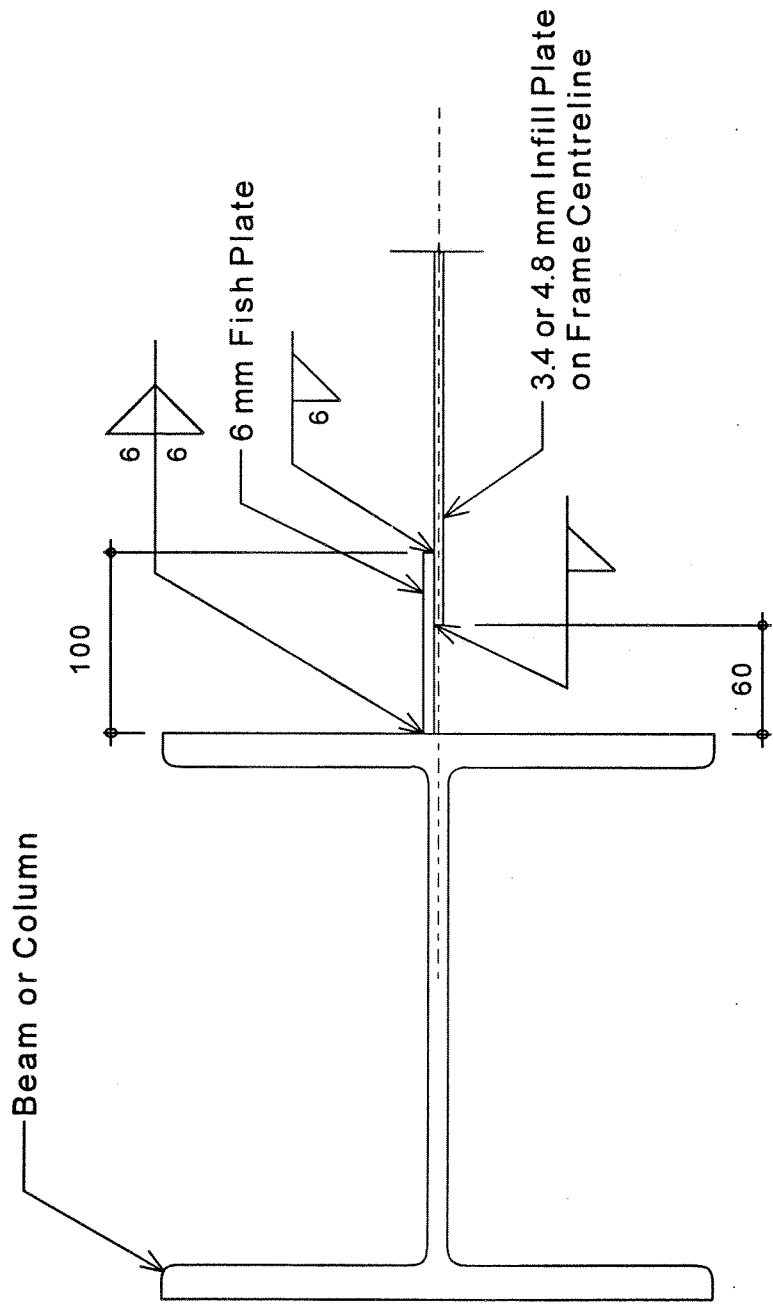


Fig. 4.2 Fish Plate Detail Used in Test Specimen

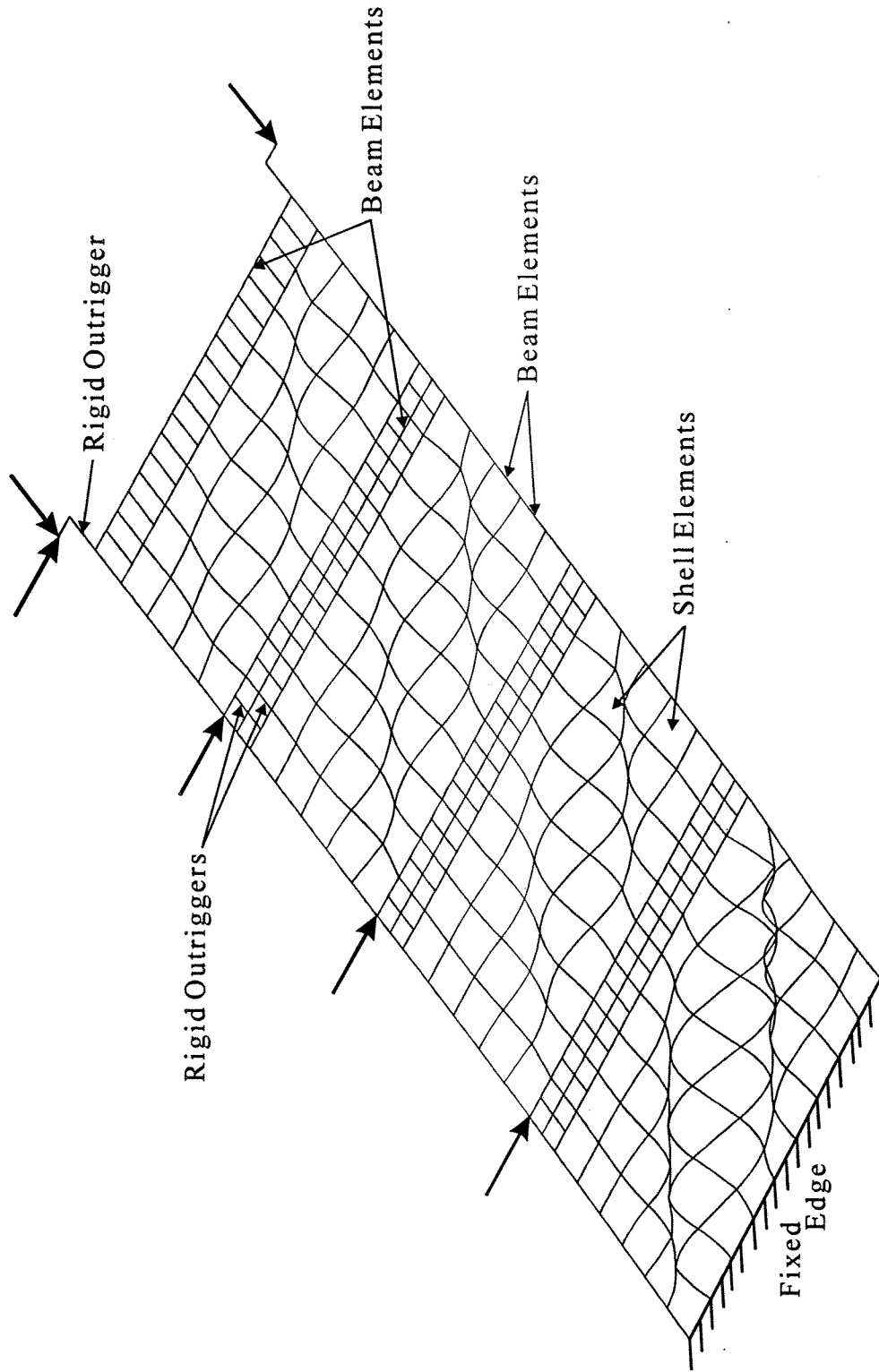


Fig. 4.3 Finite Element Model of Test Specimen (Deflected Shape)

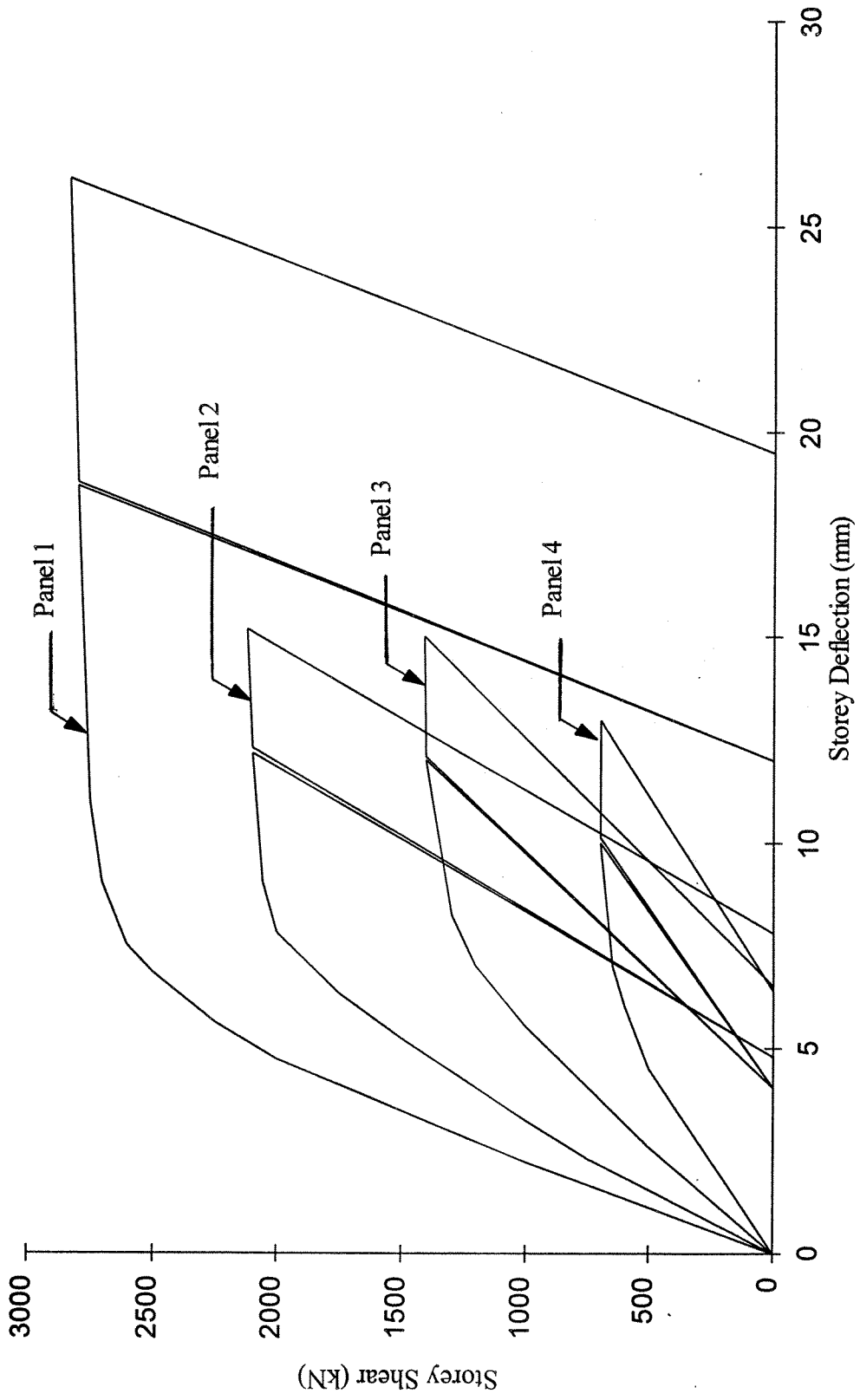


Fig. 4.4 Predicted Storey Shear vs. Storey Deflection

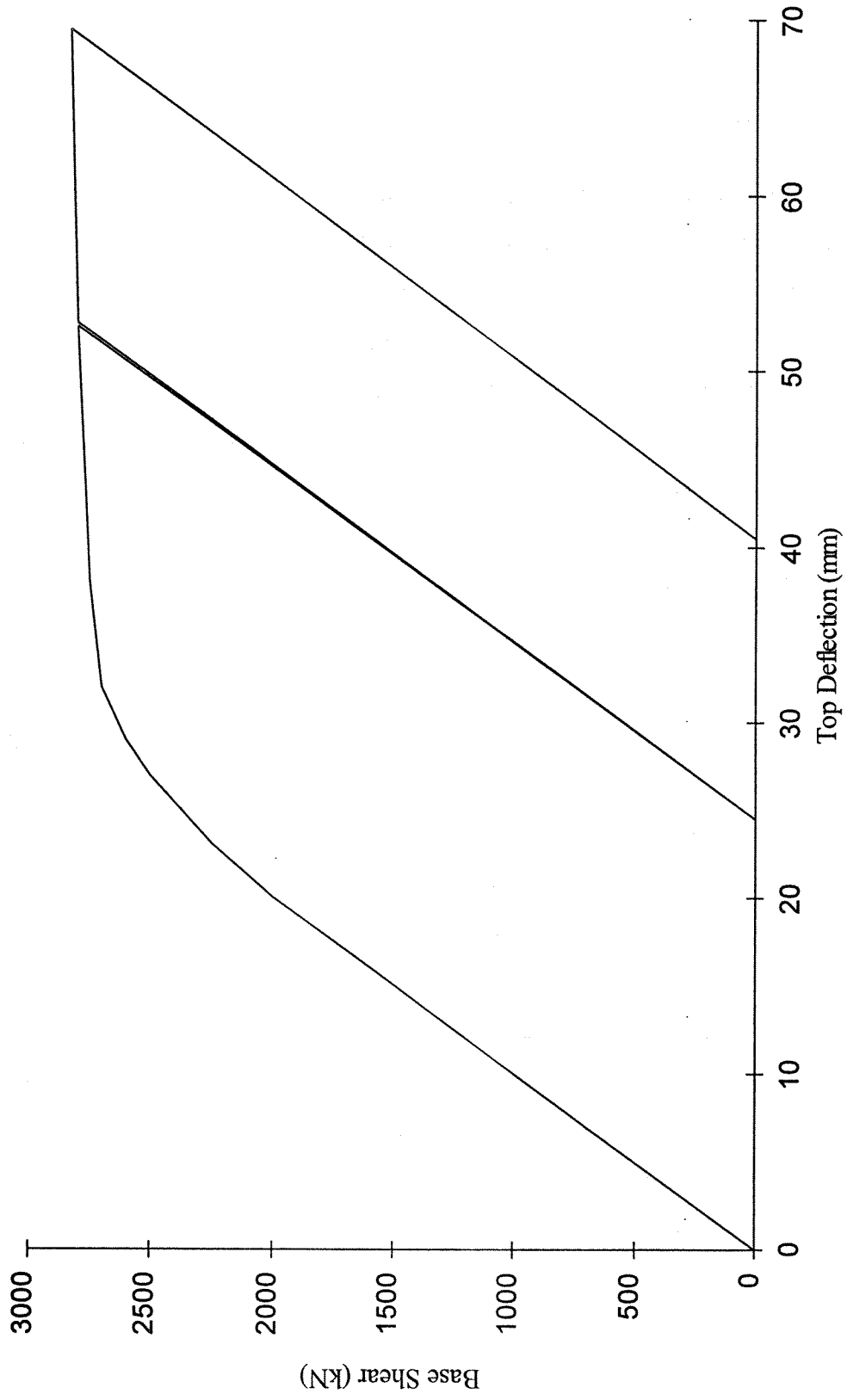


Fig. 4.5 Predicted Base Shear vs. Top Deflection

5. ANCILLARY TESTS

5.1 Introduction

Several ancillary investigations were conducted to complement the multi-storey steel plate shear wall test. A single large-scale test was performed to investigate the adequacy of the detail to be used in the panel corners for connecting the infill plates to the surrounding members. Another study determined the distribution of residual stresses in the column and beam members for use as the initial stress state in the finite element model. The material properties of all infill plates and boundary members were also determined for use in the model.

5.2 Corner Detail Test

5.2.1 Introduction

The single storey steel plate shear wall panels tested under cyclic loading by Tromposch and Kulak (1987) were similar to the panels proposed for the multi-storey test, except that shear-type beam-to-column connections were used. They reported that after 21 cycles of loading had been applied to the specimen, corner tears developed in the fish plates in two of the four corners of each panel. These tears then grew somewhat during the remainder of the test. Because of the extreme and reversing strains present in the corners of the panels during cyclic lateral loading, it was anticipated that tears might also occur in the multi-storey specimen. In order to investigate the effect of these tears on shear panel behaviour, a test was conducted using a detail proposed for the multi-storey shear wall specimen that was similar to that used by Tromposch and Kulak.

5.2.2 Test Set-up and Procedures

The test set-up, as shown in Fig. 5.1, consisted of boundary members and a portion of the infill plate representing a corner of a steel plate shear wall panel. For convenience in loading, the corner was oriented at 45° relative to its position in a real structure. The W310x129 member represents the column of the moment-resisting frame and the W530x101 member represents the beam. The fish plate detail is identical to that selected for the four storey shear wall specimen, shown in Fig. 4.2, and is also seen in Fig. 5.2 where the strap plate that provides some continuity between adjacent fish plates at the corner can also be seen. Double-acting jacks provided a means of opening and closing the joint, simulating the action of the moment-resisting frame oscillating in-plane under the action of cyclic lateral loads. A vertical tensile load—simulating the tension field that develops in the infill plate—was applied by a universal testing machine of 6000 kN capacity during the closing cycles only. During the opening cycles, no load was applied to the plate because any small compressive load that the plate could sustain was considered to be negligible. This is consistent with the observation that as the tension field develops in a panel the thin plate buckles in the orthogonal direction.

Instrumentation included cable transducers to measure the opening and closing movement of the beam and column members and to monitor any horizontal in-plane movement of the top of the plate. Linear variable displacement transformers (LVDTs) monitored the out-of-plane movement of the free ends of the beam and column members. A load cell recorded the applied testing machine load and pressure gauges were used for determining the jack loads.

The displacement criteria selected were a 6 mm in-plane displacement of the beam and column members during closing cycles and a 2 mm displacement during opening cycles, measured perpendicular to the member axes. The measurement was taken using the cable transducers adjacent to the free edge of the plate. These criteria

correspond approximately to movements determined from the finite element analysis, described in Section 4.4, during cycles near the ultimate load. In this manner, all cycles applied would be considered equivalent to the most severe cycles that would be applied to the multi-storey shear wall specimen. During the closing cycles, the vertical tensile load that represented the diagonal tension field was about equal to the yield stress of the plate over a width of 300 mm. Generally, each load or displacement was applied in two steps, alternating between the universal testing machine and the jacks. However, for the first two cycles, three steps were used in order to allow for frequent examination of the specimen in case of unforeseen behaviour.

During the first two opening cycles, severe yielding was apparent in the fish plates near the free edges of the infill plate (locations “a” in Fig. 5.1). Because this was not the area of interest, the opening displacement was reduced from 2 mm used in the first two cycles to about 1.2 mm. (In order to keep point “b” in Fig. 5.1 from moving horizontally, thereby inducing unintended forces in the infill plate, the displacements on the two sides could not be identical.) This resulted in a 30% reduction of the load from that of the first two cycles. In any case, it was anticipated that the local distortion from the closing cycles would have the greatest effect on the corner region being investigated. Load control was used in the opening cycle thereafter, with a maximum intensity of 210 kN per jack. Even so, cracking was observed at the free end of the fish plate (locations “a”) after Cycle 6. This was repaired with out-of-plane stiffeners at each end, in order to prevent failure from occurring there.

Displacement control continued to be used during closing cycles. However, an increasing residual inward (closing) displacement in the order of about 0.1 mm was observed during each cycle, although no yielding of the V-frame was apparent. By Cycle 13, the load required to reach the prescribed closing displacement of 6 mm from the original position had dropped substantially because of the increasing residual displacement. Because the cycles were intended to be of equal intensity, load control

was then adopted for the closing cycles using a load of 280 kN. This control was based on the load required for the appropriate displacement in the first cycle. For the remainder of the test, the loading was applied in this manner until a total of 35 complete loading cycles had been applied.

5.2.3 Test Results

The flaking of whitewash revealed yielding in many locations along both sides of the fish plates during Cycle 1. During the first opening cycle, yielding was observed in the infill plate along the fillet weld on the north side. (The strap plate was connected to the north side.) Some yielding was also noted in a central vertical band approximately 50 mm wide and 250 mm high on the south side of the infill plate.

By Cycle 6, both sides of the infill plate had yielded extensively in the lower corner area. On the north side, yielded areas developed in the east and west corners during opening cycles. Very little additional yielding was apparent from the whitewash in subsequent cycles.

One and one-half wavelength out-of-plane buckles developed in the infill plates on the line a-a (Fig. 5.1) at mid-height. During a closing cycle, the maximum buckle amplitude between adjacent peaks increased gradually from 27 mm in Cycle 13 to 31 mm in Cycle 35. This reduced to about 5 mm during opening cycles, and upon unloading at the end of a complete cycle the residual amplitude was about 13 mm.

The first two tears were observed during Cycle 16, both on the north side. One tear (1.60 mm long as measured using a calibrated microscope) occurred in the bottom corner of the fish plate-to-infill plate fillet weld and propagated transversely across the fillet weld by Cycle 19. The tear widened visibly and propagated during opening cycles. A second tear (1.27 mm long) formed along the fillet weld at the top of the strap plate and continued to grow in the westerly direction throughout the test,

although by the end of the final cycle the rate of growth was extremely slow. The tear extended around the top west corner of the strap plate by Cycle 30. It tended to open and propagate during closing cycles. These tears and the other two tears on the north side, described subsequently, can be seen in Fig. 5.3 during the final opening cycle. (The whitewash has been removed from these areas.)

A third tear was noted during Cycle 23 along the top of the fillet weld joining the fish plate and infill plate on the north side. It was 20 mm long and of hairline width when discovered, and grew to 36 mm by the end of the test. This tear appeared to propagate during the opening cycles.

A fourth tear (1.52 mm long) was detected during Cycle 25 in the fillet weld connecting the fish plates and infill plate on the south side at the 6 mm gap between the column fish plate and the beam fish plate. This tear did not change in subsequent cycles.

A fifth tear was noted during Cycle 30 that was actually an extension of the strap plate fillet weld tear (second tear) described above, propagating in the opposite (easterly) direction. This tear grew from 14 mm to 20 mm by Cycle 33, after which no change was observed. The tear appeared to propagate during closing cycles.

After the test was completed, the entire corner region around the strap plate was cleaned and then sprayed with dye penetrant in an attempt to reveal any as yet undiscovered tears, but none was found.

Because of the slight residual deformation of the V-frame during each cycle, the infill plate and fish plate assembly was cut out with a torch in 10 stages, with the rebound of the frame measured at each stage. A total rebound of about 1 mm on each side was recorded, representing a recovery of about 25-30% of the residual deformation.

5.2.4 Conclusion

The test specimen behaved generally as expected. Tears did form in the corner region that were similar to those observed by Tromposch and Kulak (1987) in their specimen with shear-type beam-to-column connections that cause severe plate pinching. The formation of each tear, however, caused no significant change in the load vs. deflection behaviour of the assembly. The 35 cycles that were applied were all severe cycles in terms of loading and deformations, so the damage imparted to the corners of the actual shear walls (with moment-resisting frame connections) would be less severe. It was concluded that the tears were not detrimental, and therefore the fabrication details in the corner test specimen were judged to be adequate and suitable for use in the multi-storey shear wall test.

5.3 Residual Stress Measurements

5.3.1 Introduction

The magnitude and distribution of the residual stresses in the hot-rolled wide flange sections used to construct the moment-resisting frame of the multi-storey shear wall specimen were determined because they may influence the overall behaviour. As all members of a given section size in the test specimen were cut from one piece, an additional 1500 mm length from the same piece was used for ancillary tests. Residual stress specimens were taken a minimum of 450 mm from any flame-cut edge. The specimens were cut from the ancillary piece by cold-sawing.

5.3.2 Standards and Procedures

Residual stresses were determined according to the method of sectioning outlined in Technical Memorandum No. 6 of the Guide to Stability Design Criteria for Metal Structures (Galambos 1988). A 150 mm length of the ancillary test specimen was marked off and then further marked into a series of strips. Gauge points

were located on each side of each strip 100 mm apart. At the web-to-flange junction, four sets of gauge marks were used. Hardened steel balls of 1.6 mm diameter were embedded at each of the gauge points by means of a special punch. The gauge lengths were measured using a mechanical extensometer before and after the strips were cut from the ancillary test piece. Cutting was done slowly and was carried out by cold-sawing with cutting oil. The difference in gauge length before and after longitudinal sectioning, as measured by the extensometer, is used to calculate the residual strains that were previously locked into the cross-section of the member. The flange and web moduli of elasticity used for calculating residual stresses were determined from the tension coupon tests described in Section 5.4.

The precision of the instrument used in the strain measurements is ± 0.001 mm, which in a gauge length of 100 mm corresponds to an error in stress in the elastic region of approximately ± 2 MPa in structural steel. In order to obtain a statistical confidence in the recorded measurements, the number of required measurement repetitions were determined using a particular application of the t test (e.g., Kennedy and Neville 1976). Generally, the t test is used to determine whether two samples being compared are drawn from the same population. The same principle can be used to determine whether a single sample is drawn from a particular population. In this case, the principle is applied to determine whether the sample mean (mean of the measured values) is an appropriate estimate of the population (true) mean, within a prescribed error tolerance, E , and statistical level of confidence.

The value t is defined as the number of standard deviations of the mean, $\sigma_{\bar{x}}$, that the sample mean, \bar{x} , is likely to be from the population mean, μ , within a certain level of probability. Thus:

$$|\mu - \bar{x}| = t \sigma_{\bar{x}} \quad [5.1]$$

The standard deviation of the mean is defined as the standard deviation of the means of all possible distinct samples of size n from a certain population. When the population size is infinite, as is the case when taking an arbitrary number of measurements of a single quantity, this implies that it is the standard deviation of the mean of an infinite number of samples of size n . When the population is large compared to the sample size, the standard deviation of the mean can be calculated from the standard deviation of the population, s , according to the equation (Kennedy and Neville 1976):

$$\sigma_{\bar{x}} = \frac{\sigma}{\sqrt{n}} \quad [5.2]$$

When the actual standard deviation of the population is not known but can be estimated, the standard deviation of the mean can be estimated by the equation:

$$s_{\bar{x}} = \frac{s}{\sqrt{n}} \quad [5.3]$$

where s replaces σ to indicate that the quantities are estimated. Substituting the estimated quantity $s_{\bar{x}}$ for $\sigma_{\bar{x}}$ in Eq. 5.1 leads to the equation:

$$|\mu - \bar{x}| = t \left(\frac{s}{\sqrt{n}} \right) \quad [5.4]$$

The estimate of the standard deviation of the population can in this case be obtained by using the standard deviation of the sample. The size of the sample does not need to be large for this estimate to be used, as is the case for the normal distribution test, where an approximately normal distribution within the sample is presumed.

The value of the statistic t can be obtained from tables (e.g., Kennedy and Neville 1976) based on the number of readings and the required confidence level. The number of readings is the same as that used for the estimate of s . The left side of

Eq. 5.4 is set equal to the error that can be tolerated, E , in the mean value. Therefore, the number of readings required to satisfy the error tolerance and confidence level is determined according to the equation:

$$n = \left(\frac{st}{E} \right)^2 \quad [5.5]$$

Accepting an error of 0.003 mm (6 MPa), and with a probability of 90% that the mean of the measurements will be within this error, a value of t was determined based upon the number of measurements taken in the sample. (In the specified case, the mean of the measured values will be within t standard deviations of the mean 90% of the time.) By calculating the standard deviation of the measurements at a set of gauge points, the number of measurements required in order to satisfy the acceptance criteria above was determined according to Eq. 5.5.

If the number of required measurements was greater than the number of measurements taken, an additional measurement was made and the check performed again incorporating the new value. When the number of required measurements was less than or equal to the number of measurements taken, the error of the mean value of the measurements exceeds 0.003 mm in no more than 10% of the cases. This procedure follows the recommendations of ASTM standard E122 (ASTM 1989) for the choice of statistical sampling sizes to estimate the average value of some property, but has been modified to account for the relatively small number of measurements by using the t value which is a function of the number of individual readings.

Because of the labour-intensive nature of these measurements, for the purpose of this investigation a minimum of three and a maximum of five measurements were taken at each set of gauge points. Even with this practical limitation of taking a maximum of five measurements, the acceptance criteria were not met in only 4.9% of cases. If the acceptance criteria were modified to an error, E , of 0.004 mm (8 MPa),

with a probability of 95% that the mean value will be within this error, then the acceptance criteria would not be met in 5.4% of cases. If the requirements were relaxed to an error of 0.005 mm (10 MPa), with a probability of 90% that the mean value will be within this error, only 0.8% of the cases would not be satisfied.

A gauge length on an independent steel bar was also measured at regular intervals to assess the effects of temperature fluctuations on the measurements. These effects, although slight, were taken into account in the data analysis to determine the net strains due only to the relaxation of residual stresses.

5.3.3 Results

The residual stress distributions for the three member types are plotted in Figs. 5.4, 5.5, and 5.6. Each value plotted is determined as the mean for the two sides of the strip. The moduli of elasticity used in the calculation of stresses, determined from mean values measured in the tension coupon tests, were 204 400 MPa, 207 700 MPa and 211 200 MPa for the W310x118, W310x60 and W530x82 flanges, respectively, and 198 800 MPa, 196 500 MPa, and 201 000 MPa for the W310x118, W310x60 and W530x82 webs, respectively.

For each section, the residual stress pattern is typical for hot-rolled, wide-flange steel members. Large tensile residual stresses are present at the web-to-flange junction, where cooling of the member is slowest. Maximum measured values were 92 MPa, 95 MPa, and 225 MPa for the W310x118, W310x60 and W530x82, respectively. However, some peak values may be significantly higher between the measurement locations. The central portion of all webs contained large compressive residual stresses: peak values were -152 MPa, -137 MPa, and -115 MPa for the W310x118, W310x60, and W530x82, respectively. The stresses at the flange tips varied from relatively large compressive residual stresses in the W310x118 member to small tensile residual stresses in the W530x82 member. Maximum measured

values in these regions were -76 MPa, -31 MPa, and $+21$ MPa for the W310x118, W310x60, and W530x82, respectively. The residual stresses in the flange tips of the W310x60 member appear to have been affected by the process of rotarizing, or cold-straightening. Other than this disturbance, the measured residual stresses are indicative of residual stresses derived primarily from the cooling process, during and after rolling.

In order to establish confidence in the results of the residual stress patterns determined—and in the overall experimental method—a detailed check was performed to determine how close the resulting axial forces were to reflecting static equilibrium. Residual forces were calculated for each strip. This calculation was based on the measured residual stresses (in some cases peak values between measurement points had to be estimated) and the measured areas. The calculated forces were then summed to determine the net cross-sectional force in the presence of residual stresses, which should equal zero for static equilibrium. Because of the inevitable experimental error, the tensile and compressive forces determined in each cross-section were not precisely equal. For each cross-section, the mean of the tensile and compressive forces was determined as an estimate of the magnitude of the true forces. The error of the calculated forces with respect to this estimate of the true forces gives one check on the validity of the residual stress patterns determined. These errors were 2.9%, 7.0%, and 2.5% for the W310x118, W310x60, and W530x82, respectively. Examination of the residual stress patterns indicates that they are close to doubly-symmetric and therefore the moments about the x and y principal axes are also close to zero. To correct for the slight experimental errors, a combination of a uniform axial stress and linearly varying bending stresses about the two axes could be added to satisfy the three equilibrium equations. The finite element model automatically makes the correction by establishing global equilibrium prior to application of any external loading.

5.3.4 Summary

The results of the investigation of residual stresses across the cross-sections of the column and beam members established an initial distribution of stresses present in the shear wall specimen prior to the test. For the most part, the residual stress distributions are typical of hot-rolled wide flange members with the stresses developing as a result of differential cooling rates in the various regions of the cross-section. In order to include the effect of residual stresses in the finite element model, these patterns are used as the initial stress state.

5.4 Tension Coupon Tests

5.4.1 Introduction

A total of 18 tension coupons from the three different infill plates (Panels 1 and 2 were cut from the same plate) were tested in uniaxial tension to determine the stress vs. strain behaviour. Six coupons were tested from each plate, with three taken in each rolling direction. Because of the importance of using steel with hot-rolled characteristics, from two to four of the coupons from each plate were tested prior to the main test. Plates exhibiting cold-worked or other atypical characteristics were discarded.

A total of 44 tension coupons from the three boundary members were tested in uniaxial tension. Sixteen coupons were taken from the W310x118, 12 coupons were taken from the W310x60, and 16 coupons came from the W530x82. In each case, with the exception of a small region near the web-to-flange junction, the entire cross-section was utilized.

5.4.2 Standards and Procedures

Testing of the tension coupons followed the requirements of ASTM standards A370 (ASTM 1992a) and E8M (ASTM 1992b). The coupons from the infill plate

materials were cut and machined to meet the requirements for “sheet-type” specimens that may have a thickness of up to 19 mm. The coupons cut from the boundary members were proportioned as “plate-type” specimens that are required to have a minimum thickness of 5 mm.

All coupon tests were conducted in a universal testing machine of 1000 kN capacity. Strains were recorded using an electro-mechanical extensometer with a gauge length of 50 mm. In order to determine the modulus of elasticity, approximately 20 readings were taken in the elastic region. Three static yield readings were taken on the yield plateau and one at the ultimate load for each test. The final elongation was determined using dividers on a gauge length of 50 mm for the sheet-type specimens and 200 mm for the plate-type specimens.

5.4.3 Test Results

5.4.3.1 Infill Plates

The results of the tests for the plates from Panels 1 to 4 are shown in Table 5.1. The mean, standard deviation, and coefficient of variation are given for all the key stress and strain values for each plate. Note that the mean static yield and ultimate stresses in the plates of Panels 3 and 4 are much lower than those of Panels 1 and 2. The strain-hardening strain of Panel 4 is much lower than those of Panels 1 through 3. All plates displayed extremely ductile behaviour, with failure strains in excess of 34%.

5.4.3.2 Boundary Members

The results of the tests for the boundary members—W310x118 (columns), W310x60 (beams at levels 1, 2, and 3), and W530x82 (beam at level 4)—are shown in Tables 5.2, 5.3, and 5.4, respectively. As shown in the tables, four coupons were cut from each beam flange and six from each column flange. Four coupons were cut

from each of the W310x118 and W310x60 webs, while eight coupons were taken from the deeper W530x82 web. The mean, standard deviation, and coefficient of variation are given in the tables for all the key stress and strain values for each member. The mean static yield stress is somewhat lower for the W310x118 member than for the other members, although the mean static ultimate stresses are similar. In each case, the web yield stress is higher than that for the flange, as would be expected, although for the W530x82 member the difference is not large. The modulus of elasticity was greater for the flanges than for the webs of each member. All coupons failed at a strain of approximately 26%.

The top and bottom web coupons for the W310x118 (CW1 and CW4) and the W530x82 (TBW1 and TBW8) members did not exhibit a well-defined yield plateau. Therefore, yield stresses and yield and ultimate strains for these specimens are not shown in the tables and are not included in the statistical calculations. This phenomenon is either related to the final passes of the member through the forming rolls after significant cooling had taken place or perhaps to the process of rotarizing. When these shapes are cold-straightened by rotorizing, plastic deformation is imparted to the flanges through rollers applied to the webs. This results in a severe and complex state of stress and strain from cold-working of the material in the region of the web immediately adjacent to the flanges. Large through-thickness residual strains—which would not be revealed by the residual stress measurements described in the previous section—would be present in this region. These residual strains cause early yielding and early strain-hardening of the material. All members did display evidence that some cold-straightening had taken place. Since this phenomenon is specific to members that have been cold-straightened, it should not be assumed to be generally present.

5.4.4 Summary

The results of the tension coupon tests give detailed information on the stress vs. strain material behaviour at all points in the shear wall specimen. This information—in aggregate form—is included in the finite element model so as to enable the program to simulate the material behaviour that was present in the test specimen.

Table 5.1 Infill Panel Tension Coupon Test Results

Coupon Mark	Elastic Modulus (MPa)	Upper Yield (MPa)	Lower Yield (MPa)	Static Yield 1 (MPa)	Static Yield 2 (MPa)	Static Yield 3 (MPa)	Mean Static Yield (MPa)	Static Ultimate (MPa)	Failure Stress (MPa)	Yield Strain (%)	Hardening Strain (%)	Ultimate Strain (%)	Failure Strain (%)	Comments
Panels 1&2														
5HC1	201107	367.0	357.4	337.5	333.3	338.0	336.3	456.9	374.2	0.185	2.64	20.4	32.0	
5HC2	212440	360.6	350.6	348.3	340.9	331.3	340.2	450.9	372.1	0.169	2.78	19.7	35.6	
5HC3	217784	362.6	355.8	348.0	346.1	345.6	346.6	456.9	373.6	0.164	2.62	19.5	35.2	
5HC4	205858	373.2	352.1	342.2	338.3	337.2	339.2	454.4	365.8	0.189	2.50	20.9	32.8	
5HC5	212081	369.9	355.1	347.1	341.4	341.2	343.2	457.8	359.2	0.176	2.81	19.8	35.6	
5HC6	203740	359.6	357.0	339.8	340.8	344.6	341.7	459.7	354.0	0.164	2.34	20.2	34.2	
Mean	208835	365.5	355.4	343.8	340.1	339.7	341.2	456.1	366.5	0.175	2.62	20.1	34.2	
St. Dev.	6295.6	5.44	1.90	4.61	4.20	5.29	3.52	3.07	8.36	0.01	0.18	0.52	1.53	
Coef. Var. (%)	3.01	1.49	0.53	1.34	1.23	1.56	1.03	0.67	2.28	6.11	6.79	2.57	4.47	
Panel 3														
3C1	208526	278.8	273.1	266.3	263.7	262.3	264.1	345.2	264.4	0.127	2.85	19.0	41.8	
3C2	220521	293.1	279.4	267.4	256.6	260.9	261.6	344.0	268.1	0.133	2.52	19.2	40.2	
3C3	210883	280.5	277.9	263.7	265.1	265.4	264.7	343.1	294.5	0.133	2.58	18.6	41.4	
3C4	200754	275.5	263.9	251.1	248.7	248.5	249.5	342.9	288.5	0.146	1.72	20.4	45.6	
3C5	214452	283.9	265.9	251.0	249.5	248.8	249.8	344.5	252.9	0.140	2.46	21.2	43.2	
3C6	210251	269.8	267.8	252.8	255.0	251.9	253.2	344.3	295.7	0.124	2.49	21.5	43.0	
Mean	210898	280.3	271.3	258.7	256.4	256.3	257.2	344.0	277.3	0.134	2.44	20.0	42.5	
St. Dev.	6544.9	7.91	6.45	7.88	6.89	7.42	7.14	0.87	17.91	0.01	0.38	1.23	1.86	
Coef. Var. (%)	3.10	2.82	2.38	3.04	2.69	2.90	2.78	0.25	6.46	6.21	15.40	6.13	4.38	
Panel 4														
3A2C1	224210	282.4	274.8	265.2	260.2	239.8	255.1	370.8	312.5	0.142	1.25	15.5	33.4	
3A2C2	207246	268.7	266.4	258.0	255.4	258.0	257.1	376.3	291.2	0.137	1.48	18.0	34.6	
3A2C3	202434	261.7	252.5	246.2	247.4	N/A	246.8	363.9	298.1	0.128	1.37	15.9	30.4	2 statics yield points
3A2C4	189944	275.8	274.6	264.2	262.0	263.0	263.0	378.6	301.0	0.148	1.54	18.3	36.0	
3A2C5	200356	289.6	285.6	273.6	273.9	271.5	273.0	386.8	307.1	0.150	1.45	19.5	33.8	
3A2C6	194281	297.3	289.9	259.9	282.2	279.8	274.0	375.7	306.2	0.162	2.07	18.9	36.2	
Mean	203079	279.3	274.0	261.2	263.5	262.4	261.5	375.3	302.7	0.145	1.53	17.7	34.1	
St. Dev.	12013.9	13.23	13.47	9.13	12.63	15.16	10.67	7.69	7.54	0.01	0.29	1.63	2.12	
Coef. Var. (%)	5.92	4.74	4.92	3.50	4.79	5.78	4.08	2.05	2.49	8.05	18.74	9.20	6.23	

Notes:

1. Coupon marks ending in 1, 2, or 3 are oriented perpendicular to the rolling direction.
2. Coupon marks ending in 4, 5, or 6 are oriented parallel to the rolling direction.

Table 5.2 W310x118 Tension Coupon Test Results

Coupon Mark	Elastic Modulus (MPa)	Upper Yield (MPa)	Lower Yield (MPa)	Static Yield 1 (MPa)	Static Yield 2 (MPa)	Static Yield 3 (MPa)	Mean Static Yield (MPa)	Static Ultimate (MPa)	Failure Stress (MPa)	Yield Strain (%)	Hardening Strain (%)	Ultimate Strain (%)	Failure Strain (%)	Comments
Top Flange														
CF1	216504	345.2	333.2	319.1	320.1	320.2	319.8	479.0	377.2	0.162	1.59	16.4	28.4	
CF2	219691	328.8	315.7	305.2	305.6	N/A	305.4	477.3	416.7	0.163	1.49	15.8	27.4	2 static yield points
CF3	203771	326.7	309.6	303.2	302.7	303.2	303.0	482.3	394.8	0.157	1.10	16.0	26.3	
CF4	204198	330.1	309.5	301.8	301.5	300.0	301.1	479.8	386.1	0.167	1.01	15.3	27.0	
CF5	196589	340.1	318.2	307.1	304.6	303.4	305.1	477.2	371.9	0.172	1.23	15.1	28.3	
CF6	192674	332.6	327.0	317.9	315.1	314.1	315.7	477.4	405.2	0.163	1.54	15.9	28.9	
Web														
CW1	195237	N/A	N/A	N/A	N/A	N/A	N/A	492.5	443.0	N/A	N/A	16.0	25.0	no plateau
CW2	200923	361.0	347.9	334.8	335.7	338.4	336.3	489.2	451.0	0.178	1.88	16.5	27.2	
CW3	201665	363.2	346.3	346.7	343.3	344.0	344.7	487.8	422.8	0.179	1.96	14.5	24.0	
CW4	197185	N/A	N/A	N/A	N/A	N/A	N/A	486.2	429.1	N/A	N/A	11.3	15.4	no plateau, material flaw
Bot. Flange														
CF7	204489	348.9	334.1	320.3	320.0	317.1	319.1	478.6	392.9	0.177	1.61	15.4	27.8	
CF8	206906	344.3	321.8	312.4	310.3	310.8	311.2	479.6	405.5	0.174	1.48	16.0	27.3	
CF9	193976	324.0	313.1	302.3	301.8	301.9	302.0	482.3	402.7	0.173	1.15	16.2	25.7	
CF10	219052	309.3	308.6	297.4	295.8	294.1	295.8	479.3	383.3	0.149	0.94	14.4	26.3	
CF11	206234	339.6	316.8	305.5	306.6	305.9	306.0	478.0	385.2	0.165	1.26	16.2	27.5	
CF12	188769	349.7	325.0	317.5	316.1	315.2	316.3	480.4	369.8	0.186	1.50	16.5	28.3	
Mean	202991	338.8	323.3	313.7	312.8	312.9	313.0	481.7	402.3	0.169	1.41	15.5	26.3	
St. Dev.	9239.2	14.76	12.99	13.78	13.52	14.65	13.81	4.73	24.58	0.0100	0.307	1.29	3.18	
Coeff. Var. (%)	4.55	4.36	4.02	4.39	4.32	4.68	4.41	0.98	6.11	5.89	21.7	8.34	12.1	
Mean Top Fl.	205571	333.9	318.9	309.0	308.3	308.2	308.3	478.8	392.0	0.164	1.33	15.7	27.7	
St. Dev.	10686.92	7.23	9.53	7.54	7.54	8.57	7.55	2.00	17.04	0.0050	0.246	0.49	0.98	
Coeff. Var. (%)	5.20	2.17	2.99	2.44	2.45	2.78	2.45	0.42	4.35	3.07	18.51	3.14	3.55	
Mean Bot Fl.	203238	336.0	319.9	309.3	308.4	307.5	308.4	479.7	389.9	0.171	1.32	15.8	27.1	
St. Dev.	10669.91	16.08	9.09	8.97	8.97	8.66	8.84	1.53	13.32	0.0126	0.251	0.76	0.96	
Coeff. Var. (%)	5.25	4.79	2.84	2.90	2.91	2.82	2.86	0.32	3.42	7.37	18.96	4.82	3.54	
Mean Web	198753	362.1	347.1	340.7	339.5	341.2	340.5	488.9	436.5	0.179	1.92	14.6	22.9	
St. Dev.	3055.449	1.53	1.11	8.47	5.36	3.98	5.94	2.69	12.82	0.0008	0.058	2.36	5.17	
Coeff. Var. (%)	1.54	0.42	0.32	2.48	1.58	1.17	1.74	0.55	2.94	0.43	3.02	16.19	22.59	
Mean Both Fl.	204404	334.9	319.4	309.1	308.4	307.8	308.4	479.2	390.9	0.167	1.33	15.8	27.4	
St. Dev.	10254.14	11.93	8.90	7.90	7.90	8.19	7.84	1.75	14.62	0.0098	0.237	0.61	0.97	
Coeff. Var. (%)	5.02	3.56	2.79	2.56	2.56	2.66	2.54	0.37	3.74	5.86	17.87	3.88	3.54	

Note:
Failure strains are measured on a 200 mm gauge length.

Table 5.3 W310x60 Tension Coupon Test Results

Coupon Mark	Elastic Modulus (MPa)	Upper Yield (MPa)	Lower Yield (MPa)	Static Yield 1 (MPa)	Static Yield 2 (MPa)	Static Yield 3 (MPa)	Mean Static Yield (MPa)	Static Ultimate (MPa)	Failure Stress (MPa)	Yield Strain (%)	Hardening Strain (%)	Ultimate Strain (%)	Failure Strain (%)	Comments
Top Flange														
BF1	200379	349.1	330.7	321.7	322.4	320.6	321.6	472.6	430.0	0.189	1.28	15.8	26.4	
BF2	205961	334.1	320.6	309.1	310.8	N/A	310.0	497.0	424.7	0.190	1.08	11.7	27.3	2 static yield points
BF3	226448	335.8	324.7	312.2	313.1	312.2	312.5	474.1	406.3	0.179	1.80	16.6	26.4	
BF4	207388	341.2	330.4	320.5	322.2	320.9	321.2	476.4	400.2	0.194	1.36	17.7	26.8	
Web														
BW1	198581	388.5	384.6	369.4	369.6	369.9	369.6	485.8	435.9	0.199	1.98	16.6	24.6	
BW2	192336	395.4	386.8	367.0	367.2	367.1	367.1	479.7	444.3	0.199	2.81	17.4	25.7	
BW3	201582	393.4	382.9	367.1	364.1	367.2	366.1	480.3	455.4	0.193	2.54	18.7	26.9	
BW4	193603	380.0	372.4	362.3	358.8	365.4	362.2	482.4	459.9	0.185	1.90	16.5	23.9	
Bot. Flange														
BF5	200247	347.4	328.1	313.0	316.5	317.7	315.8	471.6	426.9	0.188	1.98	17.9	26.9	
BF6	210187	334.0	321.2	308.0	306.7	306.2	307.0	470.3	431.1	0.185	1.90	18.1	25.9	
BF7	205760	332.8	321.7	308.3	308.4	309.0	308.5	472.9	415.3	0.182	1.16	17.2	26.8	
BF8	204893	348.6	332.6	316.1	321.0	320.5	319.2	473.5	439.6	0.210	1.34	17.5	27.2	
Mean	203947	356.7	344.7	331.2	331.7	334.3	331.7	478.0	430.8	0.191	1.76	16.8	26.2	
St. Dev.	8882.8	25.02	27.78	26.41	25.14	26.72	25.97	7.64	18.00	0.0088	0.542	1.79	1.04	
Coeff. Var. (%)	4.36	7.01	8.06	7.97	7.58	7.99	7.83	1.60	4.18	4.59	30.8	10.6	3.95	
Mean Top Fl.	210044	340.0	326.6	315.9	317.1	317.9	316.3	480.0	415.3	0.188	1.38	15.5	26.7	
St. Dev.	11346.41	6.73	4.85	6.17	6.05	4.94	5.96	11.42	14.29	0.0063	0.305	2.61	0.42	
Coeff. Var. (%)	5.40	1.98	1.49	1.95	1.91	1.55	1.88	2.38	3.44	3.34	22.1	16.9	1.59	
Mean Bot Fl.	205272	340.7	325.9	311.4	313.1	313.4	312.6	472.1	428.2	0.191	1.59	17.7	26.7	
St. Dev.	4074.0	8.45	5.46	3.90	6.77	6.86	5.82	1.42	10.08	0.0131	0.406	0.40	0.53	
Coeff. Var. (%)	1.98	2.48	1.67	1.25	2.16	2.19	1.86	0.30	2.35	6.84	25.4	2.2	1.98	
Mean Web	196525	389.3	381.7	366.5	364.9	367.4	366.3	482.1	448.9	0.194	2.31	17.3	25.3	
St. Dev.	4316.0	6.86	6.40	3.00	4.63	1.88	3.10	2.74	10.85	0.0067	0.438	1.01	1.28	
Coeff. Var. (%)	2.20	1.76	1.68	0.82	1.27	0.51	0.85	0.57	2.42	3.46	19.0	5.8	5.06	
Mean Both Fl.	207658	340.4	326.2	313.6	315.1	315.6	314.5	476.0	421.8	0.189	1.49	16.6	26.7	
St. Dev.	8294.2	7.08	4.79	5.35	6.31	6.14	5.80	8.64	13.38	0.0096	0.351	2.10	0.44	
Coeff. Var. (%)	3.99	2.08	1.47	1.71	2.00	1.94	1.84	1.81	3.17	5.08	23.6	12.6	1.66	

Note:
Failure strains are measured on a 200 mm gauge length.

Table 5.4 W530x82 Tension Coupon Test Results

Coupon Mark	Elastic Modulus (MPa)	Upper Yield (MPa)	Lower Yield (MPa)	Static Yield 1 (MPa)	Static Yield 2 (MPa)	Static Yield 3 (MPa)	Mean		Static Ultimate (MPa)	Failure Stress (MPa)	Yield Strain (%)	Hardening Strain (%)	Ultimate Strain (%)	Failure Strain (%)	Comments
							Static Yield (MPa)	Static Yield (MPa)							
Top Flange															
TBF1	215922	369.6	357.0	351.6	351.6	344.0	349.1	486.6	406.9	0.220	1.65	16.4	27.2		
TBF2	219125	363.2	347.3	333.0	335.8	337.7	335.5	486.6	406.9	0.197	1.72	15.8	28.1		
TBF3	205663	366.4	355.3	341.7	339.5	342.3	341.1	488.2	424.6	0.203	1.84	13.7	27.6		
TBF4	218360	378.5	367.5	352.4	350.1	350.7	351.1	492.0	420.1	0.190	1.73	14.4	26.7		
Web															
TBW1	208721	N/A	N/A	N/A	N/A	N/A	N/A	497.4	361.2	N/A	N/A	14.3	25.7	no plateau	
TBW2	188610	374.3	356.5	348.1	347.5	348.1	347.9	489.0	467.4	0.193	2.14	14.8	22.7		
TBW3	197198	386.0	368.7	354.0	357.7	354.3	355.3	492.2	417.5	0.195	2.13	16.4	27.1		
TBW4	203620	379.7	371.2	357.8	361.8	354.3	358.0	493.5	439.5	0.185	2.13	16.0	27.6		
TBW5	198033	391.8	370.9	361.8	358.4	359.8	360.0	494.3	435.2	0.199	2.28	16.9	26.4		
TBW6	205959	387.3	371.8	357.3	355.9	352.7	355.3	493.5	442.0	0.191	2.23	16.9	27.0		
TBW7	206508	378.8	361.6	349.4	350.6	347.0	349.0	489.7	443.9	0.188	1.99	17.0	27.7		
TBW8	198962	N/A	N/A	N/A	N/A	N/A	N/A	498.1	436.9	N/A	N/A	14.7	26.4	no plateau	
Bot. Flange															
TBF5	205457	368.3	363.3	348.7	350.4	342.1	347.1	495.3	419.7	0.261	1.43	15.8	26.5		
TBF6	211241	368.8	362.2	340.6	341.7	340.2	340.8	494.1	427.2	0.219	1.54	13.4	27.8		
TBF7	199890	365.5	353.2	345.4	344.2	343.0	344.2	496.3	407.4	0.209	1.52	15.4	28.0		
TBF8	214181	380.7	364.2	352.0	351.4	N/A	351.7	496.7	384.1	0.206	1.58	15.5	28.2	2 static yield points	
Mean	206092	375.6	361.5	349.5	349.8	347.4	349.0	492.7	421.3	0.204	1.85	15.5	26.9		
St. Dev.	8413.1	8.99	7.97	7.61	7.49	6.57	6.97	3.74	25.17	0.0197	0.293	1.15	1.34		
Coeff. Var. (%)	4.08	2.39	2.20	2.18	2.14	1.89	2.00	0.76	5.98	9.68	15.8	7.47	5.00		
Mean Top Fl.	214772	369.4	356.8	344.6	344.3	343.7	344.2	488.4	414.6	0.203	1.73	15.1	27.4		
St. Dev.	6211.7	6.58	8.30	9.18	7.80	5.39	7.21	2.55	9.08	0.0129	0.079	1.23	0.59		
Coeff. Var. (%)	2.89	1.78	2.33	2.66	2.27	1.57	2.09	0.52	2.19	6.38	4.6	8.18	2.14		
Mean Bot Fl.	207692	370.8	358.2	346.7	346.9	341.8	346.0	495.6	409.6	0.224	1.52	15.0	27.6		
St. Dev.	6339.4	6.76	6.42	4.88	4.75	1.44	4.61	1.17	18.83	0.0256	0.067	1.11	0.79		
Coeff. Var. (%)	3.05	1.82	1.79	1.41	1.37	0.42	1.33	0.24	4.60	11.45	4.4	7.37	2.86		
Mean Web	200951	383.0	366.8	354.7	355.3	362.7	354.2	493.5	430.5	0.192	2.15	15.9	26.3		
St. Dev.	6571.9	6.49	6.28	5.25	5.31	4.67	4.83	3.24	31.16	0.0049	0.097	1.13	1.62		
Coeff. Var. (%)	3.27	1.69	1.71	1.48	1.49	1.32	1.36	0.66	7.24	2.55	4.5	7.11	6.14		
Mean Both Fl.	211232	370.1	357.5	345.7	345.6	342.7	345.1	492.0	412.1	0.213	1.63	15.0	27.5		
St. Dev.	6934.1	6.22	6.91	6.89	6.15	4.03	5.68	4.28	13.94	0.0219	0.133	1.09	0.66		
Coeff. Var. (%)	3.28	1.68	1.93	1.99	1.78	1.18	1.65	0.87	3.38	10.26	8.2	7.21	2.39		

Note:
Failure strains are measured on a 200 mm gauge length.

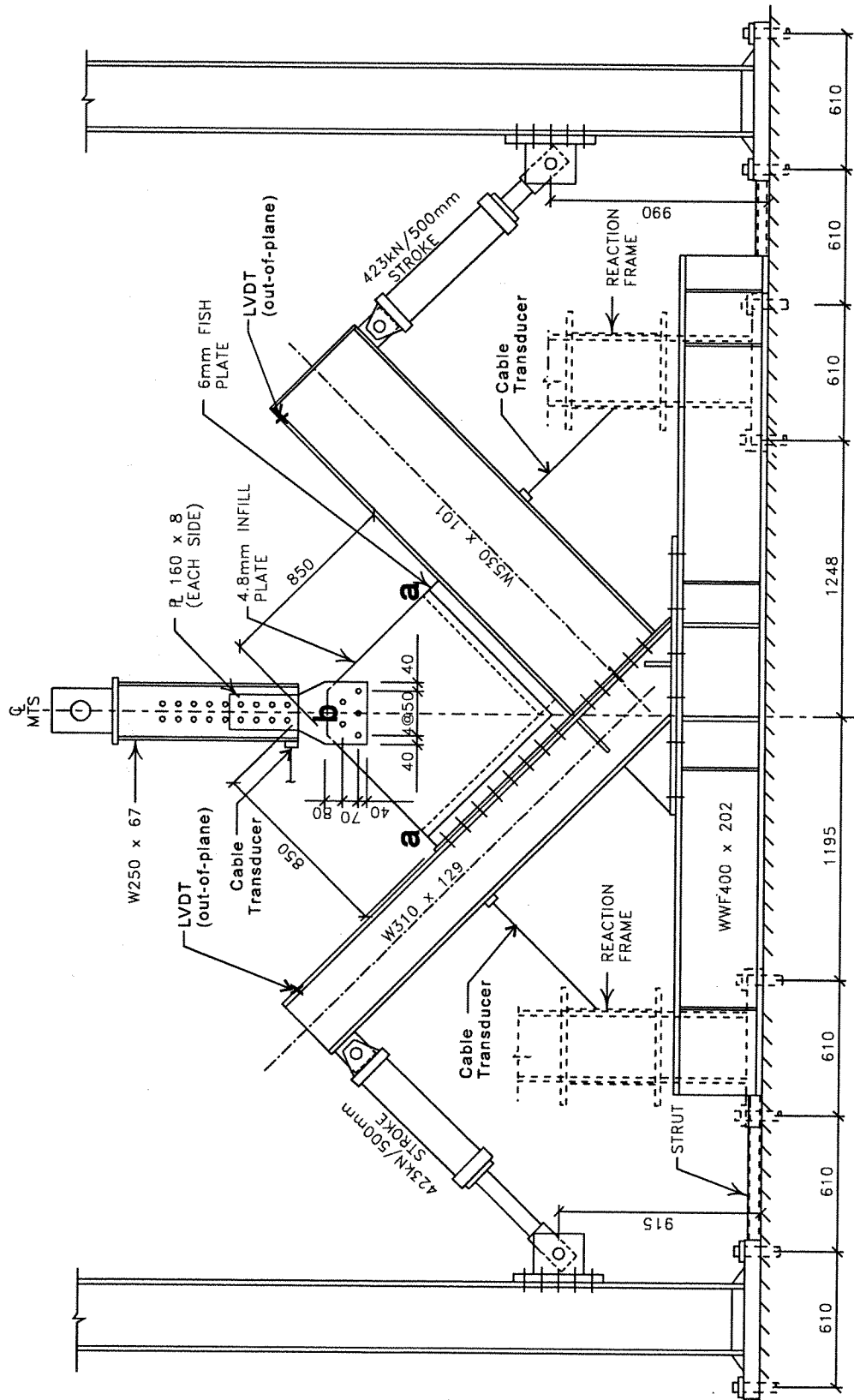


Fig. 5.1 Corner Test Set-up – South Elevation



Fig. 5.2 Corner Test Specimen (North Face)

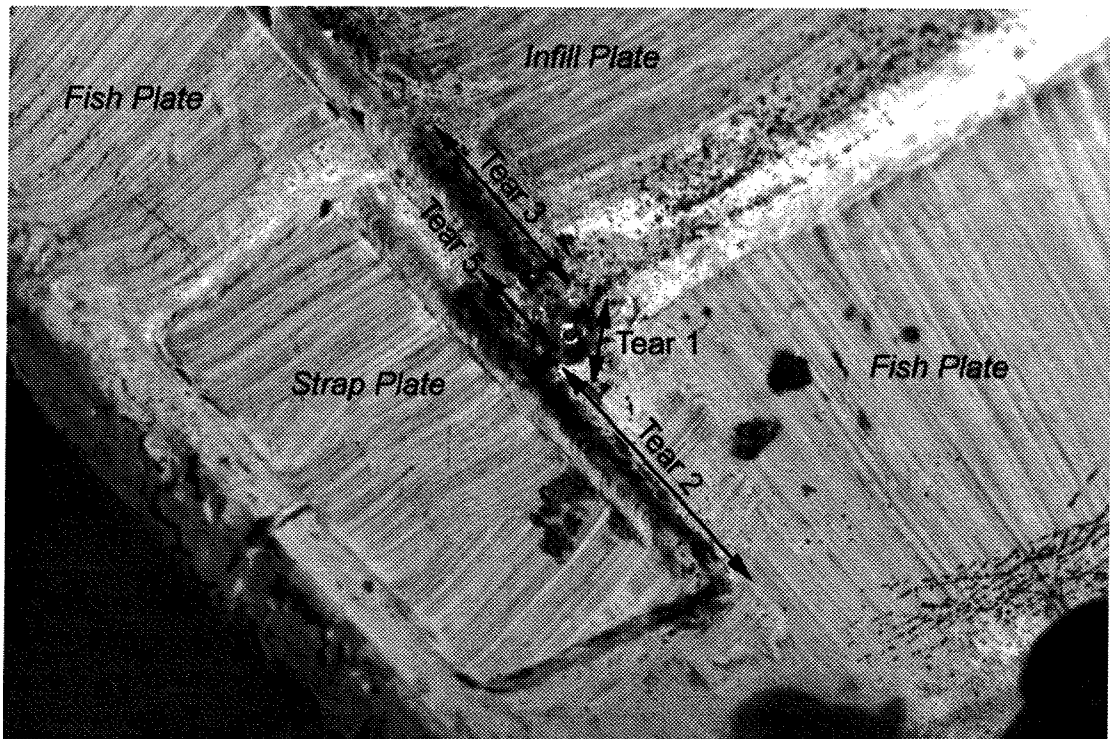


Fig. 5.3 Tears in Corner Region at Conclusion of Test (North Face)

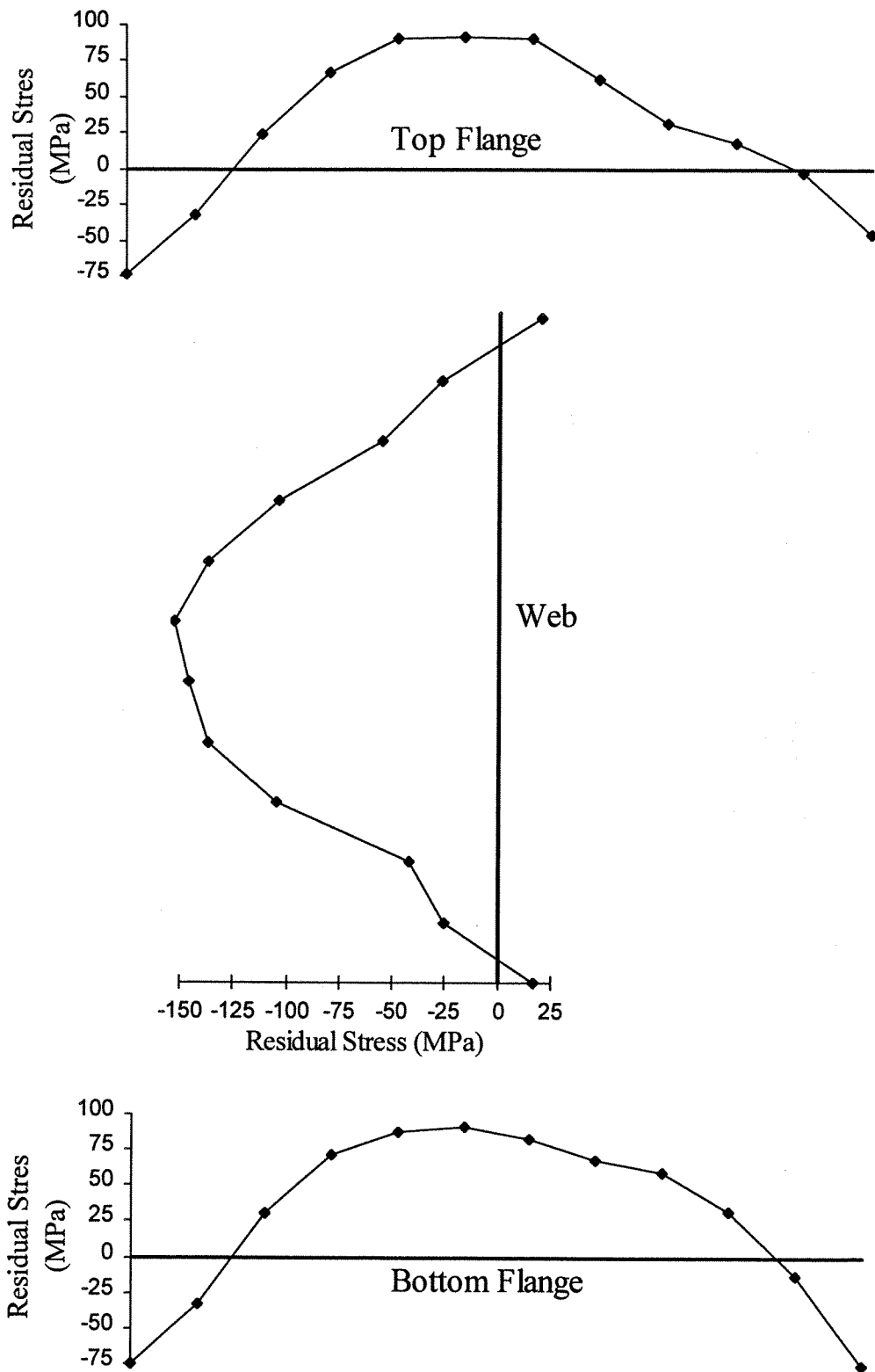


Fig. 5.4 W310x118 Residual Stress Distribution

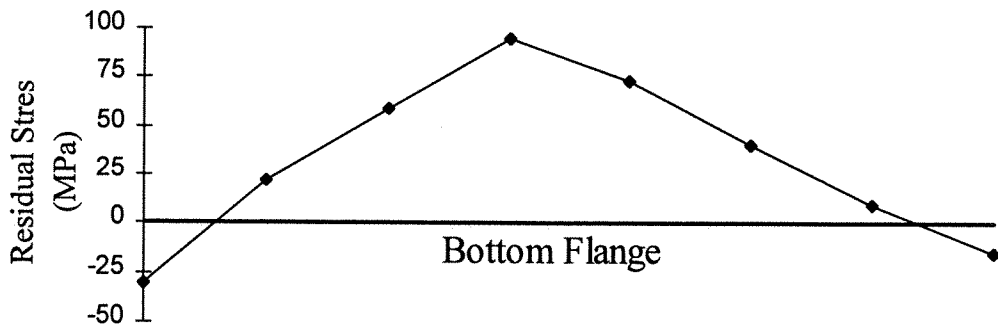
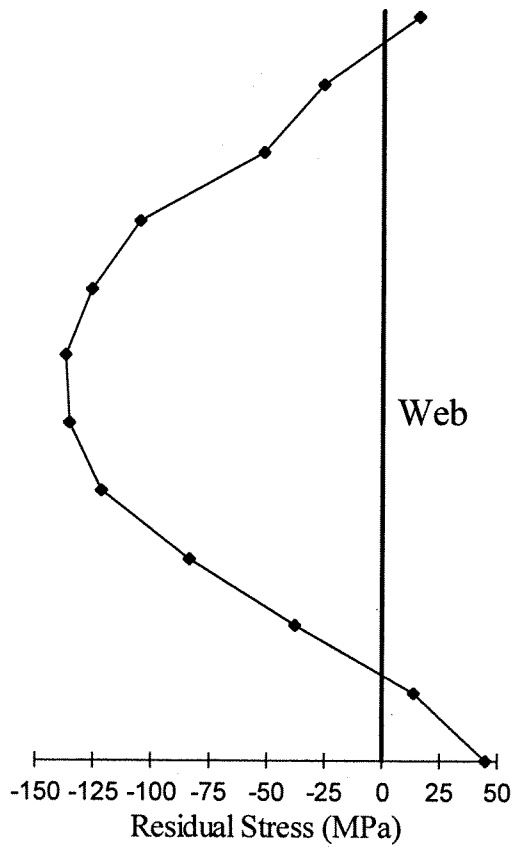
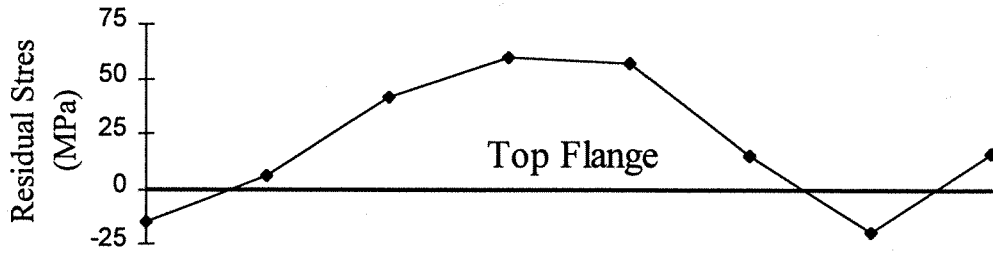


Fig. 5.5 W310x60 Residual Stress Distribution

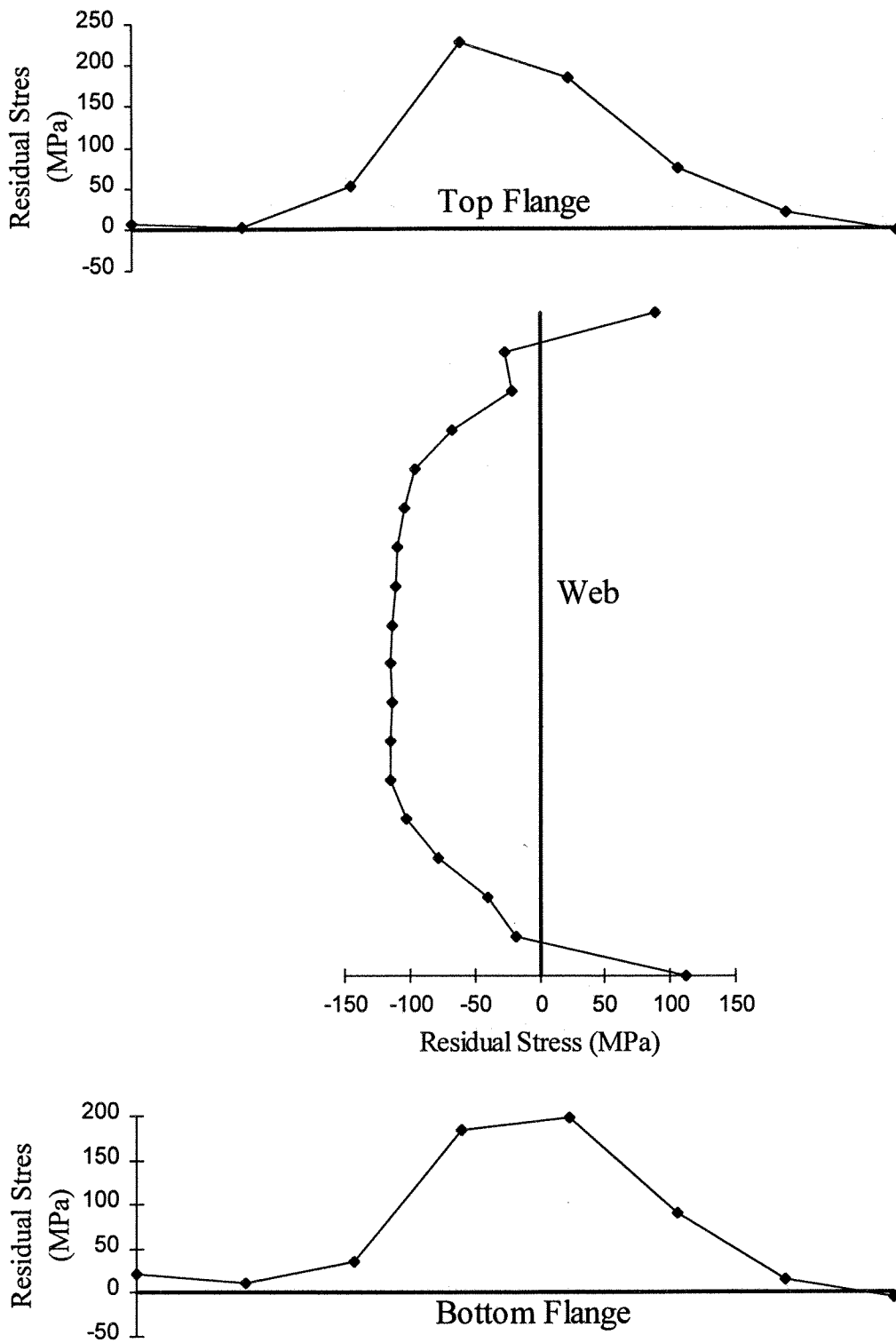


Fig. 5.6 W530x82 Residual Stress Distribution

6. MULTI-STOREY STEEL PLATE SHEAR WALL TEST

6.1 Introduction

The large-scale multi-storey steel plate shear wall specimen was tested in the spring of 1995 in the structural laboratory at the Centre for Engineering Research (C-FER) in Edmonton, Alberta. In this facility, a 500 mm thick reinforced concrete reaction wall, supported by concrete buttresses, was available for applying the horizontal loads and a prestressed concrete strong floor provided the foundation that supported the specimen at the base.

6.2 Test Set-up

The set-up for the shear wall test is depicted in Figs. 6.1, 6.2, and 6.3, and the test specimen alone is shown in Fig. 6.4. The 90 mm thick base plate of the specimen was anchored to the strong floor using 14 two inch diameter high strength steel anchor bolts. The anchor bolts were prestressed to the strong floor so as to minimize the amount of movement due to their elongation under the action of the large overturning moments. These bolts were re-stressed part way through the test to retain this benefit during the latter cycles where the loads were the most severe.

Horizontal loads were applied to the test specimen by means of 890 kN double-acting hydraulic jacks located at each of the four floor elevations. Because the jacks were supplied from a common manifold, the horizontal loads were essentially equal. The vertical loads were applied through a distributing beam at the top of the shear wall and four calibrated tension rods (see Figs. 6.1, 6.2, and 6.3) connected to four 645 kN hydraulic jacks at the base. These jacks were hydraulically independent so that they could be adjusted individually. This was necessary to keep the distributing beam outriggers horizontal, thereby avoiding the risk of unseating the distributing beam at the top of the columns. The position of the distributing beam was

monitored throughout the test by means of an electronic rotation meter (clinometer) connected to the distributing beam web.

Gravity load simulators, similar to those developed at Lehigh University (Yarimci *et al.* 1966), were used to apply the vertical loads. These devices, shown in Figs. 6.1, 6.2, and 6.3, form a pin-jointed mechanism that keeps the loads oriented close to the vertical throughout large horizontal in-plane displacements. This is accomplished without the need for manual adjustments and without causing additional restraint to the specimen. The working capacity of each gravity load simulator is 420 kN. Therefore, four were required to apply the 720 kN gravity loads to each of the two columns of the test specimen.

The shear wall was braced out-of-plane at the ends of each beam at each floor level (eight locations) using an articulated bracing system based on the principle of the Watt mechanism. One such brace is illustrated in Fig. 6.2. A derivative of a similar brace originally developed at Lehigh University (Yarimci *et al.* 1966), this brace is able to accommodate large in-plane displacements of the shear wall without offering any restraint or requiring any manual adjustments. It consists of three rigid links connected by ball-and-socket joints, plus ball-and-socket attachment brackets at each end. The brace point on the test specimen is connected to the Watt brace at the mid-point of the centre link. The brace points at the lower three beams are located on the columns 100 mm below the W310x60 beam bottom flanges in order that the centre brace link can clear the horizontal loading clevises. At the top level, the brace points are at the level of the top flange of the W530x82 beam. Watt braces were also used at each end of the distributing beam to provide the lateral support required for that member.

6.3 Instrumentation and Data Acquisition

Loads were measured at all eight jacks and at the column tops using load cells. Commercial, flat load cells of 890 kN capacity were used to measure the vertical loads applied to the tops of the columns. Four strain gauges affixed to each tension rod in a Wheatstone bridge circuit permitted calibration of the tension rods, so that they acted as additional load cells and provided a redundant set of measurements of the vertical loads.

Custom load cells manufactured at the University of Alberta, capable of measuring loads in both tension and compression, were fitted to the 890 kN hydraulic jacks for measuring the horizontal loads applied at each level. These load cells were cycled through ten complete load reversals slightly beyond the anticipated test load range to be measured before applying high-sensitivity strain gauges. This conditioning procedure improves the linearity of the calibration curve. There was no redundancy of measurement for the horizontal loads as the reaction is taken out through the floor.

In-plane and out-of-plane displacements were measured at each of the four levels of the shear wall using large displacement cable transducers. The out-of-plane measurements monitored the effectiveness of the bracing system. Additional displacement measurements were taken using linear variable displacement transformers (LVDTs) to monitor any movement of the base plate. Two LVDTs were used to measure vertical movements at the column bases and two others to measure vertical movements at intermediate locations between the anchor bolts. From these measurements, the anchorage of the base of the columns and the lowest infill plate were evaluated. Two more LVDTs and two dial gauges monitored horizontal movement and plan rotation of the base plate during the test. All translational measurement locations are depicted in Fig. 6.5. In addition, any small inclination of the tension rods connected to the gravity load simulators was monitored using four

clinometers in order to determine whether the horizontal component of the load applied to the tension rods was of significance. All electronic displacement-measuring devices were calibrated immediately prior to use in this test.

The locations of the 98 electrical resistance strain gauges that were used in the test are shown in Fig. 6.5. Thirty were in the form of ten strain rosettes affixed to Panel 2 (five on each side) in order to determine the state of strains in the panel as it stretched in one direction and buckled in the other. These data also permit the calculation of principal stresses and their orientation. The remainder of the strain gauges were positioned longitudinally on the beam and column flanges, clustered around five of the beam-to-column junctions near the bottom of the specimen where the strains were expected to be highest. From these strains, the participation of the frame in resisting the applied loading is assessed. The gauge length of the rosette strain gauges was 2 mm and the gauge length of the other strain gauges was 5 mm.

A total of 130 data acquisition channels—the capacity of the data acquisition system—were required to read the input from the electronic devices. The data was processed using a commercial software program to display the load vs. deflection curves for each storey and for the shear wall as a whole during the test on a PC monitor. Since the entire load and deflection history could not be predetermined in all its details, the display was customized to provide instantaneous values of parameters important in judging the manner in which the test would be conducted. This software also provided a means of initializing the data acquisition channels when required.

6.4 Load and Deflection History

There are numerous load and deflection histories that could be used to evaluate a structural component for seismic performance. Most slow cyclic tests, the most common approach for simulating earthquake loading, employ a horizontal in-plane load history with gradually increasing loads in successive cycles. Derecho *et al.*

(1980), however, note that in many cases the maximum deformation—or an amplitude close to the maximum—occurs early in the earthquake response. Therefore, the gradually increasing load cycle history may be unconservative. On the basis of studies of reinforced concrete shear walls, Derecho *et al.* (1980) recommend a loading history that has alternating large and small amplitude cycles. However, the traditional loading approach of using gradually increasing loads, although not a particularly good approximation of typical earthquake actions, has several advantages. First, as it is by far the most widely used approach for investigating seismic structural performance, it allows comparison with other experimental programmes. Second, the low intensity initial cycles permit any unforeseen problems to be addressed without damaging the specimen. Third, one does not have to know *a priori* what the maximum excursion should be in order to fully exploit the capabilities of the system. Finally, a “true” equivalent earthquake load history requires many assumptions regarding aspects such as the earthquake input, floor masses, and effects of non-structural elements. This would limit the scope of applicability, while at the same time add unjustified loading complexity.

As a result of this examination, it was considered that adhering to an accepted standard would facilitate the comparison of the results to the findings of other experimental research that has used the same standard. The load and deflection history selected for the shear wall test was based on the method outlined in ATC-24 (Applied Technology Council 1992). This document states that its purpose is to provide guidance in the selection of loading histories and the presentation of results for slow cyclic loading tests, thereby simplifying interpretation and comparison among different research projects. The guidelines are quite simple, but provide flexibility to the experimentalist.

ATC-24 requires that a “deformation control parameter” be selected for controlling the test. It recommends using some parameter related to interstorey drift. In this test, the drift of the lowest storey (Panel 1) was selected because that is where

the majority of the deformation and energy absorption takes place. The force quantity best related to the deformation control parameter is the storey shear in Panel 1 (i.e., the base shear). The method for arriving at a loading strategy is described in ATC-24, whereby a deformation, δ_y , and a load, Q_y , are determined to coincide with the point where “significant” yielding has occurred in the specimen. Although judgement is involved in selecting the point at which this occurs, the resultant terms δ_y and Q_y are considered sufficiently precise for use as test control parameters. The values may be determined experimentally (from a monotonic load test) or predicted analytically. Because there was to be only a single test specimen, values of $\delta_y = 6.1$ mm and $Q_y = 2600$ kN were initially estimated from the finite element analysis. Up to this point, load control was to be used in the test and, subsequently, displacement was to be the controlling parameter.

The specimen proved to be somewhat more flexible than predicted by the analysis. The yield deflection (δ_y) in Panel 1 was selected as 8.5 mm, based on observations made from the load vs. deflection curve up to that point. Prior to reaching this value, single loading cycles of ± 200 kN, ± 400 kN, ± 600 kN, ± 800 kN, and three cycles each of ± 1000 kN and ± 1950 kN were conducted to explore the elastic and the initial inelastic behaviour. These constituted Cycles 1 to 10. After three cycles with a deflection of $\delta_y = 8.5$ mm, the deflection in the first storey was increased by 8.5 mm in each subsequent deformation step. Three cycles were conducted at each deformation step up to a deflection of $3\delta_y$ (Cycles 17 to 19) and two cycles at each deformation step thereafter, following the guidelines of ATC-24.

At a deflection of $5.4\delta_y$ (46 mm), the limit of jack stroke at Level 3 was reached in the direction of loading toward the reaction wall. In all subsequent cycles, this peak deflection was maintained while the peak deflection in the opposite direction was increased as prescribed in ATC-24.

A slight unloading of the horizontal jacks occurred in Cycles 21+ and 24+ when the hydraulic reservoir had to be refilled to replace oil lost through leakage at the jack seals. (Cycles designated as + or - refer to loading in the westerly and easterly directions, respectively—i.e., away from or toward the reaction wall.) A final unplanned unloading to zero occurred in Cycle 24- because of excessive leakage of the jack at Level 2. Remedial measures were then taken to prevent such occurrences in subsequent cycles. The specimen was reloaded to complete Cycle 24- prior to proceeding to the next cycle.

For the first five cycles (up to and including the first cycle at ± 1000 kN), a gravity load of 75% of the eventual target value was applied to the top of each column. This was a cautionary approach to evaluate the effects of these loads at lower values in order to reduce the possibility of undesirable consequences. For the final two cycles at ± 1000 kN and thereafter, the full gravity load of about 720 kN per column was applied. This load represents 16% of the specified minimum yield strength of the columns. At times there was some difficulty in maintaining the gravity loads at a constant level as the shear wall was pushed horizontally back and forth. Generally, the gravity loads were maintained within $\pm 5\%$ of the target value.

Approximately two loading cycles could be performed per day. In two attempts to maintain the gravity loads overnight, leakage from the hydraulic system caused unloading to about 50–60% of the desired value. This, in addition to safety concerns, led to the decision that thereafter, the columns would be unloaded at the end of each test day and reloaded prior to applying horizontal loads the next day. This procedure is not considered to have had any effect on the overall performance of the specimen.

6.5 Specimen Behaviour During Test

6.5.1 Gravity Load Application

During the application of the initial gravity loads of 75% of the target value, no yielding of the specimen was apparent. An inspection of the thin infill panels revealed that no plate buckling occurred.

6.5.2 Cycles Prior to Significant Yielding

There was very little yielding in the first 10 cycles, as reflected by the fact that the load vs. deflection behaviour of the test specimen remained virtually linear. The earliest yielding, caused by the concentrated loads applied by the horizontal jacks, was localized near the loading clevises. Yield lines were detected during Cycle 4 in the web of the beam at Level 1 (located at the top of Panel 1), during Cycle 6 in the web of the beam at Level 2, and during Cycle 8 in the web of the beam at Level 3.

In the first attempt to reach a base shear of 1950 kN (Cycle 8), the shear wall base plate slipped about 5 mm (as measured by mechanical dial gauges) at a base shear of approximately 1550 kN. To prevent significant movement in subsequent cycles, a heavy brace designed to act in both tension and compression was welded to the base plate and then connected to the reaction wall by prestressed anchor bolts. The anchor bolts securing the shear wall base plate were also re-stressed to eliminate any prestress losses that had occurred up to that time. The dial gauges were then replaced by two additional LVDTs to monitor more precisely any subsequent movement of the base of the specimen. The brace and anchor bolt prestressing reduced the slippage to 0.38 mm at a base shear of 1950 kN.

During Cycle 8, yielding was apparent in Panel 1 and, to a lesser extent, in Panel 2. Most of the yielding was in the fish plates that connect the infill plates to the boundary members or at the periphery of the infill plates. Characteristic diagonal

tension yield patterns began to form at the top corners of Panel 1. By Cycle 10, the yielded areas on the fish plates had grown larger.

6.5.3 Cycles Subsequent to Significant Yielding

In Cycle 11 (the first cycle with $\delta = \delta_y$), the existing yield patterns became considerably more pronounced. Increased yielding was noted in the webs of the beams at Levels 1, 2, and 3, as well as in the fish plates and infill plates of Panels 1 and 2. Panels 1, 2, and 3 all buckled visibly at the maximum deflection. In addition, several loud bangs occurred in this cycle as the plate buckles popped through and reoriented themselves upon reversal of the loading direction. These noises continued to occur in all subsequent cycles.

During Cycle 14 ($\delta = 2\delta_y$), yield lines developed that covered virtually the entire area of both surfaces of Panel 1. Additional yielding occurred in Panels 2 and 3, including fairly heavy yielding across the bottom of Panel 2. The first yielding in Panel 4 was noted along the top and bottom fish plates. Yield lines developed along the web of the beam at Level 1 over its full length. The number of yield lines in this area continued to increase as the test progressed. During this cycle, the amplitude of the buckle in Panel 1 was estimated to be about 50 mm from the neutral position. After unloading, residual buckles were clearly visible in a complex surface geometry that did not favour the orientation that formed in either direction of loading.

It was noted in Cycle 15 that although the web of the beam at Level 1 and the webs of the columns above and below were extensively yielded, there was no yielding at all in the Level 1 beam-to-column joint panels. The first (very slight) yielding in this area occurred during Cycle 17 ($\delta = 3\delta_y$).

The first tear was detected during Cycle 18 in the top west corner of the south face of Panel 1. It was 6 mm long and located at the corner of the weld connecting the

infill plate to the fish plate, transverse to the weld axis. This tear did not propagate during subsequent cycles and is considered to have had a negligible effect on the behaviour of the test specimen. Residual buckles in Panel 2 after this cycle, although slight, were readily observable visually.

During Cycle 20, local buckles in the west flange of the east column and the east flange of the west column formed immediately below the beam at Level 1. These buckles were of relatively small amplitude, but they grew in size during subsequent cycles. After the lateral load had been removed at the end of this cycle, residual amplitudes of 10 mm (west column) and 40 mm (east column) were measured. In addition, a local buckle of 13 mm amplitude was discovered in the east flange of the east column near the base.

In Cycle 22, tears in the plate were seen at the top corners of Panel 1 at the toe of the fillet weld connecting the fish plate to the columns. The east tear was 120 mm long and the west tear was 80 mm long. In addition, a 50 mm tear formed at the toe of the fillet weld connecting the infill plate to the fish plate at the top west corner. Figure 6.6 shows the tears at the west side, after they had propagated during subsequent cycles. Also during Cycle 22, at a deflection of $5\delta_y$ in Panel 1, the maximum base shear of 3080 kN was reached. The load-carrying capacity of the test specimen declined very gradually during each of the remaining cycles with increasing deformations.

By Cycle 24, the local buckles in the lowest storey that began forming in Cycle 20 had become more pronounced. Local flange rotations about the longitudinal axis at the web-to-flange junction caused substantial yielding in the adjacent column webs.

Beginning at Cycle 25, tears in the interior of the Panel 1 infill plate formed as a result of kinking of the stretched plate during load reversals. The plate tended to

kink and straighten cyclically as the buckles reoriented themselves. Figure 6.7 shows one such tear. Tears also appeared in the bottom west and top east corners of Panel 1 at the toe of the fillet weld connecting the strap plates to the fish plates.

By Cycle 26, column flange distortion in the first storey was extreme. Figure 6.8 shows the distortion in the west column flanges. In each case, the distortion increased when the column was in compression and the flanges tended to straighten out partially when the column was in tension.

A total of 15 tears were present in Panel 1 by the end of the test, as shown in Fig. 6.9. The tears were distributed over the entire plate area and included tears of the types depicted in both Figs. 6.6 and 6.7, as well as those that developed in the corner test, as shown in Fig. 5.3. The tears shown on the south face (inset diagrams) in Fig. 6.9 are in the weld that surrounds the strap plate and do not extend through the entire panel thickness. No tears occurred in Panels 2, 3, or 4.

6.5.4 Specimen Failure

In Cycle 30+, a deflection of $9\delta_y$ was achieved in Panel 1. The shear wall was then unloaded and was in the process of being reloaded in the opposite direction, when the west column fractured at its base at a base shear of approximately 1750 kN. The fracture was sudden and was accompanied by a large release of energy. The fracture began at the toe of the weld connecting the west flange of the column to the base plate. The crack then propagated through the remainder of the west flange and completely through the web, as shown in Fig. 6.10.

During the first loading excursion of Cycle 30 (the final complete excursion prior to failure) the base shear reached was 85% of the maximum base shear achieved (Cycle 22). The stiffness of the shear panel itself was declining in a very gradual and stable manner, and it still maintained its integrity at the end of the test.

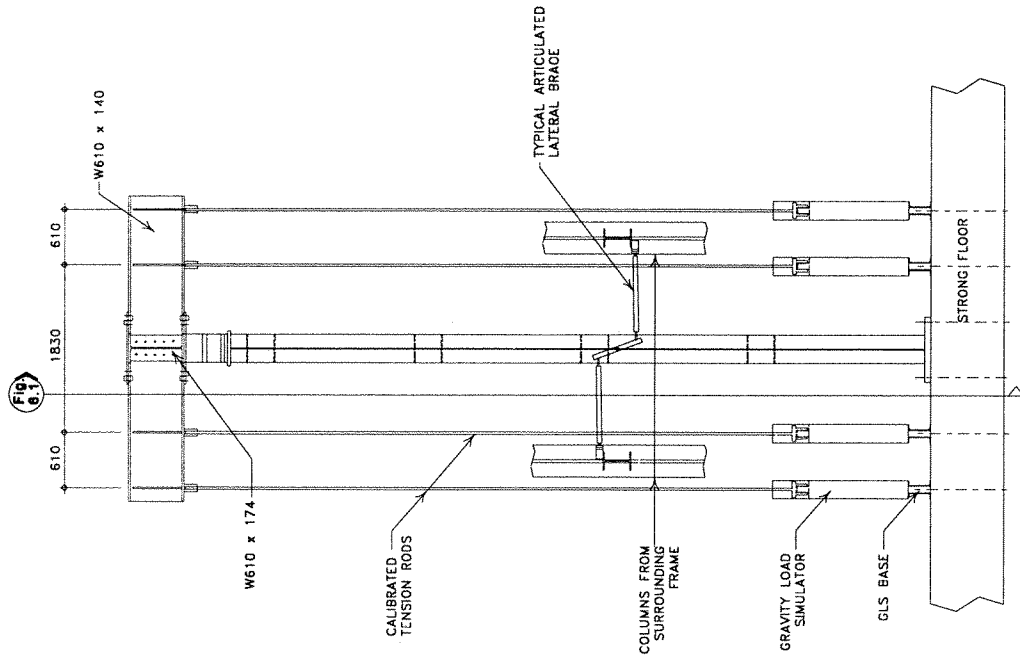


Fig. 6.1 Test Set-up – North Elevation

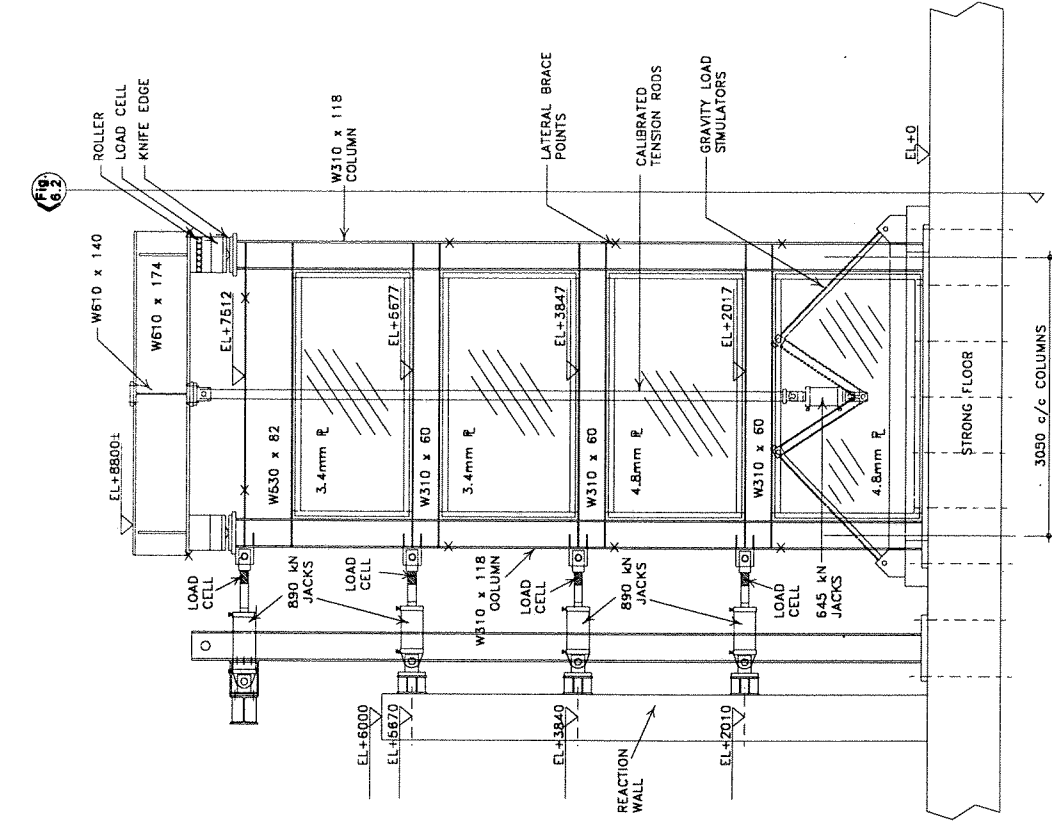


Fig. 6.2 Test Set-up – West Elevation

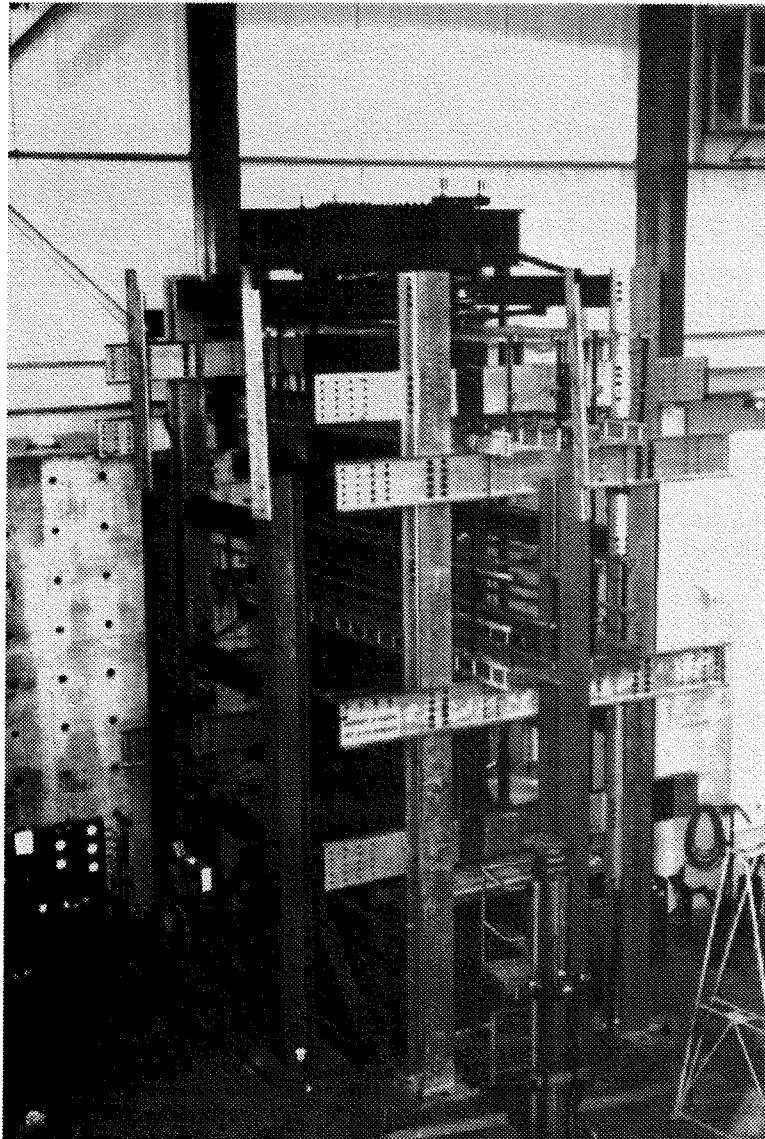


Fig. 6.3 Overview of Test Set-up



Fig. 6.4 Four Storey Shear Wall Specimen

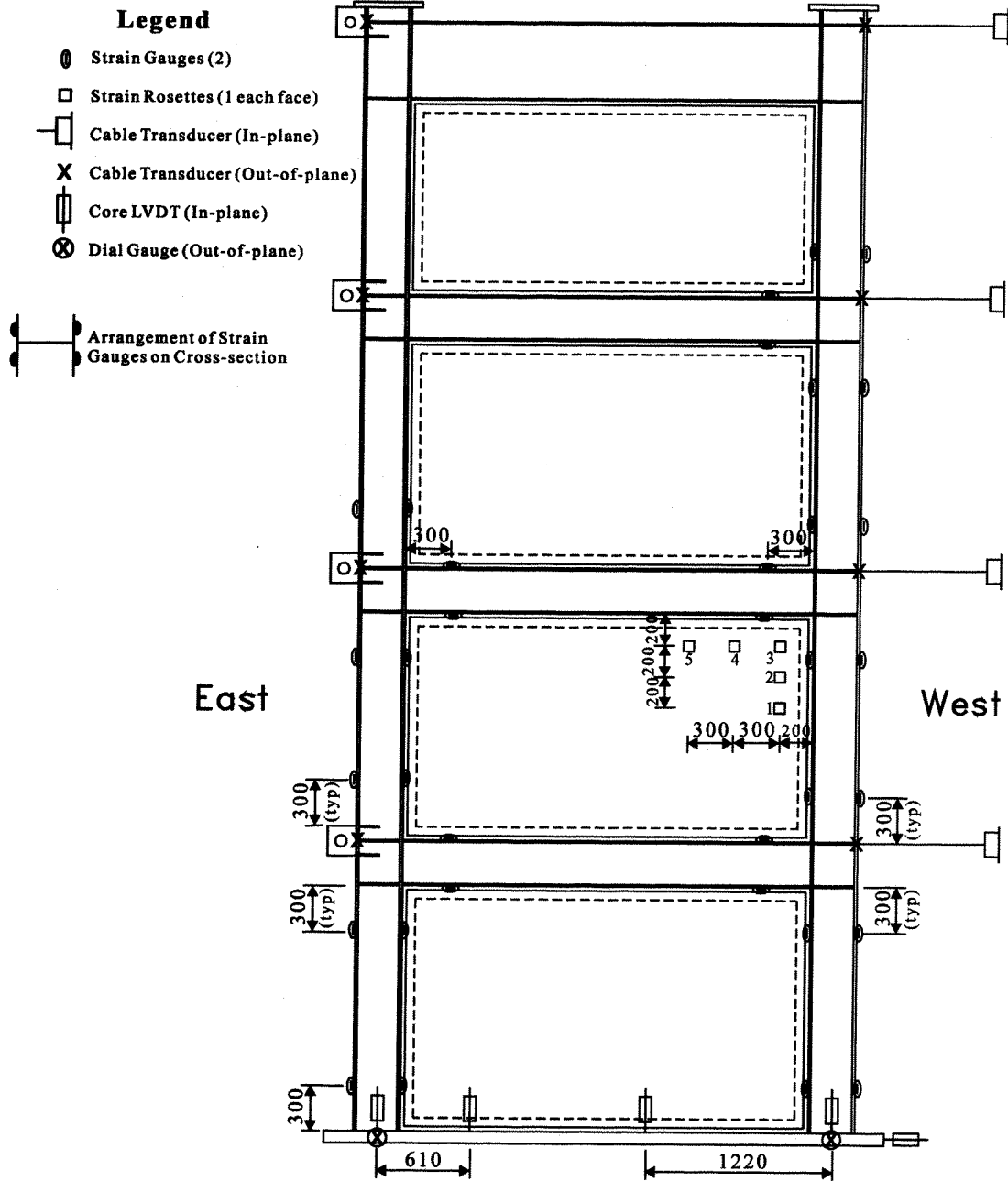


Fig. 6.5 Data Acquisition Locations

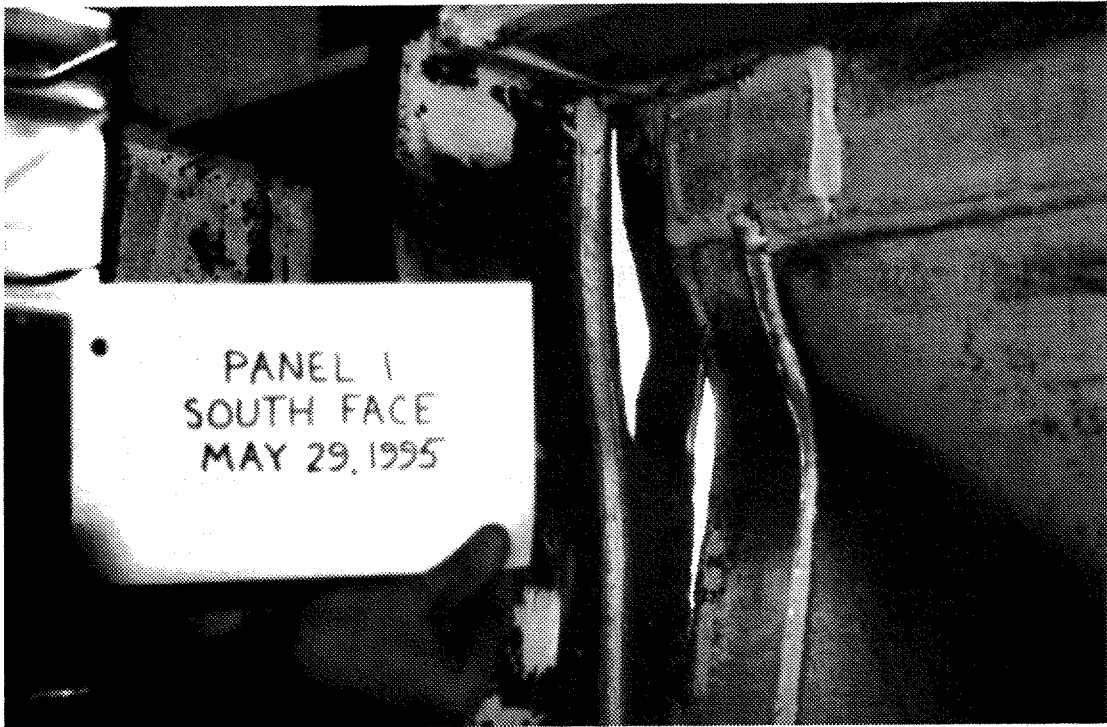


Fig. 6.6 Tears at Top West Corner of Panel 1



Fig. 6.7 Tear in Panel 1 Initiated by Cyclic Kinking

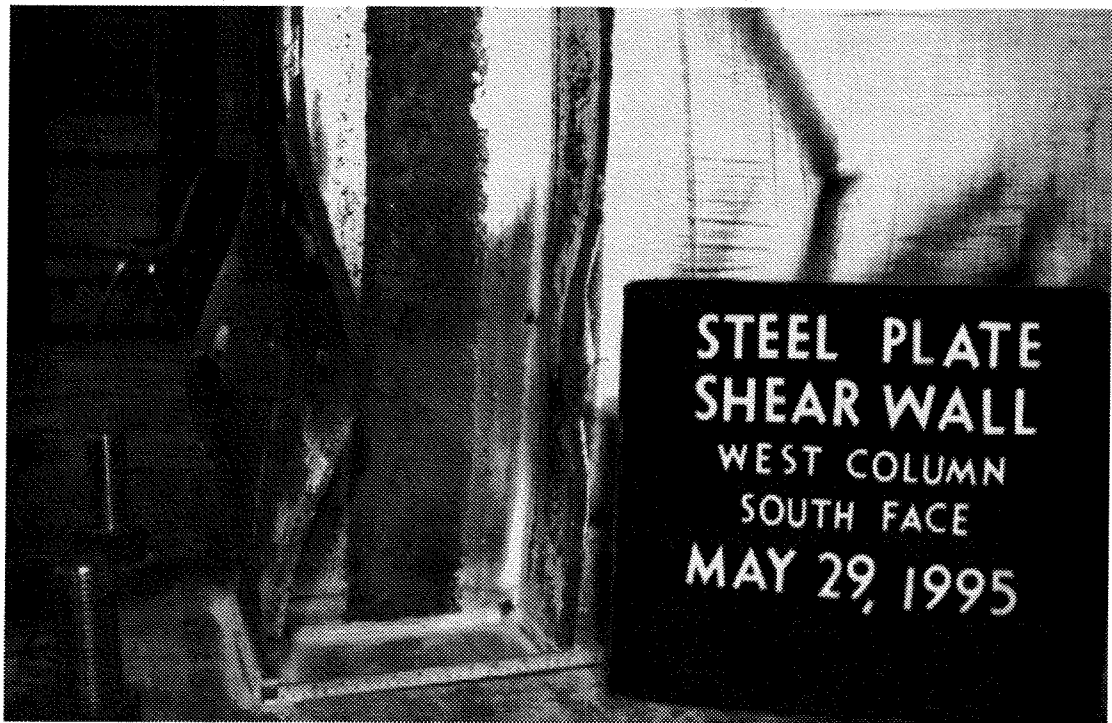


Fig. 6.8 West Column Local Distortion

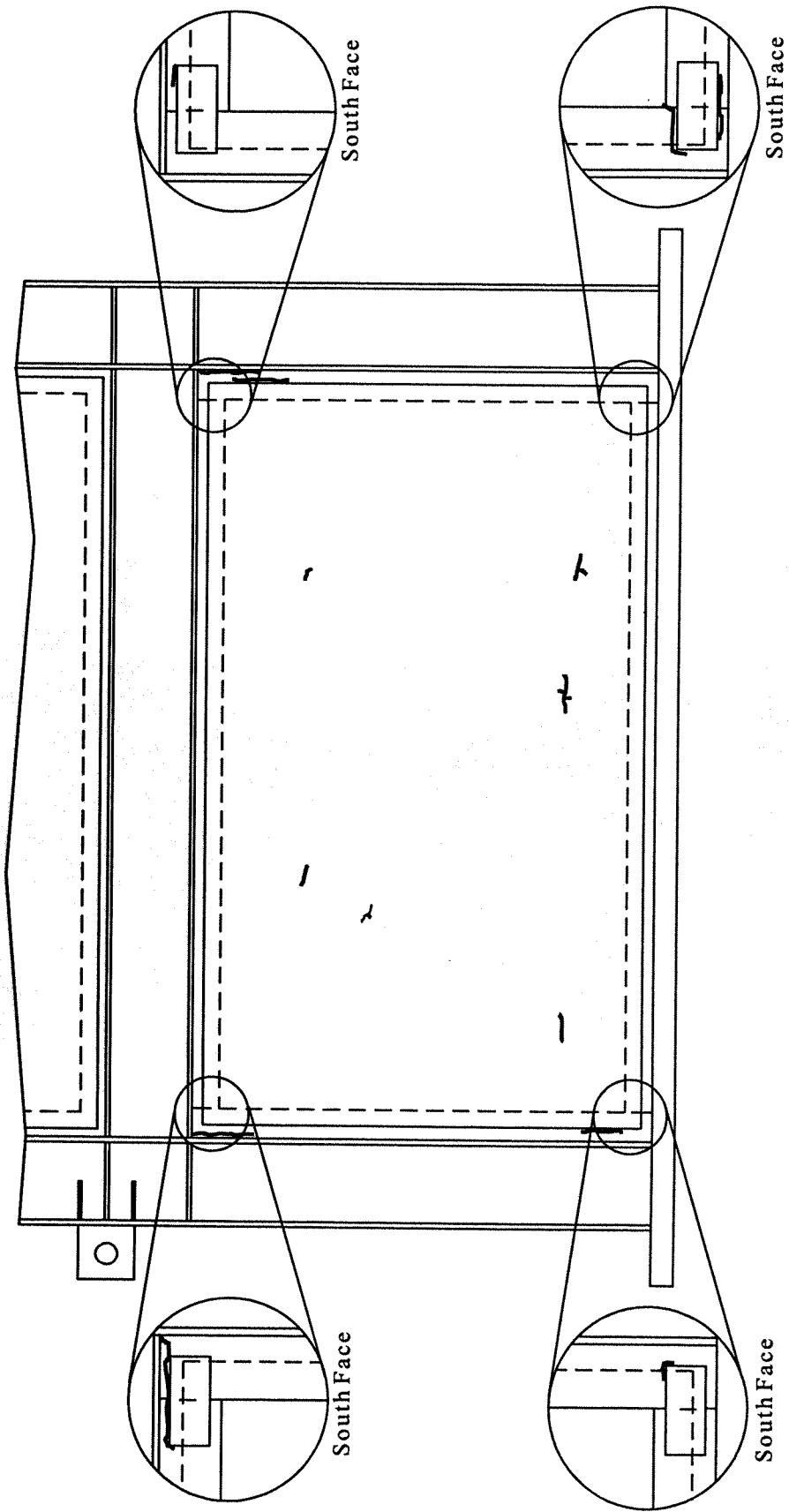


Fig. 6.9 Tears in Panel 1 at Conclusion of Test (North Face)

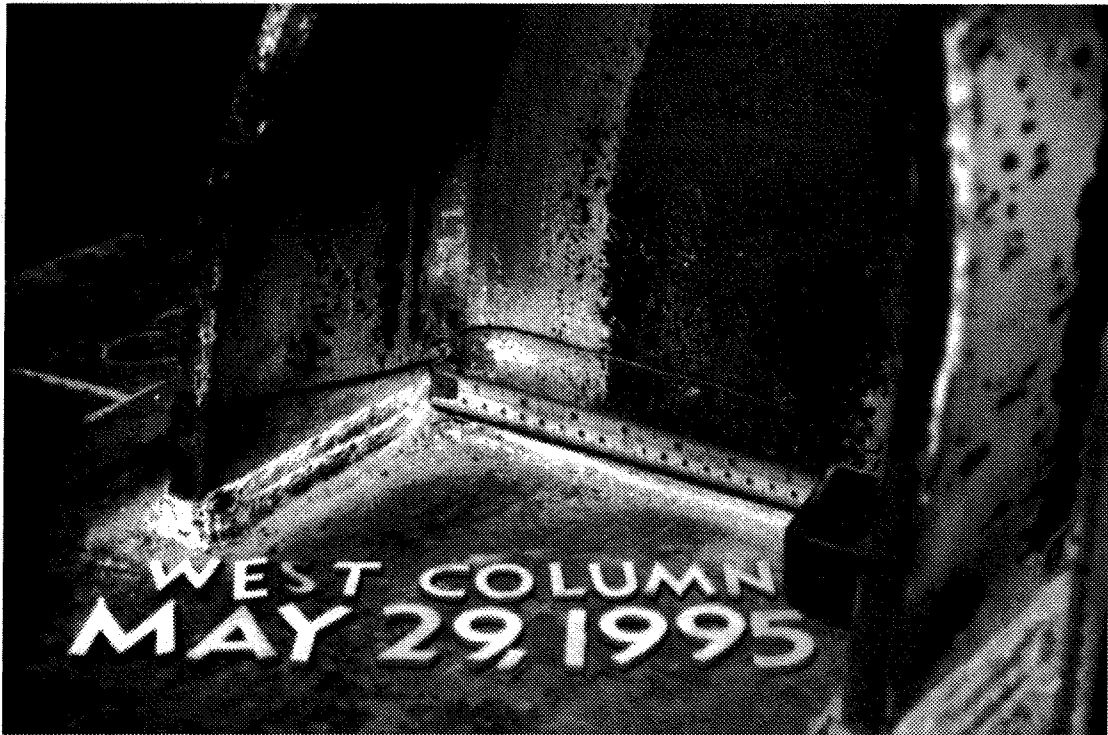


Fig. 6.10 Fracture at Base of West Column

7. DISCUSSION OF SHEAR WALL TEST RESULTS

7.1 Introduction

Generally, the multi-storey steel plate shear wall test specimen performed as expected. The ultimate load of 2890 kN predicted by the preliminary finite element model prior to the test was approximately equal to the maximum load achieved at a deflection of $3\delta_y$ and the ultimate capacity of the test specimen of 3080 kN was 1.07 times that predicted. The stiffness of the specimen was somewhat lower than that predicted by the finite element model, as discussed in Section 6.4. The ductility exhibited by the specimen provided confirmation that the configuration tested, consisting of thin plates with a moment-resisting frame, is favourable for extreme cyclic loading representative of seismic actions.

7.2 Hysteretic Behaviour

The criterion used to control the test, and which is of prime importance for defining the performance of the test specimen, is the storey shear vs. storey deflection behaviour of Panel 1. The test results are shown in Fig. 7.1, where the deflection is given both in absolute terms and also in terms of the drift ratio, δ / h_s . The hysteresis curves show many of the same characteristics that have been present in previous tests of unstiffened, thin panel steel plate shear walls (e.g., Tromposch and Kulak 1987).

In the early (elastic) loading cycles, the panel behaved in a stiff manner. As the extent of deformation increased, portions of the steel plate shear wall yielded and the frame gradually softened. After significant yielding of the infill panels had occurred, unloading and reloading in the opposite direction produced a consistent and characteristic pattern. Consider the single representative cycle (Cycle 22, modified to form a closed curve) shown in Fig. 7.2. The unloading curve a–b has a panel stiffness

similar to that in the elastic region, although with the increasing peak deflection in each excursion, the slope of these unloading curves tended to decrease gradually.

As the load reversed, the stiffness of the frame was reduced substantially (curve b-c). This reflects the redevelopment of the tension field of the panel in the opposite direction to that of the previous excursion. Because the plate had been stretched inelastically, the diagonal was longer than the opening within the moment-resisting frame upon its return to the neutral position. This was manifested during the test by significant out-of-plane buckles that were present when the shear wall was not under load. For the tension field to redevelop to the point where it again became the primary mechanism for resisting the storey shear (point c), significant storey deflection was required. When this had occurred, the curves showed an increase in stiffness (curve c-d) because the tension field that acted as a diagonal tie braces the storey. As the loads approached the ultimate strength again (curve d-e), yielding of the various components of the shear wall (primarily the infill plate) resulted in another decrease in stiffness. The subsequent curves representing the unloading and reloading of the panel in the opposite direction (curve e-f-g-h-a) are a repetition of the phenomena described for the curve a-b-c-d-e.

Each of the inelastic cycles carried out during the test resulted in the generation of similar hysteresis curves that follow the various stages described above. The primary difference in the curves is the stiffness of the shear panel during the redevelopment of the tension field, and the amount of deflection required in order for the redevelopment to occur, as seen in Fig. 7.1.

The maximum load achieved in each cycle increased slightly with each excursion to a new deflection level, until the maximum base shear of 3080 kN was reached in Cycle 22 at a deflection of $5\delta_y$. Subsequent to this, the load-carrying capacity of the shear wall declined very gradually from cycle to cycle. In the final cycle—at a deflection of $9\delta_y$ —the test specimen carried 85% of the maximum base

shear achieved (Cycle 22). Cycle 22 was also the cycle where panel tears began forming. These, along with the local buckles in the column flanges that began forming in Cycle 20, are considered to be the contributing factors in the gradual degradation of the shear wall.

The curve in Fig. 7.1 possesses a distinct asymmetry in the two loading directions because, as discussed in Section 6.4, the deflections in Panel 1 were limited to a maximum of $5.4\delta_y$ in the direction toward the reaction wall. It should be noted that this limitation was only of consequence *after* the maximum capacity of the shear wall was reached. Furthermore, it is considered unlikely that it had a significant effect on the declining cycles for excursions in the opposite direction, where the deflections were not limited by the loading device.

The distinct characteristics of the loading and unloading behaviour described above for Panel 1 are also evident in the base shear vs. top deflection graph shown in Fig. 7.3. This diagram gives a measure of the behaviour of the shear wall as a whole.

In total, 30 cycles of loading were applied to the test specimen prior to failure. Of these, 20 cycles resulted in loading the specimen well beyond the point of significant yielding. This is generally considered to be more severe than the number of inelastic cycles that a shear wall would be expected to resist during an earthquake. For example, Derecho *et al.* (1980) conducted response history analyses on concrete shear walls and determined the displacement history for earthquakes of 20 second duration. A broad range of structural periods and seismic frequency characteristics were studied. Using a total of 170 cases, they determined that the number of fully reversed large-amplitude cycles was fewer than four in 95% of cases, with an extreme value of six. (A fully reversed cycle is defined as one in which an excursion of 0.75 to 1.0 times the maximum amplitude is followed immediately by an excursion in the opposite direction of at least 0.5 times this maximum.)

Figure 7.1 clearly demonstrates the significant ductility exhibited by Panel 1. Although the maximum deflection achieved was nine times the deflection at which “significant” yielding took place, as defined in Chapter 6, the true ductility exhibited by the system is even greater. Popov (1980) defines the displacement ductility factor as being the ratio of the maximum horizontal deflection of a structure at a selected storey to the deflection at the point of significant yielding. Furthermore, the maximum horizontal deflection is taken as the *total* inelastic excursion during a half-cycle. This recognizes the increased demand on an inelastically deformed structure that must deform significantly to reach the neutral position prior to the next inelastic loading excursion in the opposite direction. Although the subjective nature of determining the point of significant yielding is acknowledged by Popov, the definition used in this research closely parallels his. According to these definitions, with a deflection of $5.4\delta_y$ in one direction followed by a deflection in the other of $9\delta_y$, the displacement ductility factor for Panel 1 of the tested steel plate shear wall is actually 14.4. Had the jack stroke at Level 3 not been restricted, the displacement ductility factor based on a half-cycle would have been greater. Measures to eliminate the local buckling of the column flanges that eventually led to fracture of the column would also have increased the ductility.

The area enclosed by the hysteresis curves is a measure of the energy dissipated by the system in resisting the particular load or displacement history imparted. Figure 7.1 shows that the curves generated are relatively wide, indicative of significant energy dissipation during each cycle. The curves exhibit some pinching due to the reduced stiffness in the region where the plate buckles reorient themselves during a load reversal and the tension field is not fully developed. However, the area enclosed is distinctly greater than the area enclosed by curves generated for steel plate shear walls with shear-type beam-to-column connections (Tromposch and Kulak 1987). The result of constructing the shear wall with a moment-resisting frame is to

increase greatly the amount of energy dissipated, as well as to provide an inherent redundancy, thereby improving seismic performance.

Figure 7.4 is a histogram that shows how the amount of energy dissipated during each cycle varies throughout the test. In the figure, the amount of energy dissipated is shown for each displacement ductility ratio, δ / δ_y , excluding $\delta / \delta_y = 9$ where failure of the column prevented the completion of the cycle. A steady increase in dissipated energy occurred from $\delta / \delta_y = 1$ to $\delta / \delta_y = 6$. Thereafter, the rate of increase in dissipated energy decreased dramatically. However, as discussed in Section 6.4, the displacement cycles starting at a displacement ductility ratio of $\delta / \delta_y = 6$ were affected by a limitation in the stroke of one of the jacks. This clearly has an effect on the results presented in Fig. 7.4.

To correct for the modification of the deflection sequence due to the limitation of the loading device, estimates were made of the additional energy that would have been dissipated had it not occurred. This is based on the assumptions that the behaviour would have been the same in the two loading directions and that the greater deflections in one direction would not affect the behaviour in the other in subsequent cycles. The adjusted histogram, shown in Fig. 7.5, indicates that the energy dissipation in the final cycles continues to increase substantially up to displacement ductility ratio of $\delta / \delta_y = 8$, although the rate of increase does decrease slightly. (Had the test not been terminated due to the fracturing of one of the columns, the increase in the amount of energy dissipated would be expected to continue for greater ductility levels.) The continued increase in energy dissipation shows that any narrowing of the hysteresis curves and reduction in capacity are more than compensated for by the increased storey deflection. This means that, although the base shear that the wall was able to carry decreased from a maximum of 3080 kN in Cycle 22, its capacity to dissipate energy actually continued to increase. Therefore, the point of maximum

capacity of the structure should not be considered to be the extent of its useful ductility.

7.3 General Observations

The uniformity of the hysteresis curves indicates that the behaviour of the steel plate shear wall test specimen under severe cyclic loading was not only very ductile, but was also extremely stable. There were no sudden losses of stiffness and, even after the peak load had been reached, deterioration was slow and controlled. Tearing of the infill plates, which is a mechanism for dissipating energy, also occurred in a gradual manner: increases in tear lengths in any given cycle were only incremental. One of the reasons that the tearing did not result in sudden decreases in stiffness is the ability of the continuous shear plate to redistribute loads to areas unaffected by the tearing. Furthermore, the tearing was distributed relatively uniformly over the area of Panel 1, as shown in Fig. 6.9, with the result that most tears remained small throughout the test. The ability of the panels to redistribute load effectively provides a redundancy in the lateral load-resisting system that is beneficial for seismic applications. The efficiency of this stress redistribution is also reflected in the fact that the tears had little effect on the overall strength of the shear wall.

Research on the behaviour of beam-to-column joint panel zones in moment-resisting frames (e.g., Krawinkler and Popov 1982; Popov *et al.* 1986) has shown that with proper proportioning they can absorb large amounts of energy through inelastic deformations. The panel zones provide a ductile fuse for the dissipation of energy under seismic forces, thereby reducing the demand on other components of the frame.

Although the steel plate shear wall tested had moment-resisting joints at the beam-to-column connections, whitewash in the joint panel zones remained intact until 16 cycles of loading had been applied, indicating that there was no significant yielding of the material in these regions. Even during Cycle 17, the extent of yielding

was limited, with only slight flaking of the whitewash detected on the north side of the west joint panel zone at Level 1. This point in the displacement history corresponds to a deflection in Panel 1 of $3\delta_y$. Furthermore, at the end of the test, inelastic deformations in the joint panel zones remained small. It is emphasized that, other than flange continuity stiffeners, no doubler plates or other forms of panel stiffening were used.

The observation that no significant deformations occurred in the joint panel zones supports the contention that the primary ductile fuse of the steel plate shear wall system is the infill plate. This means that, in the terminology of Clause 27 (Seismic Design Requirements) of the Canadian steel design standard (CSA 1994), the infill plates would be considered the “critical elements.” (In this document, elements that undergo large plastic deformations are termed critical elements.) In effect, the presence of the infill plates reduces the demand on the joint panel zone and distributes the energy dissipating mechanism over a much larger area, while at the same time stiffening the frame significantly. Because of the presence of the infill plate, there is a reduction in reliance on the moment-resisting frame for resisting the storey shears. Therefore, the joint panel zone will generally not be a critical element, and can be designed to remain essentially elastic, resulting in additional economy.

During the Northridge Earthquake in January 1994, moment-resisting joints suffered fractures in many buildings. As a result, Engelhardt and Sabol (1994), Yang and Popov (1995), and others have been studying the cause of this type of failure. In the Northridge failures, the bottom beam flanges generally fractured at the column with a number of different characteristic patterns. Slow cyclic tests have, in some cases, been able to duplicate some of these failure modes. The reduced demand on the moment-resisting frame in a steel plate shear wall due to the diagonal storey brace from the infill plate tension field tends to make the situation less severe. However, it is acknowledged that there are a number of features that may have contributed to the

fractures in the Northridge earthquake that are somewhat different from the test specimen discussed herein. These include the presence of concrete floor slabs and difficulties in making the large welds in the lower flange.

Many of the Northridge fractures initiated at the natural notch formed by the backing bar used during the welding operation at the beam flanges. The SAC Joint Venture, a group representing a broad cross-section of industry organizations, recommends (FEMA 1995) removal of the backing bar and run-off tabs, back gouging, and redepositing weld material at the bottom of the flange in an overhead operation. The procedure is then completed by grinding the weld and testing it using non-destructive techniques. All these operations are expensive and reduce the competitiveness of the system in the marketplace. Costs are further increased due to the recommendation for various types of joint reinforcement or haunches in order to force the plastic hinge away from the connection. The backing bars and run-off tabs used in the fabrication of the steel plate shear wall test specimen were left in place in all locations and no such reinforcement was used. However, no distress of any kind was noted in the areas of the beam-to-column connections, in spite of the very large deformations imparted to the test specimen and the large number of loading cycles applied.

Because of the large deflections accommodated by the lowest storey, a comparison is made with the seismic drift limitations prescribed by building codes. The National Building Code of Canada (NBCC 1995a) specifies a limitation on interstorey drift of $0.01h_s$ for structures that are designed as post-disaster buildings and $0.02h_s$ for all other buildings. For the steel plate shear wall test specimen, this is equivalent to a deflection at Level 1 ($h_s = 1928$ mm) of 19.3 mm ($2.3\delta_y$) for post-disaster buildings and 38.6 mm ($4.5\delta_y$) for other buildings.

In a similar manner to the National Building Code of Canada, recommendations under the National Earthquake Hazards Reduction Program

(NEHRP) limit the interstorey drift depending upon the seismic hazard grouping (FEMA 1994). Buildings in group 3 (those having essential facilities that are required for post-earthquake recovery), group 2 (those that have a substantial public hazard due to occupancy or use), and group 1 (those not assigned to groups 3 or 2) are limited to an interstorey drift of $0.010h_s$, $0.015h_s$, and $0.020h_s$, respectively. For the test specimen, this is equivalent to deflections at Level 1 of 19.3 mm ($2.3\delta_y$), 28.9 mm ($3.4\delta_y$), and 38.6 mm ($4.5\delta_y$), respectively. In buildings of four storeys or fewer where the non-structural elements are specially designed to accommodate large displacements, somewhat more liberal limits may be used. The largest permissible interstorey drift under these circumstances is $0.025h_s$ for buildings in seismic hazard group 1. For the test specimen, this is equivalent to a deflection at Level 1 of 48.2 mm ($5.7\delta_y$).

Thus, the range of permissible levels of interstorey drift for the steel plate shear wall test specimen, without special requirements for the non-structural elements, is 19.3 mm ($2.3\delta_y$) to 38.6 mm ($4.5\delta_y$). In the test, the ultimate strength was reached in Cycle 22 with a deflection at Level 1 of 42.5 mm ($5\delta_y$), which is greater than the drift limitation in these cases. Therefore, even if drift were to *control* the design of the shear wall, deflections would not be expected to reach the post-ultimate region. Even for the most liberal case, where deflections of $0.025h_s$ are allowed, the resulting deflection in the test specimen would still not lead to any significant strength degradation. The deflections imposed during the test were, therefore, much more severe than would take place in a properly designed structure. Nevertheless, the shear wall panel exhibited excellent performance throughout the test.

7.4 Failure Mode

The test specimen failed in Cycle 30 by the sudden fracturing of the west column at its base. A metallurgical examination revealed that the fracture began in the heat-affected zone of the outer column flange near the toe of the complete penetration groove weld that connected the column to the base plate.

The crack began at the flange tip and propagated approximately 30 mm along the flange in a relatively tough manner, as is apparent from the 45° shear lips on the fracture surface. Examination of the crack surface showed that of the initial 30 mm, only the last 10 mm occurred in the final cycle of loading (Cycle 30), exhibiting a classical ductile failure surface appearance. The initial 20 mm crack surface (at the tip of the flange) had been deformed in compression during one or more of the earlier load cycles.

When the crack reached 30 mm in length, the cross-sectional area had been sufficiently reduced such that a brittle cleavage fracture was initiated, with the failure surface perpendicular to the plane of the flange. Growth occurred completely through the outer flange and through the web to the inside of the inner flange. The final fracture happened with a large release of energy.

Although failure of the column occurred at a very large deflection and after a large number of inelastic reversals, the failure *mode* is also of importance in assessing the suitability of a structural system for seismic applications. Certainly, the failure mode of sudden fracture of the column is not desirable and should be avoided.

The reason for this failure mode is evident. During Cycle 20 (near the ultimate load), local buckles began forming in the column flanges at the top and bottom of the column segment adjacent to Panel 1. As the frame deflections became more severe, the amplitudes of the local buckles grew. At large deflections, the buckle amplitudes at the column bases grew to approximately 90 mm when the column was in

compression. As the column went into tension when the loads were reversed, the local buckles tended to straighten. This action caused a severe cyclic bending of the flanges at the column base, eventually causing the material to fracture. The problem was compounded by the fact that when the flange is in tension, the heavy weldment at the base plate effectively restrains the through-thickness contractions (the Poisson effect). This creates a condition of triaxial tensile stresses that significantly reduces the local ductility of the material.

One way to prevent the local flange movements that contributed to the fracture of the column is to install full-depth horizontal stiffeners between the column flanges. Adding column stiffeners near the top and bottom of the storeys in locations where strains are expected to be several times the yield strain would restrain the formation of these local buckles. The test demonstrated that local buckles may form in the absence of sufficient stiffening under extreme lateral deformations even if Class 1 beam-column sections are used. This occurs because the ductility demands far exceed those required to reach and maintain the plastic moment, which defines the width-to-thickness ratios for elements of Class 1 sections. The most critical location for stiffening is at the column base, where the presence of heavy welding increases the likelihood of a low-cycle fatigue failure. Non-destructive inspection of the welds to ensure high quality is also recommended at these locations.

Another measure that may improve the performance of the connection at the column base is to force the plastic hinge away from the area that is restrained by welding. One way in which this could be achieved is by strengthening the columns at their bases by adding cover plates to the flanges. Tapered cover plates could be used to avoid an abrupt change in stress at their ends.

Because the shear panel still maintained its integrity when the column fracture occurred, had this failure mode been prevented there is reason to expect that the very gradual deterioration of capacity would have continued. However, because the load-

carrying capacity of the test specimen during Cycle 30 had already decreased to 85% of the maximum, no repair of the column was attempted.

7.5 Force Modification Factor, R (NBCC 1995a)

Although earthquake design methodologies vary throughout the world, a common approach used to account for inelastic seismic performance of a particular structural system is to reduce the elastic design forces to a level that would be encountered if significant inelastic behaviour occurred. Structural systems that are capable of effectively dissipating seismic energy inelastically are permitted larger reductions than those that are not. The National Building Code of Canada (NBCC 1995a) accomplishes this through a factor called the “force modification factor,” R. Considerations in establishing a value for the factor include ductility, the capability to dissipate energy through several load reversals within acceptable deformations and without failure, redundancy, previous performance in major and moderate earthquakes, and design and construction experience (NBCC 1995b). Clearly, engineering judgement is required in making an appropriate assessment. No information is available about steel plate shear wall structures that have been subjected to major or moderate earthquakes. However, the test reported herein has shown that the ductility of the test specimen and its energy dissipation capacity over many cycles are excellent. Furthermore, the redundancy of the shear wall system with both shear panels and moment-resisting frames is desirable for seismic applications.

Provisions for the design of all types of steel plate shear walls are stated in Appendix M of Canadian standard CAN/CSA-S16.1-94 (CSA 1994). In the National Building Code of Canada (NBCC 1995a), they have been conservatively assigned values of the force modification factor based on engineering judgement and the limited data available at the time. Three values were assigned as follows:

1. $R = 4.0$: Ductile steel plate shear walls, with moment connections provided between the beams and columns that are proportioned in accordance with the requirements of Clause 27.2 of Canadian standard CAN/CSA-S16.1-94 (CSA 1994).
2. $R = 3.0$: Nominally ductile steel plate shear walls, with moment connections provided between the beams and columns that are proportioned in accordance with the requirements of Clause 27.3 of Canadian standard CAN/CSA-S16.1-94 (CSA 1994).
3. $R = 2.0$: Ordinary steel plate shear walls proportioned with no requirements beyond the provisions of Appendix M of Canadian standard CAN/CSA-S16.1-94 (CSA 1994).

The values of the force modification factor for ductile and nominally ductile steel plate shear walls are the same as those assigned to the enclosing steel frames alone and, therefore, do not recognize the potentially improved behaviour of the steel plate shear wall.

Uang (1991) showed how the value of R can be quantified within the framework of the NEHRP provisions (FEMA 1988). In order to determine a value for R , the relationship between the actual response and the theoretical elastic response and design base shear must be estimated in some manner. Although not stated explicitly, the National Building Code of Canada (NBCC 1995a) incorporates an implied definition of R based solely on the ductility of the structural system. The design base shear is defined as:

$$V = \left(\frac{V_e}{R} \right) U \quad [7.1]$$

where V_e is the base shear that would result if the structure were to remain elastic, U is a calibration factor, and R is the force modification factor. The factor U was established with a value of 0.6 in order to maintain design base shears at the same level as in the previous edition of the Code (NBCC 1995b). The inverse of U is generally considered to be an “overstrength factor” that attempts to account for the fact that buildings have a reserve strength beyond that assumed in design. Tso (1992) suggests that some reasons that overstrength occurs are that member sizes may have been selected to meet stability or drift requirements or strength requirements of other load cases, redundancy not accounted for in the design may improve the actual behaviour, and non-structural elements may contribute to the lateral strength of the building. Materials also generally have strengths well in excess of their nominal values.

Figure 7.6 shows three base shear vs. deflection responses of a structural system. The actual response, an approximate bilinear response, and the response if the system were to remain elastic are all shown. If the system were to remain elastic and there were no overstrength, it would have to be designed for a base shear V_e . However, structures are generally able to undergo some inelastic deformation that allows them to be designed for a lesser base shear, which is addressed by the factor R . Therefore, from Eq. 7.1, the reduced base shear is obtained as:

$$\frac{V_e}{R} = \frac{V}{U} \quad [7.2]$$

which represents the base shear expected during the actual response, V_{\max} , as shown in Fig. 7.6. Therefore:

$$V_{\max} = \frac{V_e}{R} \quad [7.3]$$

Rearranging Eq. 7.3 leads to the definition of the force modification factor, R :

$$R = \frac{V_e}{V_{\max}} \quad [7.4]$$

The overstrength factor $1/U$ reduces the base shear given in Eq. 7.3, V_{\max} , to the design value, V , as defined in Eq. 7.1 and as shown in Fig. 7.6.

The elastic deflections shown in Fig. 7.6 corresponding to the base shears V , V_{\max} , and V_e are δ_v , δ_y , and δ_{ve} , respectively. It is emphasized that δ_y has the same definition as that used previously in discussions about the test results. The deflection δ_{\max} , defined here as the maximum deflection at which a base shear of V_{\max} can be maintained, occurs at the intersection of the actual and approximate bilinear response curves. The National Building Code of Canada (NBCC 1995a), gives the maximum inelastic deflection to be expected during an earthquake, δ_{NBC} , as R times the elastic deflection resulting from the design earthquake forces, or $R\delta_v$, that is:

$$\delta_{NBC} = R\delta_v \quad [7.5]$$

From Fig. 7.6, it is evident that:

$$\delta_v = \delta_y \frac{V}{V_{\max}} \quad [7.6]$$

Substituting the expression for δ_v in Eq. 7.6 into Eq. 7.5 and solving for R :

$$R = \frac{\delta_{NBC}}{\delta_y} \frac{V_{\max}}{V} \quad [7.7]$$

Substituting expressions for V and V_{\max} from Eqs. 7.1 and 7.3, respectively:

$$R = \frac{\delta_{NBC}}{U\delta_y} \quad [7.8]$$

Setting the deflection δ_{NBC} , which represents the maximum inelastic deflection of the structure, equal to the maximum inelastic deflection achieved in tests, δ_{max} , gives:

$$R = \frac{\delta_{max}}{U\delta_y} \quad [7.9]$$

The value of U is 0.6 and the values δ_y and δ_{max} can be determined through an experimental determination of the load vs. deflection response of the system. Therefore, according to the procedures outlined above, the value of R can be determined experimentally.

Figure 7.7 shows the envelope of cyclic response curves for Panel 1 of the four storey shear wall test specimen. Assuming that the response beyond the point where the descending curve intersects the approximate bilinear curve cannot be utilized, then:

$$\frac{\delta_{max}}{\delta_y} = 6 \quad [7.10]$$

and from Eq. 7.9, the force modification factor is determined to be $R = 10$ for the steel plate shear wall.

For comparison, another interpretation of the relationship between the elastic and inelastic response curves is presented. For all but very short period structures, and assuming linearly elastic – perfectly plastic response, the maximum inelastic deflection of a structure is approximately equal to the deflection if it were to remain elastic under the same earthquake excitation (Clough and Penzien 1993), that is:

$$\delta_{ve} \approx \delta_{max} \quad [7.11]$$

Therefore, if δ_{ve} is taken equal to δ_{max} , Eq. 7.4 becomes:

$$R = \frac{V_e}{V_{\max}} = \frac{\delta_{ve}}{\delta_y} = \frac{\delta_{\max}}{\delta_y} \quad [7.12]$$

Based on the assumption stated in Eq. 7.11, from Eqs. 7.10 and 7.12, the force modification factor is determined to be $R = 6$ for the steel plate shear wall. Although this method has a sound rational basis, it may be overly conservative due, in part, to the fact that the elastic base shear itself, V_e , tends to be conservative (Tremblay *et al.* 1993).

The experimentally derived value of the force modification factor based on the implicit definition of R in the National Building Code of Canada (NBCC 1995a) was determined to be 10, while a more conservative interpretation leads to a value of 6. Moreover, even though there was a slight degradation in the maximum base shear carried at large deflections, the energy dissipated continued to increase up to a deflection of $\delta / \delta_y = 8$. If an evaluation were made on this basis alone, a force modification factor of 8 to about 13 could be assigned. The system is also inherently redundant and exhibited excellent energy dissipation characteristics. Thus, based on this evaluation of the test results, the value of $R = 4.0$ assigned to ductile steel plate shear walls in the National Building Code appears to be very conservative.

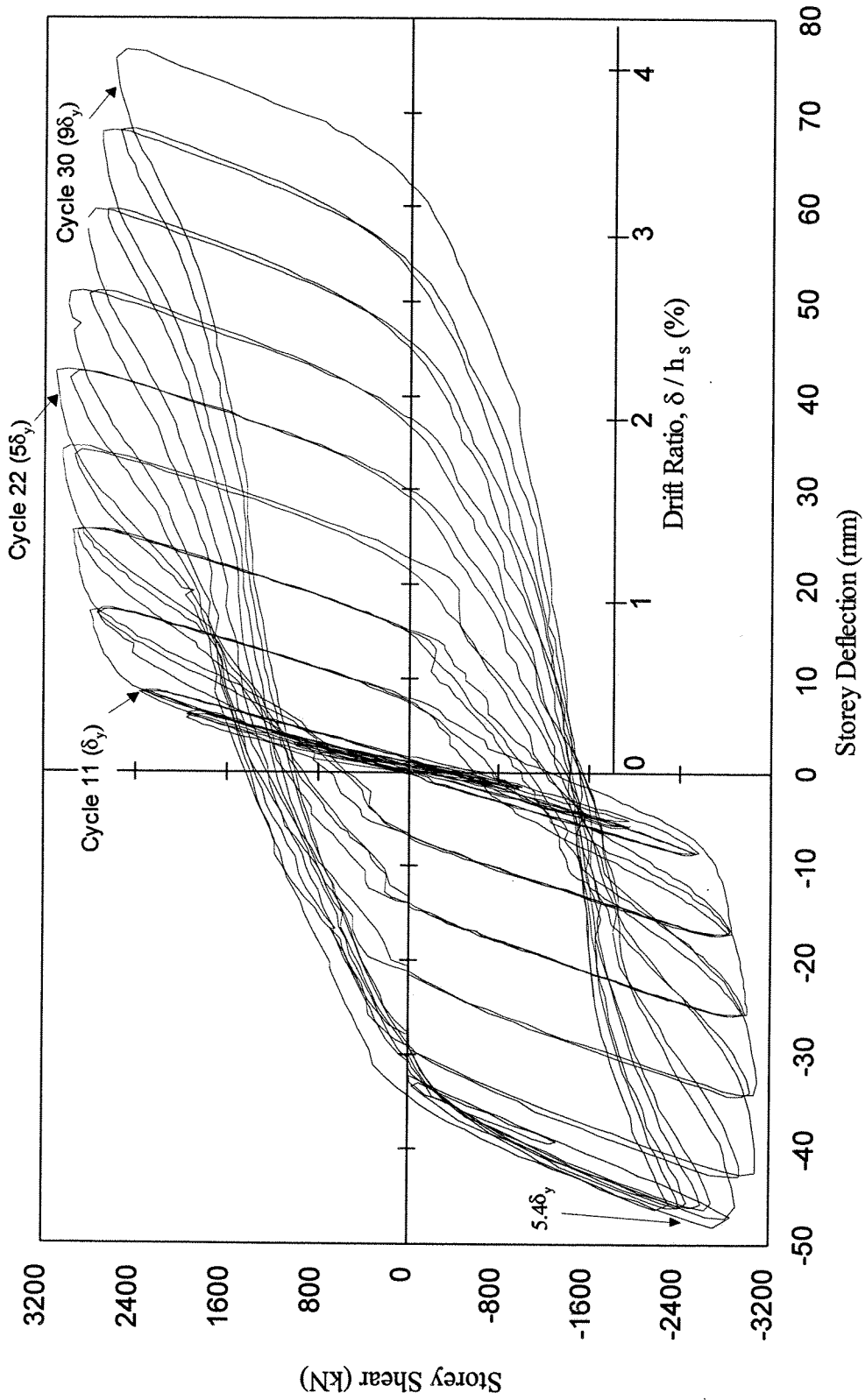


Fig. 7.1 Storey Shear vs. Storey Deflection – Panel 1

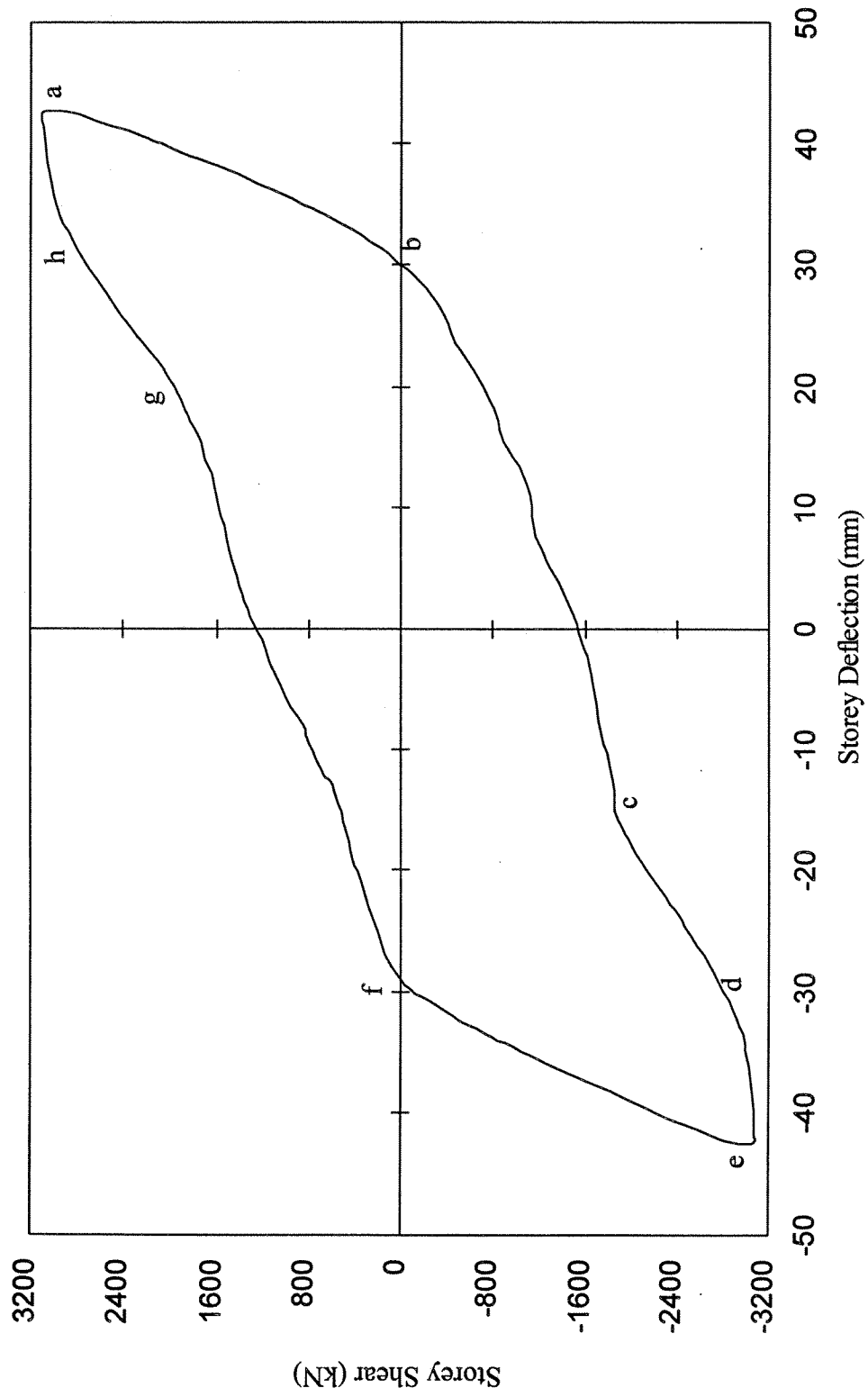


Fig. 7.2 Typical Loading Cycle – Panel 1

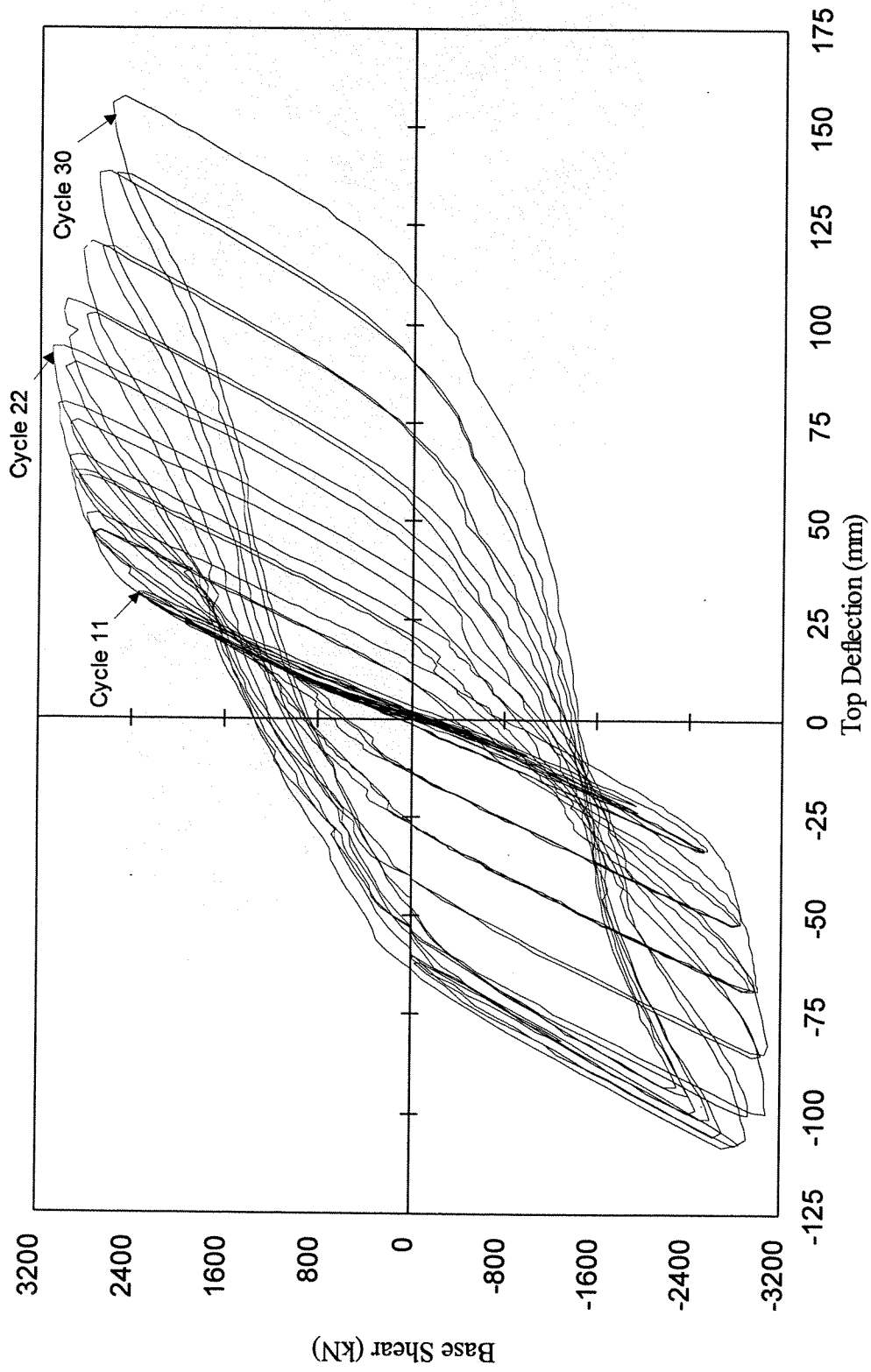


Fig. 7.3 Base Shear vs. Top Deflection

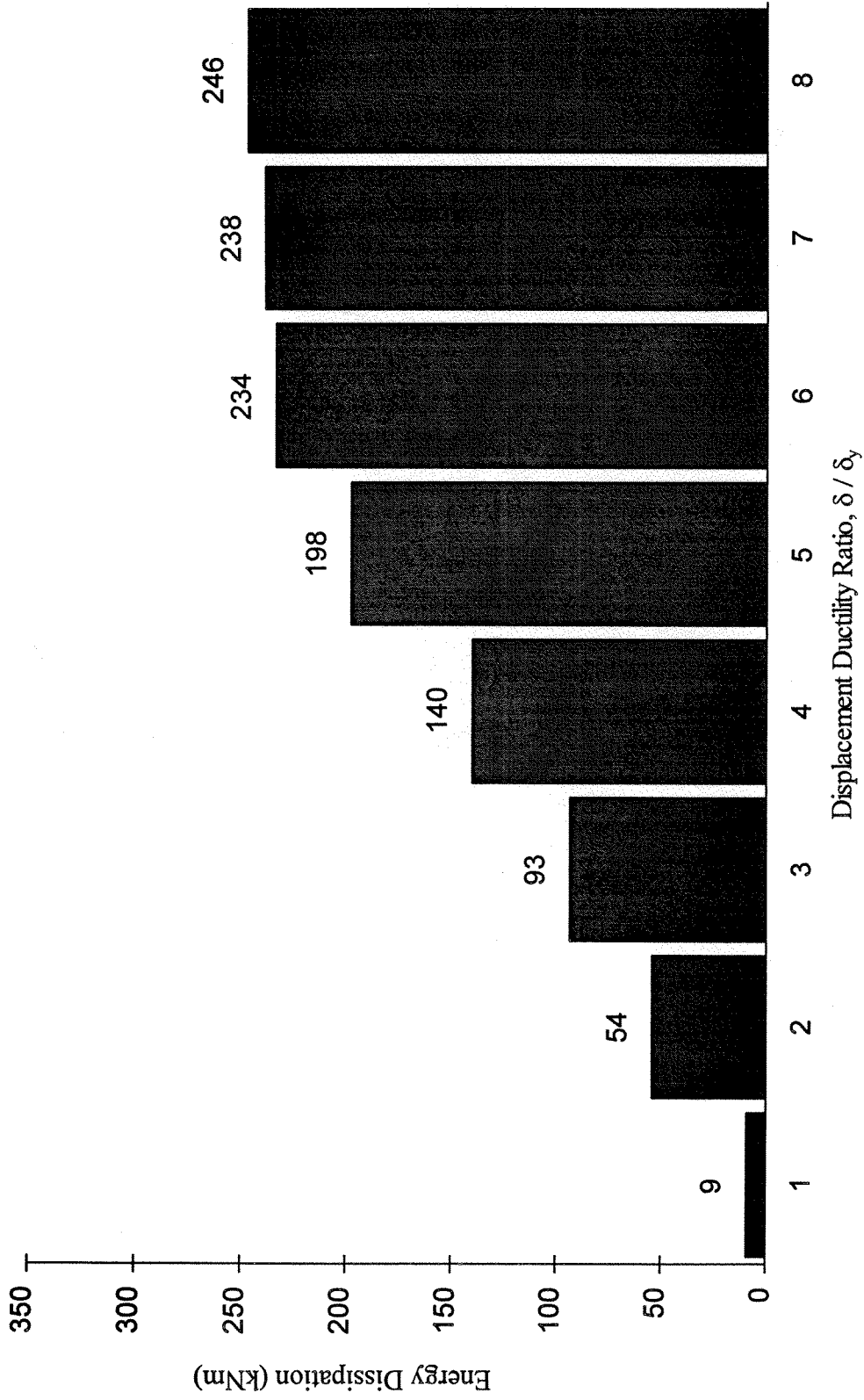


Fig. 7.4 Actual Energy Dissipation During Test

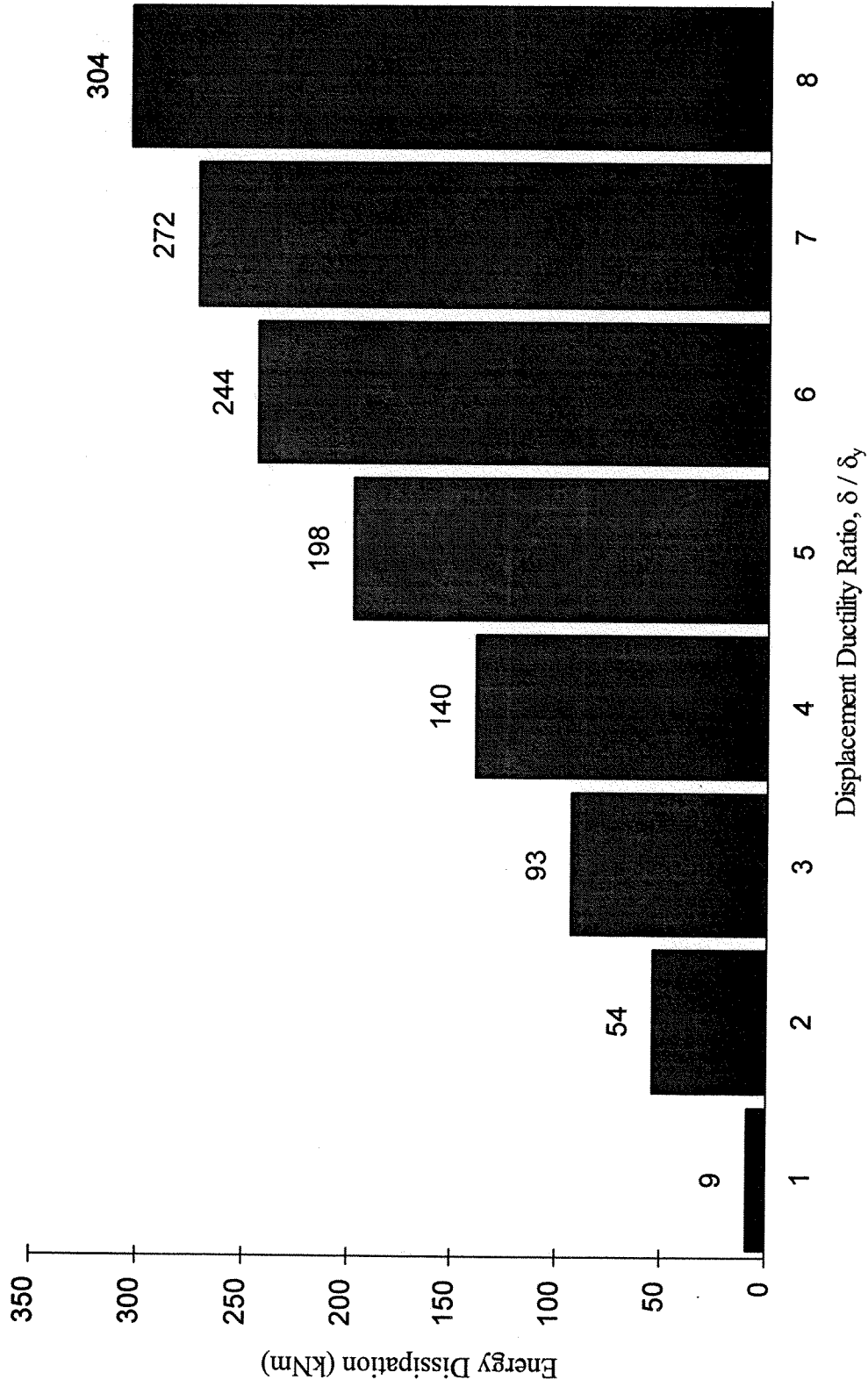


Fig. 7.5 Adjusted Energy Dissipation During Test

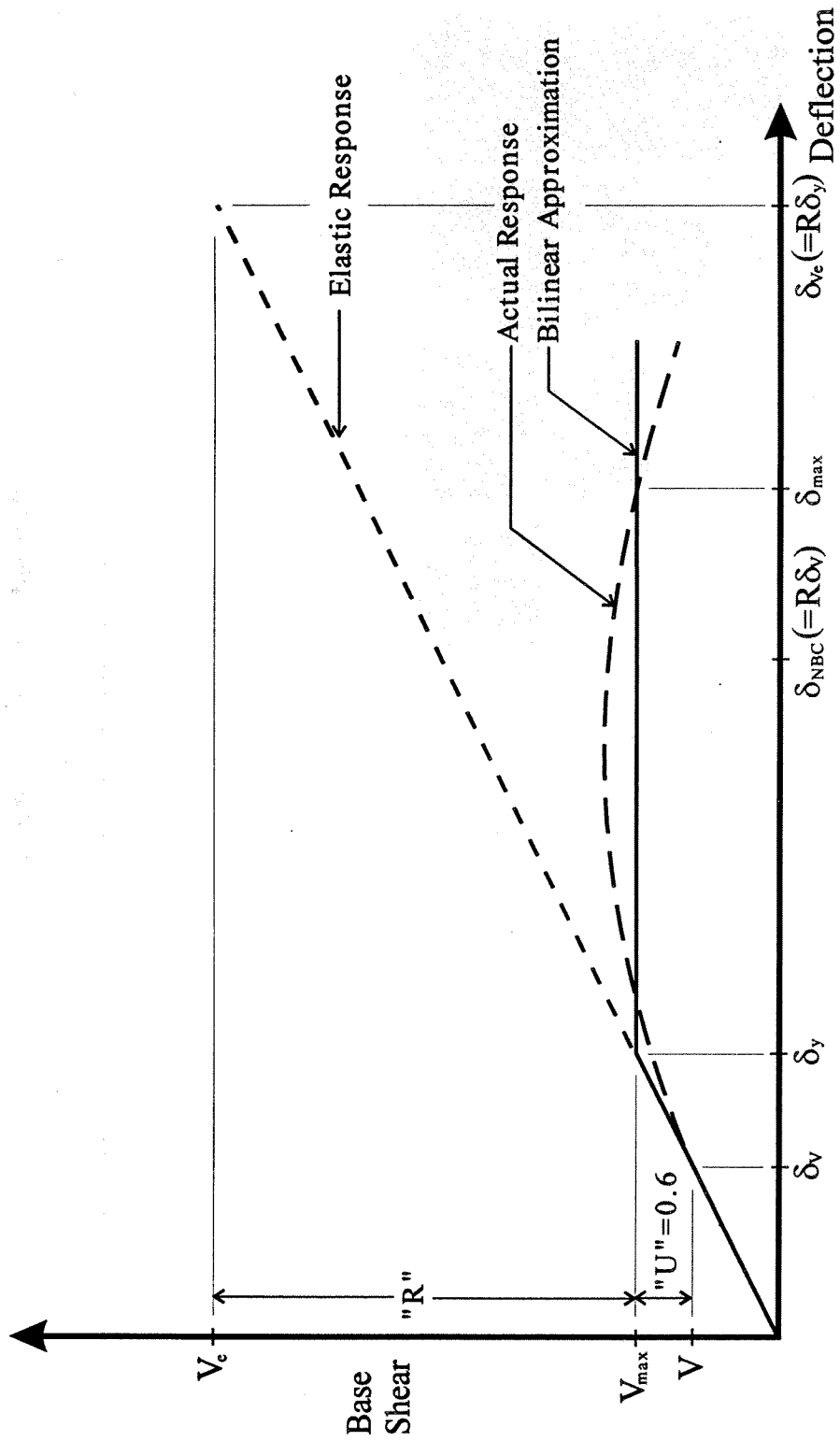


Fig. 7.6 Elastic and Inelastic Response of a Structural System

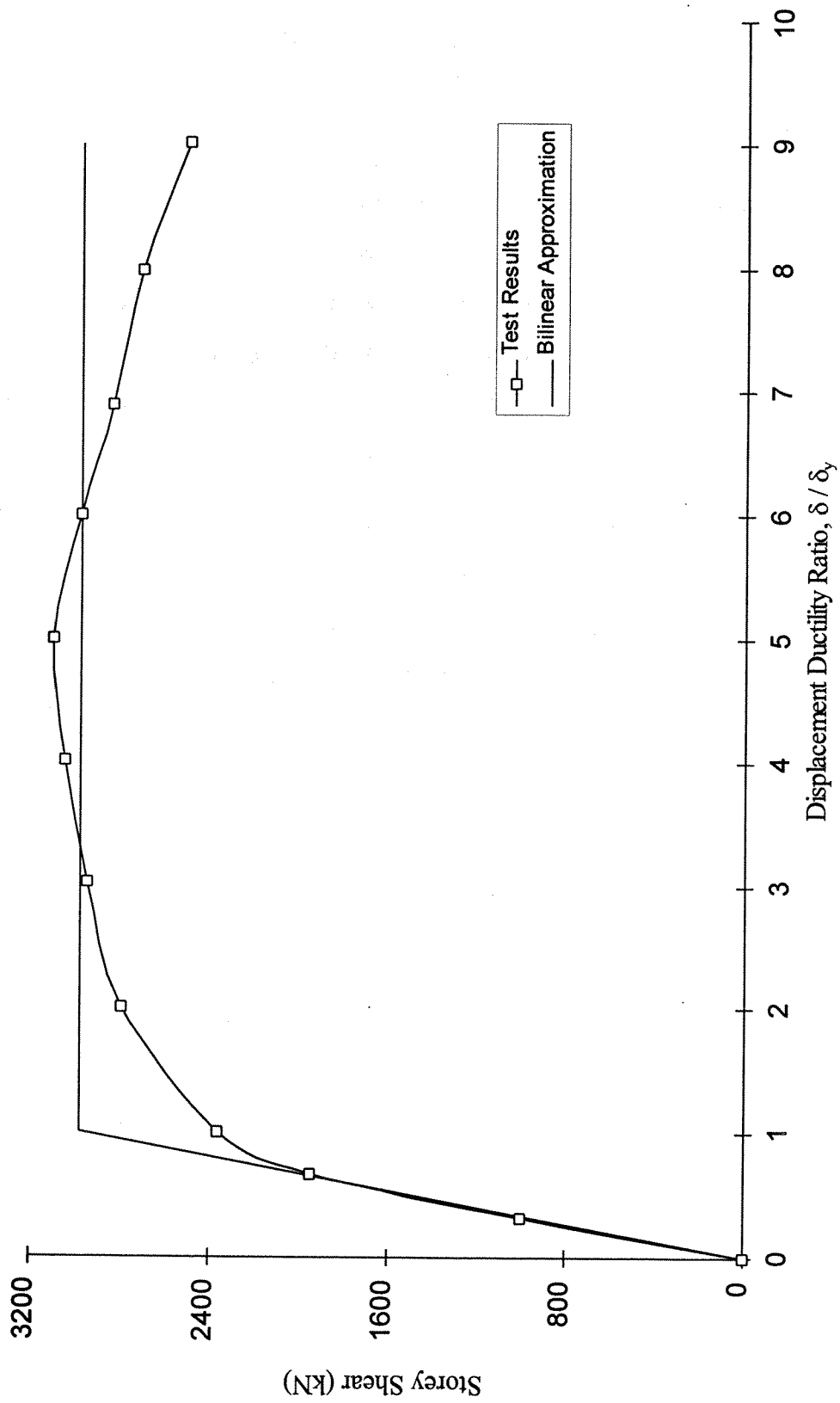


Fig. 7.7 Envelope of Cyclic Test Curves

8. FINITE ELEMENT ANALYSIS OF TEST SPECIMEN

8.1 Introduction

A preliminary finite element model for the analysis of steel plate shear walls is described in Chapter 3. Basic features of the model, such as the types of elements and the solution strategy used are discussed. An analysis using the model is compared to the results of a shear wall test conducted by Timler and Kulak (1983). In Chapter 4, these modelling concepts are applied to the four storey steel plate shear wall test specimen and predictions of its behaviour are made.

After the completion of both the main test and the ancillary tests, the finite element model was refined to represent more closely the test specimen as constructed. This chapter presents details of the refined model and the results of the associated analyses. Some of the most important basic features of the model described in Chapter 3 are repeated here for completeness, together with a discussion of modifications and refinements.

8.2 Description of Model

8.2.1 Elements

The basic components of the steel plate shear wall model were not changed for the final analyses. The beams and columns were modelled using a quadratic, shear-flexible beam element that allows for large axial strains. An I-shaped cross-section was used with 13 integration points so as to allow an accurate depiction of the stresses that vary non-linearly over the cross-section.

The shear wall infill plates were modelled using a quadratic shear-flexible plate/shell element. Five integration points were used through the thickness to permit an accurate representation of non-linear constitutive material behaviour. As in the

preliminary model, a 6x9 element mesh was used for Panel 1, a 4x9 mesh was used for Panel 4, and a 5x9 mesh was used in the remaining panels.

Further details of the elements used in the model are described in Section 3.2.1. Figure 4.3, representing the preliminary model, is also applicable for the refined model.

8.2.2 Geometry

Before conducting the shear wall test, the specimen was measured extensively to determine the as-built dimensions to be used in the subsequent analyses. The measured camber and sweep of the beams and columns and the column out-of-plumb were considered to be negligibly small and, therefore, they were not included in the model.

The cross-sectional dimensions of the beams and columns were measured at 34 locations. Mean values were used in the finite element model for the flange and web dimensions of each member type. The thickness of each panel was measured at 12 locations and the mean values were used in the model. A summary of the as-built dimensions is presented in Section 4.5.

The fish plate connection tabs were omitted from the model, as was done for the preliminary model. The suitability of this idealization is discussed in Section 3.3.1. The infill plate was taken to have an initial out-of-flatness corresponding to the third plate buckling mode of the shear wall loaded in the same manner as for the subsequent strength analyses. This mode occurred at an applied lateral load of 49.0 kN per floor. The third mode was selected because it was the lowest mode that resulted in the peak non-dimensional amplitude occurring within Panel 1, where the greatest plate deformations occur. The peak amplitude was set to an out-of-plane displacement of 10 mm, as in the preliminary model.

8.2.3 Connectivity and Bracing

Line elements are used for both the beam and the column members. The element nodes may be located eccentric to the centroid of the cross-section, as shown in Fig. 3.1. The column elements lie immediately adjacent to the infill plates and are connected directly to them at each node. Rigid outrigger elements are required at the tops of the columns in order to apply the concentric vertical loads.

The beam elements lie on the beam centreline. Rigid elements project upward and downward by a distance equal to one half the depth of the beam at each node and are in turn connected to the infill plate. In this manner, deformation compatibility is assured between the beams and infill plates.

The column bases and the lower edge of Panel 1 are fully fixed. The model also includes the out-of-plane bracing that was present in the physical test at each end of each beam.

8.2.4 Residual Stresses

In order to include the effects of residual stresses in the finite element model, extensive residual strain measurements were taken at various locations on the cross-sections of each type of member in the shear wall frame, as described in Section 5.3.

The finite element program, ABAQUS (Hibbitt *et al.* 1994), allows initial stress states to be specified only at integration points. The elements were modelled using 13 integration points across the cross-section, as described in Section 3.2.1. Integration is then performed internally according to Simpson's rule.

In order to incorporate the measured residual stresses into the model, certain assumptions were made. It was clear from the measured data that the residual stress patterns were essentially doubly-symmetric. Therefore, no distinction was made between the two flanges of each member or between the two halves of each flange

and web. The data was mirrored about the flange and web centrelines and the data from the two flanges were superimposed. This results in four data points at each measurement location for the flanges and two data points for the webs. However, the three data points that were apparently disturbed by rotorizing of the W310x60 member (see Section 5.3.3) were discarded. The resulting data for the flanges of the W310x118 member are presented in Fig. 8.1. The approach of mirroring the data points necessarily results in a doubly-symmetric residual stress distribution. There are two advantages to this. First, internal static moment equilibrium is enforced about the two principal axes and, second, the assumed residual stress distribution is independent of the orientation in which the member is installed into the frame.

A best-fit curve was applied to the measured data, as shown in Fig. 8.1. In all but two cases, a second order polynomial was sufficient to result in a suitable correlation coefficient ($r^2 \geq 0.95$). In one of these exceptions, use of a fourth order polynomial was able to achieve this level of correlation. In the other case, a sixth order polynomial limit was invoked for the W310x60 flange data, which showed considerable scatter, resulting in a value of $r^2 = 0.92$. Residual stresses were then determined from the curves at the integration points in the finite element model and used as the initial stress conditions for the numerical analyses.

When a user-defined initial stress condition is *imposed* upon the model, a situation may exist where global equilibrium is not satisfied in the structure. Therefore, an initial analysis step was performed prior to the application of any external loading that incrementally adjusted the initial stress pattern until equilibrium was achieved. It was observed that the residual stresses were not altered significantly by this analysis step.

8.2.5 Material Properties

In the final analytical study, most of the material properties were taken as prescribed for the preliminary model. A simple rate-independent constitutive behaviour is assumed in the model that is identical in tension and compression and the yield criterion is the von Mises yield surface model.

Measured material properties form the basis for the stress vs. strain relation for both the infill plates and the boundary members in the final model. Because of the large number of high level strain reversals, a kinematic hardening rule is invoked to simulate the Bauschinger effect in the cyclic runs. When kinematic hardening is specified, ABAQUS requires that the plastic strain relation have only a single hardening modulus. Thus, material behaviour determined from tension coupon tests must be modelled with a bilinear representation. The bilinear stress vs. strain response selected extended from the origin to the mean value of the static yield point (the slope is equal to the mean modulus of elasticity) and then to the mean static ultimate stress and corresponding strain. Any strains beyond this point are considered by the program to occur at a constant stress level. In order to facilitate comparisons, this same bilinear stress vs. strain relation is also used in the monotonic loading case.

8.2.6 Geometric Non-linearity

Refinements such as the inclusion of initial residual stresses resulted in a relatively complex model. With the consideration of geometric non-linearities, the analysis program was unable to trace the equilibrium path fully to the ultimate capacity. Therefore, for the monotonic loading case up to the ultimate capacity and for the cyclic loading case, the geometric non-linearities were not considered. To assess the impact of this approximation, a monotonic loading case was investigated with these non-linearities included, up to the point where the solution would no

longer converge. This is equivalent to a deflection at Level 1 of approximately 8.5 mm. The results of this comparison are described in Section 8.3.1.

8.3 Results of Analyses

8.3.1 Monotonic Loading

Using the refined model, but excluding geometric non-linearities, an ultimate strength analysis was performed in a manner similar to the preliminary numerical study. (A partial analysis that includes the geometric non-linearities is described subsequently.) After the initial analysis step to equilibrate the residual stress distributions in the beam and column members, gravity loads of 720 kN were applied to the top of each column. This magnitude is equal to the target gravity load used in conducting the physical test.

Equal horizontal in-plane forces were then applied at each floor level. The horizontal loads were increased until the deflection at Level 1 reached a value equal to $7\delta_y$ (59.5 mm), which is well beyond the deflection where the ultimate strength was reached.

Figures 8.2 to 8.5 show to the same scale the resulting storey shear vs. storey deflection response for Panels 1 through 4, respectively. Figure 8.6 shows the base shear plotted against the horizontal deflection at the top of the model. (Figure 8.6 uses a reduced horizontal scale as compared with Figs. 8.2 to 8.5.) In each case, there is excellent agreement with the test results up to a base shear of about 400 kN, or about one-eighth of the maximum value attained. At higher loading levels, where the model is still essentially elastic, it predicts stiffer behaviour than that exhibited by the test specimen. This discrepancy is considered to occur for two reasons. First, the non-linear geometric effects, not taken into account in the model, tend to become more significant as the deflections increase. Second, the cyclic nature of the loading applied to the test specimen generally results in a slightly decreasing storey stiffness with an

increasing number of cycles of loading applied. (It is noted that the significant yield deflection, δ_y , was first reached during the eleventh loading cycle.) This slight stiffness degradation is not modelled in the monotonic loading of the finite element analysis.

The results for all panels and for the overall shear wall behaviour show that the finite element model accurately predicts the ultimate load. This load level occurred in the test at a deflection of $5\delta_y$ (42.5 mm) at Level 1.

The gradual post-ultimate strength degradation exhibited by the test specimen (Cycles 24 to 30) is not seen in the finite element results because the tearing and local buckling behaviour of the shear wall were not included in the model. This degradation is derived primarily from these phenomena. In any case, current earthquake engineering practice (e.g., NBCC 1995a; FEMA 1994) prohibits the utilization of ductility levels that result in storey deflections of the magnitudes experienced in Panel 1 during these cycles. However, if ductility demands of this magnitude *were* required of the structure during an earthquake, the physical test has demonstrated that no sudden loss in stiffness will occur in a properly detailed steel plate shear wall.

In order to assess the effect of omitting geometric non-linearities in the analysis, a second monotonic analysis was conducted with the geometric non-linearities included. The equilibrium path was traced up to a load and deflection level where it became very difficult to achieve convergence.

The results of the two analyses (including and excluding geometric non-linearities) are compared in Figs. 8.7 to 8.11, where the loading excursions for Cycles 5+, 8+, and 11+ of the test are also shown. The softening effect of including the geometric non-linearities is evident in each of the figures. The decrease in slope in the elastic portion of the responses varies from 11% to 20%. The response that includes geometric non-linearities also tends to deviate from the linear initial response

at a lower load level than the response that excludes this effect. Moreover, when the applied shear is sufficiently high in Panel 1, the softening effect of multiple loading cycles can be seen by a comparison of Cycles 8 and 11 (Fig. 8.7). Had the test specimen been loaded with a *monotonic* loading history, the results of the model that includes geometric non-linearities would agree even more closely with the test results. It is also evident that for Panels 2 to 4 (Figs. 8.8 to 8.10, respectively), which underwent considerably less distortion and degradation, the analysis that includes the geometric non-linearities shows excellent agreement with the test results.

It is recommended that, wherever feasible, geometric non-linearities should be included in the finite element analysis of steel plate shear walls. However, where severe numerical difficulties are encountered, an excellent approximation of the ultimate strength is obtained even by neglecting this effect. For estimating the structural stiffness at low and medium load levels, a partial analysis including geometric non-linearities should be conducted to as high a load level as practicable.

8.3.2 Cyclic Loading

The monotonic loading analyses provide a means of estimating the envelope of the cyclic response up to the ultimate capacity. However, in order to fully describe the cyclic behaviour, the finite element model must be able to trace the unloading and reloading responses with reasonable accuracy.

A cyclic analysis was performed on the steel plate shear wall with loading similar to that applied to the test specimen. The storey shear vs. storey deflection results of this analysis are shown in Fig. 8.12 for Panel 1. For practical reasons, only the loading for Cycles 5, 11, 17, 22, and 26+ was applied. A reduced gravity load was used in the early cycles of the test, which affected only Cycle 5 of the analysis. The target gravity load from the test of 575 kN per column was applied during this cycle and the load was then increased to 720 kN for all subsequent cycles.

The effects of non-linear geometric behaviour were not included for reasons stated previously. A kinematic hardening rule was used to simulate the Bauschinger effect during load reversals.

The stiffness at very low loading and the ultimate strength are both predicted well by the model, as was the case for monotonic loading. The stiffness of the model at intermediate load levels is somewhat higher than the stiffness exhibited by the test specimen. This is considered to be chiefly due to the exclusion of the non-linear geometric effects.

An important feature of the hysteretic behaviour that is not duplicated by the model is the pinching of the hysteresis curves. The test specimen exhibited significantly reduced stiffness during the early reloading phase after a load reversal, as shown in Fig. 8.12. This occurred prior to the full development of the diagonal tension field in the infill plate. This reduced stiffness did not occur in the numerical analysis. This is primarily because, although the infill plate is deflected significantly out-of-plane, the local second order effects have been neglected. Further work is required so that the second order effects can be included in the finite element analysis to model properly the pinching characteristic of the shear wall hysteretic behaviour. A relatively simple behavioural model that does reflect the pinching characteristic is presented in Chapter 9.

8.4 Summary

The preliminary finite element model presented in Chapter 3 was refined in order to represent the four storey test specimen as closely as practicable, but the basic features of the model such as the element types and the model mesh were retained. As-built dimensions and measured material properties were used in the model. An initially deformed geometry was used to represent initial out-of-plane deformations in the infill plates and the residual stresses of the boundary members were modelled.

The model predicts the ultimate strength of the shear wall very well for all storeys. The initial stiffness of the model is also in good agreement with the test results. However, at somewhat higher load levels, the model overestimates the stiffness of the test specimen. This is attributed primarily to the fact that the second order geometric effects were neglected in the analysis in order to be able to achieve convergence to the solution at large deflections. A slight decrease in stiffness of the test specimen during low and moderate intensity loading cycles also contributed to this discrepancy.

Although the main monotonic and cyclic analyses were conducted without the consideration of geometric non-linearities due to numerical difficulties, a separate study including the non-linearities led to substantially better comparisons with the test results. Additional research is required to obtain solutions at large deflections with the inclusion of the second order geometric effects.

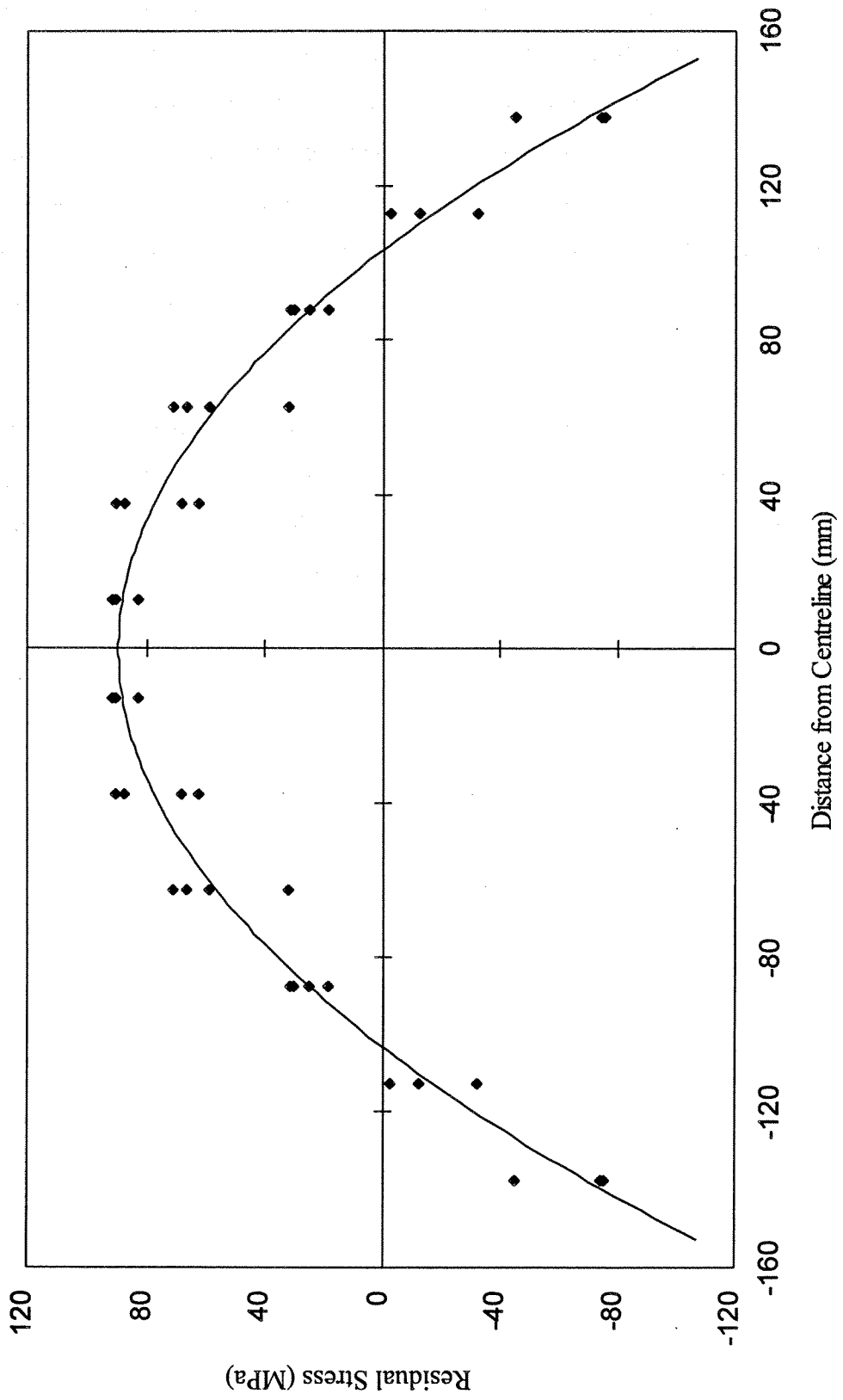


Fig. 8.1 W310X118 Flange Residual Stresses

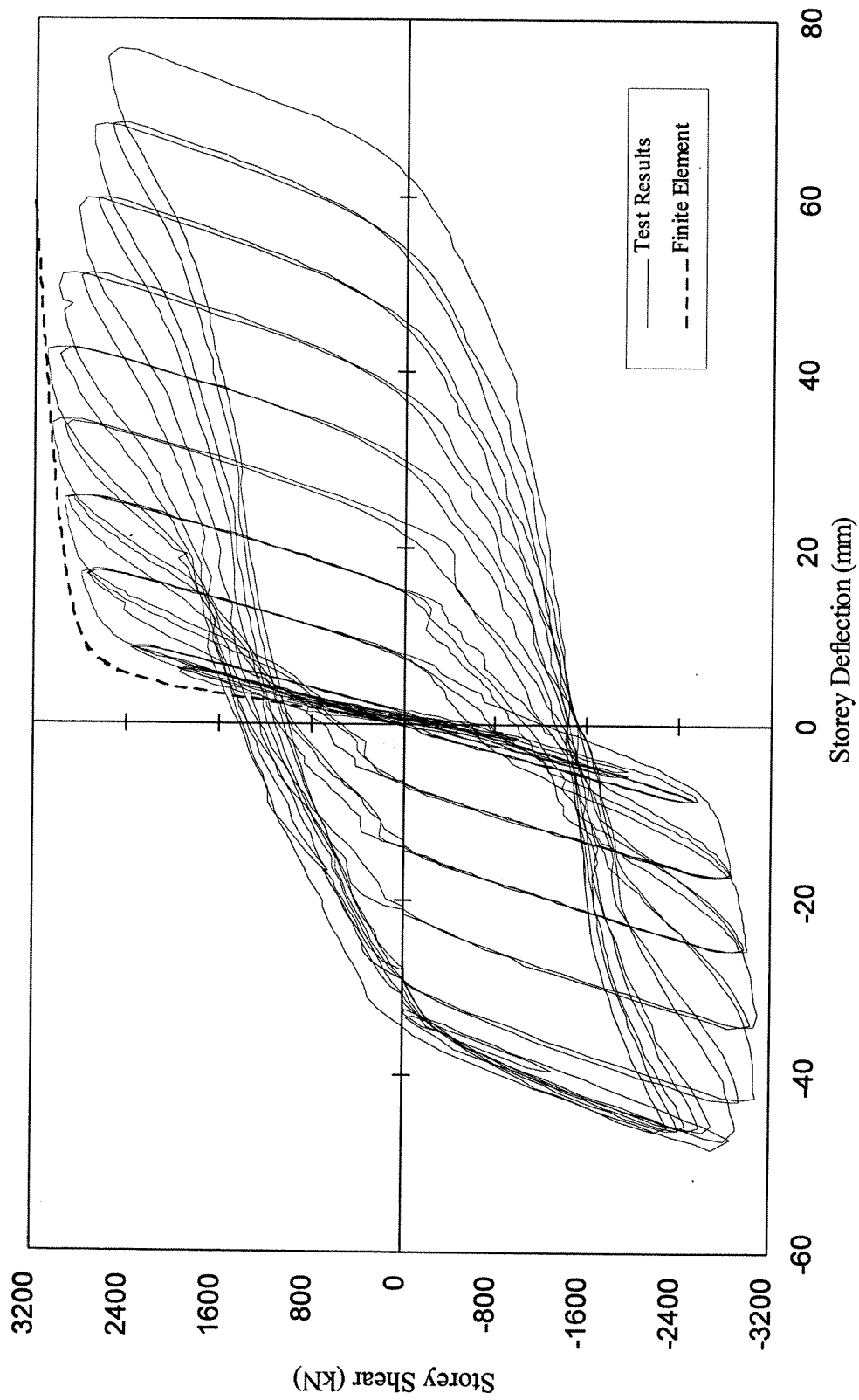


Fig. 8.2 Comparison of Monotonic Finite Element Analysis with Test Results – Panel 1

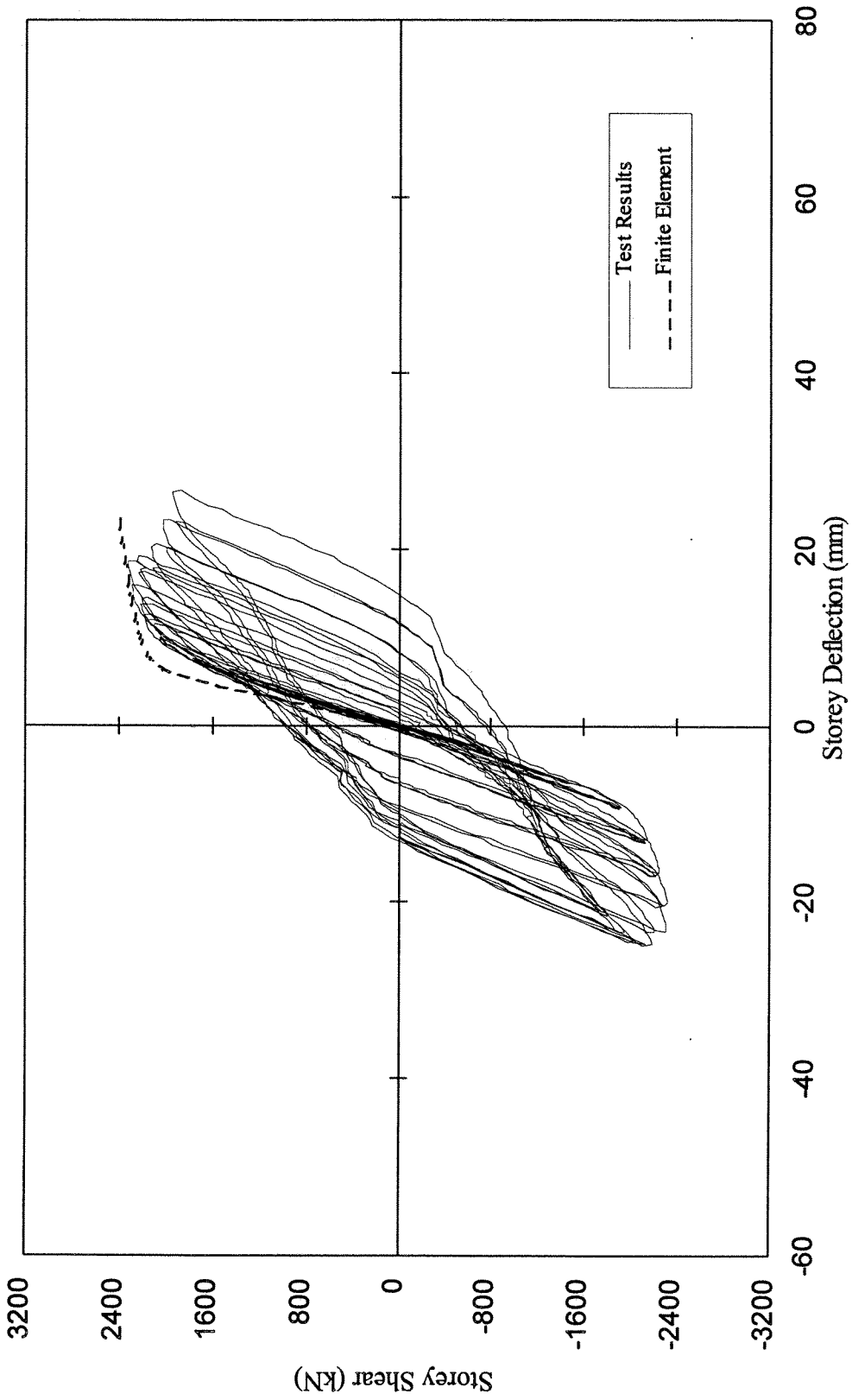


Fig. 8.3 Comparison of Monotonic Finite Element Analysis with Test Results – Panel 2

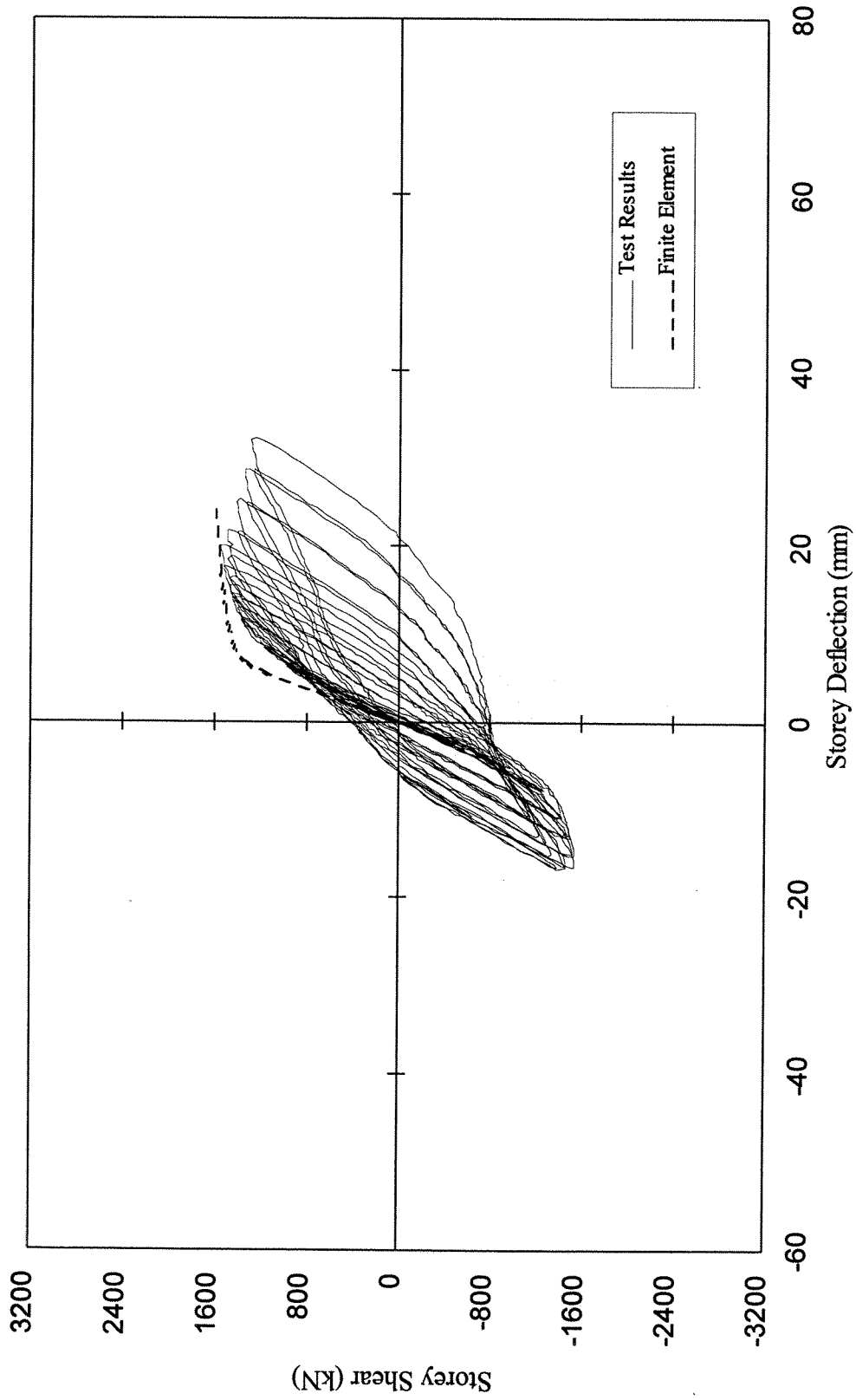


Fig. 8.4 Comparison of Monotonic Finite Element Analysis with Test Results – Panel 3

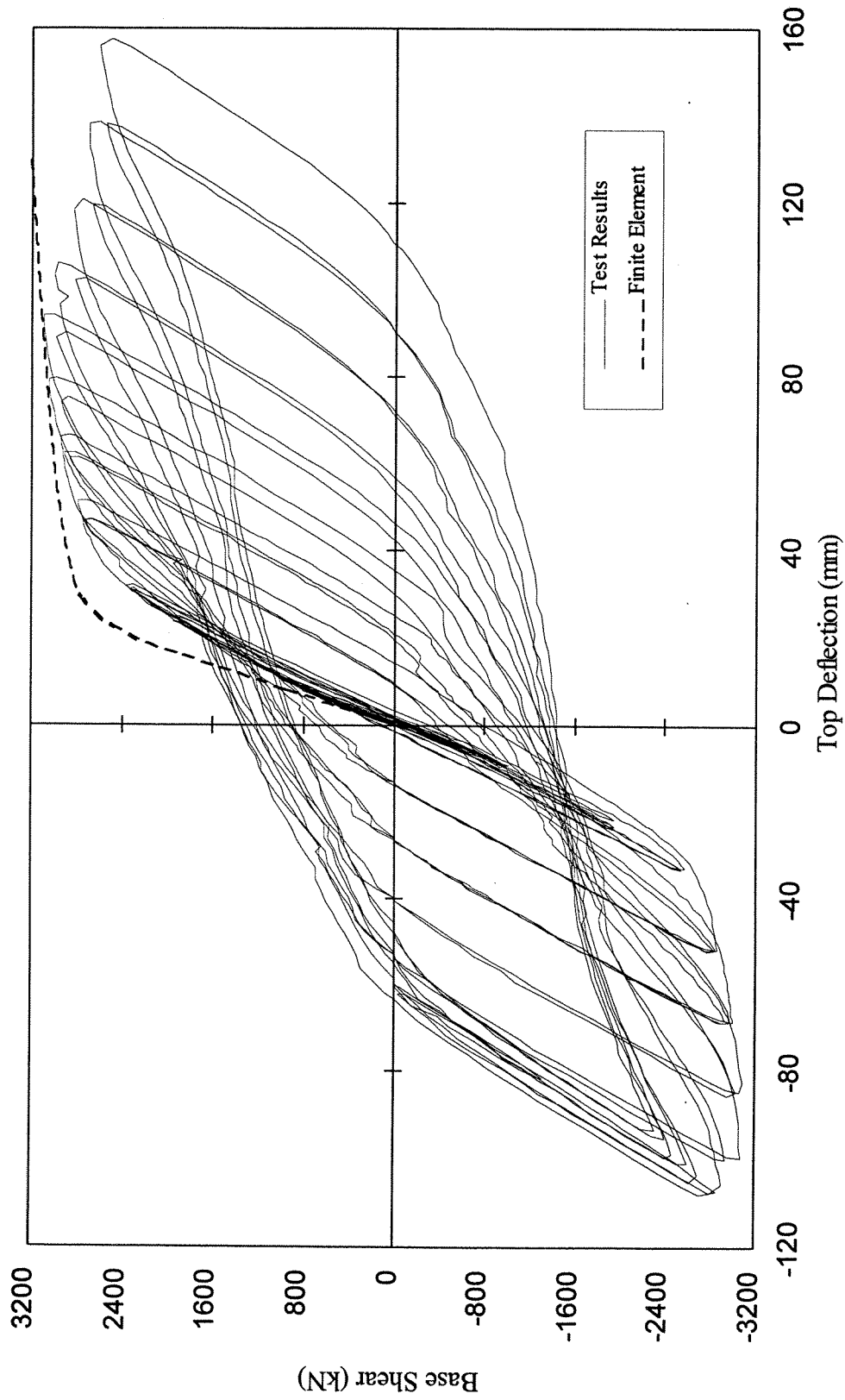


Fig. 8.6 Comparison of Monotonic Finite Element Analysis with Test Results – Overall

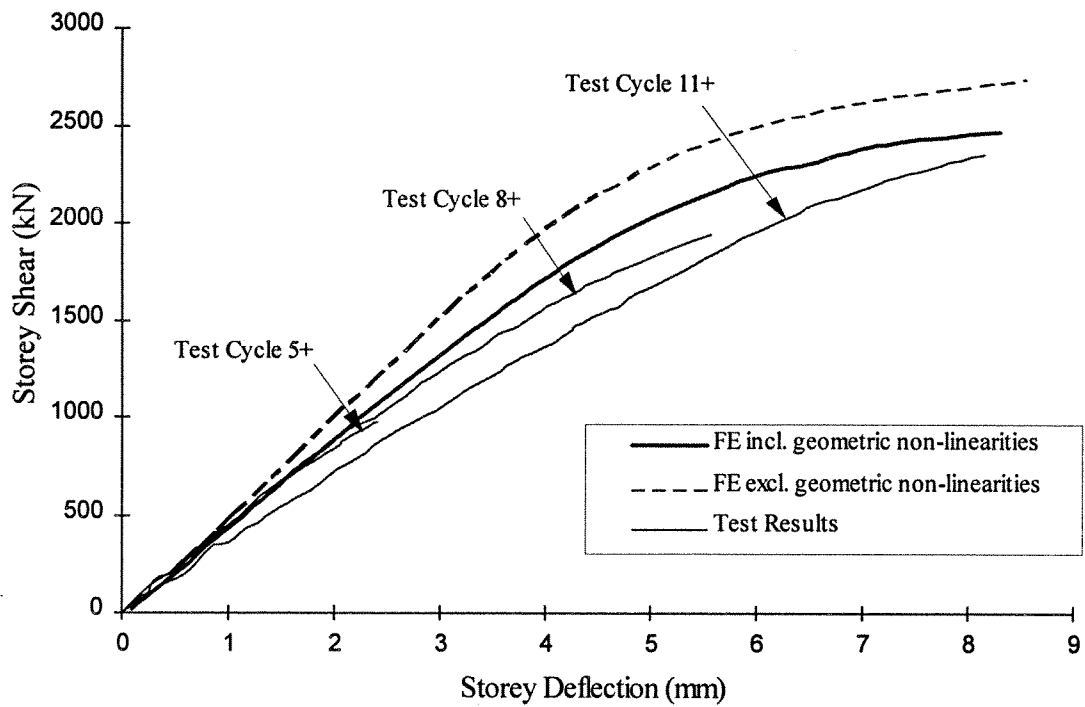


Fig. 8.7 Comparison of Initial Finite Element Curves with Test Results – Panel 1

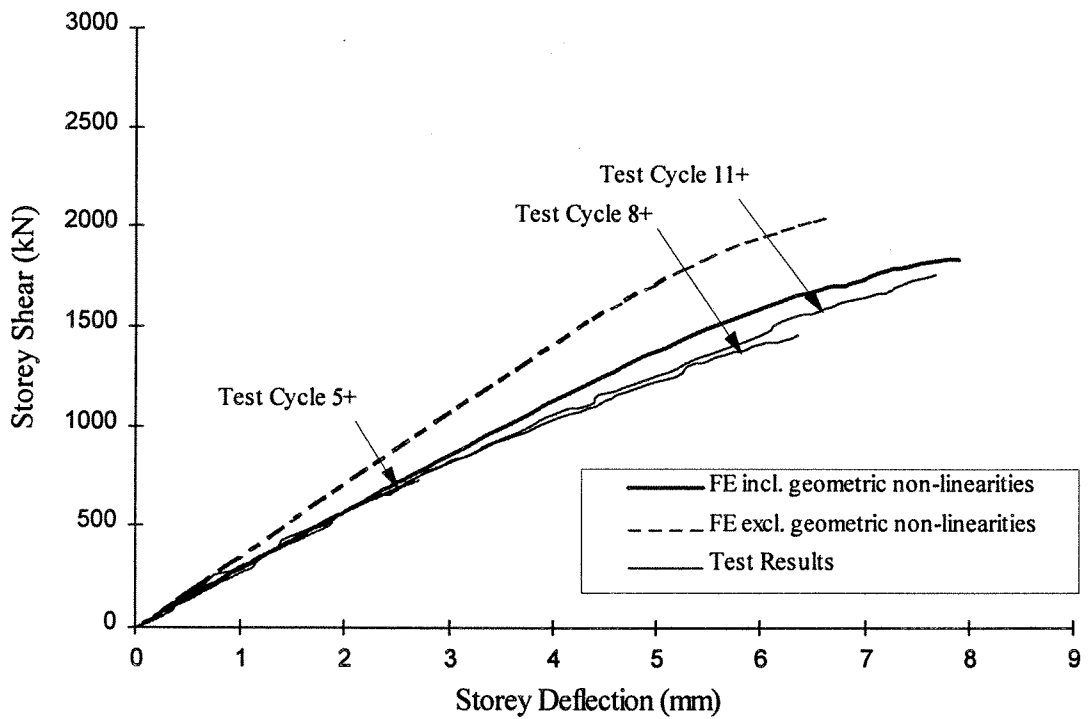


Fig. 8.8 Comparison of Initial Finite Element Curves with Test Results – Panel 2

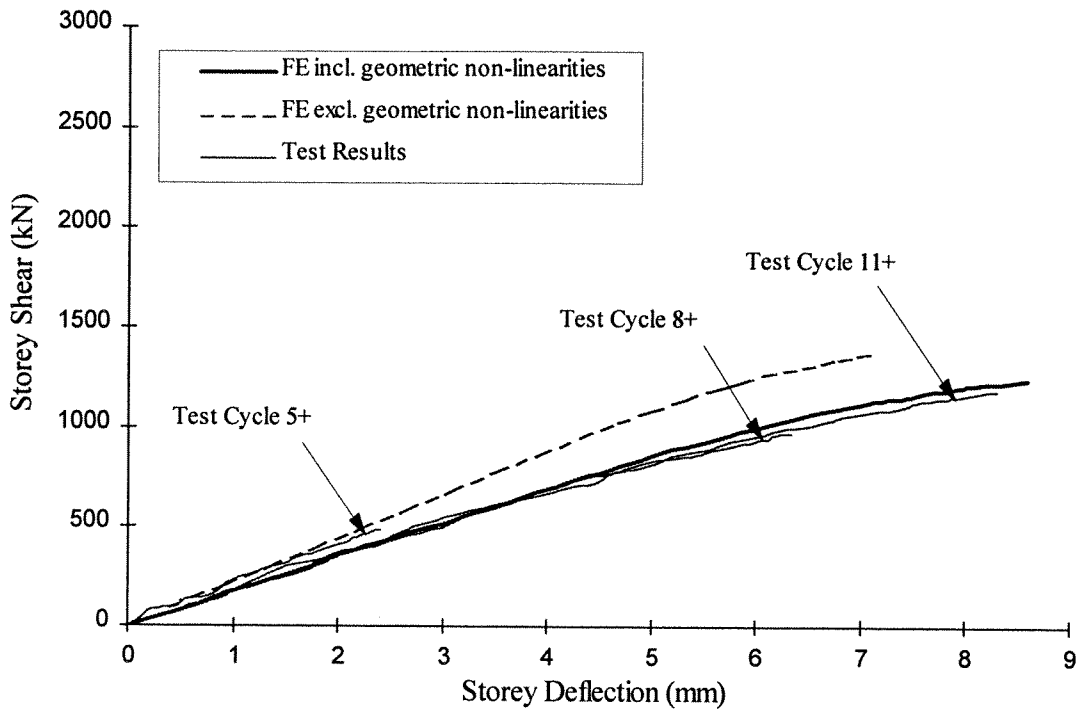


Fig. 8.9 Comparison of Initial Finite Element Curves with Test Results – Panel 3

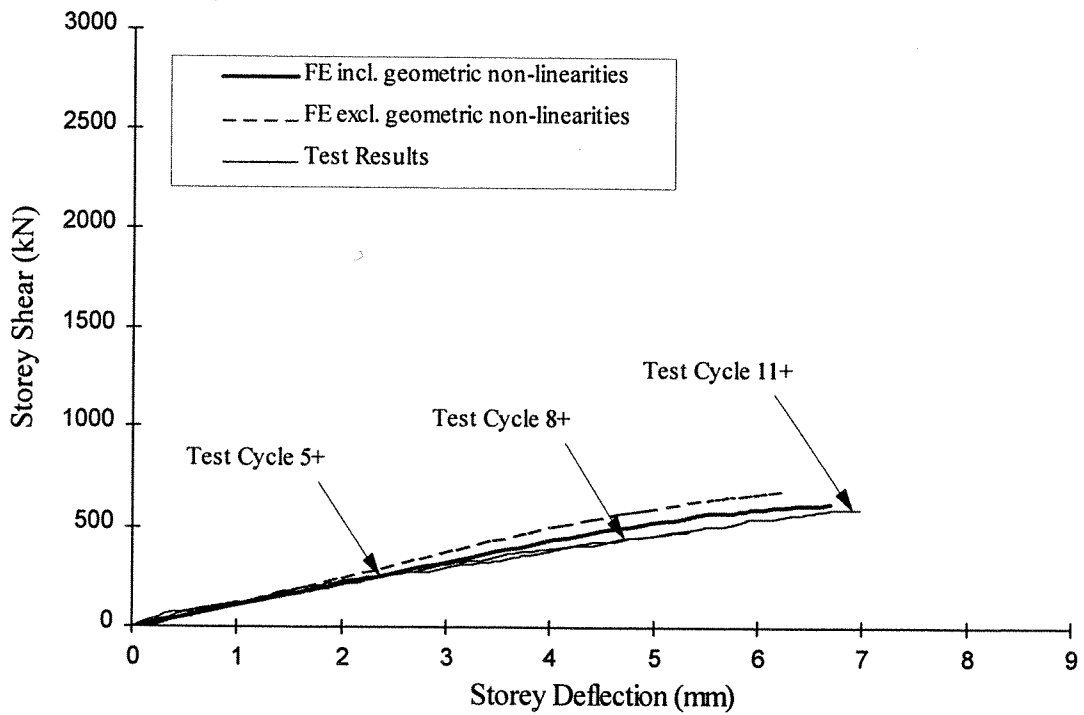


Fig. 8.10 Comparison of Initial Finite Element Curves with Test Results – Panel 4

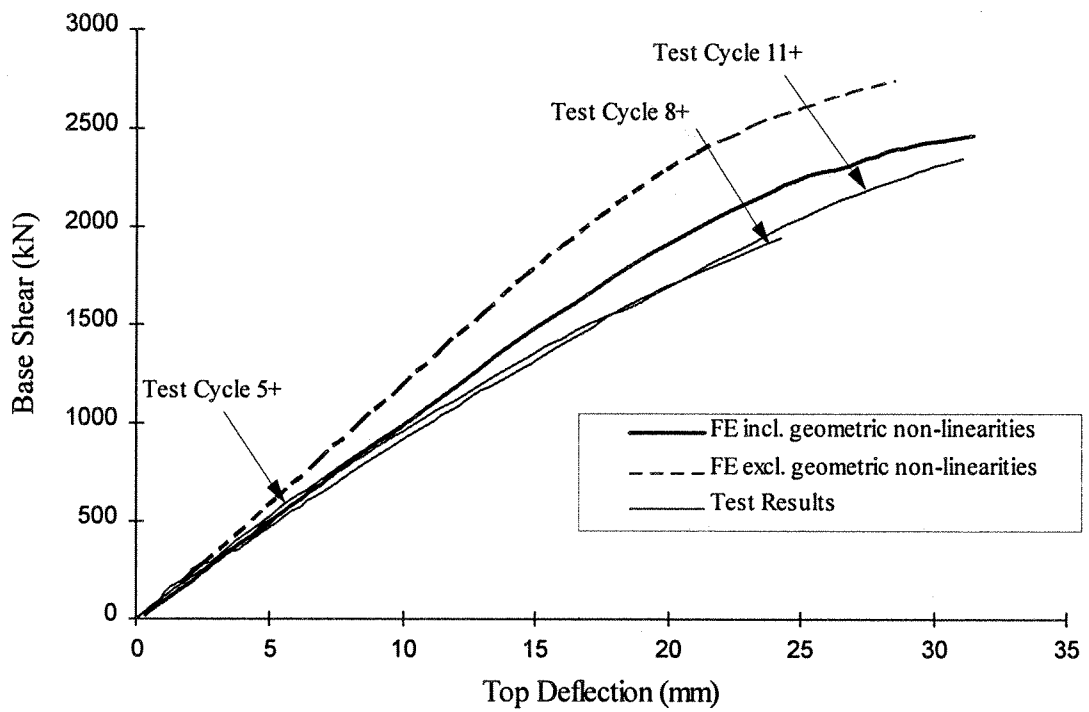


Fig. 8.11 Comparison of Initial Finite Element Curves with Test Results – Overall

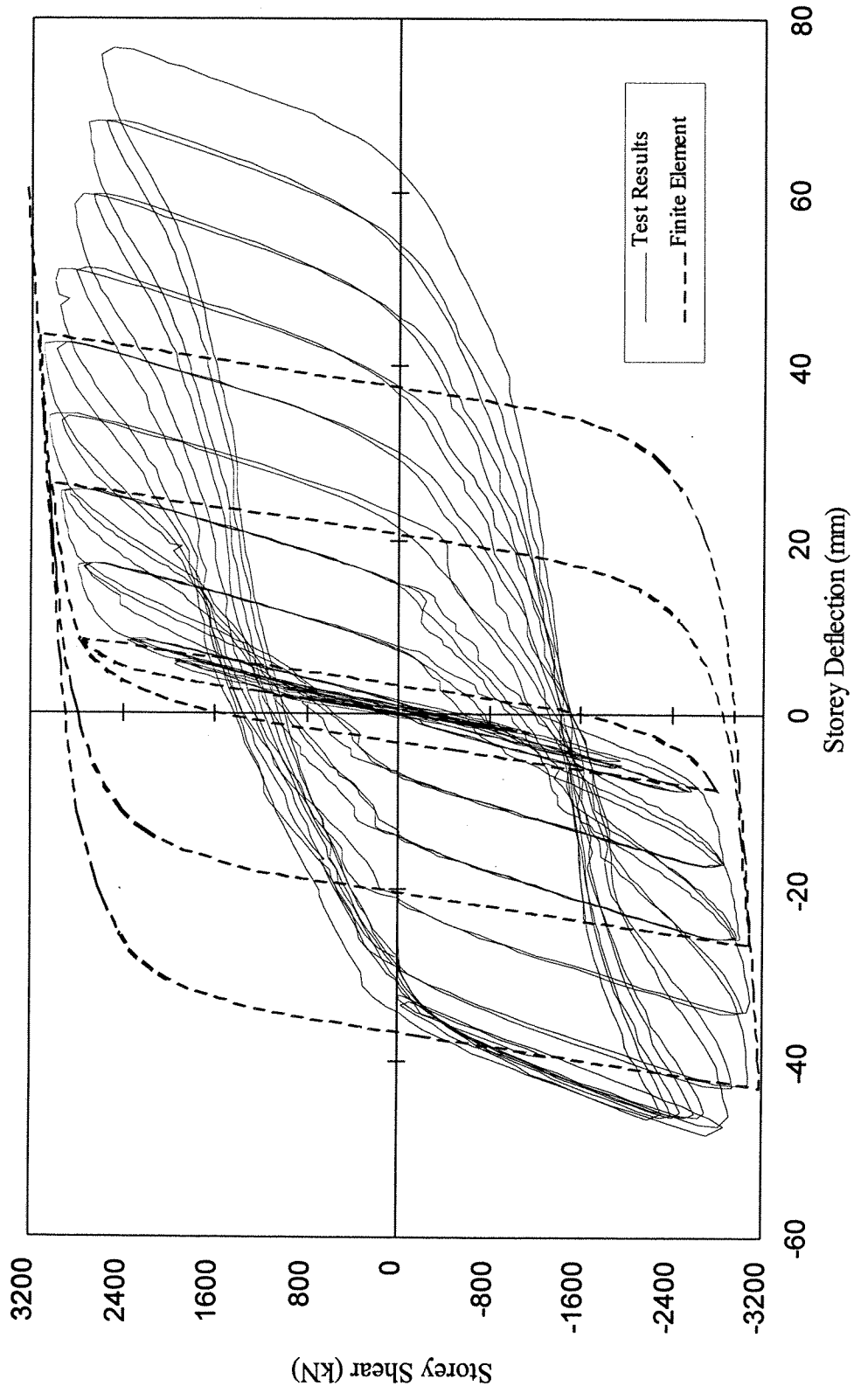


Fig. 8.12 Comparison of Finite Element Hysteresis Analysis with Test Results – Panel 1

9. SIMPLIFIED ANALYSIS

9.1 Introduction

The finite element method provides a powerful technique for modelling the behaviour of complex structures. However, the resources for conducting such an analysis are not universally available. In the case of routine analysis of building components, designers generally require simpler methods that can be processed with commonly available computing resources.

A simplified method for analysing thin-panel steel plate shear walls—the strip model—was presented originally by Thorburn *et al.* (1983). This model represents the buckled infill plates as a series of discrete, pin-ended strips inclined in the direction of the tension field. The model can be analysed using any commercially available plane frame analysis package, making the method accessible to almost all structural design offices.

Results from a strip model analysis have been compared with good results to the physical tests done by Timler and Kulak (1983) and by Tromposch and Kulak (1987). However, the shear wall test conducted as part of this research affords the first opportunity to evaluate the strip model by comparing it to a test employing a multi-storey configuration, for which it was originally developed.

This chapter discusses the assumptions inherent in the plane-frame strip model and the multi-step approach for determining the envelope of the load vs. deflection behaviour. Results of strip model analyses of the test specimen are compared to the test data and the results of the finite element analysis described in Chapter 8. The sensitivity of the strip model analysis to various parameters is also discussed.

Two models for predicting hysteretic behaviour of steel plate shear walls are presented. A model developed by Tromposch and Kulak (1987), which is a revised

version of a model originally developed by Mimura and Akiyama (1977), is described and a new model is proposed that explicitly separates the contributions of the moment-resisting frame and the infill panel at all stages of the loading cycle. The models are used to predict three cycles of response from the test curves and comparisons between the two models are made.

9.2 Strip Model

9.2.1 Analysis Method

The strip model assumes that the dominant action that resists a storey shear is the diagonal tension field that develops after the thin, unstiffened infill plate buckles. Generally, buckling occurs at relatively low lateral loads because of the large size of the panel with respect to its thickness and because of the inevitability of some initial out-of-plane imperfections. Because of the dominance of this behaviour, the tension field is modelled as a series of discrete, pin-ended strips inclined with the same orientation as the tension field. This assumes that the compression in the orthogonal direction is negligible and that the angle of inclination of the tension field can be reasonably predicted. The strips are assigned an area equal to the plate thickness multiplied by the width of the strip. In a previous study (Thorburn *et al.* 1983), modelling each panel with a series of ten strips was found to provide sufficient accuracy. However, for comparison, the use of 20 strips was also studied herein. This comparison is presented in Section 9.3.2. Figure 9.1 shows the plane frame model used for the analysis of the test specimen.

Because most common plane frame computer programs are only capable of representing elastic behaviour, a full analysis up to the ultimate strength requires a multi-step approach. When the lateral load applied to the model reaches a level such that any strip reaches its tensile yield capacity, that strip is removed from the model and replaced by equivalent forces at each end. This approach models the strip

implicitly as having a bilinear elastic – perfectly plastic stress vs. strain curve, i.e., the member maintains its yield load, but is unable to carry additional load as the applied forces increase. Assuming that the infill plate in the real structure has properties typical of hot-rolled structural steel, this is a good behavioural approximation. It should be recognized that, although the yield stress of the material is generally not known in advance, a good estimate is required for an accurate prediction of the response of the frame. In most design situations, simply using the nominal yield strength leads to conservative results because the mean yield strength generally exceeds the nominal value by a considerable margin. However, in seismic design, if the actual yield stress is greater than that assumed, overstressing of other components can occur during an earthquake. In some cases, a pair of analyses to bracket likely extremes may be appropriate. In the multi-storey test examined herein, the properties of all materials used were known from ancillary tests.

Inelasticity in the moment-resisting frame must also be represented in the analysis in order to model properly the shear wall behaviour. In a manner analogous to that used for the material response in the tension strips, the members of the frame are assumed to form a plastic hinge when the cross-section is fully yielded under the combined actions of axial and flexural forces. This results in a softening of the shear wall boundary frame. Appendix M of the Canadian steel design standard (CSA 1994) requires that columns forming an integral part of a steel plate shear wall shall be proportioned as Class 1 beam-columns. This means that a fully plastic condition can be achieved without the onset of local buckling. However, the possibility of overall member buckling is not addressed by this planar analysis and must be checked separately.

For axial compression plus uniaxial bending about the major axis, the cross-sectional capacity of a Class 1 I-shaped beam-column can be described (CSA 1994) by the equation:

$$\frac{C}{C_y} + \frac{0.85 M}{M_p} = 1.0 \quad (M \leq M_p) \quad [9.1]$$

where C and M are the applied compressive force and moment, respectively, and C_y and M_p are the actions that cause full plasticity under the effects of compression or bending acting alone. (The load and resistance factors have been omitted from Eq. 9.1.) When the lateral loads reach a level where this equation is satisfied anywhere in the frame, a plastic hinge is modelled at that location. Clearly, it is necessary that the yield strength for the material again must be estimated. The use of nominal values of cross-sectional proportions is considered appropriate for design.

Modelling a plastic hinge in an elastic plane frame analysis requires the introduction of a true hinge plus opposing moments on each side of this joint equal in magnitude to the moment that was present when the hinge formed. Thus, at the hinge location, the frame will maintain the current moment as the lateral loads increase in subsequent loading steps. Because of the nature of the hinge in the model, the cross-section will continue to accept axial load. Although with perfectly plastic behaviour this model is not strictly correct, neglected effects such as strain hardening make this a reasonable approximation.

It should be recognized that the formation of a plastic hinge is actually a gradual process and that varying amounts of plasticity exist over a finite length of the member. However, the assumption that elastic behaviour is maintained up to the point of full plastification of the cross-section and that the hinge ultimately forms at a point are considered to be reasonable approximations. Moreover, it is considered adequate to examine the frame for plastic hinges only at the ends of the members. Thus, plastic hinges are modelled when they form at the end of the beams or in the columns at a floor level only. Residual stresses in the boundary members are neglected.

Gravity loads expected to be present in combination with the lateral loads are applied in the first load step and maintained throughout the analysis. Some method of accounting for second-order effects due to these gravity loads acting on a deflected frame is required: in an ultimate strength analysis deflections can rapidly become significant. Most commercial plane frame computer programs can accommodate the second-order geometric effects.

The multi-step analysis procedure consists of applying lateral loads until yielding occurs in one or more tension strips or a plastic hinge forms at some point in the moment-resisting frame. The analysis to this point provides load and deflection information for the frame at the limit of elastic behaviour. The model is then modified by replacing yielded tension strips with forces and replacing plastic hinges with true hinges and moments according to the methods described above. This softened model is then loaded with lateral forces greater than those in the previous step. Loading continues until yielding occurs in one or more of the remaining tension strips or another plastic hinge forms. The process is repeated until a mechanism forms or until the load vs. deflection curve approaches zero slope.

Experience has shown that it is good practice to rerun the analysis after tension strips are removed or hinges inserted and the associated forces added, initially *without* increasing the lateral loads. Should the results of the two analyses differ significantly, the modelling errors can be identified and corrected. An increment in the lateral load may then be applied.

9.2.2 Angle of Inclination of Tension Field

In order to formulate a steel plate shear wall strip model, the angle of inclination of the tension field (and thus of the tension strips) must be estimated. A method of estimating this angle based on the principle of least work was derived by Thorburn *et al.* (1983) and later refined by Timler and Kulak (1983). The derivation

was similar to that of Kuhn *et al.* (1952), which, in turn, was based on the theory of pure diagonal tension originally developed by Wagner (1931).

According to Timler and Kulak (1983), the angle of inclination, α , for steel plate shear walls having pin-ended beams is (some symbols differ from those in the original work):

$$\alpha = \tan^{-1} \sqrt[4]{\frac{1 + \frac{tL}{2A_c}}{1 + t h_s \left(\frac{1}{A_b} + \frac{h_s^3}{360 I_c L} \right)}} \quad [9.2]$$

where the variables are as defined in the list of symbols. Although the formulation of Eq. 9.2 involves a number of simplifying assumptions, Timler and Kulak demonstrated that reasonable agreement was obtained between the predicted value and those measured in the infill panel of their test specimen.

There is considerable added complexity in extending Eq. 9.2 for use in steel plate shear walls having moment-resisting beam-to-column connections. This arises because the storey shear is shared in a complex interaction between the moment-resisting frame and the diagonal tension field. Rather than making further approximations, in Section 9.3.2 it is demonstrated that for the four-storey test specimen, the load vs. deflection behaviour is relatively insensitive to the angle of inclination selected in the range near 45° . In shear walls of typical proportions, the angle of inclination would not be expected to differ from 45° by more than a few degrees. Therefore, an angle of 45° can be used for preliminary analyses.

The bending moments measured near the beam-to-column joints during the four storey test were relatively low and would also be expected to be low in other similar shear walls because of the dominance of wall behaviour observed in the test as opposed to frame behaviour. Therefore, it is suggested for the final analysis that

Eq. 9.2 remains a valid method for estimating this angle for shear walls with moment-resisting beam-to-column connections.

9.3 Comparison with Test Results

9.3.1 Introduction

Strip model analyses of the test specimen were carried out in order to compare the results with the behaviour exhibited during the physical test. In order to demonstrate the effect of varying the angle of inclination of the tension strips, models with two different angles, judged to be near the lower and upper end of the typical range, were used. In each of the two cases, the same angle of inclination was used in all four storeys.

In general, it is recommended that ten strips be used in each storey. However, in order to investigate the effect of the number of strips used in the model, another analysis was conducted using 20 strips in the lowest storey. The use of ten strips was retained for the top three storeys.

In all analyses, gravity loads that were equivalent to those applied to the test specimen were included. Equal lateral loads were applied at each floor level in a monotonic manner until the ultimate capacity of the frame was reached.

9.3.2 Analyses and Results

The analyses presented in this section were performed using the commercial three-dimensional structural analysis computer program S-FRAME (Softtek Services 1995). The features utilized for the analysis are available in most commercial two-dimensional frame analysis programs, however.

In conducting P-delta analyses that reflect the deflected shape, the S-FRAME program considers both the effects of axial loads acting on a member deflected

between its end points (the so-called $P-\delta$ effects) and the effects of axial loads acting on a member with one end laterally displaced with respect to the other (the $P-\Delta$ effects). The technique follows a two-cycle iterative approach. In this procedure, nodal displacements, $\{X\}$, are determined initially using a linear analysis:

$$[K]\{X\} = \{R\} \quad [9.3]$$

where $[K]$ is the structure stiffness matrix and $\{R\}$ is the load vector. Using these displacements, the member forces are determined and used to form the structure geometric stiffness matrix, $[K_G]$, that accounts for both the $P-\delta$ and $P-\Delta$ effects. In the second cycle, the nodal displacements are recalculated according to:

$$([K] + [K_G])\{X\} = \{R\} \quad [9.4]$$

which includes an approximation of the second-order geometric effects. Final member forces are then determined from the updated nodal displacements.

In order to create a strip model, the angle of inclination of the tension field, α , must be estimated. As a starting point, the numerical model developed for the test specimen was created using an angle of inclination for the tension strips calculated according to Eq. 9.2. This equation identified angles for Storeys 1 through 4 of 42.0° , 41.8° , 42.4° , and 43.5° , respectively. The mean value of 42.4° (referred to in subsequent discussions as 42°) was used in each storey for the model. Figure 9.1 shows a diagram of the model with the infill plates modelled as ten pin-ended strips in each storey. Figures 9.2 to 9.6 show the results of the analysis for each of the four storeys and for the shear wall as a whole. (For ease of comparison, the scales are identical for the four individual panels.) The curve in each figure depicting the behaviour of the moment-resisting frame acting alone serves to demonstrate the significant contribution of the infill panels in resisting the storey shears and increasing the stiffness of the structure.

The areas of the tension strips were calculated using the mean measured thickness of the infill panels of the test specimen. However, nominal values were used for the cross-sectional properties of the frame members. Extensive measurements showed that the mean quantities did not differ appreciably from the nominal values. In all cases, the mean measured static yield stress was used to determine the onset of plastic behaviour.

In the initial loading step, the full gravity loads were applied to the column tops and equal lateral loads were applied at the four floor levels. The lateral loads were set to a value where inelastic action first occurred, according to the criteria outlined in Section 9.2.1. The numbers in the diagram of the frame shown in Fig. 9.7 indicate the loading steps of the numerical analysis during which plastic hinges formed or tension strips yielded. Inelastic action first occurred through the formation of a plastic hinge at the base of the column on the opposite side of the frame to the applied lateral loads. This establishes the limit of elastic behaviour for the strip model curves of Figs. 9.2 to 9.6. The numerical model was then modified to include the behaviour of this plastic hinge and the lateral loads were increased further, up to a point where a second plastic hinge formed. This took place in the same column, below the beam at Level 1. In the third step, a plastic hinge formed in the other column at the base. In the fourth step, three of the diagonal strips in the third storey yielded in tension and were then removed from the model for subsequent steps. The loading of the numerical model continued in this manner until the ultimate strength of the shear wall was reached. Figure 9.7 shows the complete sequence of yielding. Although a collapse mechanism was not yet present, Fig. 9.2 shows that the stiffness of the frame was approaching zero. The complete analysis required 14 load steps.

When determining whether yielding had occurred in a tension strip or whether a plastic hinge had formed in a boundary member, a tolerance of 5% of the theoretical values was used in order to reduce the computational effort. This does not result in a

significant loss of accuracy. A stricter tolerance would result in an associated increase in the number of steps required for the ultimate strength analysis.

It can be seen from Figs. 9.2 to 9.6 that the strip model gives a good representation of the load vs. deflection behaviour of the test specimen. In each case, the ultimate strength is in excellent agreement with the test value, particularly for Panel 1 (Fig. 9.2), which is the critical panel. The amount of inelastic behaviour predicted by the analysis for Panel 4 was negligible, whereas in fact some inelasticity in the panel was observed in the test prior to reaching the maximum base shear.

The initial stiffness of the numerical model is consistently less than the stiffness measured during the test, as may be seen by comparing the initial slopes of the curves. The differences in stiffness vary from 6% to 30%, reflecting the fact that the mechanism for resisting storey shears at low load levels is not as well represented by tension strips as it is at the higher load levels. It is noted however, that a slight decrease in stiffness of the test specimen was observed with each cycle of loading, even at very low load levels. Since the numerical model is elastic at these load levels, this feature is not represented. The *effective* stiffness of the real structure (after some cycling at low load levels) is somewhat less than the *initial* stiffness, and therefore the discrepancies are actually somewhat smaller than those reported above. This is because the initial cycling deforms the infill plate, increasing the role of the diagonal tension field in resisting storey shears.

In each case, the stiffness predicted by the strip model became equal to the stiffness measured in the test when the loads reached approximately 55% to 65% of the ultimate capacity, which occurred at about the point of first yield in the analysis. This represents a transition region, wherein the diagonal tension field becomes the dominant mechanism for resisting the storey shears.

There are several factors that contribute to the stiffness of the shear wall at low load levels that are not modelled by the strip analysis, which is a simplified representation of the real structure. These are discussed in detail in Section 9.5.

The analysis described above is based on the assumption that the angle of inclination of the tension field is $\alpha = 42^\circ$. For comparison, a similar analysis was conducted on a numerical model that used $\alpha = 50^\circ$ in each panel. This value is the angle measured in Panel 1 at the end of the test. The multi-step analysis was conducted in the same manner as described for the first model and, once again, 14 steps were required to reach the ultimate strength. The results are also presented in Figs. 9.2 to 9.6.

Examination of the curves in Figs. 9.2 to 9.6 reveals that the change in the angle of inclination from 42° to 50° does not have a significant effect on the ultimate strength of the model, either for each of the panels individually or for the shear wall as a whole. By increasing α from 42° to 50° , the initial stiffness decreases slightly. This decrease varies from 0% to 9% for the cases depicted in Figs. 9.2 to 9.6. These facts indicate that the behaviour of the model up to the ultimate strength is relatively insensitive to the angle of inclination selected. A full parametric investigation is beyond the scope of this research, and further study is desirable in order to confirm this as a general conclusion.

As a means of substantiating the use of only ten strips to model the continuous infill plates, the analysis for the model with an angle of inclination of 50° was repeated using 20 strips in Panel 1. The method of analysis was identical, but 17 steps were now required to reach the ultimate capacity. This simply reflects the larger number of strips that require removal from the model as yielding takes place. There was no significant difference in the sequence of yielding in the model with the larger number of strips.

Figure 9.8 shows a comparison of the storey shear vs. storey deflection behaviour of Panel 1 for the models using ten and 20 strips. The figure clearly shows that there is no significant loss in accuracy when the ten strip discretization is used as compared with 20 strips. It is possible that further research into this aspect might reveal that even fewer than 10 strips could be used.

9.4 Hysteresis Models

9.4.1 Hysteresis Model of Tromposch and Kulak (1987)

The ability to predict the amount of energy that a particular steel plate shear wall configuration is capable of dissipating under inelastic cyclic loading is valuable in assessing its seismic performance. Tromposch and Kulak (1987) have presented a method for predicting hysteresis curves for thin-panel steel plate shear walls loaded cyclically. The method is a modified version of a model originally developed by Mimura and Akiyama (1977). The hysteresis curves are predicted using the monotonic load vs. deflection curve generated by a strip model analysis and using a series of assumptions regarding hysteretic behaviour. A full description of the method and the assumptions upon which it is based can be found in Tromposch and Kulak (1987).

Figure 9.9 shows the hysteresis model proposed by Tromposch and Kulak (1987). The envelope of curves (curve O-A-P) is an idealized bilinear representation of the strip model analysis. Identical envelope curves are used in the two loading directions.

Consider the first cycle, O-A-B-C-D-E-F-G. During the initial stage of loading, the shear wall response is assumed to follow the elastic curve O-A. Upon loading beyond point A, a reduced stiffness is assumed as the wall deflects by an arbitrary amount along the envelope of curves (curve A-B). The unloading curve (curve B-C) is assumed to be parallel to the elastic curve (curve O-A) until the shear

reduces to zero. Implicit in the assumption that the panel shear reduces to zero at exactly zero applied load is that both the panel and the moment-resisting frame behave in an elastic – perfectly plastic manner and that they both become inelastic at the same deflection. This assumption is a reasonable approximation for most typical steel plate shear wall configurations. This issue is discussed further in the description of the proposed hysteresis model in Section 9.4.2.

Reloading consists of a phase wherein the stiffness is only that of the moment-resisting frame (curve C-D), followed by a phase dominated by tension field action (curve D-E). The first of these reloading phases occurs prior to reaching the deflection where the stretched plate forms a tension field (point D) and it assumes elastic frame behaviour. The extent of deflection in the first phase depends upon the amount of permanent inelastic deformation imposed in the previous half cycle (O-C). Because of the reduction in length of the compression diagonal during the deflection A-B (the Poisson effect), the deflection O-C is not fully recovered at the onset of the second reloading phase (point D). The hysteresis model assumes a Poisson's ratio for plastic behaviour of 0.5, and therefore the deflection along curve C-D is equal to 0.5 times the distance O-C. This is analogous to the procedure recommended by Mimura and Akiyama (1977), described in Chapter 2. The curve is then assumed to simply extend linearly from point D to the cusp of the envelope of curves in the reloading direction (point E). As the model is deflected farther in this direction by an arbitrary amount, it follows the inelastic curve E-F. It is then unloaded elastically to point G.

In all cycles after the first, the two-phase reloading curve is determined in a manner that reflects the inelastic behaviour from the previous cycles. Consider the reloading curve G-H-B. Once again, the slope of the first phase reloading curve (curve G-H) is based on the elastic stiffness of the moment-resisting frame acting alone. However, the *extent* of deflection is taken to be equal to the permanent deformation from the previous cycle in the same direction of loading (O-C) plus one-half of the permanent deformation from the half cycle just completed in the opposite

loading direction (O-G). This reflects the previous stretching of the diagonal plus the shortening of the diagonal due to the Poisson effect. The second phase extends linearly from the end of the first phase (point H) to the point on the envelope curve where unloading began in the previous cycle (point B). Further deflections take place along the envelope curve (curve B-I), and thereafter, unloading and subsequent reloading take place in the manner described for curve F-G-H-B-I. For cycles with relatively large deformations, during the redevelopment of the tension field the moment frame may undergo deflections large enough to form a mechanism. Beyond this deflection, the curve is assumed to have zero slope until the tension field forms. Curve M-M'-N illustrates a curve where a mechanism forms in the moment-resisting frame at point M'.

In order to assess the efficacy of this model, it was used to predict hysteresis curves for Panel 1 for Cycles 15, 18, and 21. The monotonic load vs. deflection curves of both the strip model and the moment-resisting frame acting alone were used in the model. The comparisons between the experimental results and the predictions are shown in Figs. 9.10, 9.11, and 9.12. The panel deflections for these cycles are equal to $2\delta_y$, $3\delta_y$, and $4\delta_y$, respectively. At cycles with larger deflections and after a greater number of load reversals, effects such as plate tearing, local buckling, and extensive frame inelasticity render the assumptions less valid. The strip model used had the tension strips inclined at an angle of 50° from the vertical, although there is no significant difference for an angle of 42° , as shown in Fig. 9.2.

The procedure for generating the hysteresis curve for a single cycle with equal deflections in the two directions can be carried out as described above. The maximum deflection is located at a value equal to the maximum recorded for that cycle in the test. (If the procedure is to be used to *predict* behaviour—as opposed to comparing the analytical method to existing test results—this value can be selected for any

arbitrary deflection.) The corresponding load is equal to the load at which this deflection is reached in the strip model analysis.

Figures 9.10, 9.11, and 9.12 show that the predicted curves tend to underestimate the energy dissipation. The test/predicted ratios of the energy dissipation for Cycles 15, 18, and 21 are 1.63, 1.24, and 1.25, respectively.

In Cycle 15, the slopes of the predicted unloading curve and the second phase reloading curve (where tension field action dominates) show good agreement with those of the test curve. The primary reason that the model underestimates the energy dissipation is that the slope of the first phase reloading curve (based on the elastic stiffness of the moment frame) is less than the stiffness exhibited by the test specimen. This is because any stiffness contributed by the infill plate has been neglected.

The predicted curve for Cycle 18 shows good agreement with the test results in the unloading region and in the reloading phase where the moment-resisting frame remains elastic. The marked change in stiffness where the frame forms a mechanism is not seen in the test curve.

In Cycle 21, the slopes of the predicted unloading curve and the reloading curve where the moment-resisting frame is elastic show good agreement with those of the test curve. As in Cycle 18, the complete loss of stiffness at the point where the moment frame forms a mechanism is not seen in the test curve, although a slight decrease in stiffness did occur.

9.4.2 Proposed Hysteresis Model

In order to represent more precisely the contributions of the moment-resisting frame and the infill panels in the hysteretic behaviour of thin-panel steel plate shear walls, a new model is proposed. It is based on the previous work of both Mimura and

Akiyama (1977) and Tromposch and Kulak (1987). In this model, the behaviour of the shear wall is divided in two distinct components—that of the frame and that of the panel. The load vs. deflection behaviour of both the frame and the panel are assumed to be bilinear, but the deflections at which they become inelastic are not necessarily equal. Therefore, the resulting shear wall behaviour is trilinear.

Figure 9.13 shows the idealized curves based on the strip model ($\alpha = 50^\circ$) and moment-resisting frame analyses shown in Fig. 9.2. Because the slopes of the shear wall and moment frame curves taken from the analyses subsequent to the point where the frame yields (K_3 and K_{f2} , respectively) are approximately equal, the *panel* stiffness in this region, K_{p2} , is assumed to be zero. The shear resisted by the panel after the moment frame yields is determined by subtracting the shear resisted by the frame from the total shear. The deflection at which the moment-resisting frame becomes inelastic, Δ_{yf} , is reflected by a cusp on the overall shear wall curve. Immediately prior to this, the shear wall possesses a stiffness equal to that of the frame, K_{f1} , since the stiffness of the panel in this region is assumed to be zero. The wall and frame curves are completed by initial segments having a slope equal to their elastic stiffnesses, K_1 and K_{f1} , respectively. The intersection of the first two segments of the shear wall curve represents the point at which the panel curve becomes inelastic (at a deflection Δ_{yp}), establishing the elastic panel curve with a stiffness K_{p1} .

In determining the unloading curves, the panel and frame are assumed to unload according to their elastic stiffnesses. Because they did not yield at the same deflection, they also do not unload through the same deflection. The panel becomes completely unloaded in a deflection Δ_{up} . At this point, the frame (and therefore the overall shear wall) still resists some shear. Upon further unloading of the shear wall, the panel is assumed to buckle immediately as it begins to become loaded in the opposite direction. Therefore, the stiffness of the shear wall decreases to that equal to

the elastic stiffness of the moment-resisting frame acting alone. The bilinear panel and frame curves are used to determine the hysteretic behaviour of the shear wall based on their respective contributions during each phase of the loading cycle.

Figure 9.14 shows the proposed hysteretic model. The initial elastic curve O-A has a stiffness equal to the initial stiffness of the wall, K_1 , as determined from the strip model analysis. Beyond point A, at a deflection Δ_{yp} (see Fig. 9.13), the panel behaves inelastically and the shear wall stiffness reduces to that of the moment-resisting frame, K_{f1} . At point B, at a deflection Δ_{yf} , the moment frame yields and the shear wall stiffness reduces to the post-yield stiffness of the moment-resisting frame, K_{f2} . The shear wall then deflects following this path up to an arbitrary deflection at point C. Unloading then takes place along the line C-D with a stiffness equal to the elastic stiffness of the shear wall, K_1 . Because the deflection of the panel and frame at the limit of elastic behaviour (Δ_{yp} and Δ_{yf} , respectively) are different, they do not become completely unloaded at the same time. At point D (after a deflection of Δ_{up} during unloading from point C), the panel shear has reduced to zero and the moment-resisting frame resists the entire remaining load. If the panel had the same stiffness in both directions, a further reduction in load would then result in not only a reduction in load carried by the moment-resisting frame but also a reloading of the panel in the opposite direction. However, as was assumed by Tromposch and Kulak (1987), the thin panel is assumed to buckle immediately. Therefore, the panel remains unloaded as the moment frame unloads elastically along the path D-E with a stiffness K_{f1} . At point E, the frame has recovered by a distance Δ_{uf} , which is dependent upon the deflection at point C since $K_{f2} \neq 0$. At point E, both the panel and the frame are completely unloaded.

Loading in the opposite direction continues along the path E-F with a slope equal to the elastic stiffness of the moment-resisting frame, K_{f1} . The total deflection from point C to point F, where the moment frame becomes inelastic, is $2\Delta_{uf}$. From

point F to point G, the shear wall is assumed to have the post-yield moment frame stiffness, K_{f2} . The total deflection required for the tension field to redevelop in the new loading direction (from point D to point G) is determined in the manner described by Mimura and Akiyama (1977) and Tromposch and Kulak (1987) that assumes a Poisson's ratio equal to 0.5, as discussed in Chapter 2. Therefore, the absolute deflection at point G is one-half that of point D, where the panel became completely unloaded. (Note that the tension field may develop *before* the moment frame yields. In that case, the region of reduced stiffness—curve F-G—would not exist.) Further loading follows the path G-H, with a stiffness $K_{p1} + K_{f2}$. In this region, the tension field is developed and the moment-resisting frame possesses its post-yield stiffness. Point H is located on the strip model curve for the shear wall. Continued loading in the same direction follows a path with the slope $K_3 = K_{f2}$ up to an arbitrary deflection at point J.

Unloading and reloading follow the path J-K-L-M-N-P-C in a manner similar to that described above. In determining the abscissa of point N (i.e., for cycles beyond the first), the procedure of Tromposch and Kulak (1987) is adopted. Therefore, the deflection from point K to point N is equal to the absolute deflection at point D (in the previous cycle in the same direction) plus one-half the absolute deflection at point K (in the previous half-cycle). This implicitly assumes that the inelastic stretching of the panel in the previous half-cycle begins when the overall deflection is zero. In fact, this is not necessarily the case according to the curves generated from these models. For example, point H does not necessarily lie on the vertical axis. However, this assumption yields good agreement with the test results of both Tromposch and Kulak and the four storey shear wall test and gives a resulting *effective* Poisson effect. Unloading and reloading from point C in the second cycle follows the path C-D-E-F-G'-H'. The increase in deflection from point G to point G' reflects the additional stretching of the panel that did not exist during the first cycle.

By dividing the shear wall into two distinct components, the hysteresis behaviour can be modelled with the contributions of each component known explicitly at each stage. This is conducive to the analysis of other steel plate shear wall configurations such as one proposed by Xue and Lu (1994), wherein the moment-resisting frame spans several bays with infill plates installed in only one.

Figures 9.10, 9.11, and 9.12 show the hysteresis curves derived from the proposed model for Cycles 15, 18, and 21 of the test. The test/predicted ratios of the energy dissipation for these cycles are 1.33, 1.16, and 1.11, respectively.

In Cycle 15, the unloading curve shows good agreement with the test results. In the loading region where the tension field has not yet developed, the stiffness of the test specimen is greater than that predicted by the model. This indicates that the panel stiffness, which is neglected in the model, is significant during this cycle. The slope of the predicted curve during the phase where the tension field is developed is somewhat greater than that of the test curve. The curves bisect one another, which tends to offset the underestimate of the energy dissipation in the first reloading phase. (Reasons for discrepancies between the test and predicted curves are discussed subsequently.)

The predicted curve for Cycle 18 shows good agreement with the test results in the unloading region and in the reloading phase where the moment-resisting frame remains elastic. The significant loss in stiffness predicted by the model as the moment-resisting frame forms a mechanism is not reflected by the test results. Again, the predicted stiffness during the loading phase where the tension field is developed is somewhat higher than that of the test specimen.

In Cycle 21, the slopes of the predicted unloading curve and the reloading curve where the moment-resisting frame is elastic show good agreement with those of the test curve. The model predicts a great reduction in stiffness where a mechanism

forms in the moment frame, whereas only a small reduction in stiffness was seen in the test. The predicted stiffness in the phase where the tension field is developed is greater than that of the test specimen.

In each cycle, the deflection at which the tension field in the panel becomes effective, as seen by a sharp increase in the slope of the response, is predicted very well by the proposed model. Similarly, a reduction in slope is seen in Cycle 21 at the deflection where the moment-resisting frame is predicted to form a mechanism. Also in Cycle 21, and to a lesser extent in Cycles 15 and 18, the predicted reduction in the slope of the *unloading* curve at a storey shear somewhat greater than zero is reflected in the test curve by a gradual reduction in slope. This feature was even more prominent in the hysteresis behaviour of the shear wall specimen tested by Tromposch and Kulak (1987), as seen in Fig. 2.6.

For relatively large deflection cycles (Cycles 15 and 21), the elastic stiffness of the moment-resisting frame alone (assuming no stiffness in the panel) gives an excellent estimate of the shear wall stiffness up to the point where a mechanism forms. Even for smaller deflection cycles, a good estimate of the stiffness would likely result for very thin panels or for panels that had previously undergone severe deformations. However, because of the incremental decrease in slope during this loading phase in each successive cycle of the test (see Fig. 9.2), caution is advised in extending this method to cycles with extremely large deflections. However, approximate hysteresis curves can still be generated if a good estimate of the stiffness can be made.

The underestimate of the stiffness during the reloading phase that occurs after a mechanism forms in the moment-resisting frame is attributed to the forces that develop in the corners of the infill panels that tend to prop the frame. This phenomenon is discussed in Chapter 10. The stiffening effect becomes significant at

relatively large deflections from the point where the panel first became unloaded. Strain hardening may also play a role in the stiffness being higher than predicted.

The overestimate of the stiffness in the reloading phase where the tension field action is dominant is attributed to a softening effect resulting from the deterioration of the panel during the test. This is substantiated by the incremental decrease in slope during this loading phase in each successive cycle of the test (see Fig. 9.2). However, it is interesting to note that during the *initial* excursion at a particular peak deflection level, the shape of the response curve at high load levels is very similar to that predicted by the proposed model. This can be seen best by examining in Fig. 7.1 the first excursion curves for deflections of $2\delta_y$, $3\delta_y$, and $4\delta_y$, where steep loading curves followed by curves with very low stiffness near the ultimate load are evident. The second cycles at each respective peak deflection level were presented in Figs. 9.10, 9.11, and 9.12 because it was felt that the extra energy dissipation seen in the first excursion cannot be relied upon should previous excursions have occurred that are equal or greater in magnitude. Even with the reduced energy dissipation during the second cycle, the proposed model conservatively estimates its value.

The test curves presented in Figs. 9.10, 9.11, and 9.12 exhibit all of the stages represented in the proposed hysteresis model, although they are not as clearly differentiated. This model, although approximate, is a relatively simple means of estimating the hysteresis curves that would result from loading a steel plate shear wall cyclically including significant inelastic behaviour. It is also useful in providing comparisons of the amount of energy dissipation that can be expected among different shear wall configurations.

9.4.3 Comparison of Hysteresis Models

An important reason for modelling the hysteretic behaviour of structural systems is to estimate the amount of energy dissipated during inelastic cyclic loading.

Tromposch and Kulak (1987) compared their hysteresis model with the behaviour of the shear wall specimen they tested at two different deflection levels. During cycles with peak deflections of about 8 mm ($h_s / 275$) and 17 mm ($h_s / 129$), the test/predicted ratios of energy dissipation reported were 1.36 and 0.83, respectively. They attributed the discrepancies, in part, to the uncertainty of the behaviour of the beam-to-column joints, which were bolted shear-type connections. In the case of the four storey shear wall specimen with moment-resisting joints, the connection behaviour can be predicted more reliably.

Test/predicted ratios of the energy dissipated by the four storey shear wall in Cycles 15, 18, and 21 were presented in previous sections for both the Tromposch and Kulak (1987) model and the proposed model. In all cases, the proposed model resulted in a test/predicted ratio closer to 1.0. The *mean* test/predicted ratios of the three cycles for the Tromposch and Kulak model and the proposed model are 1.37 and 1.20, respectively. Therefore, the proposed model gives a mean estimate of the energy dissipation in these cycles that is improved by 12.4% over that of the previous model. It should be noted that the cycles presented had peak deflections that were considerably greater than those examined by Tromposch and Kulak, as described above. During Cycles 15, 18, and 21, peak deflections were reached of 17 mm ($h_s / 113$), 25.5 mm ($h_s / 76$), and 34 mm ($h_s / 57$), respectively.

The proposed model, therefore, provides an improved estimate of the energy dissipation of the four storey shear wall. This, combined with the fact that it explicitly models the respective contributions of the infill panel and the moment-resisting frame at each stage of loading, make it an effective method for predicting hysteretic shear wall behaviour.

9.5 General Discussion

As discussed in Section 9.3.2, the initial stiffness of the test specimen was somewhat underestimated by the strip model. Several factors may contribute to this. By modelling the infill panels as a series of discrete diagonal strips, only the phenomenon of pure tension field action is modelled. However, it is obvious that the true behaviour of the panels is somewhat more complex.

The justification for modelling the continuous panel as a series of separate strips of plate is that the proportions of the panels and the presence of initial imperfections lead to out-of-plane deformations at low loads. The compressive forces perpendicular to the tension field are, therefore, limited. However, at low loads the buckle amplitudes are small and are restrained by the perpendicular tension band. If the compression struts were nearly fully effective, the behaviour would approach that of a planar plate in a state of pure shear. It is recognized that this limiting condition cannot be true even at very low levels of loading, because of the initial out-of-plane deformations that inevitably are present in the large panels. However, it is proposed that, up to a moderate load level, the pure shear model provides a reasonable approximation of the true behaviour. The precise level of loading up to which this approximation is valid is a matter of judgement, and a parametric study would be required to make recommendations that are generally applicable.

The pure shear condition can be simulated with the strip model by using an equivalent strain energy approach. By equating the elastic strain energy resulting from a panel shear resisted in pure diagonal tension to the elastic strain energy resulting from the same panel shear resisted in pure shear, an effective plate thickness can be determined for use in the strip model. Timler and Kulak (1983) showed that the elastic strain energy in a panel approximated as a series of discrete diagonal tension strips (the strip model) can be written as:

$$U_{\sigma} = \frac{V^2 h_s}{2 E t L \cos^2 \alpha \sin^2 \alpha} \quad [9.5]$$

where the variables are as defined in the list of symbols. However, if the panel behaves in pure shear, the elastic strain energy as an integral over the plate volume is:

$$U_{\tau} = \int \frac{\tau_{xy}^2}{2 G} dVol. \quad [9.6]$$

The panel shear stress, τ_{xy} , is constant over the volume and is equal to the panel shear, V , divided by tL . The volume of the panel is given by $tL h_s$. Therefore, Eq. 9.6 can be re-written as:

$$U_{\tau} = \frac{V^2 h_s}{2 G t L} \quad [9.7]$$

Equating U_{σ} in Eq. 9.5 to U_{τ} in Eq. 9.7 and referring to the panel thickness for the pure diagonal tension case as the *effective* panel thickness, t_e :

$$\frac{V^2 h_s}{2 E t_e L \cos^2 \alpha \sin^2 \alpha} = \frac{V^2 h_s}{2 G t L} \quad [9.8]$$

Solving for the effective panel thickness:

$$t_e = \frac{G t}{E \cos^2 \alpha \sin^2 \alpha} \quad [9.9]$$

Assuming a Poisson's ratio of 0.3 for steel, the relationship between E and G is:

$$E = 2.6 G \quad [9.10]$$

Therefore, the effective panel thickness can be written as:

$$t_e = \frac{t}{2.6 \cos^2 \alpha \sin^2 \alpha} \quad [9.11]$$

where t is the actual plate thickness and α is the angle of inclination of the tension field from the vertical. As shown in Fig. 9.13, within the usual range of α values for steel plate shear walls (say, $\alpha = 40^\circ$ to $\alpha = 50^\circ$), the effective thickness is always about 1.55 times the actual thickness. However, even with this increase in stiffness in the model, the behaviour is still less stiff than that of the test specimen. This indicates that other phenomena are present that increase the stiffness of the structure.

Although the compression field in the infill plate has limited effectiveness, there are zones in two opposite corners (where the compression diagonals perpendicular to the tension field are short) that can support significant compressive loads. This region provides additional stiffness that is not present in the strip model. Taking an effective width approach, a portion of the infill plate in the corners could be modelled as pin-ended compression struts. Judgement is required in determining the effective width of the compression band and further research would be required to determine whether the effect of this stiffened region is significant.

Another stiffening phenomenon that is not included in the strip model is the increase in axial stiffness of the tension column afforded by the continuous infill plate along its boundary. Some portion of the plate acts with the column in resisting the tension as a result of overturning moments, thereby increasing the shear wall stiffness. Because the tension area of even relatively thin plates can be a significant fraction of the adjacent column area, the stiffening effects could be appreciable. The strip model could be modified by adding vertical strips in the region of vertical tension in order to model this phenomenon.

A further source of stiffening is the presence of strain hardening, which has been neglected. As each tension strip yields, it is removed from the model and replaced by forces equal to the yield force. For higher loads, these strips have no axial

stiffness. Similarly, modelled plastic hinges do not accept additional moments when the material reaches the hardening strain. However, except for localized effects, strains as high as the hardening strain are not expected to occur at low loads, which is where the shear wall stiffness is underestimated by the model.

The foregoing discussion summarizes characteristics of steel plate shear wall behaviour that are not represented in the simplified strip model. The results presented in Figs. 9.2 to 9.6 clearly demonstrate that these characteristics do not have a significant effect on the ultimate strength: it is predicted very well by the model in all cases. However, these characteristics may be significant at lower load levels. It is postulated that the higher initial stiffness exhibited by the test specimen comes from a combination of the characteristics described in this section.

9.6 Summary

The strip model provides a relatively simple means of predicting the envelope of load vs. deflection curves for a steel plate shear wall loaded cyclically into the inelastic region. The procedure can be conveniently performed using a personal computer and any commercial plane frame analysis computer program.

The basis of the model is the representation of the tension field in the thin infill panels as a series of discrete, pin-ended diagonal tension strips. It was determined that, within the scope of this study, the angle of inclination of the tension strips has little effect on the overall behaviour, providing it does not vary significantly from 45° . As yielding in the strips occur, they are removed from the model and replaced by forces equal to the yield force of the strip. Plastic hinges are also modelled so as to simulate the softening of the surrounding frame. Good agreement with the test results was achieved for each of the panels and for the shear wall as a whole. However, the initial stiffness of the steel plate shear wall test specimen is

consistently underestimated by the model. Several phenomena have been described that might account for this moderate discrepancy.

Two methods are also presented in this chapter for predicting the hysteresis behaviour of steel plate shear walls, thereby reflecting the energy dissipation of the system. They are both based on the results of a monotonic strip model analysis, an analysis of the moment-resisting frame acting alone, and several assumptions regarding hysteresis behaviour. One method is that presented by Tromposch and Kulak (1987), which was based on a model developed by Mimura and Akiyama (1977). Also presented is a proposed new model that explicitly separates the contributions of the moment-resisting frame and the infill panel at all stages of the loading cycle. The amount of energy dissipation predicted by the proposed model for cycles at three different levels of deformation showed very good agreement with the test results and resulted in an improved estimate over the previous model.

The agreement of the analytical results outlined in this chapter with the test results validates the procedures presented. The strip model, combined with the proposed hysteresis model, provides an effective means of predicting the complete cyclic behaviour of steel plate shear walls and of comparing different shear wall configurations.

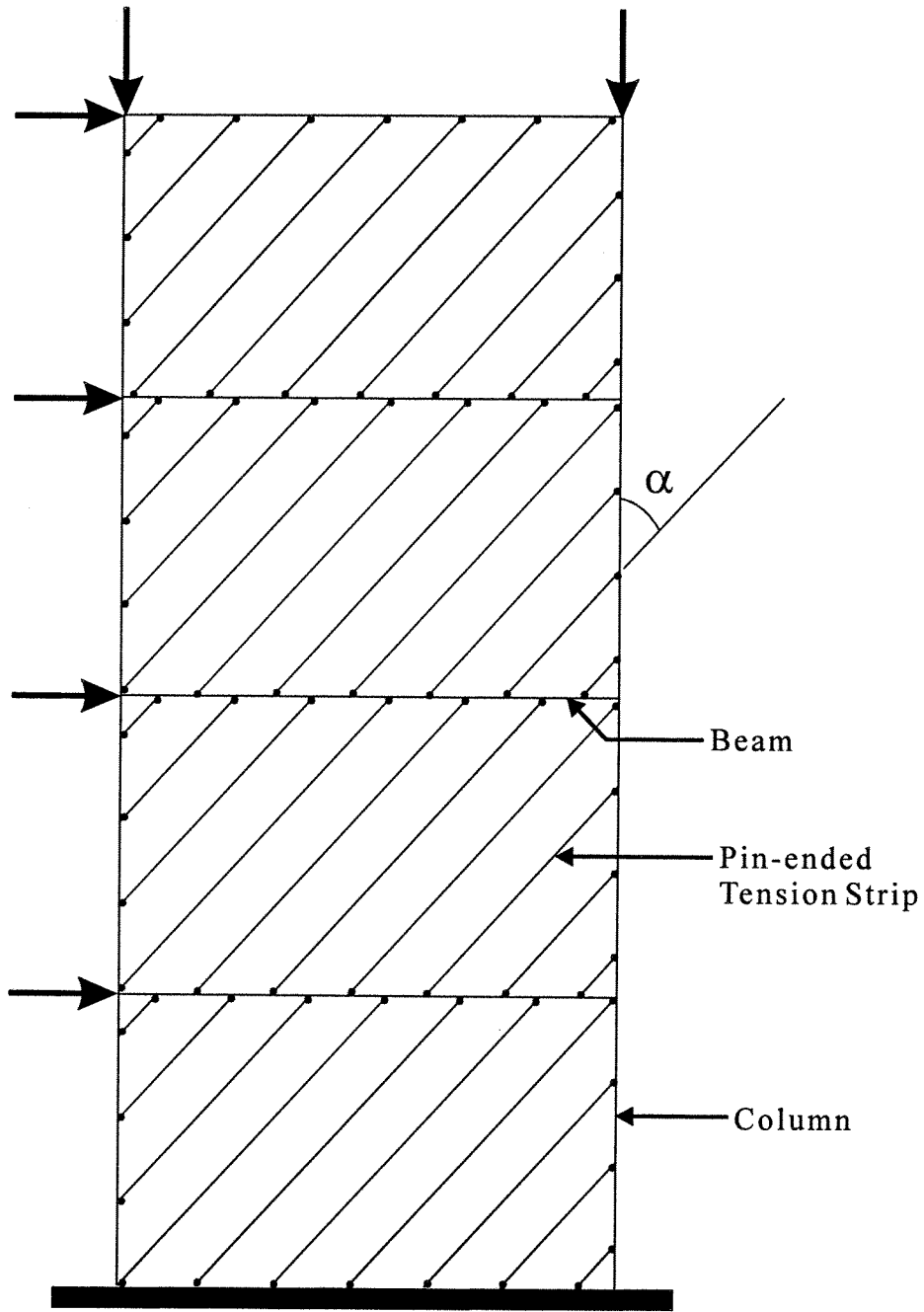


Fig. 9.1 Plane Frame Strip Model of Test Specimen

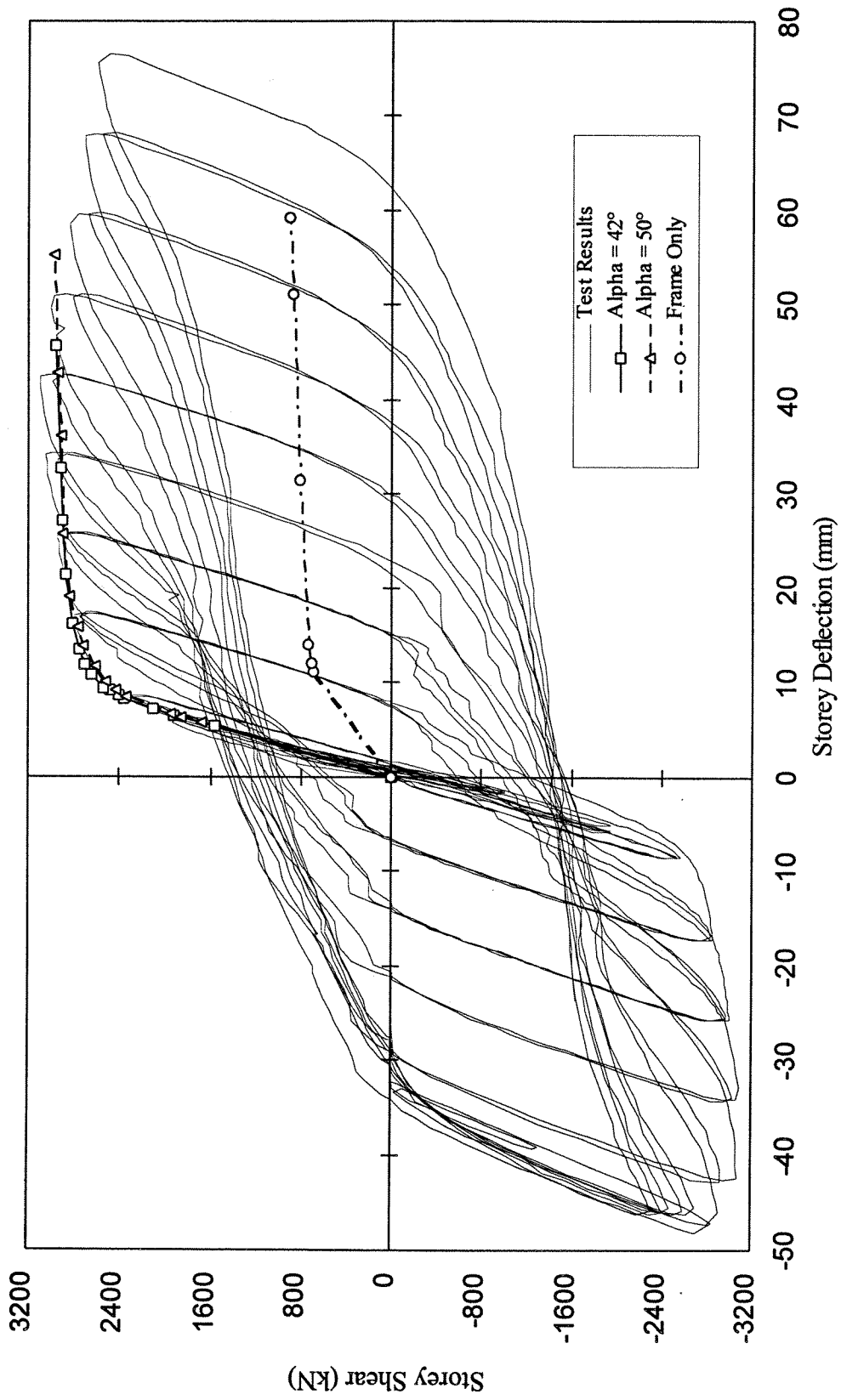


Fig. 9.2 Comparison of Strip Model Analyses with Test Results – Panel 1

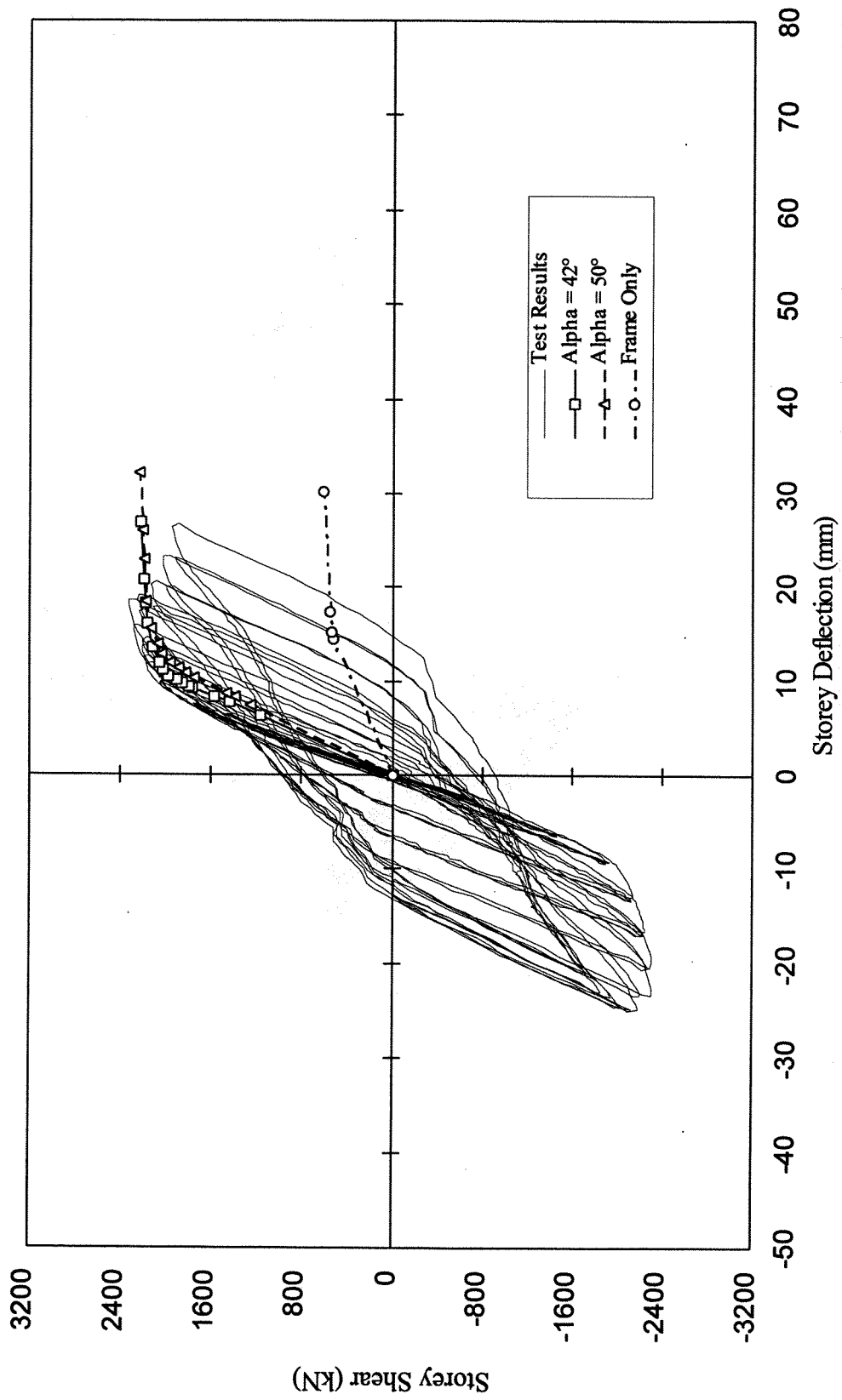


Fig. 9.3 Comparison of Strip Model Analyses with Test Results – Panel 2

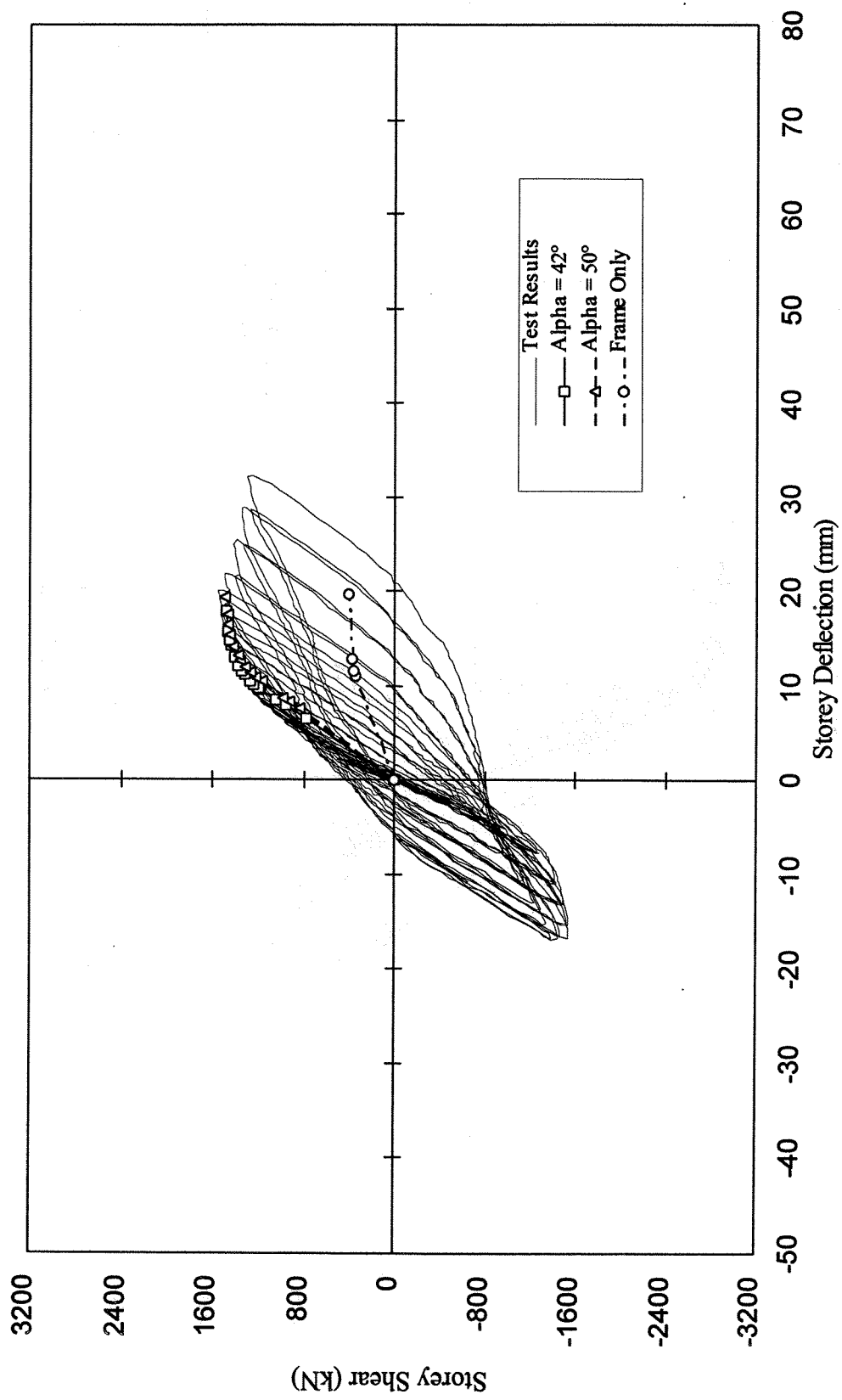


Fig. 9.4 Comparison of Strip Model Analyses with Test Results – Panel 3

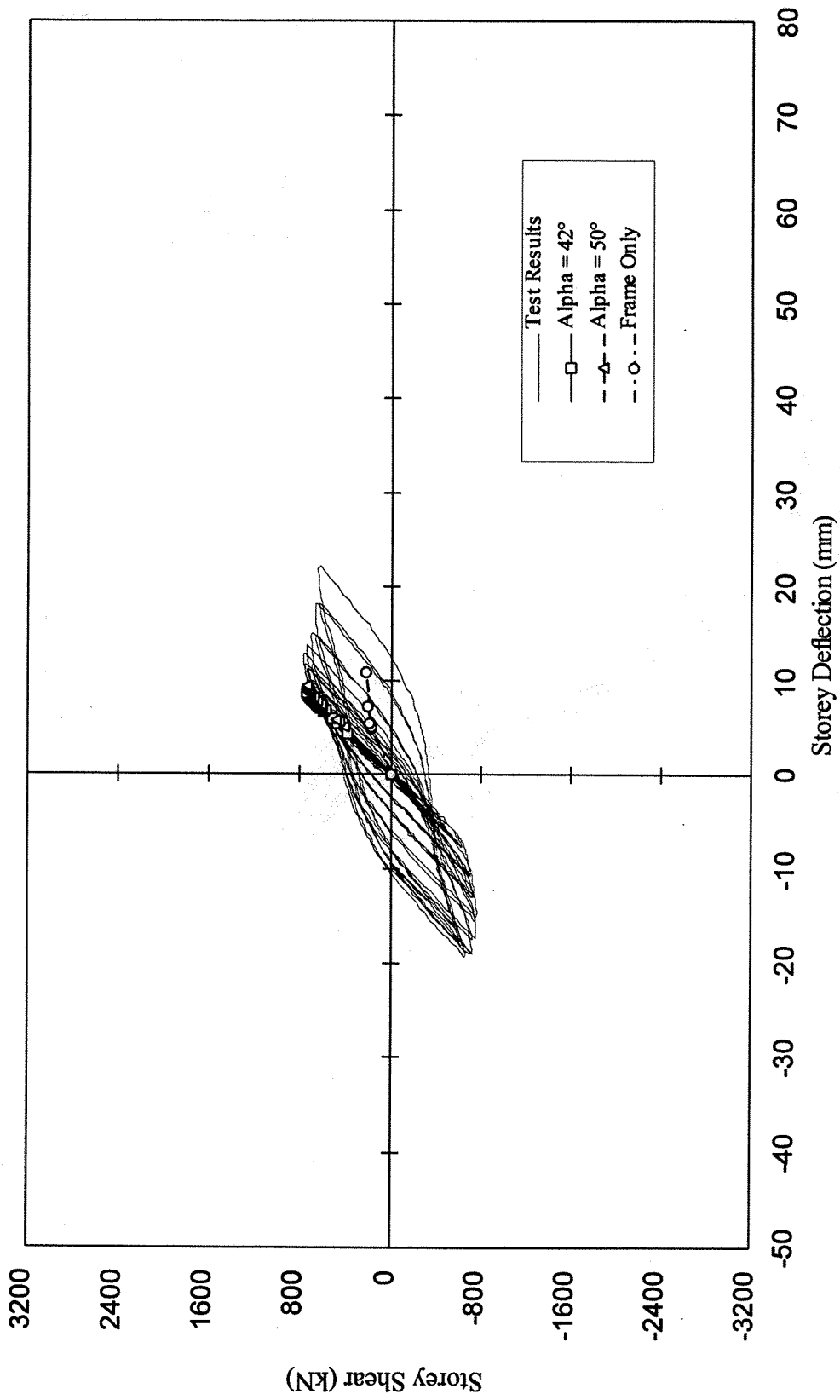


Fig. 9.5 Comparison of Strip Model Analyses with Test Results – Panel 4

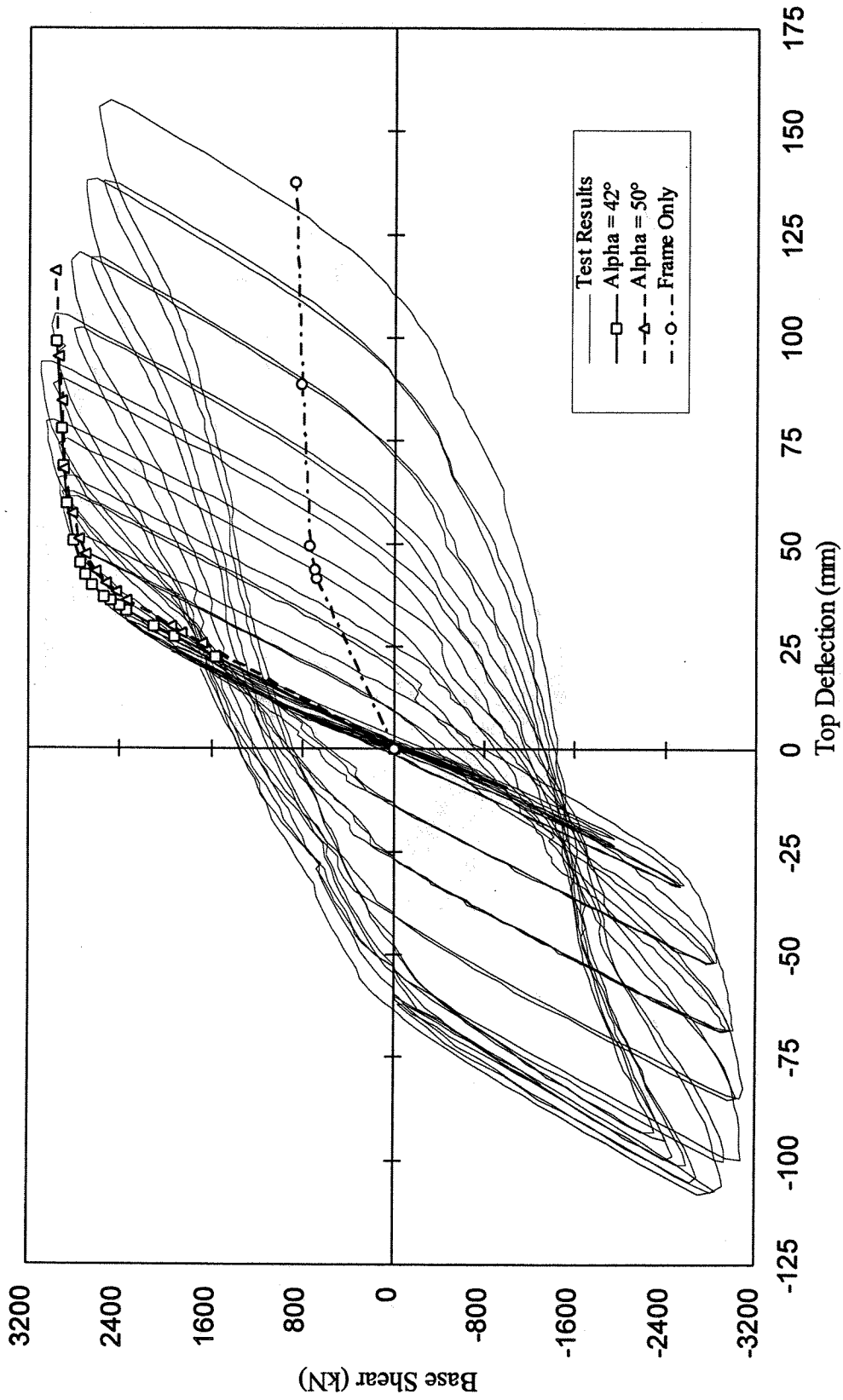


Fig. 9.6 Comparison of Strip Model Analyses with Test Results – Overall

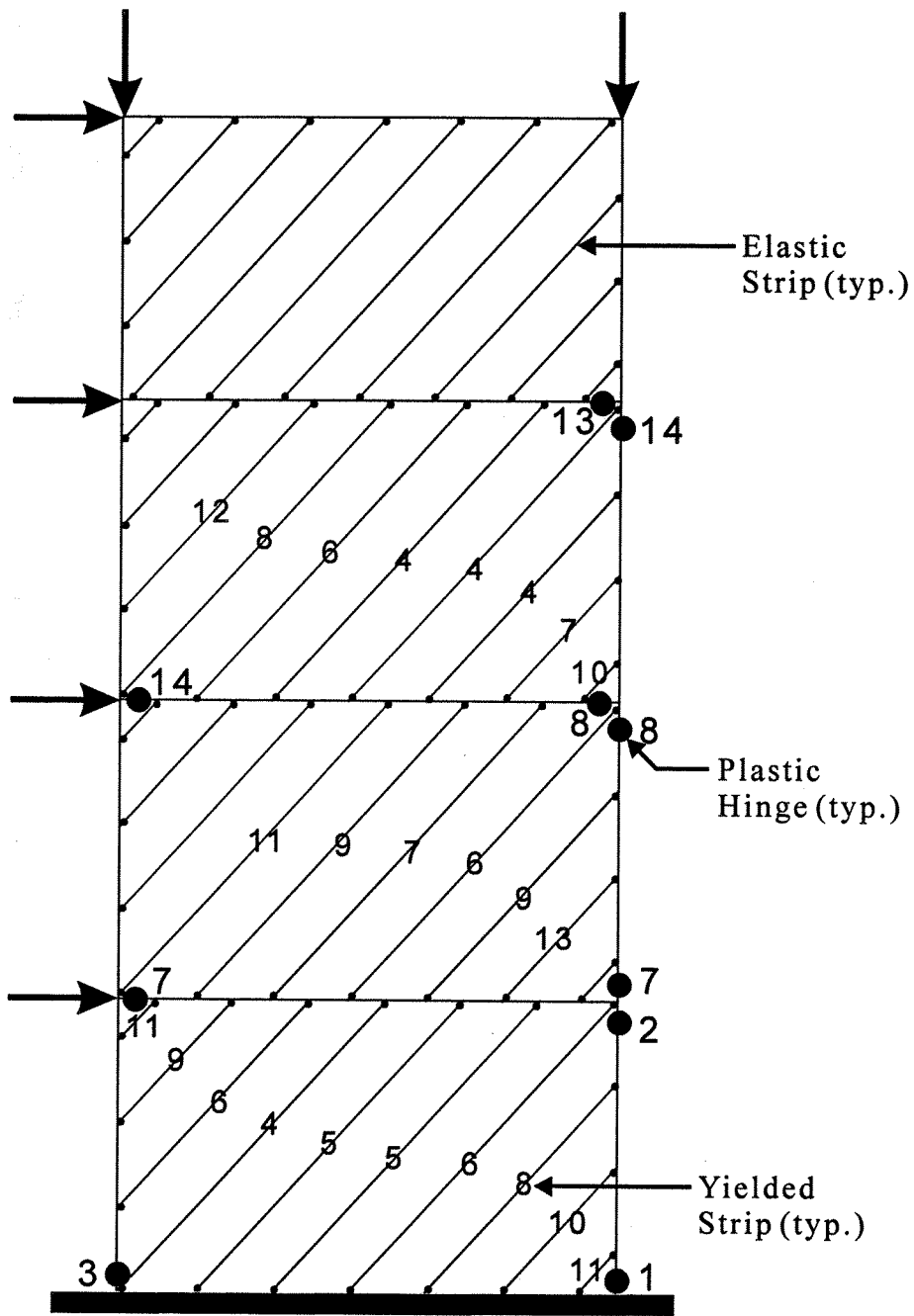


Fig. 9.7 Sequence of Plastic Hinging and Strip Yielding

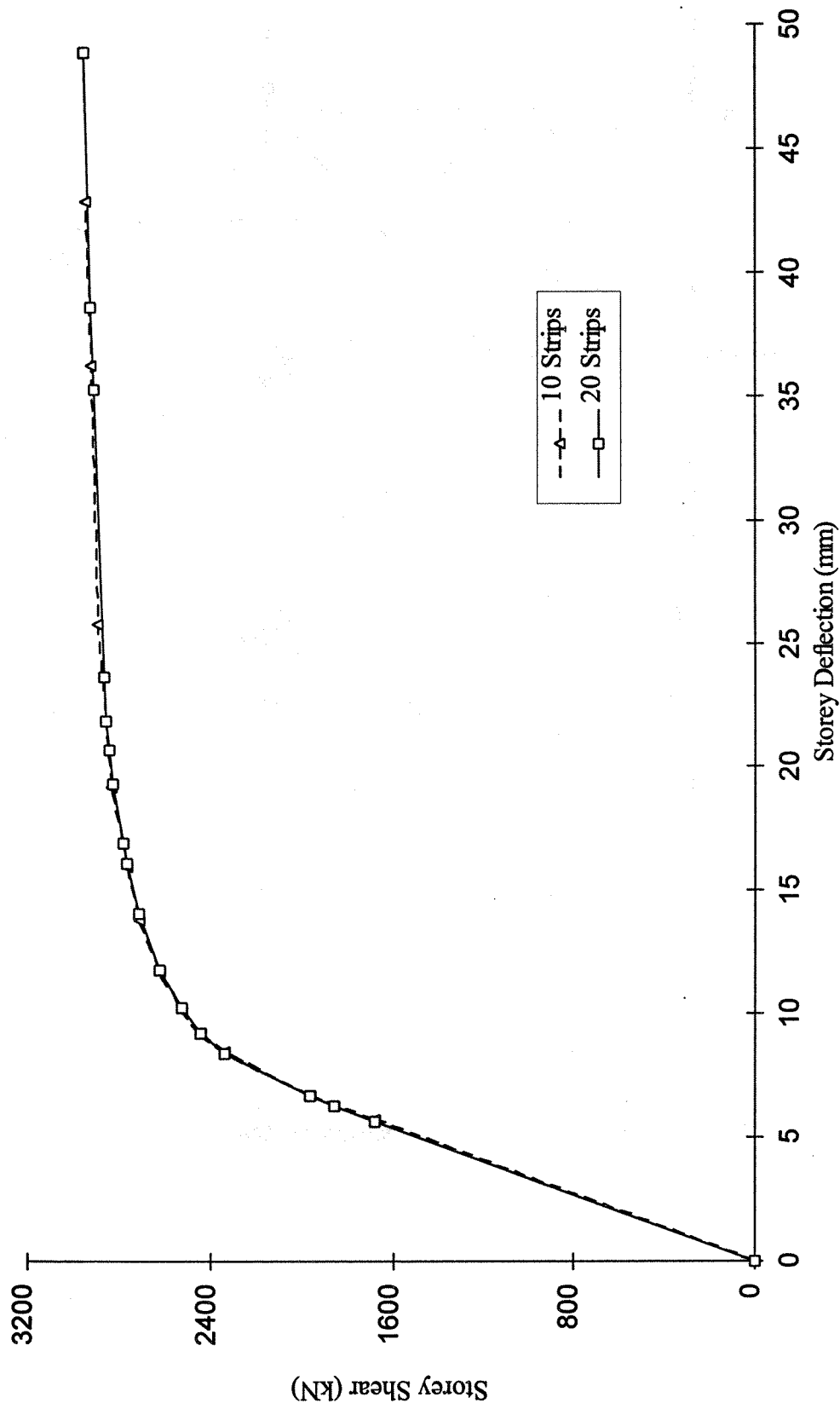


Fig. 9.8 Effect of Number of Tension Strips in Strip Model – Panel 1

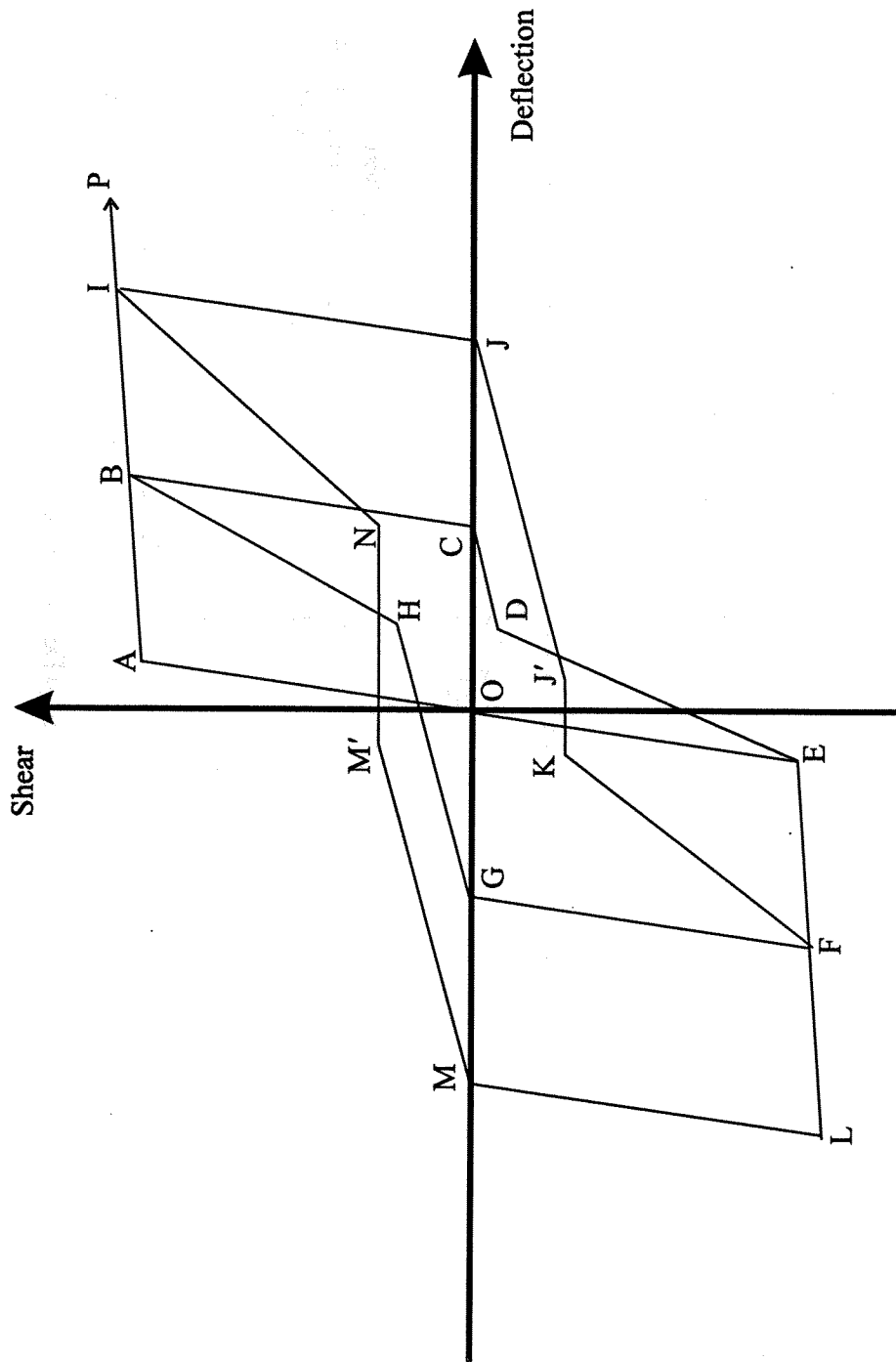


Fig. 9.9 Hysteresis Model (Tromposch and Kulak 1987)

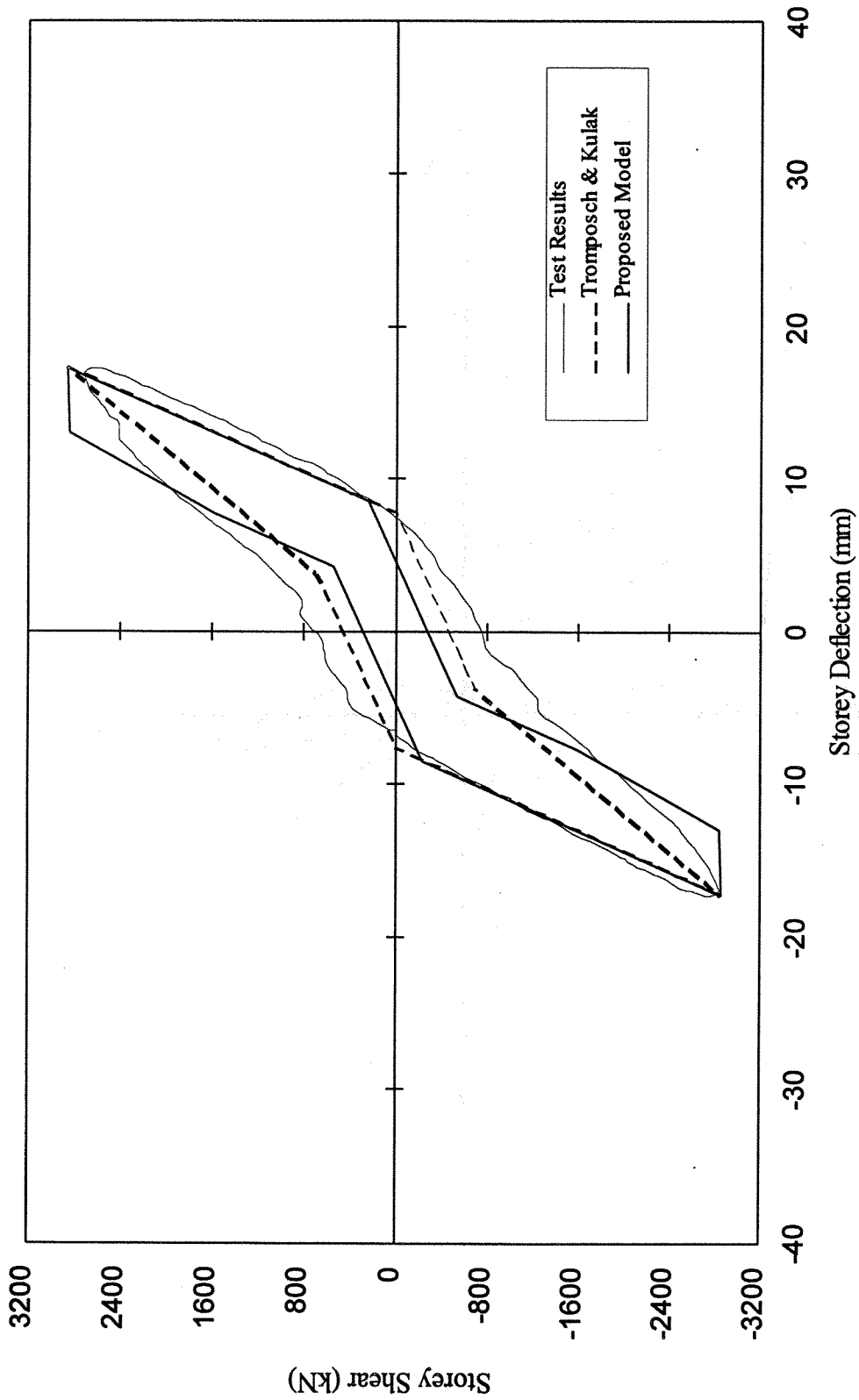


Fig. 9.10 Comparison of Hysteresis Models with Test Results – Panel 1 / Cycle 15

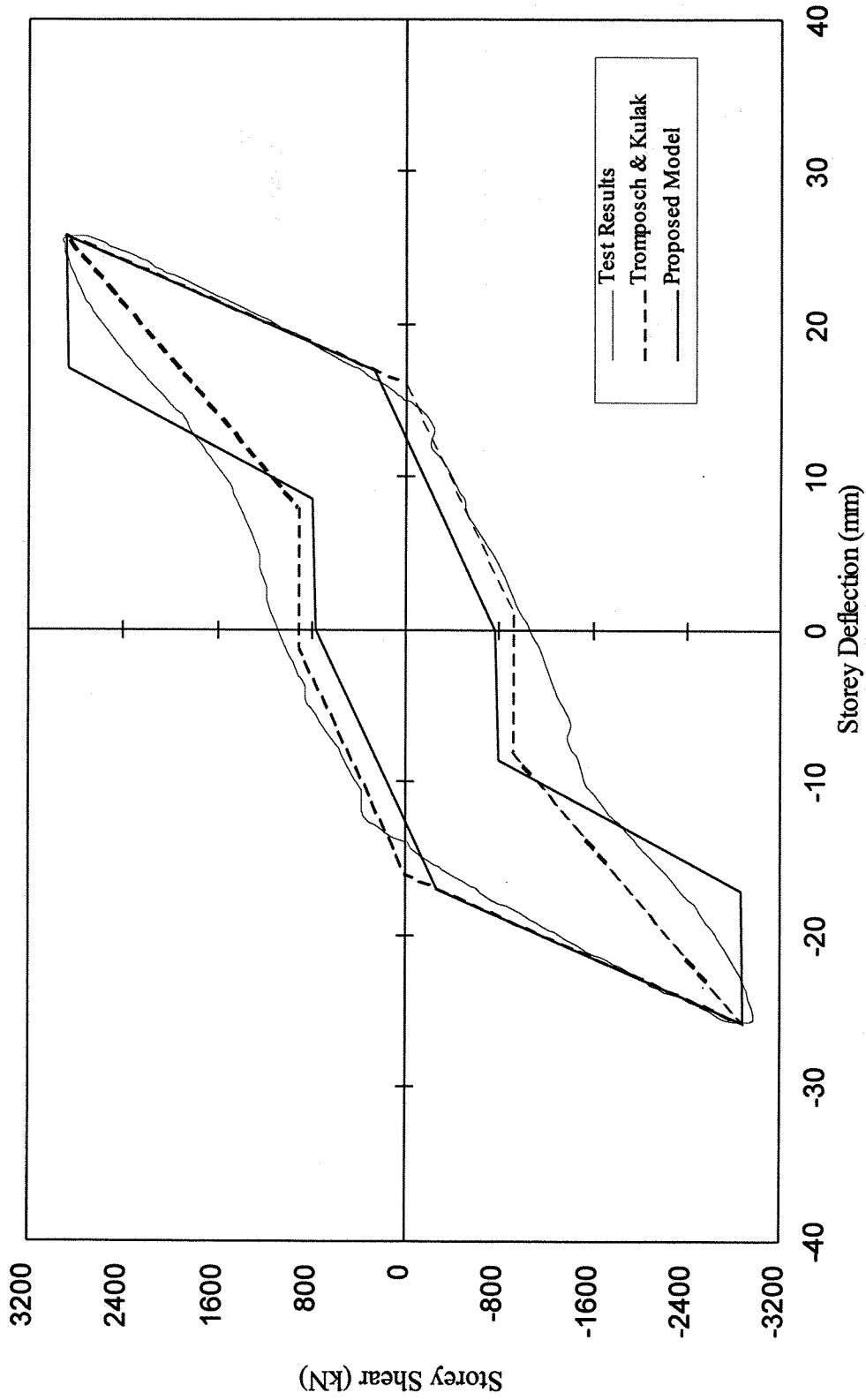


Fig. 9.11 Comparison of Hysteresis Models with Test Results – Panel 1 / Cycle 18

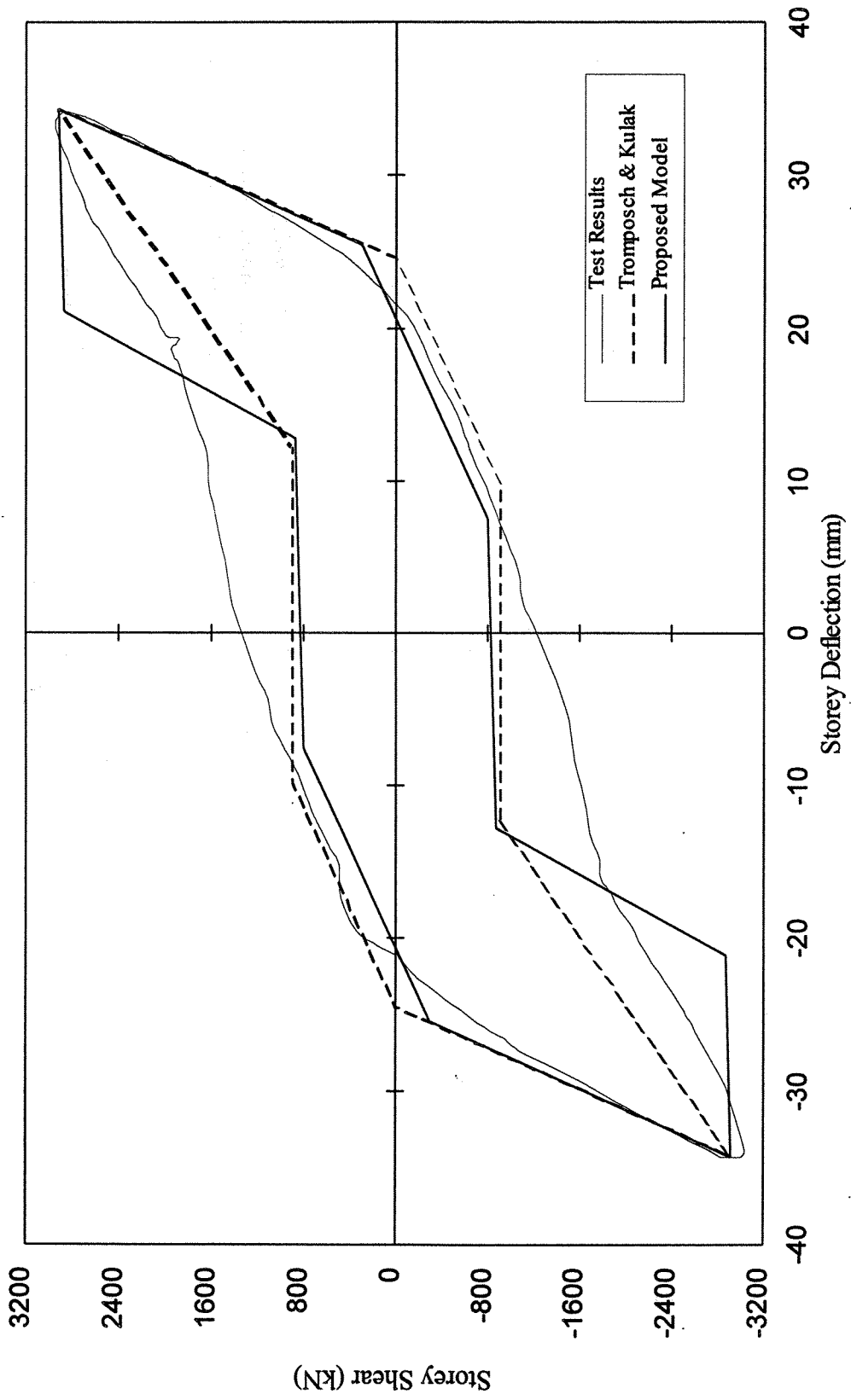


Fig. 9.12 Comparison of Hysteresis Models with Test Results – Panel 1 / Cycle 21

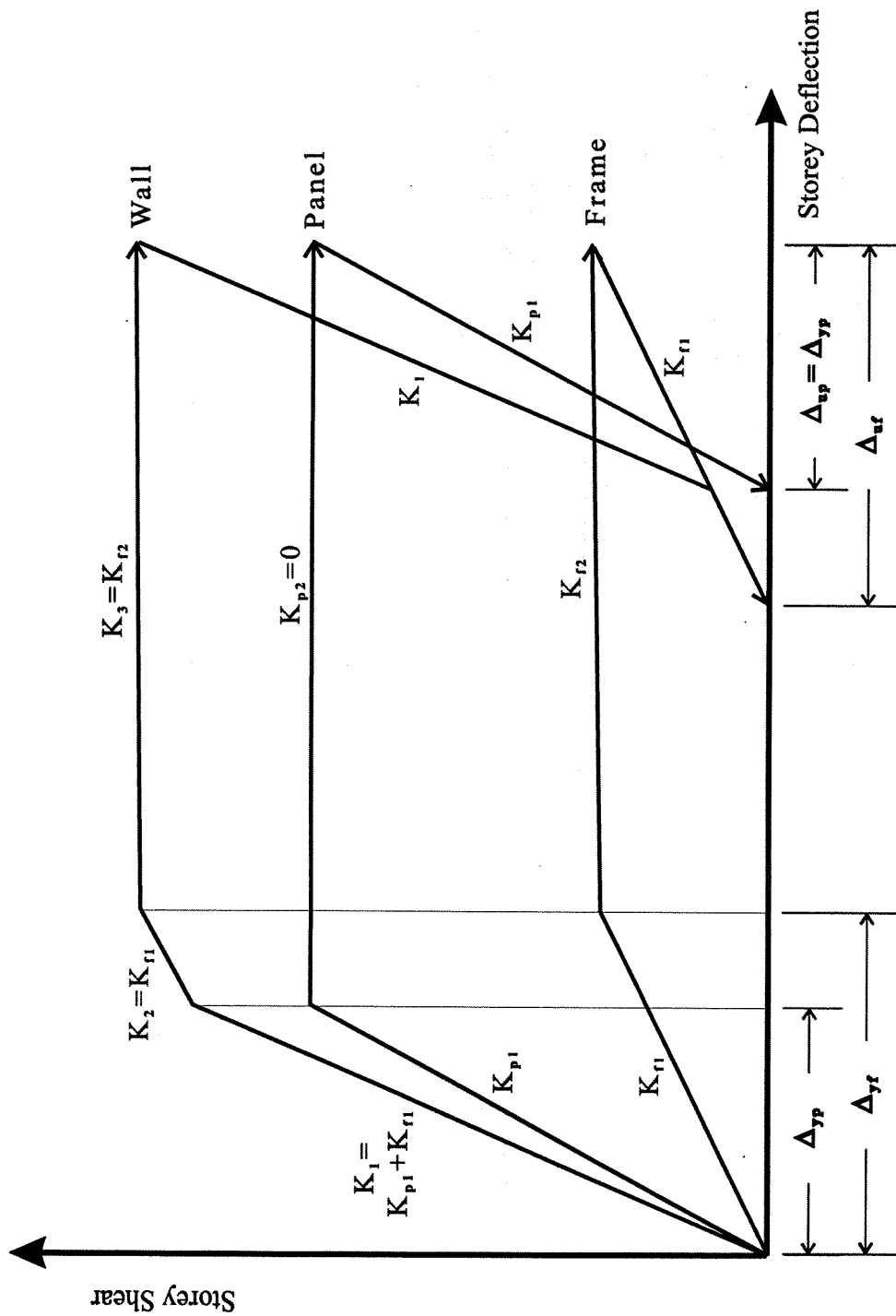


Fig. 9.13 Storey Shear vs. Storey Deflection Behaviour of Shear Wall Components

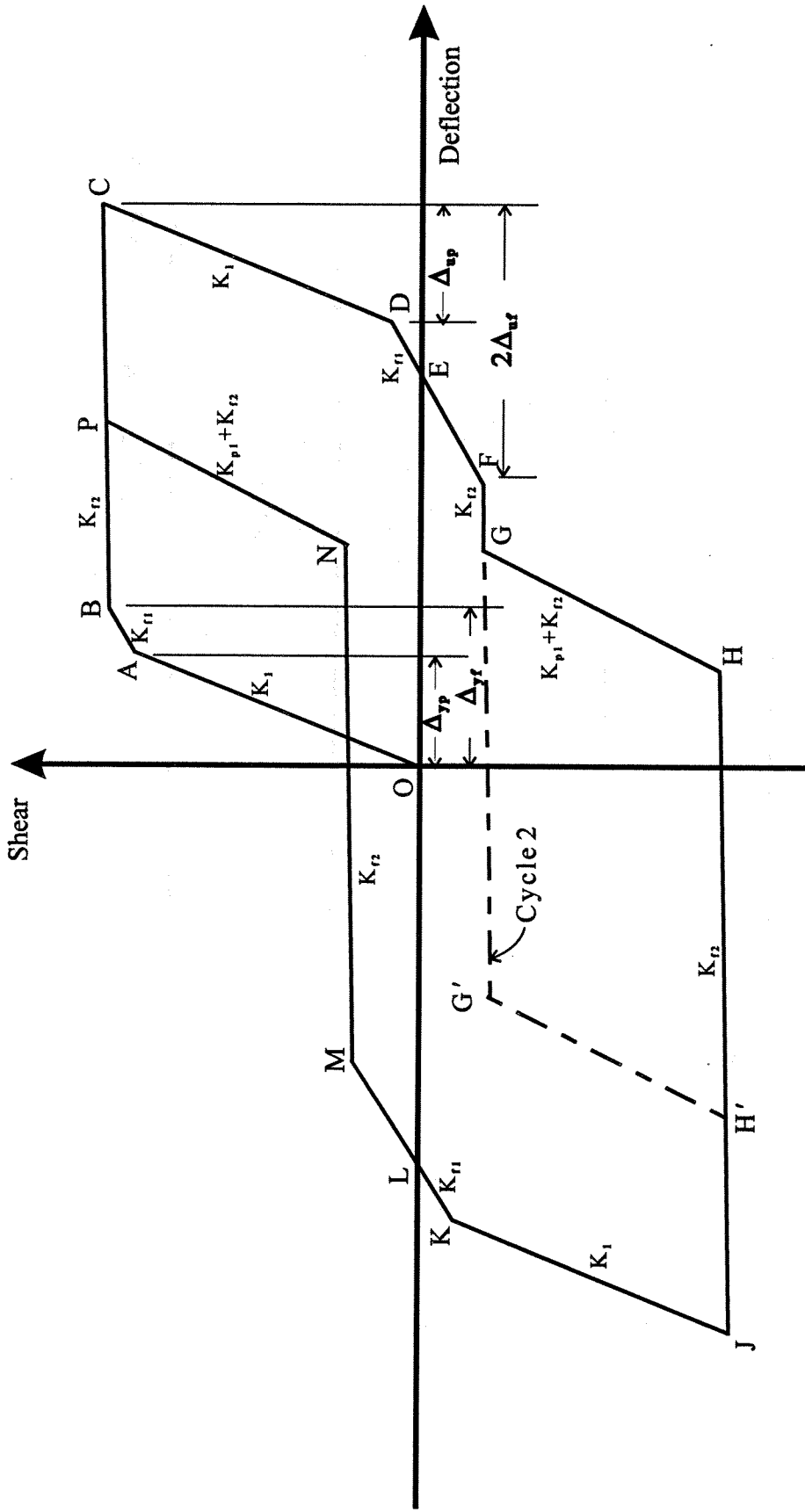


Fig. 9.14 Proposed Hysteresis Model

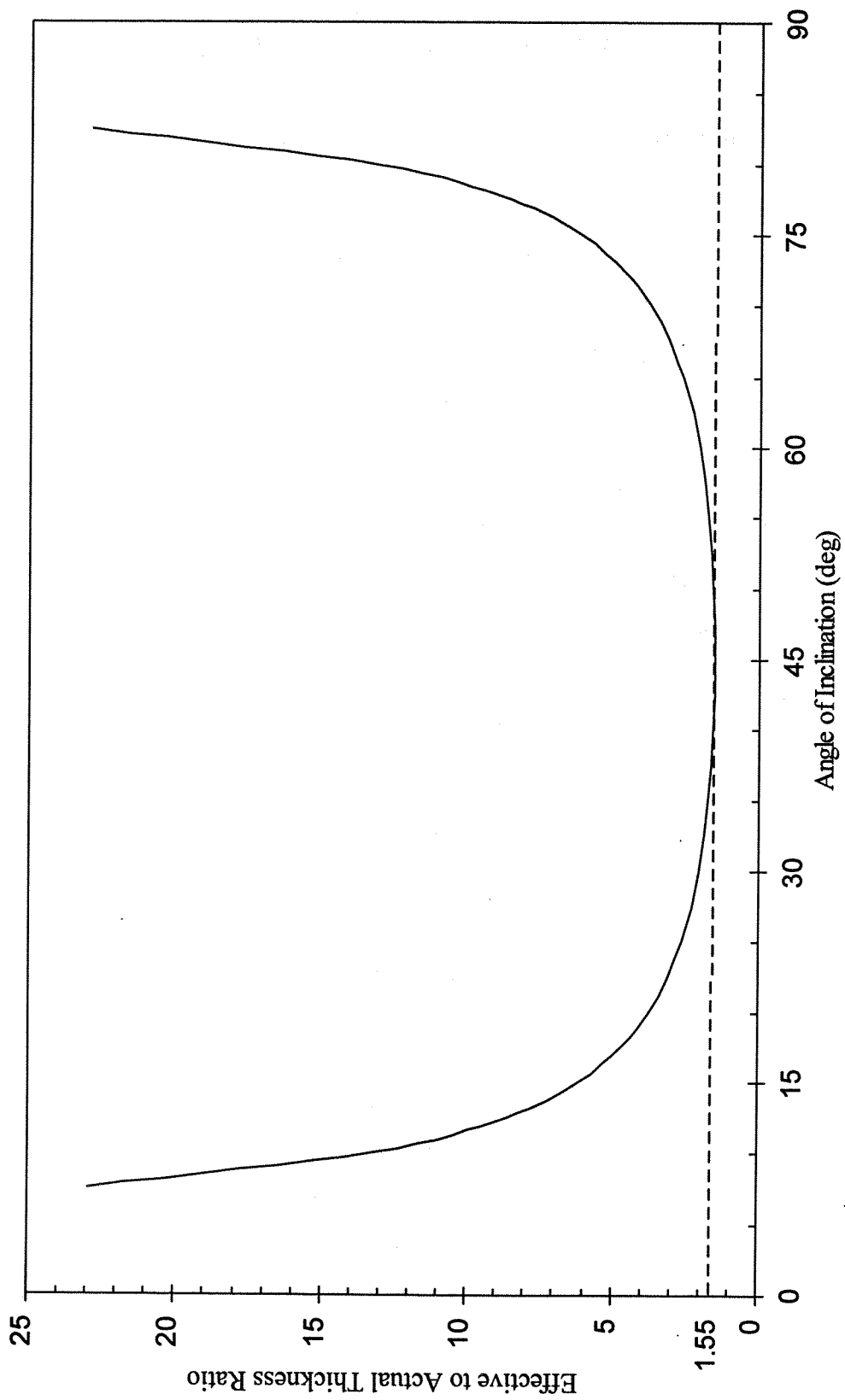


Fig. 9.15 Panel Thickness Ratio vs. Angle of Inclination of Tension Field

10. EVALUATION OF STRAIN DATA

10.1 Introduction

Figure 6.5 shows the locations of the 98 strain gauges used in the test. Thirty of the gauges were in the form of ten 45° strain rosettes and the others were linear gauges. In this chapter, the strain data from the lower two storeys of the steel plate shear wall specimen are discussed. Comparisons are made to the finite element results and to strip models with tension strips inclined at 42° and 50° from the vertical.

Section 10.2 reports the analyses of the strain data for the boundary members in each of Storeys 1 and 2 at two load levels. (Storey 1 includes the columns in the lowest storey and the beam at Level 1. Similarly, Storey 2 includes the columns between Levels 1 and 2 and the beam at Level 2.) For each storey, the greater load level selected is near the limit of elastic behaviour for the most highly strained gauge location in the group considered. Another, lower, load level is also considered for each storey. In this case, the same load level is used for each of the two storeys. The base shears selected for Storey 1 are 2021 kN and 994 kN and those for Storey 2 are 2570 kN and 994 kN. For convenience, base shears of 994 kN, 2021 kN, and 2570 kN are referred to in the subsequent discussion as low, medium, and high load levels, respectively. For the data collected from the rosettes affixed to Panel 2, all three load levels are discussed. This information is reported in Section 10.3.

The test results from the low, medium, and high load levels were extracted from the data obtained during Cycles 7+, 11+, and 14+, respectively. This means that the forces applied at the four floor levels are oriented in a westerly direction. In each case, the material at the relevant strain gauges remained elastic throughout its strain history up to the load level considered. The finite element and strip model results are taken from a monotonic loading case up to the load level considered. Second-order geometric effects are included in the analyses.

10.2 Beam and Column Strains

Comparisons of the strain data from the test with the numerical model predictions for the beams and columns are made in the form of bending moments and axial forces. Figures 10.1 to 10.6 show the bending moments in each member and Figs. 10.7 to 10.12 show the axial forces, each at two load levels. Bending moments are plotted on the compression side of the member, axial tension is designated as positive, and axial compression is considered negative. For ease of comparison, the same scale is used for all plots for each member type (beam or column). All plots represent the *clear* extent of the members, that is, the beam-to-column joint regions are excluded from the member length.

In order to determine the axial force and bending moment from the strain gauges at a particular cross-section, uniaxial bending was assumed. Therefore, the readings from the two gauges on each flange were averaged to obtain the strain at the outer surface of each flange. Between these two points, a linear strain distribution is assumed. The mean measured value of the modulus of elasticity (see Chapter 5) was used to determine the associated stresses.

The bending moment diagrams resulting from the strip model analyses show a linear variation between tension strip nodes (Figs. 10.1 to 10.6), whereas the axial force diagrams are stepped (Figs. 10.7 to 10.12). This occurs only because of the discretization of the infill plate into a number of tension strips. These features of the curves (cusps and steps) are therefore dependent upon the number of strips used and their locations. However, it is recognized that the real structure would not exhibit these localized features.

Figures 10.1 and 10.2 show the bending moments in the east and west columns of Storey 1. In each case, and at both the low and the medium load levels, the bending moments predicted by all models near the top of the column agree well with the test values. The predicted moments near the bottom of the columns are

generally much higher than those measured, although the general trend from very small moments at the top to much larger moments at the bottom is evident in all cases. The shape of the curves from the finite element model and the strip models are similar, but in all cases the finite element model gives the closest agreement with the test results. Furthermore, the difference in the shapes of the curves for the two columns reflects the fact that where the infill plate is on the tension side of the column (in this case, the west column), it tends to significantly restrain the rotation of the column at the base. The agreement of the finite element results with the test results for the west column at the medium load level is excellent. In all other cases, where the measured bending moments near the column bases are lower than predicted, it appears that the infill plate in the test specimen helped restrain the rotations of the columns at their base more effectively than was modelled by the numerical analyses.

Figures 10.3 and 10.4 show the bending moments in the east and west columns of Storey 2. The bending moments near the top of the columns are predicted reasonably well by all models, although the finite element model consistently gives the best results. The moments near the bottom of the two columns considered are predicted with varying degrees of success. The best prediction in this region is by the finite element model at the low load level for the east column. The bending moment is significantly overestimated by all models near the base of the west column at the high load level. Because the infill plate is modelled only as a series of discrete tension strips in the strip model, the resulting tension forces are higher than would be present from the tension field in the actual continuous infill plate. This is reflected in the figures by bending moments at the mid-height of the columns that are significantly larger than those exhibited by the finite element model. There is also no evidence of these large bending moments in the test specimen, although the data available are near the column ends only. In general, the magnitudes of the measured moments are relatively small in the columns of Storey 2, which is consistent with the observed

deformed shape that exhibited a reversing curvature near Level 2. This deformed shape is typical of shear wall structures and confirms the effectiveness of the infill plates in contributing to the behaviour of the shear wall.

Figures 10.5 and 10.6 show the bending moments in the beams at Levels 1 and 2. All of the models predict similar moment curves, although the finite element model generally shows the best agreement with the test results. The trend is from a positive moment at the east end of the beam to a negative moment (or a lesser positive moment) at the west end. This is what would be expected from a moment-resisting frame loaded in the same manner. However, the values of moments are relatively small. At the load levels investigated, the maximum ratio of measured moment to plastic moment of the beam cross-section is only about 0.1. This indicates that the contribution of beam bending to the stiffness of the shear wall is relatively small and that the specimen behaved more like a wall than a frame when the tension field was well developed. However, the strip model implies a higher dependence on frame action. This is manifested by larger moments at the beam ends as compared with the finite element model and the test results.

The measured bending moments are small at all locations of the moment frame, with the exception of the column bases. This supports the evidence (such as the low degree of yielding in the beam-to-column joint panel zones reported in Section 7.3) that the infill panels significantly reduce the demand on the moment-resisting frame.

Figures 10.7, 10.8, 10.9, and 10.10 show the axial forces in the east and west columns of Storeys 1 and 2. The measured compression forces in the west column and tension forces in the east column are greater at the base of the columns than at the top. Furthermore, the differences between the forces at the top and bottom increase as the applied horizontal load increases. These characteristics reflect the transfer of the vertical component of the tension fields to the columns and their contributions to the

axial force distributions. In this respect, the models provide a reasonable prediction of the trends of the curves, but the actual values are predicted satisfactorily only in some of the cases. The ability of the models to predict the trends indicates that they model adequately the transfer of the vertical component of the tension field to the columns. The best results are from the finite element model for the east column in Storey 1 (Fig. 10.7), where both the trends and the particular values are predicted well. In all other cases, the compression forces in the west column are lower than predicted by the models and the tension forces in the east column are greater than predicted. (The lower tension forces in the east column are, in fact, occasionally compression forces.) This is consistent with the observation above that in the strip model the tension forces in the strip are greater than would be expected in the tension field of the actual infill plate. The variation in column axial forces from the top to the bottom are, thus, necessary for vertical static equilibrium. The predicted values are consistently closer to the measured values for the east column than for the west column at the same load level.

Figures 10.11 and 10.12 show the axial forces in the beams at Levels 1 and 2. In general, these forces are predicted reasonably well by the finite element model. However, the compressive forces are consistently overestimated by the strip model. This is due to the steep moment gradients (high shear forces) in the columns of Storeys 2 and 3 adjacent to the beams, which arise from the high tensile forces in the strips. These steep moment gradients are not present in the finite element results and, of course, are not expected to be present in the actual structure.

It should be noted that although the finite element model consistently gave better agreement with the test results than the strip model, the simpler strip model tended to produce conservative estimates of the member forces. This applies to all of the bending moments and the compressive axial forces in both the columns and the beams. The underestimate of the tensile column forces (in this case, in the east column) is not likely to be detrimental because the design forces would be established

from the case where the loading occurs in the opposite direction and the column is in compression.

10.3 Panel 2 Strains

Figure 6.5 shows the location of the strain rosettes affixed to Panel 2. In each location, rosettes were used on both sides of the panels and the associated readings were averaged to account for the effect of local plate bending. Stresses through the thickness of the plate are assumed to be negligible. For convenience of reference, the rosette pairs are numbered from 1 to 5 in Fig. 6.5. Results from the rosettes were sampled at the low, medium, and high load levels, as described in Section 10.1. Comparisons are made only with the finite element model because in the strip model the plate is not modelled as continuous in two directions.

Table 10.1 presents the major and minor principal stresses (σ_1 and σ_2 , respectively), the major principal stress direction (α , angular measurement from the vertical), and the maximum shear stress (τ_{\max}). The stresses are determined from the strain measurements using the mean measured value of the modulus of elasticity of the plate material, presented in Chapter 5. Results are shown at the five rosette locations for each of the three load levels, with one exception: the results of Rosette 3 are not presented at the high load level because one of the strain gauges had ceased to function properly. Tensile stresses are positive and compressive stresses negative.

In general, the angle α tends to decrease from the location of Rosette 1 to Rosette 5. As the horizontal loads increased from the low load to the high load level, the angle α determined from the test data stayed virtually constant for Rosettes 1 and 2 and decreased for Rosettes 3 to 5. This trend was reversed in the finite element results, where the angle stayed virtually constant for Rosettes 3 to 5 and decreased for Rosettes 1 and 2. Nevertheless, the decreases in angle described above were seldom more than 10° and the finite element model predicted the orientation of the principal

stresses adequately in most cases. A possible reason for any discrepancy between the test and predicted results is the fact that the fish plate connection was not included in the finite element model. The strain rosettes were mounted only 100 mm from the inside edge of the fish plate, and this may have had an effect on the state of stress in the region.

The predicted values of the principal stresses show good agreement with the test results in some cases and relatively poor agreement in the remainder. The predicted major principal stress magnitude is in all cases higher than the test value and the predicted minor principal stress magnitude is lower than the test value in nearly all cases. However, the predicted maximum shear stress, τ_{\max} , equal to one half the algebraic *difference* between the major and minor principal stresses, is in good agreement with the test values in most cases. The mean test/predicted ratio is 0.97 and the coefficient of variation is 0.16. This good agreement for the maximum shear stress indicates that although the principal stresses are not predicted well, the finite element model tends to underestimate the minor principal stress magnitude and to overestimate the major principal stress magnitude by a similar amount. Therefore, the stiffness of the infill plate in the direction of the minor (compressive) principal stress is greater in the test specimen than in model in the region near the edge of the panel where the strains were measured. This is likely due to the stiffening effect of the thicker fish plates that are not present in the model.

The test results also show that the minor (in this case, compressive) principal stresses can be very significant, a feature that is not fully represented by the finite element model and is neglected by the strip model entirely. Moreover, the magnitude of the experimental compressive principal stress is *greater* than that for the tension principal stress in virtually all cases considered. These results indicate that although the infill plates are relatively thin, considerable compressive stresses can be sustained near the panel corners, partly because of the stiffening effect of the fish plates. This

provides an additional mechanism that contributes to the shear resistance and stiffness of the panel.

10.4 General Discussion

The models predict the test results well in some cases and rather poorly in others. One location where the test results are not predicted particularly well by the finite element model is at the base of the shear wall. The bending moment at the base of the east column and the axial force in the west column are both predicted to have higher magnitudes than those determined from the measured strains. This applies to both the low and medium load levels. In order to gain an understanding of the consequence of this, the internal forces were examined in the columns and infill plate at the elevation of the lowest set of strain gauges, which were positioned 300 mm above the base plate.

Since the axial forces and bending moments in each column are known for both the finite element model and the test results at each load level, the net vertical force and bending moment in the infill plate can be determined simply by the application of the equations of global static equilibrium. These calculated force effects are shown in Table 10.2. As a check on the resulting forces, and to investigate the actual stress distribution across the infill plate at this elevation, the vertical stresses from the finite element analysis were plotted. These curves are shown in Fig. 10.13 for both the low and medium load levels. Numerical integration of the area under the curves leads to the net vertical force and bending moment present in the infill plate at that elevation. Based on this information, as well as the axial forces and bending moments in the columns at the same elevation, an overall statics check can be performed. This calculation indeed shows that the equations of static equilibrium are satisfied at each load level in the finite element analysis.

The general features of the two curves in Fig. 10.13 show several distinct similarities. In the region of the tensile stresses, the stress distribution is relatively uniform, with a slight undulation that reflects the buckled configuration of the plate. In the compression zone, the stress gradient is steep and the compressive stresses adjacent to the column flange are relatively high. Furthermore, the neutral axis occurs at approximately the same location in each case. The stress magnitudes merely increase with increasing load applied to the structure.

The stress distributions across the plate are in stark contrast to those that would be expected in the web of a beam in bending, when the web is relatively stocky. In that case, the web would have a linearly varying elastic stress distribution from one edge to the other. The net force in the web would be compressive because of the applied compressive axial load (the gravity loads). The force effects that would result in the infill plate under these circumstances are also shown in Table 10.2 for comparison.

Although the stress distribution in the infill plate of the test specimen cannot be uniquely determined, certain qualitative statements can be made. Table 10.2 indicates that at the low load level, the axial force and bending moment in the infill plate are better predicted by elastic beam theory than by a finite element analysis. However, at the medium load level, the vertical force is approximately equal to the force determined from the finite element analysis, whereas the moment is more similar to the moment resulting from elastic beam theory. This implies that the true behaviour lies between the two predictive models.

The infill plate in the test specimen resists significantly more of the overturning moment than predicted by the finite element model, as shown in Table 10.2. It is likely that improved agreement would result had the fish plates been included in the model. The stiffening effect of the fish plates would lead to higher stresses than those predicted adjacent to the columns. Because of the large moment

arm from these regions to the shear wall centreline, significantly larger bending moments would result, with a relatively small increase in stress.

Another factor may have had an effect on the comparisons between the analytical and test results. This is the fact that the physical test specimen had undergone numerous loading cycles prior to the sampling of the data presented, whereas the data for the numerical models are from a monotonic loading case. Although load levels were selected such that inelastic straining had not occurred at the locations where the strains were measured, such straining could have occurred in other locations. This may have resulted in a redistribution of stresses from the elastic case. Furthermore, some damage (such as small undetected plate tears) may have accumulated in the test specimen that was not modelled, although this effect is expected to be small.

Residual stresses may also have had an effect on the results. Residual stresses were included in the boundary members of the finite element model, but those in the infill plate that result from weld shrinkage around the perimeter of the panel were not included. Residual stresses were not included in the strip models. The presence of residual stresses affects the load level at which material yielding occurs.

10.5 Summary

A large amount of data was collected from the strain gauges affixed to the four storey steel plate shear wall test specimen. Longitudinal gauges were used to measure strains in the flanges of the beams and columns and strain rosettes were used to measure the state of strain in Panel 2. Results at three load levels were compared to the results obtained from the finite element model and the strip model.

It was found that the moments and axial forces in the boundary members were predicted well by the numerical models in some cases, but rather poorly in others. Generally, the finite element model predicted the test results better than the strip

model. In almost all cases, the two models displayed the same trends in the bending moment and axial force diagrams. The strip model tended to produce conservative estimates of the member forces for design.

The orientation of the principal stresses in Panel 2 were predicted well by the finite element model in most cases. Discrepancies are attributed, at least in part, to the fact that the strain rosettes were placed relatively close to the fish plate connection, which is not included in the model. Although the principal stress magnitudes generally differed from the predicted values, the maximum shear stresses showed relatively good agreement with the test results. Although the infill plates are relatively thin, they can develop significant compressive stresses in the corners that contribute to the strength and stiffness of the shear wall.

Table 10.1 Panel 2 Stress Data at Rosette Locations

Low Load	Rosette 1		Rosette 2		Rosette 3		Rosette 4		Rosette 5	
	Test Results	Finite Element	Test Results	Finite Element	Test Results	Finite Element	Test Results	Finite Element	Test Results	Finite Element
α (deg)	62.8	65.8	60.2	61.4	57.0	52.8	50.5	36.1	47.6	36.9
σ_1 (MPa)	31.6	36.9	20.6	63.1	10.0	47.6	29.3	65.0	28.1	49.8
σ_2 (MPa)	-97.2	-77.6	-97.6	-83.2	-99.8	-120.0	-94.0	-56.9	-81.5	-57.5
τ_{max} (MPa)	64.4	57.2	59.1	73.1	54.9	83.8	61.6	60.9	54.8	53.7

Medium Load	Rosette 1		Rosette 2		Rosette 3		Rosette 4		Rosette 5	
	Test Results	Finite Element	Test Results	Finite Element	Test Results	Finite Element	Test Results	Finite Element	Test Results	Finite Element
α (deg)	64.3	59.9	60.1	55.0	48.8	48.0	40.5	37.9	40.3	36.5
σ_1 (MPa)	102.5	119.3	76.5	171.8	54.3	155.4	86.8	139.8	104.9	151.5
σ_2 (MPa)	-161.4	-103.8	-188.9	-71.4	-278.0	-248.4	-161.5	-113.9	-131.6	-79.4
τ_{max} (MPa)	132.0	111.5	132.7	121.6	166.1	201.9	124.2	126.9	118.2	115.5

High Load	Rosette 1		Rosette 2		Rosette 3		Rosette 4		Rosette 5	
	Test Results	Finite Element	Test Results	Finite Element	Test Results	Finite Element	Test Results	Finite Element	Test Results	Finite Element
α (deg)	63.9	56.4	61.3	50.4	-	-	38.2	38.4	38.3	35.3
σ_1 (MPa)	164.0	208.9	124.4	238.1	-	-	135.2	231.6	165.9	242.3
σ_2 (MPa)	-174.4	-122.8	-207.1	-62.6	-	-	-166.2	-157.3	-144.1	-104.4
τ_{max} (MPa)	169.2	165.9	165.7	150.4	-	-	150.7	194.5	155.0	173.3

Note: Angle of major principal stress direction, α , is measured from the vertical.

Table 10.2 Force Effects at Base of Panel 1

	Low Load		Medium Load	
	Axial Force (kN)	Moment (kNm)	Axial Force (kN)	Moment (kNm)
Test Results	-327	648	487	747
Finite Element	14	78	463	224
Elastic Beam Theory	-411	481	-409	973

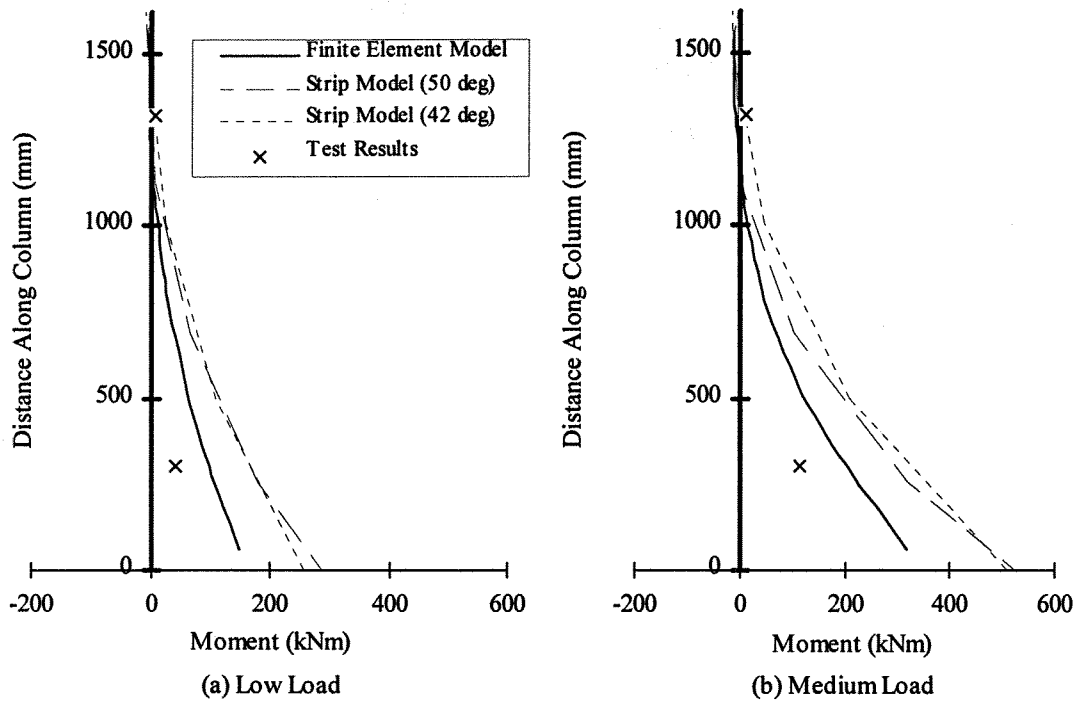


Fig. 10.1 Bending Moment Diagrams – Storey 1 / East Column

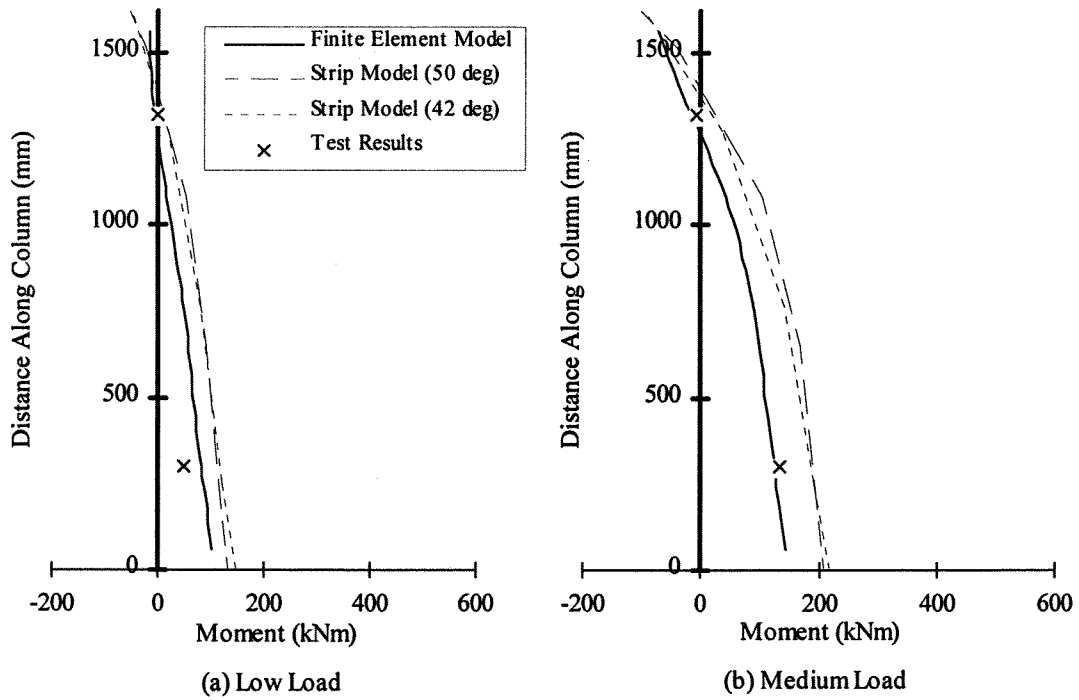


Fig. 10.2 Bending Moment Diagrams – Storey 1 / West Column

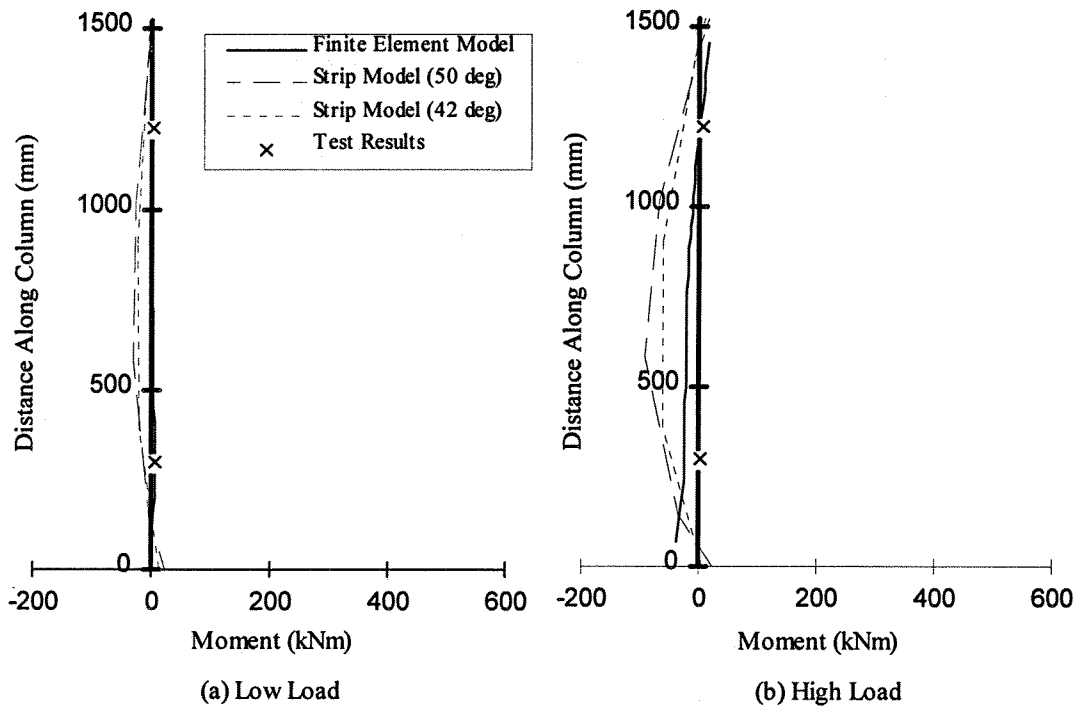


Fig. 10.3 Bending Moment Diagrams – Storey 2 / East Column

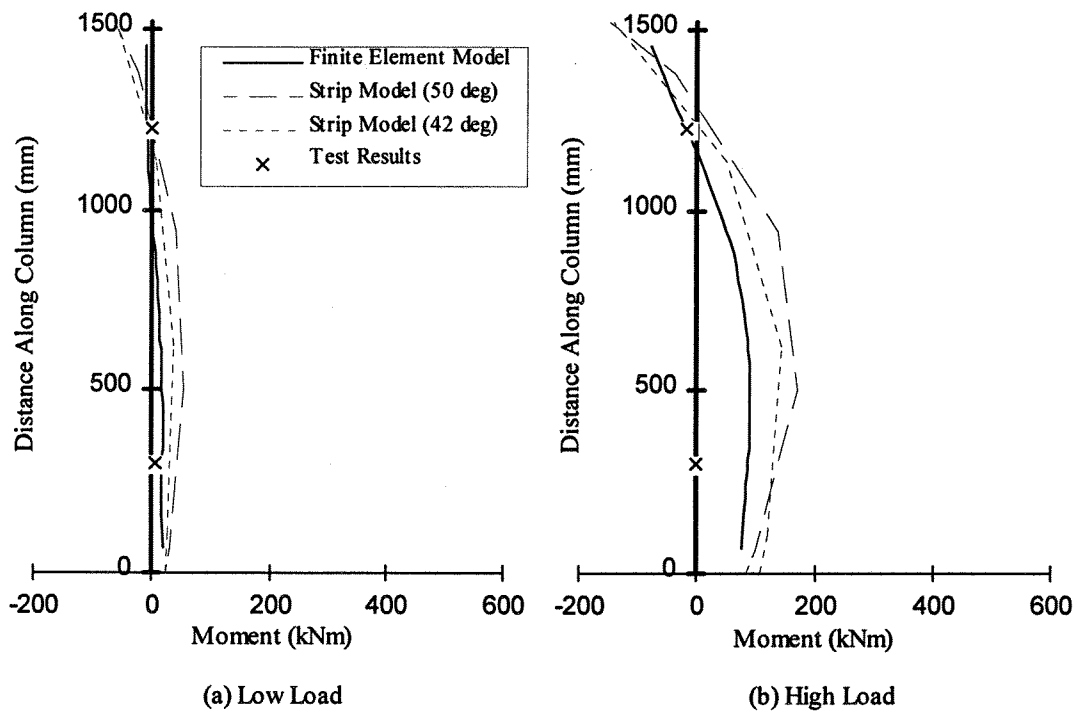
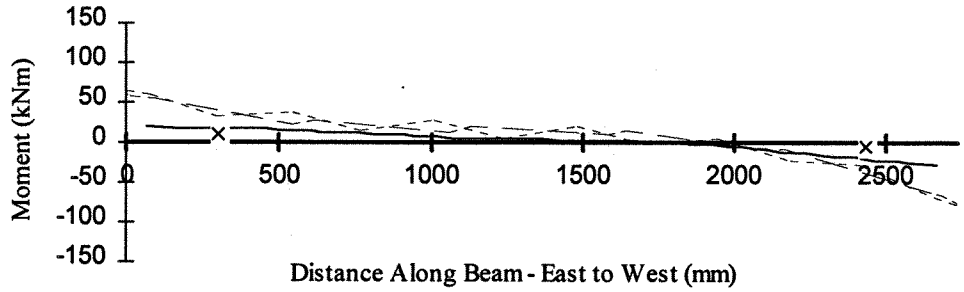
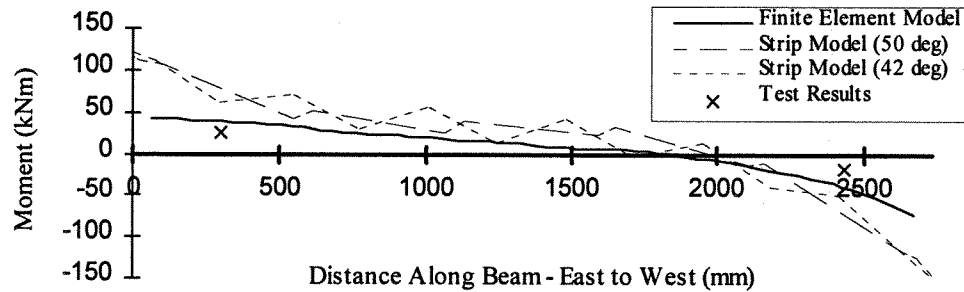


Fig. 10.4 Bending Moment Diagrams – Storey 2 / West Column

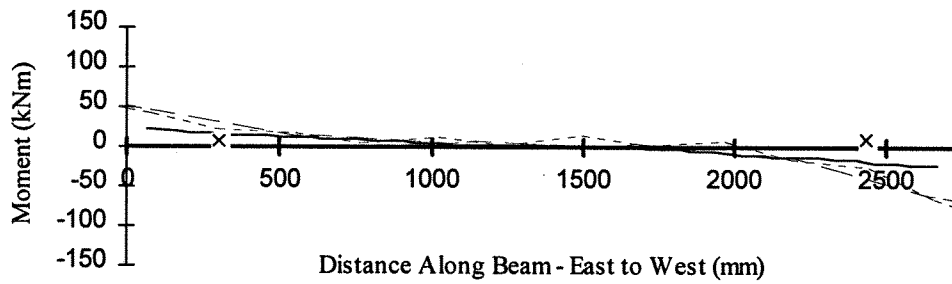


(a) Low Load

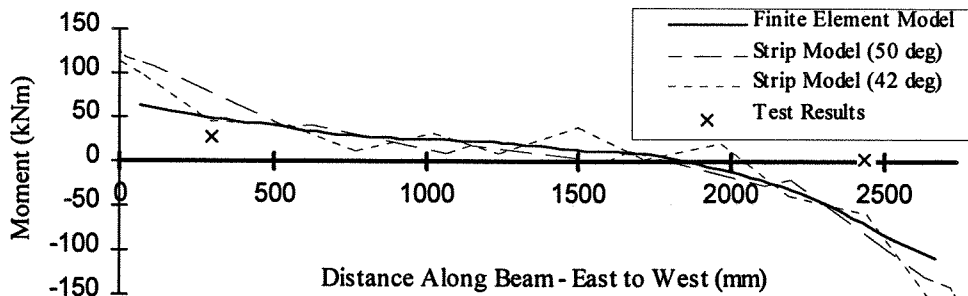


(b) Medium Load

Fig. 10.5 Bending Moment Diagrams – Level 1 Beam



(a) Low Load



(b) High Load

Fig. 10.6 Bending Moment Diagrams – Level 2 Beam

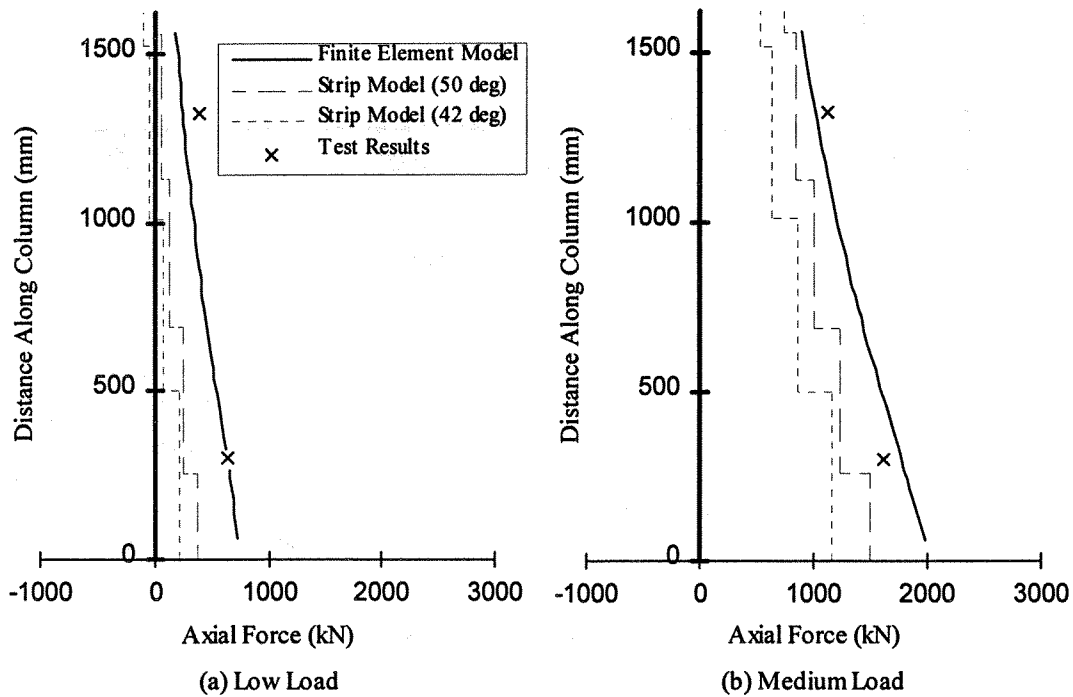


Fig. 10.7 Axial Force Diagrams – Storey 1 / East Column

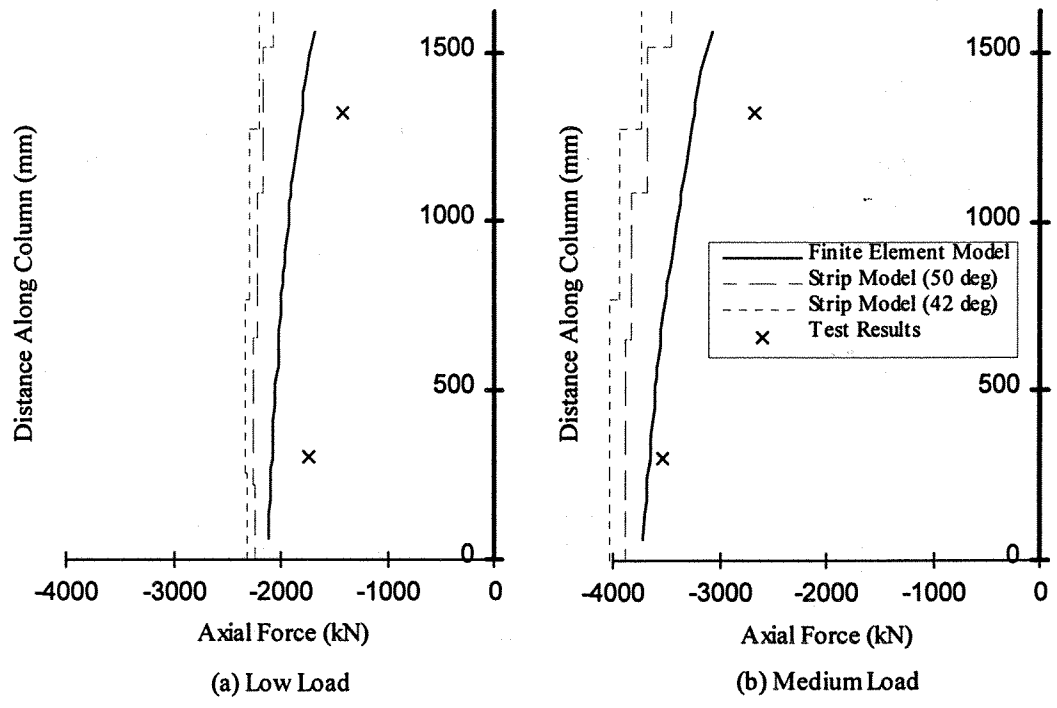


Fig. 10.8 Axial Force Diagrams – Storey 1 / West Column

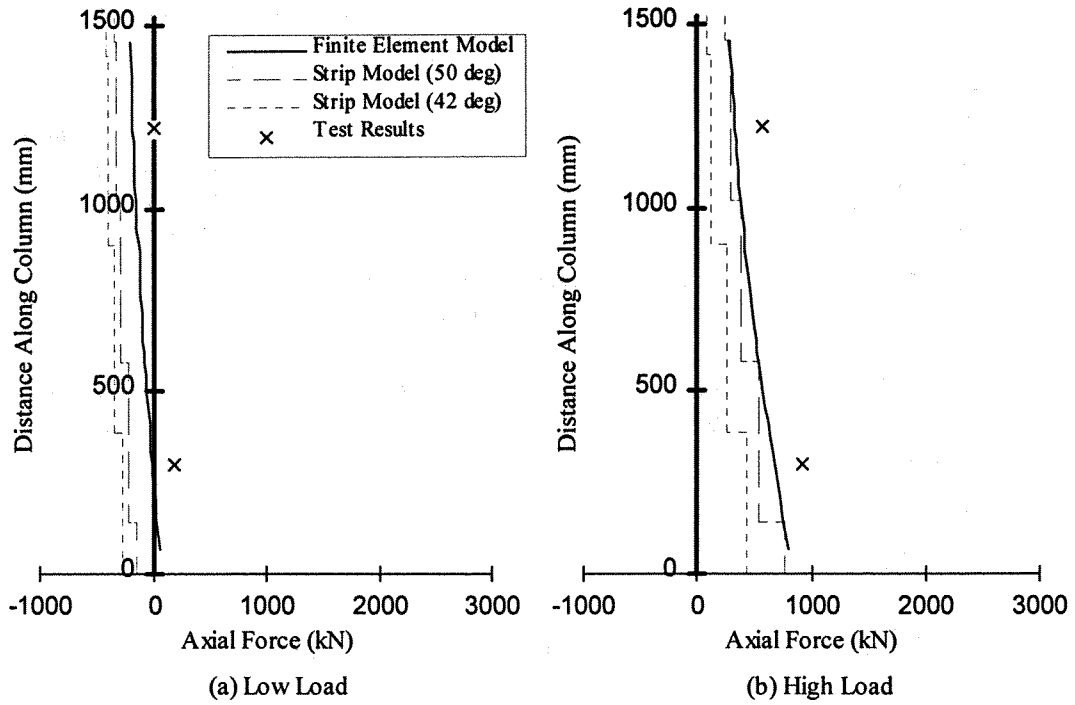


Fig. 10.9 Axial Force Diagrams – Storey 2 / East Column

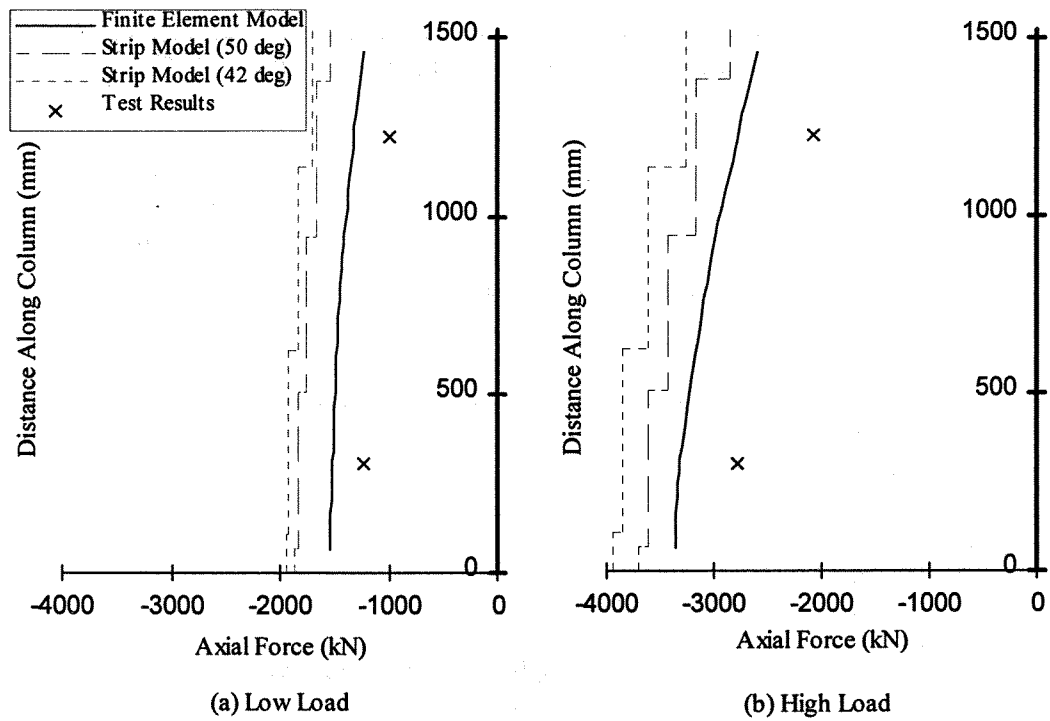


Fig. 10.10 Axial Force Diagrams – Storey 2 / West Column

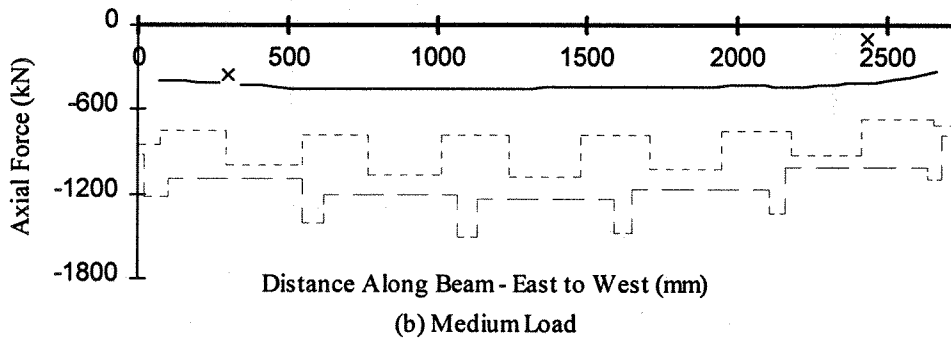
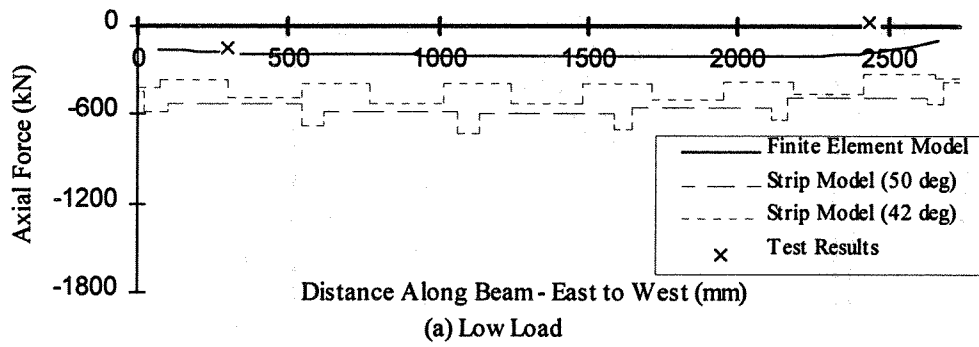


Fig. 10.11 Axial Force Diagrams – Level 1 Beam

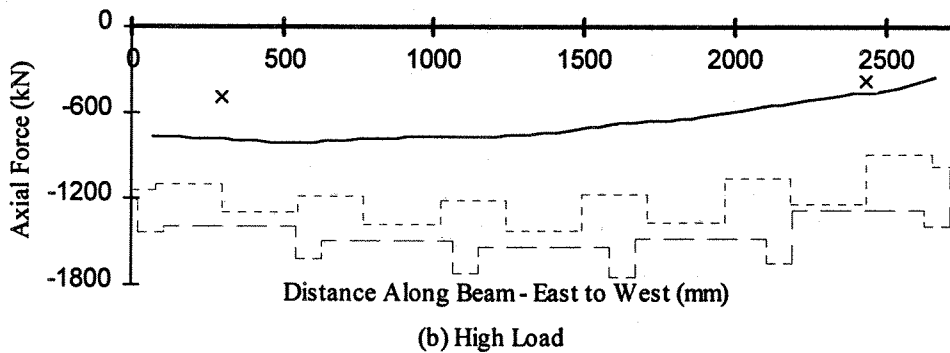
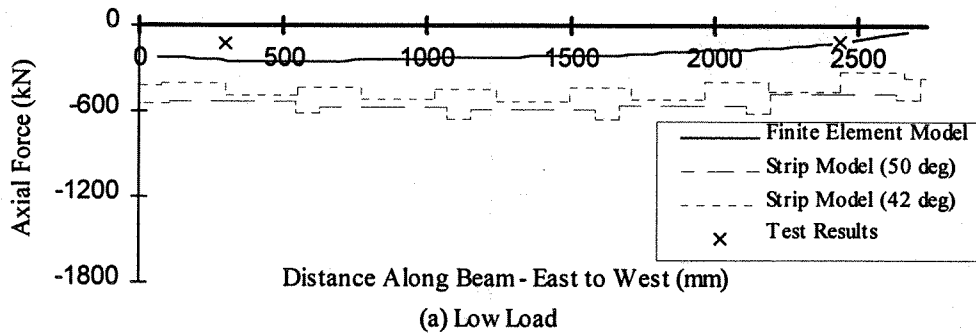
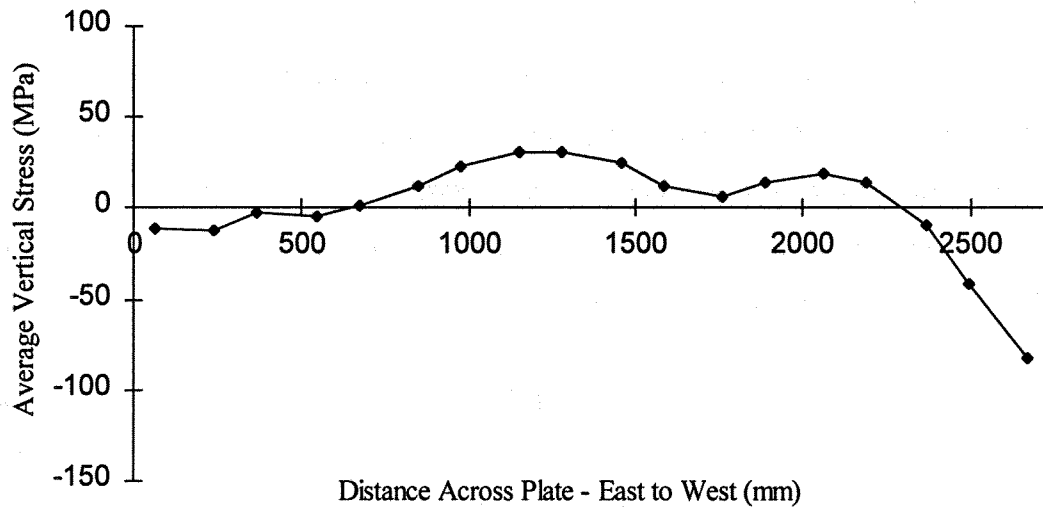
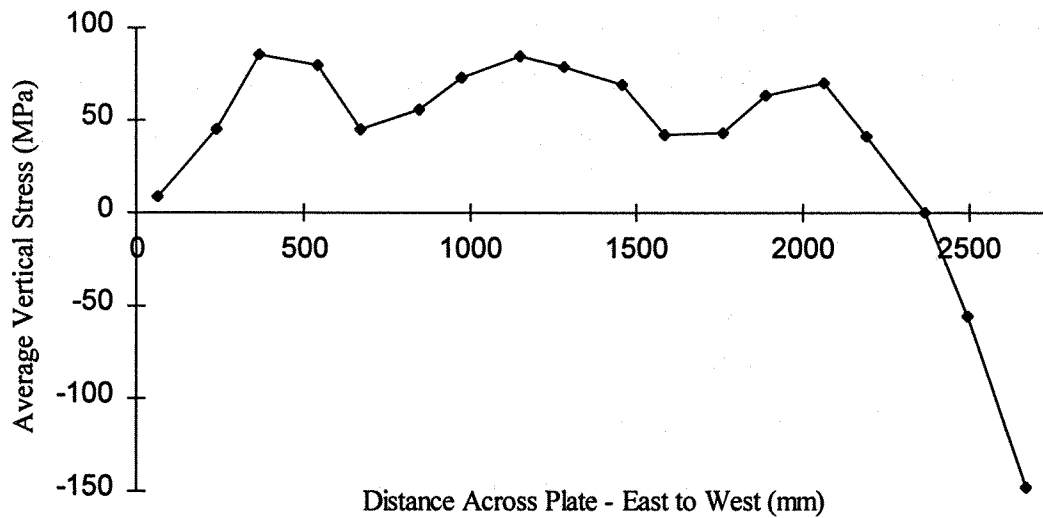


Fig. 10.12 Axial Force Diagrams – Level 2 Beam



(a) Low Load



(b) Medium Load

Fig. 10.13 Panel 1 Stress Distribution – Finite Element Model

11. SUMMARY, CONCLUSIONS, and RECOMMENDATIONS

11.1 Summary

This research project consisted of three main components: a physical testing programme, a finite element study, and an analytical study based on simplified models. In addition to providing a means of assessing the performance of steel plate shear walls subjected to severe cyclic loading, the test results were used to confirm the validity of the numerical models.

A four storey, single bay steel plate shear wall with unstiffened infill panels and moment-resisting beam-to-column connections was tested under a sequence of loading intended to simulate a severe seismic event. Gravity loads were applied to each column and equal cyclic in-plane horizontal loads were applied at each floor level. The cyclic deflection amplitudes were gradually increased according to the recommendations outlined in ATC-24 (Applied Technology Council 1992) until significant degradation of the shear wall was evident. The test specimen was able to resist increasingly higher loads in each successive cycle until a deflection of five times the deflection corresponding to the point of first significant yielding was reached, after which degradation of the load-carrying capacity was gradual and stable. The cycle in which the peak capacity occurred coincided approximately to that in which plate tears and local column flange buckling began to take place in the lowest storey. Prior to failure of the specimen, a deflection in the lowest storey of nine times the yield deflection had occurred. The test specimen proved to be initially very stiff, showed excellent ductility and energy dissipation characteristics, and exhibited stable behaviour at very large deformations and after many cycles of loading

Prior to conducting the four storey test, a large-scale specimen that represented a corner of one shear wall panel was tested. Thirty-five cycles of loading were applied in order to evaluate the performance of the corner connection detail

planned for use in the main test. The detail exhibited no significant deterioration and the detail was incorporated into the four storey specimen. Other ancillary tests included an evaluation of residual stresses in the shear wall frame members and a series of material tests on the members and infill plates.

A finite element model for steel plate shear walls was developed that used quadratic beam elements to represent the beams and columns and quadratic plate/shell elements to model the infill plates. As-built dimensions and measured material properties were incorporated into the model. An estimate of the initial out-of-flatness of the panels and the residual stresses obtained experimentally were also included. Because of the difficulty in achieving a solution when geometric non-linearities were included in the model, they were excluded for both the monotonic ultimate strength analysis and the cyclic analysis. In order to assess the effect of this on the model response, a comparative monotonic analysis that included geometric non-linearities was conducted up to a point where significant yielding had occurred and severe difficulties were encountered in achieving convergence. The non-linear analysis was found to be in excellent agreement with the experimental data, while the analysis that excluded the geometric non-linearities tended to overestimate the initial stiffness somewhat. However, the full response analysis (with the geometric non-linearities excluded) resulted in an excellent prediction of the ultimate strength. The cyclic finite element analysis was performed using a kinematic hardening rule. The analytical results agreed well with the test data in most respects, but because the non-linear geometric effects were neglected the response of the model did not display the moderate degree of pinching seen in the response of the test specimen.

The strip model, originally presented by Thorburn *et al.* (1983), was used to predict the envelope of cyclic curves obtained in the test. Inelastic behaviour in both the inclined tension strips and in the frame members was modelled. Although the model slightly underestimated the elastic stiffness of the test specimen, excellent agreement was obtained with the experimentally observed ultimate strength.

Two methods were presented for predicting the hysteretic behaviour of steel plate shear walls. A method proposed by Tromposch and Kulak (1987), which is based on a model developed by Mimura and Akiyana (1977), and a proposed new model were used to predict the behaviour of the four storey test specimen. The proposed model, which is based on combining the individual contributions of the moment-resisting frame and the infill panels, resulted in improved estimates of the amount of energy dissipated.

11.2 Conclusions and Recommendations

The four storey steel plate shear wall test specimen exhibited excellent performance. The hysteretic behaviour, shown in Fig. 7.1 for Panel 1, indicates that the shear wall configuration tested possesses an extremely high degree of ductility. This quality is generally considered to be one of the most important for structures subjected to seismic loading. Even at the end of the test, the main ductile component of the shear wall—the infill panel—was still able to carry shears nearly equal to those resisted at the ultimate load level. The hysteresis curves were also very stable throughout the response and they did not show any sudden drops in capacity. The post-ultimate degradation was gradual and controlled and significant degradation occurred only after a large number of displacement cycles and at very large deflections. Furthermore, the amount of energy dissipated during the loading cycles was significantly greater than that shown by similar shear walls but with shear-type beam-to-column connections (Tromposch and Kulak 1987). The amount of energy dissipated also increased steadily with each cycle of increased deflection. Based on the results of this large-scale four storey test, *it is concluded that the steel plate shear wall configuration tested represents an excellent lateral load-resisting system for seismic loading.*

It was shown in Chapter 7 that the force modification factor, R , in the National Building Code of Canada (NBCC 1995a) for a lateral load-resisting system

can be derived from experimental data. Two possible means for determining this factor were presented. The definition of the force modification factor that is implied by the method prescribed for calculating inelastic deflections in the National Building Code led to a value of $R = 10$, whereas a more conservative alternate approach led to a value of $R = 6$. The current value of the force modification factor for "ductile steel plate shear walls" in the National Building Code is $R = 4.0$, equivalent to the value assigned to ductile moment-resisting frames and ductile eccentrically braced frames. Based on the experimentally derived values and the excellent energy dissipation characteristics exhibited by the test specimen, *it is concluded that the value of $R = 4.0$ in the National Building Code for "ductile steel plate shear walls" is very conservative.*

When the test specimen reached deflections greater than five times the significant yield deflection, a gradual decrease in capacity occurred. This degradation was from a combination of small tears that formed in the infill plate and local buckling of the column flanges. In Chapter 7, it was noted that design codes tend to limit inelastic deflections to values that generally do not exceed an equivalent of 4.5 times the yield deflection in the case of the shear wall specimen. Therefore, *it is concluded that in a properly designed steel plate shear wall structure, significant degradation as a consequence of plate tearing and local buckling is unlikely to occur in a design earthquake.*

Towards the end of the test, where large deflections were imposed, severe local flange buckling occurred in the columns of the lowest storey immediately above the base and also below the beam at Level 1. Under dynamic earthquake loading, this condition could occur in other storeys. *It is recommended that even for Class 1 cross-sections, column flanges be stiffened to prevent local buckling due to a potential overload at locations in the frame where an analysis indicates that fully plastic behaviour will occur.* In any case, the interface between the shear wall and the foundation is effectively an abrupt change in stiffness of the lateral load-resisting

system. It was the local buckling deformations at this interface that appear to have led to the eventual fracture at the base of the west column during the test. Therefore, *it is recommended that in all cases, precautions be taken to prevent local buckling at the column bases and at other locations of abrupt changes in stiffness.* Further research is required to investigate the most effective means to accomplish this.

Because of the interaction of the shear panel and the moment-resisting frame, a good estimate of the yield stress of the panel material must be made in order to produce reliable results from an ultimate strength analysis. Furthermore, the tension field in the infill panel is anchored by the columns and the beams, and therefore the stress developed in the panel has a direct impact on the demands on the boundary members. However, the yield stress of structural steel can exceed its nominal value by a considerable amount. Therefore, to prevent overstressing the frame members due to an unexpected material overstrength, *it is recommended that both a minimum and a maximum yield stress be specified for the infill plates in construction documents.* An alternative would be to conduct pairs of analyses using likely minimum and maximum values of the yield stress.

Both the finite element model and the strip model gave excellent predictions of the ultimate capacity of the test specimen. The best prediction of the elastic and initial inelastic response was obtained through the use of the finite element model with non-linear geometric effects taken into account. Furthermore, the finite element model gave the best predictions of the internal member forces. Therefore, *it is recommended that for research purposes a finite element model including geometric non-linearities be used to obtain accurate results.* This method can also be used by structural design offices that have the appropriate computing resources.

Although the strip model tended to underestimate the elastic stiffness of the shear wall specimen by a small margin and was somewhat less accurate in predicting internal member forces than the finite element model, the results were still considered

to show generally good agreement with the test data and to produce conservative results for design. Therefore, *it is recommended that for design purposes the strip model be used to predict the monotonic response of steel plate shear walls.*

It was found that the hysteresis model presented by Tromposch and Kulak (1987) generally led to reasonable predictions of the amount of energy dissipated by the test structure. However, a new hysteresis model has been proposed that results in improved estimates of energy dissipation and offers the ability to isolate the respective contributions of the shear panels and the moment-resisting frame at all stages of the cycle. *It is recommended that the proposed new hysteresis model be used to predict the hysteretic response of steel plate shear walls.*

11.3 Recommendations for Future Research

The results of the large-scale four storey steel plate shear wall test described herein represent a significant advance in the understanding of the behaviour of these structures under severe cyclic loading. However, additional experimental investigations would be useful for the further study of certain aspects. For example, more detailed experimental data should be obtained about moment-resisting joints in steel plate shear walls to confirm the assertion that the presence of infill panels allows great ductility without severe demands on the frame joints. Because the storey shears are resisted largely by the stiff infill panels, beam-to-column joint demands tend to be less severe than for moment-resisting frames without infill panels. Measured joint moments were relatively small in all cases and no signs of joint distress were observed. This was supported by the observation that very little yielding occurred in the joint panel zones of the test specimen, even at large deflections. However, the possibility of a need for some of the special joint detailing requirements (FEMA 1995) to prevent failures of the kind that took place in the 1994 Northridge earthquake should be investigated further.

The infill plate in Panel 1 maintained its integrity throughout the test despite the large deflections and the large number of cycles imposed. This suggests that means to prevent the severe local buckling that led to the fracturing of the column should be studied in order to enhance the ductility of the system even further. It is likely that there are cost-effective ways to delay further the degradation of steel plate shear walls associated with local buckling of the column flanges.

Steel plate shear walls with nominally ductile moment-resisting frames and those with shear-type beam-to-column connections—assigned values of $R = 3.0$ and $R = 2.0$, respectively (NBCC 1995a)—should be tested in a similar manner to the shear wall test conducted during this research to determine the appropriateness of these values. It is likely that these force modification factors are conservative representations of their actual performance. It might also be found that the current requirements for achieving $R = 4.0$ may be relaxed, resulting in economies.

In order to allow for the passage of electrical and mechanical services through steel plate shear walls, the effect of panel penetrations should be investigated.

The finite element model developed during this research gave an excellent prediction of the ultimate strength and, when the effects of geometric non-linearities were included, was also able to give a good prediction of the elastic and initial inelastic response and the internal member forces. Additional work is required to refine the model such that the complete response can be traced with the inclusion of the non-linear geometric effects. It is likely that this would also lead to improved predictions of the hysteretic behaviour.

This study supports the use of the strip model as a relatively simple means of analysing the monotonic behaviour of steel plate shear walls. However, the discretization of the panel into a series of strips results in a moderate underestimation of the stiffness of the shear wall. It is desirable to develop a means of accounting for

the small but significant effects of the compressive stresses in the panel that tend to stiffen the shear wall. It is suggested that this may also result in improved estimates of the internal column and beam forces. However, the method must be relatively easy to implement so as not to detract from the advantages of the simplicity of the model.

REFERENCES

- Agelidis, N. and Mansell, D.S. 1980. Element design for a steel services core. Proceedings of the 7th Australasian Conference on the Mechanics of Structures and Materials, Perth, Australia, pp. 52-57.
- Agelidis, N. and Mansell, D.S. 1982. Steel plate cores in tall buildings. Civil Engineering Transactions of the Institution of Engineers, Australia, **CE24(1)**: 11-18.
- Anon. 1989. An eight-storey steel frame in 15 weeks; design incomplete at tender stage. Steel Construction (South African Institute of Steel Construction), **13(5)**: 5.
- Aoyama, H. and Yamamoto, Y. 1984. Aseismic strengthening of existing RC buildings by steel panel shear walls with rims. Transactions of the Japan Concrete Institute, **6**: 733-740.
- Applied Technology Council 1992. Guidelines for cyclic seismic testing of components of steel structures. Report No. 24, Applied Technology Council, Redwood City, CA.
- ASTM. 1989. E122-89, Standard practice for the choice of sample size to estimate a measure of quality for a lot or process. American Society for Testing and Materials, Philadelphia, PA.
- ASTM. 1991. A569/A569M-91a, Standard specification for steel, carbon (0.15 maximum percent), hot-rolled sheet and strip commercial quality. American Society for Testing and Materials, Philadelphia, PA.

- ASTM. 1992a. A370-92, Standard test methods and definitions for mechanical testing of steel products. American Society for Testing and Materials, Philadelphia, PA.
- ASTM. 1992b. E8M-92, Standard test methods for tension testing of metallic materials [metric]. American Society for Testing and Materials, Philadelphia, PA.
- Baldelli, J.A. 1983. Steel shear walls for existing buildings. AISC Engineering Journal, (2): 70-77.
- Basler, K. 1961. Strength of plate girders in shear. ASCE Journal of the Structural Division, 87(ST7): 151-180.
- Caccese, V., Elgaaly, M., and Chen, R. 1993. Experimental study of thin steel-plate shear walls under cyclic load. ASCE Journal of Structural Engineering, 119(2): 573-587.
- Clough, R.W. and Penzien, J. 1993. Dynamics of structures, Second edition. McGraw-Hill, Inc., New York, NY.
- CSA. 1992a. CAN/CSA-G40.20-92, General requirements for rolled or welded structural quality steel. Canadian Standards Association, Rexdale, ON.
- CSA. 1992b. CAN/CSA-G40.21-92, Structural quality steels. Canadian Standards Association, Rexdale, ON.
- CSA. 1994. CAN/CSA-S16.1-94, Limit states design of steel structures. Canadian Standards Association, Rexdale, ON.

- Derecho, A.T., Iqbal, M., Fintel, M., and Corley, W.G. 1980. Loading history for use in quasi-static simulated earthquake loading tests. ACI Publication SP63, Reinforced Concrete Structures Subjected to Wind and Earthquake Forces. American Concrete Institute, pp. 329-356.
- Elgaaly, M. and Caccese, V. 1990. Steel plate shear walls. Proceedings of the AISC National Steel Construction Conference, Chicago, IL, pp. 4-1 – 4-28.
- Elgaaly, M., Caccese, V., and Du, C. 1993. Postbuckling behavior of steel-plate shear walls under cyclic loads. ASCE Journal of Structural Engineering, **119**(2): 588-605.
- Engelhardt, M.D. and Sabol, T.A. 1994. Testing of welded steel moment connections in response to the Northridge earthquake. Progress report to the AISC Advisory Subcommittee on Special Moment Resisting Frame Research.
- FEMA. 1988. NEHRP Recommended provisions for the development of seismic regulations for new buildings. Federal Emergency Management Agency, Washington, DC.
- FEMA. 1994. NEHRP Recommended provisions for seismic regulations for new buildings. Federal Emergency Management Agency, Washington, DC.
- FEMA. 1995. Interim guidelines: evaluation, repair, modification and design of welded steel moment frame structures (SAC Joint Venture). Publication No. 267, Federal Emergency Management Agency, Washington, DC.
- Galambos, T.V. (Editor) 1988. Guide to stability design criteria for metal structures, Fourth edition. Structural Stability Research Council. John Wiley and Sons, Inc., New York, NY.

- Hibbitt, Karlsson, and Sorenson 1994. ABAQUS. Hibbitt, Karlsson, and Sorenson, Inc., Pawtucket, RI.
- Kennedy, D.J.L., Kulak, G.L., and Driver, R.G. 1994. *Discussion of Postbuckling behavior of steel-plate shear walls under cyclic loads* by Elgaaly, M., Caccese, V., and Du, C. ASCE Journal of Structural Engineering, **120**(7): 2250-2251.
- Kennedy, J.B. and Neville, A.M. 1976. Basic statistical methods for engineers and scientists, Second edition. Harper and Row Publ., New York, NY.
- Krawinkler, H. and Popov, E.P. 1982. Seismic behavior of moment connections and joints. ASCE Journal of the Structural Division, **8**(ST2): 373-391.
- Kuhn, P., Peterson, J.P., and Levin, L.R. 1952. A summary of diagonal tension, Part I – Methods of analysis. Technical Note 2661, National Advisory Committee for Aeronautics, Washington, DC.
- Kulak, G.L., Kennedy, D.J.L., and Driver, R.G. 1994. *Discussion of Experimental study of thin steel-plate shear walls under cyclic load* by Caccese, V., Elgaaly, M., and Chen, R. ASCE Journal of Structural Engineering, **120**(10): 3072-3073.
- Mimura, H. and Akiyama, H. 1977. Load-deflection relationship of earthquake-resistant steel shear walls with a developed diagonal tension field. Transactions of the Architectural Institute of Japan, **260**(Oct.): 109-114. (in Japanese)
- Nakashima, M., Iwai, S., Iwata, M., Takeuchi, T., Konomi, S., Akazawa, T., and Saburi, K. 1994. Energy dissipation behaviour of shear panels made of low yield steel. Earthquake Engineering and Structural Dynamics, **13**: 1299-1313.

- NBCC. 1995a. National building code of Canada. National Research Council of Canada, Ottawa, ON.
- NBCC. 1995b. National building code of Canada structural commentaries. National Research Council of Canada, Ottawa, ON.
- Popov, E.P. 1980. Seismic behavior of structural subassemblages. ASCE Journal of the Structural Division, **106**(ST7): 1451-1474.
- Popov, E.P., Amin, N.R., Louie, J.J.C., and Stephen, R.M. 1986. Cyclic behavior of large beam-column assemblies. AISC Engineering Journal, (1): 9-23.
- Ramm, E. 1981. Strategies for tracing the nonlinear response near limit points. Nonlinear Finite Element Analysis in Structural Mechanics, Edited by E. Wunderlich, E. Stein, and K.-J. Bathe, Springer-Verlag, Berlin, pp. 63-89.
- Riks, E. 1979. An incremental approach to the solution of snapping and buckling problems. International Journal of Solids and Structures, **15**(7): 529-551.
- Roberts, T.M. and Sabouri-Ghomi, S. 1991. Hysteretic characteristics of unstiffened plate shear panels. Thin-walled Structures, **14**: 145-162.
- Sabouri-Ghomi, S. and Roberts, T.M. 1991. Nonlinear dynamic analysis of thin steel plate shear walls. Computers and Structures, **39**(1/2): 121-127.
- Sabouri-Ghomi, S. and Roberts, T.M. 1992. Nonlinear dynamic analysis of steel plate shear walls including shear and bending deformations. Engineering Structures, **14**(5): 309-317.
- SAE. 1994. Chemical compositions of SAE carbon steels – SAE J403. Society of Automotive Engineers, Inc., Warrendale, PA.
- Softtek Services 1995. S-FRAME for windows. Softtek Services, Ltd., Richmond, BC.

- Sugii, K. and Yamada, M. 1996. Steel panel shear walls, with and without concrete covering. Proceedings of the 11th World Conference on Earthquake Engineering., Acapulco, Mexico.
- Takahashi, Y., Takemoto, Y., Takeda, T., and Takagi, M. 1973. Experimental study on thin steel shear walls and particular bracings under alternative horizontal load. Preliminary Report, IABSE Symposium on Resistance and Ultimate Deformability of Structures Acted on by Well-defined Repeated Loads, Lisbon, Portugal, pp. 185-191.
- Thorburn, L.J., Kulak, G.L., and Montgomery, C.J. 1983. Analysis of steel plate shear walls. Structural Engineering Report No.107, Department of Civil Engineering, University of Alberta, Edmonton, AB.
- Timler, P.A. and Kulak, G.L. 1983. Experimental study of steel plate shear walls. Structural Engineering Report No. 114, Department of Civil Engineering, University of Alberta, Edmonton, AB.
- Timoshenko, S.P. and Goodier, J.N. 1970. Theory of elasticity, Third edition. McGraw-Hill Book Co., Inc., New York, NY.
- Tremblay, R., Stierner, S.F., and Filiatrault, A. 1993. *Discussion of Overview of seismic provision changes in National Building Code of Canada 1990 by Tso, W.K.* Canadian Journal of Civil Engineering, **20**(2): 334-339.
- Tromposch, E.W. and Kulak, G.L. 1987. Cyclic and static behaviour of thin panel steel plate shear walls. Structural Engineering Report No. 145, Department of Civil Engineering, University of Alberta, Edmonton, AB.
- Tsai, K.C. and Wang, R.J. 1996. Shear beam for seismic energy dissipation. Proceedings of the 5th International Colloquium on Structural Stability, Structural Stability Research Council, Rio de Janeiro, Brazil, pp. 187-198.

- Tso, W.K. 1992. Overview of seismic provision changes in National Building Code of Canada 1990. *Canadian Journal of Civil Engineering*, **19**(3): 383-388.
- Uang, C.-M. 1991. Establishing R (or R_w) and C_d factors for building seismic provisions. *ASCE Journal of Structural Engineering*, **117**(1): 19-28.
- Wagner, H. 1931. Flat sheet metal girders with very thin webs, Part I – General theories and assumptions. Technical Memo. No. 604, National Advisory Committee for Aeronautics, Washington, DC.
- Xue, M. and Lu, L.-W. 1994a. Interaction of infilled steel shear wall panels with surrounding frame members. Proceedings of the Structural Stability Research Council Annual Technical Session, Bethlehem, PA, pp. 339-354.
- Xue, M. and Lu, L.-W. 1994b. Monotonic and cyclic behavior of infilled steel shear panels. Proceedings of the 17th Czech and Slovak International Conference on Steel Structures and Bridges, Bratislava, Slovakia.
- Yamada, M. 1992. Steel panel encased R.C. composite shear walls. Proceedings of the ASCE Engineering Foundation Conference on Composite Construction in Steel and Concrete II, pp. 899-912.
- Yamamoto, Y. and Aoyama, H. 1985. Behaviors of existing reinforced concrete frames strengthened with the steel shear panel governed by flexural strength. *Transactions of the Japan Concrete Institute*, **7**: 615-622.
- Yang, T.-S., and Popov, E.P. 1995. Experimental and analytical studies of steel connections and energy dissipators. Report No. UCB/EERC-95/13, Earthquake Engineering Research Center, University of California, Berkeley, CA.

Yarimci, E., Yura, J.A., and Lu, L.-W. 1966. Techniques for testing structures permitted to sway. Fritz Engineering Laboratory Report No. 273.40, Lehigh University, Bethlehem, PA.

201. *Strength and Installation Characteristics of Tension-Control Bolts* by Scott T. Undershute and Geoffrey L. Kulak, August 1994.
202. *Deformational Behavior of Line Pipe* by Magdi Mohareb, Alaa E. Elwi, Geoffrey L. Kulak and David W. Murray, September 1994.
203. *Behavior of Girth-Welded Line Pipe*, by Nader Yoosef-Ghodsi, Geoffrey L. Kulak and David W. Murray, September 1994.
204. *Numerical Investigation of Eccentrically Loaded Tied High Strength Concrete Columns* by Jueren Xie, Alaa E. Elwi, and James G. MacGregor, October 1994.
205. *Shear Strengthening of Concrete Girders Using Carbon Fibre Reinforced Plastic Sheets* by Efrosini H. Drimoussis and J.J. Roger Cheng, October 1994.
206. *Shrinkage and Flexural Tests of a Full-Scale Composite Truss* by Michael B. Maurer and D.J. Laurie Kennedy, December 1994.
207. *Analytical Investigation of the Compressive Behavior and Strength of Steel Gusset Plate Connections* by Michael C.H. Yam and J.J. Roger Cheng, December 1994.
208. *The Effect of Tension Flange Movement on the Strength of Point Loaded I-Beams* by Dean Mullin and J.J. Roger Cheng, January 1995.
209. *Experimental Study of Transversely Loaded Continuous Steel Plates* by Kurt P. Ratzlaff and D.J. Laurie Kennedy, May 1995.
210. *Fatigue Tests of Riveted Bridge Girders* by Daniel Adamson and Geoffrey L. Kulak, July 1995.
211. *Fatigue of Riveted Tension Members* by Jeffery DiBattista and Geoffrey L. Kulak, November 1995.
212. *Behaviour of Masonry Cavity Walls Subjected to Vertical Eccentric Loads* by Ru Wang, Alaa E. Elwi, Michael A. Hatzinikolas and Joseph Warwaruk, February 1996.
213. *Thermal Ice Loads on Structures* by Azita Azarnejad and Terry M. Hruday, November 1996.
214. *Transmission of High Strength Concrete Column Loads Through Concrete Slabs* by Carlos E. Ospina and Scott D.B. Alexander, January 1997.
215. *Seismic Behaviour of Steel Plate Shear Walls* by Robert G. Driver, Geoffrey L. Kulak, D.J. Laurie Kennedy and Alaa E. Elwi, February 1997.